

INMATEH -

**AGRICULTURAL
ENGINEERING**

JANUARY - APRIL

No liability is assumed by the editorial staff for the content of scientific papers and opinions published in this volume. They represent the author's point of views

Editorial

The National Institute of Research-Development for Machines and Installations designed to Agriculture and Food Industry - INMA Bucharest has the oldest and most prestigious research activity in the field of agricultural machinery and mechanizing technologies in Romania.

Short History

- ✓ In 1927, the first research Center for Agricultural Machinery in Agricultural Research Institute of Romania - ICAR (Establishing Law was published in O. D. no. 97/05.05.1927) was established;
- ✓ In 1930, was founded The Testing Department of Agricultural Machinery and Tools by transforming Agricultural Research Centre of ICAR - that founded the science of methodologies and experimental techniques in the field (Decision no. 2000/1930 of ICAR Manager - GHEORGHE IONESCU ȘIȘEȘTI);
- ✓ In 1952, was established the Research Institute for Mechanization and Electrification of Agriculture - ICMA Băneasa, by transforming the Department of Agricultural Machines and Tools Testing;
- ✓ In 1979, the Research Institute of Scientific and Technological Engineering for Agricultural Machinery and Tools - ICSITMUA was founded - subordinated to Ministry of Machine Building Industry - MICM, by unifying ICMA subordinated to MAA with ICPMA subordinated to MICM;
- ✓ In 1996 the National Institute of Research-Development for Machines and Installations designed to Agriculture and Food Industry - INMA was founded - according to G.D. no. 1308/25.11.1996, by reorganizing ICSITMUA, G.D. no. 1308/1996 coordinated by the Ministry of Education and Research G.D. no. 823/2004;
- ✓ In 2008 INMA has been accredited to carry out research and developing activities financed from public funds under G.D. no. 551/2007, Decision of the National Authority for Scientific Research - ANCSno. 9634/2008.

As a result of widening the spectrum of communication, dissemination and implementation of scientific research results, in 2000 was founded the institute magazine, issued under the name of SCIENTIFIC PAPERS (INMATEH), ISSN 1583 – 1019.

Starting with volume 30, no. 1/2010, the magazine changed its name to INMATEH - *Agricultural Engineering*, appearing both in print format (ISSN 2068 - 4215), and online (ISSN online: 2068 - 2239). The magazine is bilingual,

being published in Romanian and English, with a rhythm of three issues / year: January-April, May-August, September-December and is recognized by CNCSIS - with B⁺ category. Published articles are from the field of AGRICULTURAL ENGINEERING: technologies and technical equipment for agriculture and food industry, ecological agriculture, renewable energy, machinery testing, environment, transport in agriculture etc. and are evaluated by specialists inside the country and abroad, in mentioned domains.

Technical level and performance processes, technology and machinery for agriculture and food industry increasing, according to national requirements and European and international regulations, as well as exploitation of renewable resources in terms of efficiency, life, health and environment protection represent referential elements for the magazine „INMATEH - *Agricultural Engineering*”.

We are thankful to all readers, publishers and assessors.

Editor in chief,
Ph. D. Eng. Vladut Valentin

Managing Editorial Board - INMA Bucharest**Editor in Chief**

VLĂDUȚ Nicolae-Valentin
General Manager, Ph.D.Eng, SR I

Executive Editor

POPA Lucreția
Ph.D.Eng, SR I

Logistic support, database

MURARU Vergil, Ph.D.Eng, SR I
ȚICU Tania, techn.

Scientific Secretary

CÂRDEI Petre, math.

Official translators

RADU Daniela-Cristina
Prof.English, French

E-mail: inmatehjournal@gmail.com

Editorial Board

- Acad. HERA Cristian - Romania, Honorary President of ASAS - Academy of Agricultural and Forestry Sciences "Gheorghe Ionescu Șişești", member of Romanian Academy;
- Acad. Prof. Ph.D. SIN Gheorghe - Romania, President of ASAS - Academy of Agricultural and Forestry Sciences "Gheorghe Ionescu Șişești";
- Prof.Ph.D. NICOLESCU I. Mihai - Romania, Vicepresident of ASAS - Academy of Agricultural and Forestry Sciences "Gheorghe Ionescu Șişești";
- Hon.Prof.Ph.D.Eng. GĂNGU Vergil - Romania, President of the Department of Agricultural Mechanization of ASAS - Academy of Agricultural and Forestry Sciences "Gheorghe Ionescu Șişești";
- Ph.D. Eng. NICOLESCU C. Mihai - Romania, Scientific General Secretary of the ASAS-Academy of Agricultural and Forestry Sciences "Gheorghe Ionescu Șişești";
- Assoc.Prof. Ph.D. Eng. BELC Nastasia - Romania, IBA Bucharest;
- Ph.D. Eng. BUȚU Alina - Romania, INSB Bucharest;
- Prof. Ph.D. Eng. PARASCHIV Gigel - Romania, P.U. Bucharest;
- Prof. Ph.D.Eng. BIRIȘ Sorin - Romania, P.U. Bucharest;
- Prof. Ph.D. Eng. NICULIȚĂ Petru - Romania, USAMV Bucharest;
- Prof. Ph.D. Eng. VLASE Sorin - Romania, "Transilvania" University Brașov;
- Prof. Ph.D. Eng. ROȘ Victor - Romania, Technical University Cluj Napoca;
- Prof. Ph.D. Eng. FILIP Nicolae - Romania, Technical University Cluj Napoca;
- Prof. Ph.D. Eng. VOICU Gheorghe - Romania, P.U. Bucharest;
- Prof. Ph.D. Eng. GERGEN Iosif - Romania, USAMVB Timișoara;
- Prof. Ph.D. Eng. ȚENU Ioan - Romania, USAMV Iași;
- Assoc.Prof.Ph.D.Eng. BUNGESCU Sorin - Romania, USAMVB Timișoara;
- Prof. Ph.D.Eng. FENYVESI László - Hungary, Hungarian Institute of Agricultural Engineering Godolo;
- Prof.Ph.D.Eng. KOSUTIC Silvio - Croatia, University of Zagreb;
- Ph.D. BIOCCA Marcello - Italy Agricultural Research Council, Agricultural Engineering Research Unit;
- Prof.Ph.D.Eng. MIHAILOV Nikolay - Bulgaria, University of Rousse;
- Assoc.Prof. Ph.D.Eng. ATANASOV At. - Bulgaria, University of Rousse;
- Assoc.Prof. Ph.D. ERTEKIN Can - Turkey, Akdeniz University Antalia;
- Prof. Ph.D.Sc. Eng. VARTUKAPTEINIS Kaspars - Latvia, Latvia University of Agriculture, Institute of Agricultural Machinery;
- ir. HUYGHEBAERT Bruno - Belgium, Walloon Agricultural Research Center CRA-W;
- Prof. Ph.D. Eng. FABBRO Dal Inacio Maria - Brazil, Campinas State University;
- Prof. Ph.D. Eng. DE WRACHIEN Daniele - Italy, State University of Milan;
- Prof. Ph.D. Guanxin YAO - P.R.China, Along Agriculture R&D Technology and Management Consulting Co., Ltd;
- Prof. Ph.D. Eng. GONZÁLEZ Omar - Republic of Cuba, Central University "Marta Abreu" de las Villas;
- Assist.Prof.Dr. KABAŞ Önder –Turkey, Akdeniz University.
- Asist.Prof.Dr. SELVİ Kemal Çağatay - Turkey, Ondokuz Mayıs University.

In the present, *INMATEH - Agricultural Engineering* journal is indexed in the next international databases: [ULRICH'S Web](#): Global Serials Directory, [CABI](#), [SCIPRO](#), [ELSEVIER /SciVerse SCOPUS](#), [Index COPERNICUS International](#), [EBSCO Publishing](#), [Elektronische Zeitschriftenbibliothek](#)

INMATEH - Agricultural Engineering

vol. 51, no.1/ 2017

NATIONAL INSTITUTE OF RESEARCH-DEVELOPMENT FOR
MACHINES AND INSTALLATIONS DESIGNED TO
AGRICULTURE AND FOOD INDUSTRY - INMA Bucharest

6 Ion Ionescu de la Brad Blvd., sector 1, Bucharest

Three issues per year,
eISSN: 2068 – 2239
pISSN: 2068 – 4215

Edited by: INMA Bucharest

Copyright: INMA Bucharest / Romania

CONTENT

		Pag.
1.	<p style="text-align: center;">CONSTRUCTION OF CENTRIFUGAL WORKING DEVICE FOR MINERAL FERTILIZERS SPREADING / КОНСТРУКЦІЯ ВІДЦЕНТРОВОГО РОБОЧОГО ОРГАНУ ДЛЯ РОЗКИДАННЯ МІНЕРАЛЬНИХ ДОБРИВ Prof. Ph.D. Eng. Kobets A.S.¹⁾, Lect. Ph.D. Eng. Ponomarenko N.O.¹⁾, Prof. Ph.D. Agri.Sci. Kharytonov M.M.¹⁾ Dnipropetrovsk State Agrarian and Economics University, Faculty of Agrarian Engineering, Dnipro / Ukraine</p>	5
2.	<p style="text-align: center;">PARTICLE MOTION OVER THE SURFACE OF A ROTARY VERTICAL AXIS HELICOID / РУХ ЧАСТИНКИ ПО ПОВЕРХНІ ГЕЛІКОЇДА, ЯКИЙ ОБЕРТАЄТЬСЯ НАВКОЛО ВЕРТИКАЛЬНОЇ ОСІ Prof. Ph.D. Eng. Pylypaka S.F.¹⁾, Ph.D. Eng. Klendii M.B.²⁾, Ph.D. Eng. Klendii O.M.²⁾ ¹⁾National University of Life and Environmental Sciences of Ukraine / Ukraine; ²⁾Separated Subdivision of National University of Life and Environmental Sciences of Ukraine Berez hany Agrotechnical Institute / Ukraine</p>	15
3.	<p style="text-align: center;">THEORETICAL ANALYSIS OF THE TECHNOLOGICAL FEED OF LIFTED ROOT CROPS / ТЕОРЕТИЧНИЙ АНАЛІЗ ТЕХНОЛОГІЧНОЇ ПОДАЧІ ВИКОПАНОГО ВОРОХУ КОРЕНЕПЛОДІВ Dr. Prof. Baranovsky V.M.¹⁾, P.G. Potapenko M.V.²⁾ ¹⁾ Ternopil Ivan Pul'uj National Technical University, Ternopil / Ukraine; ²⁾ Berez hany Agrotechnical Institute, Berez hany / Ukraine</p>	29
4.	<p style="text-align: center;">MECHANICAL BEHAVIOR OF CORN STALK PITH: AN EXPERIMENTAL AND MODELING STUDY / 玉米秸秆内瓤的力学特性试验与模拟研究 Lect.Ph.D. Stud. Lixian Zhang ¹⁾, Prof. Ph.D. Zhongping Yang ^{*1)}, Prof. Ph.D. Eng. Qiang Zhang ²⁾, Prof. Xinhua Zhu ¹⁾, Lect.Ph.D. Haijun Hu ³⁾ ¹⁾ Department of Mechanical and Electronic Engineering, Northwest A&F University, Shaanxi / China; ²⁾ Department of Biosystems Engineering, University of Manitoba, Manitoba / Canada; ³⁾ College of Water Resources and Architectural Engineering, Northwest A&F University, Shaanxi / China</p>	39
5.	<p style="text-align: center;">FEASIBILITY STUDY OF MIXTURE TRANSPORTATION AND STIRRING PROCESS IN CONTINUOUS-FLOW CONVEYORS / ТЕХНІКО-ЕКОНОМІЧНЕ ОБГРУНТУВАННЯ ПРОЦЕСУ ТРАНСПОРТУВАННЯ ТА ЗМІШУВАННЯ СУМІШЕЙ ТРУБЧАСТИМИ КОНВЕЄРАМИ Prof. Ph.D. Eng. Hevko R.B.¹⁾, Prof. Ph.D. Eng. Yazlyuk B.O.¹⁾, Assoc. Prof. Ph.D. Eng. Liubin M.V.²⁾, Assoc. Prof. Ph.D. Eng. Tokarchuk O.A.²⁾, Ph.D. Eng. Klendii O.M.³⁾, Eng. Pankiv V.R.⁴⁾ ¹⁾Ternopil National Economical University / Ukraine; ²⁾ Vinnitsa National Agrarian University / Ukraine; ³⁾Separated Subdivision of National University of Life and Environmental Sciences of Ukraine Berez hany Agrotechnical Institute / Ukraine; ⁴⁾Ternopil Ivan Pul'uj National Technical University</p>	49
6.	<p style="text-align: center;">INVESTIGATION OF CONSTRUCTIVE GEOMETRICAL AND FILLING COEFFICIENTS OF COMBINED GRINDING SCREW CONVEYOR / ДОСЛІДЖЕННЯ КОНСТРУКТИВНОГО ГЕОМЕТРИЧНОГО КОЕФІЦІЄНТА ТА КОЕФІЦІЄНТА ЗАПОВНЕННЯ КОМБІНОВАНОГО ГВИНТОВОГО ТРАНСПОРТЕРА-ПОДРІБНЮВАЧА P.G. Pankiv V.R.¹⁾, Ph.D. Eng. Tokarchuk O.A.²⁾ ¹⁾ Ternopil Ivan Pul'uj National Technical University, Ternopil / Ukraine; ²⁾ Vinnitsa National Agrarian University, Vinnitsa / Ukraine</p>	59
7.	<p style="text-align: center;">INVESTIGATION OF DYNAMICAL IMPACT LOADS IN SCREW CONVEYER DRIVES WITH SAFETY CLUTCHES / ДОСЛІДЖЕННЯ ДИНАМІЧНИХ НАВАНТАЖЕНЬ В ПРИВОДАХ ГВИНТОВИХ КОНВЕЄРІВ З ЗАПОБІЖНИМИ МУФТАМИ Prof.Ph.D.Eng.Lutsiv I.V, Prof.Ph.D.Eng. Hevko I.B., Prof.Ph.D.Eng. Lyashuk O.L., Dubynyak T.S. Ternopil Ivan Pul'uj National Technical University, Ternopil / Ukraine</p>	69

		Pag.
8.	<p>A SWITCHING CONTROL STRATEGY OF GREENHOUSE COOLING SYSTEM BASED ON TEMPERATURE PREDICTION MODEL FOR ENERGY SAVING / 基于温度预测模型的温室降温系统的节能切换控制 Ph.D. Stud. Zhenfeng Xu¹⁾, Prof. Ph.D. Junjie Chen^{*1)}, Assoc. Prof. Ph.D. Gang Yu²⁾, Ms. Yahui Wang¹⁾ ¹⁾ School of Instrument Science and Engineering, Southeast University / China; ²⁾ Jiangsu Academy of Agricultural Sciences / China</p>	77
9.	<p>ENERGY BALANCE ANALYSIS AND MECHANIZATION INDEX FOR GREENHOUSE VEGETABLE PRODUCTION IN SOUTHERN OF ALGERIA. AN OVERVIEW OF BISKRA PROVINCE / تحليل الميزان الطاقي ومؤشر المكننة لزراعة البيوت المحمية في الجزائر. نظرة عن ولاية بسكرة Ph.D.Eng. Nourani A., As. Ph.D. Stud. Eng. Bencheikh A. Scientific and Technical Research Centre on Arid Regions (CRSTRA), Biskra/Algeria</p>	85
10.	<p>INTEGRATED USE OF BIOENERGY CONVERSION TECHNOLOGIES IN AGROECOSYSTEMS КОМПЛЕКСНЕ ВИКОРИСТАННЯ ТЕХНОЛОГІЙ БІОЕНЕРГЕТИЧНОЇ КОНВЕРСІЇ У АГРОЕКОСИСТЕМАХ Doctor of technical sciences Golub G.A.¹⁾, Doctor of technical sciences Kukharets S.M.²⁾, Ph.D. Eng. Yarosh Y.D.²⁾, Ph.D. Econ. Kukharets V.V.²⁾ ¹⁾National University of Life and Environmental Sciences of Ukraine / Ukraine, ²⁾Zhytomyr National Agroecological University / Ukraine</p>	93
11.	<p>STABILITY OF EPS SYSTEM OF AGRICULTURAL VEHICLES UNDER VIBRATION ENVIRONMENT / 农用车辆振动环境下电动助力转向系统的稳定性研究 Ph.D. Zhipeng Li, M.S. Songzhuo Shi School of Transportation, Northeast Forestry University, Harbin, Heilongjiang / China</p>	101
12.	<p>THE EFFECT OF DRIPPER DISCHARGE ON THE WATER AND SALT MOVEMENT IN WETTED SOLUM UNDER INDIRECT SUBSURFACE DRIP IRRIGATION / 滴头流量对间接地下滴灌下湿润体内土壤水盐运移的影响 Assoc.Prof. Qiaoxia An¹⁾, Assoc.Prof. Ph.D.Stud. Sanmin Sun^{*1,2)}, M.S. Rong Xu¹⁾ ¹⁾College of Water Conservancy and Architecture Engineering, Tarim University, Alar / China ²⁾College of Water Resources and Civil Engineering, China Agricultural University, Beijing / China</p>	111
13.	<p>MATHEMATICAL MODEL VALIDATION AND ANALYSIS OF SOIL WATER AND NITROGEN TRANSPORT IN WATER STORAGE PITS / 蓄水单坑土壤水氮运移的数学模型验证分析研究 Master Zhonghua Ni College of Engineering and Technology, Shangqiu Polytechnic, Shangqiu, Henan / China</p>	117
14.	<p>BIOREMEDIATION OF AGRICULTURAL SOIL CONTAMINATED WITH LEAD USING INTERACTION: COMMON BARLEY <i>HORDEUM VULGARE</i> AND EARTHWORM <i>LUMBRICUS SP</i> / BIOREMEDIATION D'UN SOL AGRICOLE CONTAMINÉ AU PLOMB A L'AIDE D'INTERACTION: ORGE COMMUNE <i>HORDEUM VULGARE</i> ET VER DE TERRE <i>LUMBRICUS SP</i> As. Ph.D. Boukirat D.^{*1)}, Prof. Ph.D. Maatoug M.¹⁾, As. Ph.D. Zerrouki D.,¹⁾ As. Ph.D. Lahouel H¹⁾, Prof. Ph.D. Dr. Heilmeier H.²⁾, Prof. Ph.D. Dr. Kharytonov M.³⁾ ¹⁾Laboratory of Agro Biotechnology and Nutrition in Semi-arid Zones, Faculty of Natural Sciences and Life; Ibn-Khaldun University – Tiaret / Algeria; ²⁾ Institute of Biosciences, TU Bergakademie Freiberg / Germany, ³⁾ State Agrarian-Economic University, Dnipropetrovsk / Ukraine</p>	125
15.	<p>EXPERIMENTAL STUDY ON THE EFFECT OF WATER QUALITY ON RAINFALL EROSION / 水质对土壤降雨侵蚀影响的实验研究 As.Ph.D.Stud. Ji Hengying^{1,2)}, Prof. Ph.D. Shao Ming-an^{*3,4)}, Ph.D. Jia Xiaoxu⁴⁾ ¹⁾College of Resources and Environment, Northwest A & F University, Shaanxi/China ; ²⁾ College of Chemistry and Chemical Engineering, Xinjiang Normal University, Urumqi/ China; ³⁾ State Key Laboratory of Soil Erosion and Dryland Farming on the Loess Plateau, Institute of Soil and Water Conservation, Northwest A & F University, Shaanxi /China; ⁴⁾Key Laboratory of Ecosystem Network Observation and Modeling, Institute of Geographic Sciences and Natural Resources Research, Chinese Academy of Sciences, Beijing / China</p>	135

CONSTRUCTION OF CENTRIFUGAL WORKING DEVICE FOR MINERAL FERTILIZERS SPREADING

КОНСТРУКЦІЯ ВІДЦЕНТРОВОГО РОБОЧОГО ОРГАНУ ДЛЯ РОЗКИДАННЯ МІНЕРАЛЬНИХ ДОБРИВ

Prof. Ph.D. Eng. Kobets A.S.¹⁾, Lect. Ph.D. Eng., Ponomarenko N.O.¹⁾,
Prof. Ph.D. Agri.Sci. Kharytonov M.M.¹⁾

Dnipropetrovsk State Agrarian and Economics University, Faculty of Agrarian Engineering, Dnipro / Ukraine;
Tel: 0973456227; E-mail: envteam@ukr.net

Keywords: fertilizer, airflow, centrifugal spreader, disk

ABSTRACT

The original methods for determining the critical velocity impact on a metal surface, taking into account the moisture content of the granules and the influence of the wind on the final distribution have been developed. The research technique of influence on the airflow make possible to determine the effect of speed, both in laminar and turbulent modes.

The proposed rotary working body designs, structural features of which enable to improve the dispersion evenness of mineral fertilizer, are presented.

РЕЗЮМЕ

Розроблені оригінальні методи визначення критичної швидкості удару об металеву поверхню з урахуванням вологості гранул і впливу дії повітря на кінцевий розподіл. Методика досліджень швидкості повітряного потоку дозволяє визначити вплив швидкості, як у ламінарному, так і в турбулентному режимах.

Запропонований роторний робочий орган, конструкційні особливості якого дозволяють покращити рівномірність розкидування мінеральних добрив.

INTRODUCTION

It is known that, in Europe, over 90% of the granular fertilizers are distributed using spinning disc spreaders. Fertilizer efficiency largely depends on proper method, combinations of their dressing into soil (Ning et al, 2015). Depending on the terms and standards, there are main pre-sowing fertilizing and top-dressing.

There are two ways to use granular fertilizers: solid surface spreading and subsoil fertilization (Antille et al., 2013; Fertilizer Manual, 1998). The granular fertilizers must be especially properly handled and distributed (Hofstee, 1992).

The most common granular fertilizer application device is the centrifugal disk spreader (Petcu et al., 2014; Tijsskens et al., 2008). The main advantages of this spreader are the large spread width, the simple construction and the low cost (Petcu et al., 2015). Meantime the distribution pattern of fertilizer is affected by many variables. It depends on machinery model, working conditions and physical characteristics of fertilizer (Allaire and Parent, 2004; Macmillan, 2007; Šima T. et al., 2013). In this case disks with the possibility of working with mixture application on the soil surface at an angle to the horizon are used.

First of all, it is explained by the versatility of aggregate. By disc reorienting, we can get high quality fertilizing and achieve high performance by coverage.

However, lack of a clear interpretation of numerous design features of the working body and the car, in general, creates problems for the implementation of agro-technical requirements and increases the burden on the environment (Biocca et al., 2015). It is known that the optimal dose of fertilizing for each crop is recommended for specific soil and climatic conditions (Fertilizer Manual, 1998).

Methods and terms of fertilizing depend on biological and varietal characteristics of culture, predecessors, soil conditions, specific farm possibilities. Usually local and dispersing methods are used. Dispersed and local fertilizing can be main, pre-sowing or top-dressing.

Fertilizing is one of the indicators of agronomic requirements for such operations like irregularity in the distribution by coverage - 25%, while aggregate moving - 10%.

Unfortunately, national machines for mineral fertilizing provide application evenness near 50-60%, leading to deterioration of the quality and quantity of crops (*Kravchuk et al., 2004; Vasylieva N., 2016; Velychko O., 2015*). It was established that the uneven application of mineral, organic fertilizers and lime leads to significant yield losses and deterioration of its quality. Another negative consequence is environmental pollution.

The main disadvantages of centrifugal machines for mineral fertilizing are:

- high distribution unevenness by coverage;
- fractions redistribution by coverage;
- coverage instability.

It is clear that the quality of national spreading machines should be raised, but it requires significant expenditures in Ukraine. That is why improvement of the technical level of machines should be focused on economically reasonable limits. All these indicate the need for further research regarding the fertilizing process.

During the analytical research we have created mathematical model of the granular fertilizer which uses a centrifugal disk. The construction diagram of our own design spreader has been suggested.

The objective of experimental research is to determine the effect of wind direction on uniformity of fertilizing by the fertilizer spreader working body.

According to the goals we identified the following tasks such as:

- to develop a methodology for determining:
 - parameters of granules distribution by the soil surface in laboratory conditions;
 - wind impact on the parameters of the distribution of the granules by the soil surface.
- to develop constructive scheme of experimental installation and produce experimental stand;
- to produce disk model with the main design parameters;
- to perform laboratory experiments according to the research program;
- to perform mathematical analysis of the results.

MATERIAL AND METHODS

Achievements of the laboratory research were:

- determination of basic mechanical and technological properties of the fertilizers used in experiments;
- establishing granules distribution by kinematic and geometrical parameters: rate of disk rotation n , rad/s; angles $\gamma_1, \gamma_2, \gamma_3$ of flow setting, deg; angles $\alpha_1, \alpha_2, \alpha_3$, – tilting angles of blades to disk rotation area, deg;
- calculation of distribution parameters by the surface of each stream separately and simultaneously from all streams for different fractional composition of fertilizers;
- determination of the design parameters of the disk in which distribution is closest to even;
- research of the impact of different wind speed and direction on the final distribution of fertilizers;
- establishing the impact on fertilizers final distribution by axial vibrations of the disk and tilting angle relative to surface of soil.

Several field testing trials were included into the program, namely:

- making prototype of the disk with structural and kinematic characteristics, which was determined by results of laboratory and field research;
- determining the quality of surface fertilization under different applying rules;
- comparative analysis of fertilizing quality by serial and developed centrifugal working body.

Major mechanical and technological properties of fertilizers that have been used for the research, were determined during the experiment.

Standard methods were used to determine moisture, specific gravity, coefficient of internal and external friction, metal restitution ratio on hit. Methods of acceptable impact velocity of granules by the metal surface and determining of their aerodynamic properties can be considered as original.

Acceptable impact velocity can be determined by the scheme (fig. 1).

Laboratory installation consists of a blade disc 1 with a vertical rotation axis, bin 2, driving gear 3 with installed r.p.m. meter, percentage feeder 4, light-absorbing screen 5, collector of waste material – bag 6 and bin 7.

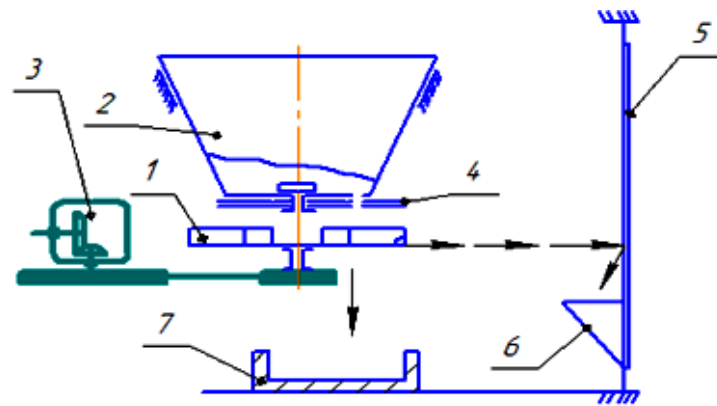


Fig. 1 - The scheme for determining acceptable impact velocity of fertilizer granules by metal surface

1 – blade disc; 2 – tanker; 3 – driving gear; 4 – percentage feeder; 5 – light-absorbing screen; 6 – bag; 7 – bin

Critical velocity was determined on sailing classifier with somewhat modified design (fig. 2), where the flow rate is measured directly by anemometer 3. In this device airflow is formed by fan 5, which is powered by transformer 7. The flow rate is regulated by excluder 6. Using of the anemometer 3 instead of the Pitot tube makes possible to measure velocity directly without performing assistive calculations.

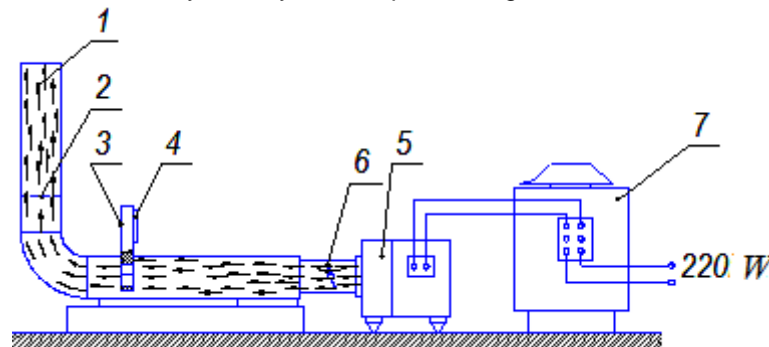


Fig.2 - Scheme of modified sailing classifier:

1 – tube; 2 – net; 3 – anemometer; 4 – anemometer screen; 5 – throttle; 6 – fan; 7 – transformer

The laboratory installation was constructed to perform the research program (fig. 3).

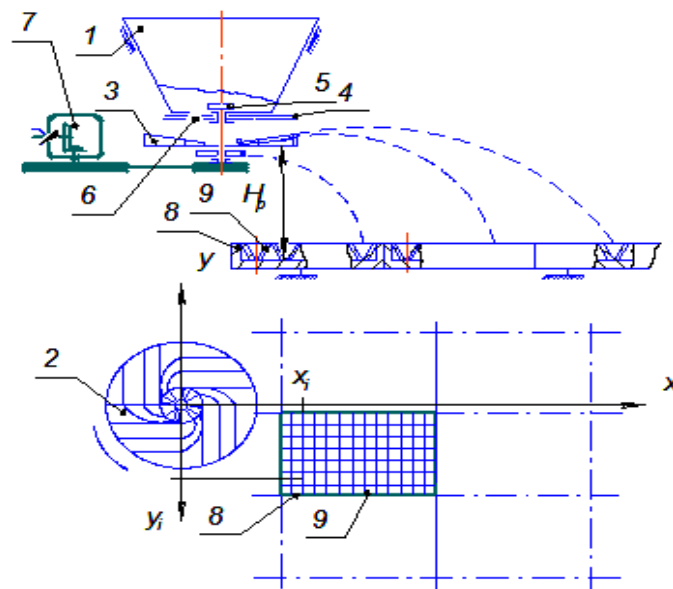


Fig. 3 - Scheme of laboratory installation

1 – tanker; 2 – disk; 3 – blade; 4 – percentage feeder; 5 – activator; 6 – activator's window; 7 – reducer; 8 – bin; 9 – samplers

Bins with installed samplers, which take falling granules, are used to determine the distribution parameters. It provides opportunities to determine the distribution of the granules coordinate-wisely (X_i, Y_i). Only one bin was used because of distribution parameters which have been pre-installed coordinate-wisely.

Wind flow was created by the bladed fan. Speed and direction of air flow were regulated by changing the position of the fan 3 relatively to bin 2. The flow rate was measured by anemometer 4 (fig. 4).

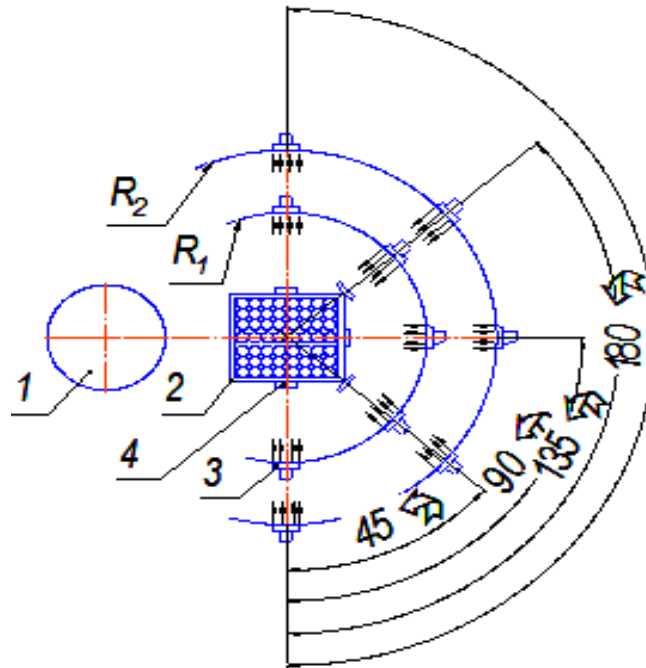


Fig. 4 - Research scheme of airflow action

1 – disk spreader; 2 – bin with samplers; 3 – fan; 4 – anemometer

At higher speeds unevenness dramatically increases and exceeds the allowable agrotechnical limits. The obtained data testify that the airflow negatively affects the evenness. The direction of the flow is also an important factor that determines evenness.

The lowest effect is observed when the wind direction is perpendicular to aggregate motion. This can be explained by receiving the smallest dose by outermost bins.

The biggest impact was at the action of two angles: 45° and 135°. It was revealed that the influence of the wind is selective, that air flow which is directed at an angle from 45° to 135° has the greatest impact on evenness distribution of fertilizer by the surface. If the wind speed is greater than 2.0 m/s than the fertilizing quality indicators deteriorate dramatically.

However, the value of unevenness in the presence of airflow in general, was within agrotechnical requirements.

Field tests were performed using two serial machines, equipped with disks of our own design. Sizes of the disk, its fastening elements and driving gear fully correspond to the serial disk sample. The only difference was establishment of a special adapter on the shaft. It gives the possibility to change the height position of the disk above soil.

Provision of butting overlap has been provided using GPS navigator.

The tightly placed bins were placed (one to each other) to evaluate the evenness of the surface distribution of granules. They were identical to those ones, used in the laboratory experiments.

RESULTS

Despite the fundamental researches in theory of granules interaction with disk and numerous improvements of working body construction, the question of uneven distribution of fertilizers which is provided by existing spreaders, is still not resolved fully, because the aim of analytical researches was to create a design disk, which is able to provide technologically sufficient evenness while fertilizers spreading.

One of the significant reasons of uneven distribution explained by scheme – Fig.5.

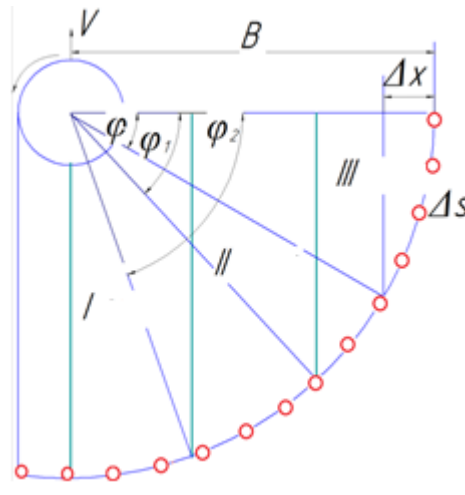


Fig. 5 - Scheme for analysis of uneven sowing of fertilizer by capture width according to even rotation of centrifugal working body

Assuming that all the granules during disc discharge are thrown at the same distance B toward the center, on the condition the aggregate does not move, then, if the granules are evenly distributed over a radius of circle B while the aggregate moves, it becomes obvious a dense distribution at the edge of the distribution strip.

Based on accepted assumption it can be argued that the number of granules, which falls on the strip Δx by capture width is proportional to length of corresponding arc Δs (Fig.5). This allows to characterize intensity of the area sowing which is processed, by formula $\Delta s/\Delta x = \psi$. The most intense sown area, the width of which is determined by one third of half of width and corresponds to the angle $\varphi_2 \approx 0,841$ rad ($48,19^\circ$) – Fig.6.

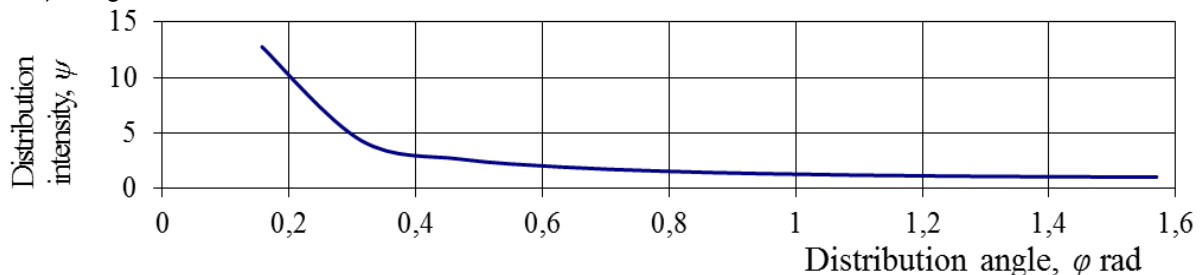


Fig. 6 - Dynamics of uneven distribution of fertilizers by the area which is processed

If half of operating width split into three equal areas (Fig. 5), then the third area will account 53.54% of the fertilizer, the second, determined angles φ_1 and φ_2 ($\varphi_1 = 70,53^\circ$) – 24.83 % from total amount of fertilizers, and on the first - 21.63% of amount that accounts for half of operating width.

It is evident that actual distribution scheme will be different from the considered idealized version, but the overall picture of densified sowing operation width on stripes edges is observed in real conditions.

As seen from the above considerations, it is necessary to provide escaping of multiple streams of granules from disk with different initial velocities, while avoiding flows cross during flight.

The design of centrifugal working body, which is proposed for problem solving, provides opportunity of additional simultaneous distribution zones I and II to achieve an average density that is realized in zone III (Fig.5). The constructive scheme of a fertilizer spreader is shown in Fig. 7.

Disk 1 is equipped with four blades (sectors) 2, inclined to the horizontal disk surface at an angle α . On working surface of each blade three vertical directing ribs 3 are mounted, longitudinal axis of which is perpendicular to the radial crossing line of blade and disk plane. Fertilizers are served to the center of disk and by centrifugal forces entering onto blades. Each blade fertilizer stream is divided into three independent streams that will have different velocities while escaping from surface, and besides on the longest edge granules are provided with the largest relative, and hence, the largest absolute escaping velocity; the lowest velocity will be developed on the short edge.

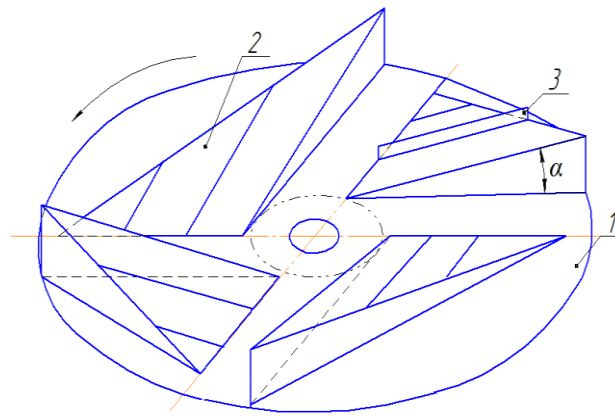


Fig. 7 - Constructive scheme of a fertilizer spreader
 1 – disc; 2 – blades (sectors); 3 – one of the guide ribs

Considering that angles of escaping from each edge will be different, we can say that separate streams of fertilizer will be spaced and trajectories crossing will not happen. The inclination angle of each blade α is selected according to the ability to deliver material on strip which is specified for this.

When designing the centrifugal working body it is necessary to provide the following material delivery: on long edge $0,62V$; on average $0,26V$; on short $0,11V$. To determine escaping velocity of granules from edge, which starts at an arbitrary distance a from disk center ($a = 00_1$), theorem of velocity addition is used.

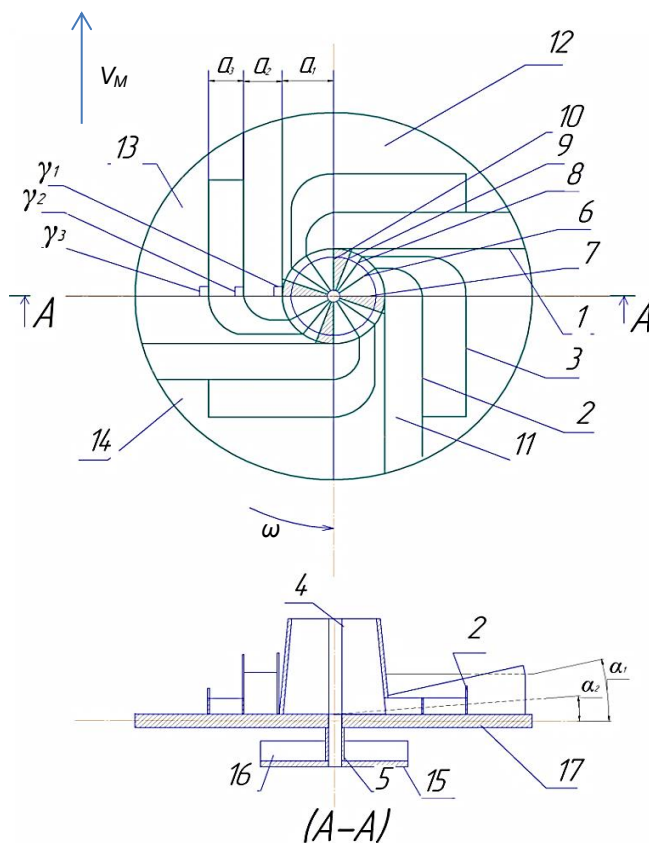


Fig. 8 - Constructural and technological scheme of centrifugal working body for fertilization

Analysis of possible options of centrifugal working body designs for fertilizing allowed to accept scheme, construction of which involves forming allocation of granules flows while loading (fig.8). Spreader consists of disk 17, four blades (sectors 11-14) each of which is formed by two vanes side walls which are formed by vertical edges and bottoms are inclined at angles α_1 and α_2 to the disk horizontal surface. Each edge (1-3) is perpendicular to the joint crossing line of blades bottoms and disk plane (on Fig.4 direction of each edge is marked with angles $\gamma_1, \gamma_2, \gamma_3$ severally). In the center of disk there is a conical feeder 4, interior space of which is divided into separate sectors with radial vertical plates (6-10). Each plate at it bottom part go beyond feeder on edge height and with bottom edge accedes to horizontal center disk part. The lateral edge of protruding from feeder (conical) part is connected to the curved section of edge 2, which is placed on the horizontal plane of the disk.

In the same way edge 3 is connected with protruding side part of the plate 8, and edge 1 – with 9. In each quarter of the centrifugal working body where the working blade is, feeder is divided into four sectors by plates. Three of them workable, through two blades fertilizer fall on upper disk, and on the second sector

accounts 53.6 % amount of fertilizer from first, and onto the last – third – the least 11.24 % of the same amount. From this sector fertilizer falls onto disk 15, which is situated lower on 60 mm from the upper which is provided by cup 5, on which are placed perpendicular one to each other guiding edges 16. One of feeder sectors closed from above (fig.1, shaded). Sectors areas are assigned proportional to the expenditure of

material which falls on each edge. The material getting into the sectors falls on the horizontal surface of the disc from which, moves between the curved portions of edges gets to the inclined blades.

Mathematical model for investigation of granules flight suggests that environmental resistance is proportional to velocity (fig.9). We consider general case of a particle motion as a material point in air after escaping from the working body if wind presents:

- gravity $m\vec{g}$, where $g = 9.81 \text{ m/s}^2$ – acceleration of gravity;
- total resistance force (pressure) of environment:

$$\vec{R} = k \cdot m \cdot g (\vec{V} - \vec{V}_B) \tag{1}$$

where k – resistance coefficient;

\vec{V} – particle velocity at an arbitrary time t (forms an angle α with horizon), m/s;

\vec{V}_B – wind velocity which is directed at angle β relative to particle, m/s;

\vec{V}_0 – initial velocity of material particle M (forms an angle α_0 with horizon), m/s.

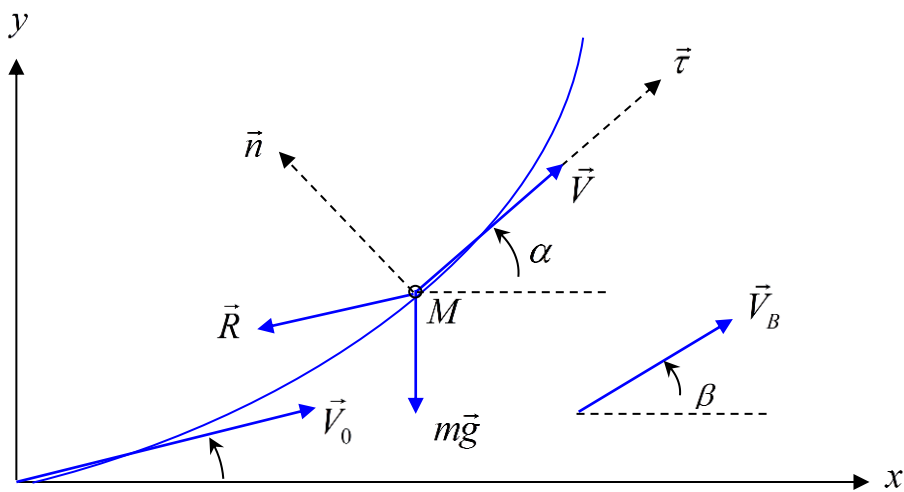


Fig. 9 - Scheme to the mathematical model of granules movement in the air

In true coordinate system (τ, n) system of differential equations of particle motion looks like:

$$m \frac{dV}{dt} = F_\tau, \quad m \frac{V^2}{\rho} = F_n,$$

$$\begin{cases} m \frac{dV}{dt} = -m \cdot g \cdot \sin \alpha - k \cdot m \cdot g \cdot [V - V_B \cdot \cos(\beta - \alpha)]; \\ m \frac{V^2}{\rho} = -m \cdot g \cdot \cos \alpha + k \cdot m \cdot g \cdot V \cdot \sin(\beta - \alpha), \end{cases} \tag{11}$$

where

$$\frac{1}{\rho} = \frac{d\alpha}{ds} \text{ – trajectory curvature;}$$

s – arc trajectory coordinate.

After the conversion and integration mathematical dependences we have:

$$x(\alpha) = \frac{1}{k \cdot g} \cdot \frac{A}{k} \left[\cos \varphi \cdot \ln \frac{\sin(\alpha + \varphi + \Omega)}{\sin(\alpha + \varphi)} - \sin \Omega \cdot \cos(\varphi + \Omega) \cdot \text{ctg}(\alpha + \varphi + \Omega) \right] + C_1, \tag{12}$$

$$y(\alpha) = \frac{1}{k \cdot g} \cdot \frac{A}{k} \left[-\sin \varphi \cdot \ln \frac{\sin(\alpha + \varphi + \Omega)}{\sin(\alpha + \varphi)} + \sin \Omega \cdot \sin(\varphi + \Omega) \cdot \text{ctg}(\alpha + \varphi + \Omega) \right] + C_2,$$

where C_1 and C_2 are obtained from the initial conditions: $x(\alpha_0) = 0 \quad y(\alpha_0) = 0$

The range of granules flight, which escapes from scapula was calculated with the following initial data: wind velocity (V_B) – 3 m/s, fertilizers density (ρ)–1000 kg/m³, granule diameter (R) – 0.001-0.005 m, blade inclination angle to disk rotation plane (α_1)– 13°, environment viscosity (η) for air – 0.000018 kg/(m s). For initial velocity V_0 , and escaping angle α_0 from formulas (9) and (10) we obtained the values $V_0 = 18.19$ m/s, $\alpha_0 = 8^\circ$.

The result of mathematical model graph solution is drawn and represented in Fig.10.

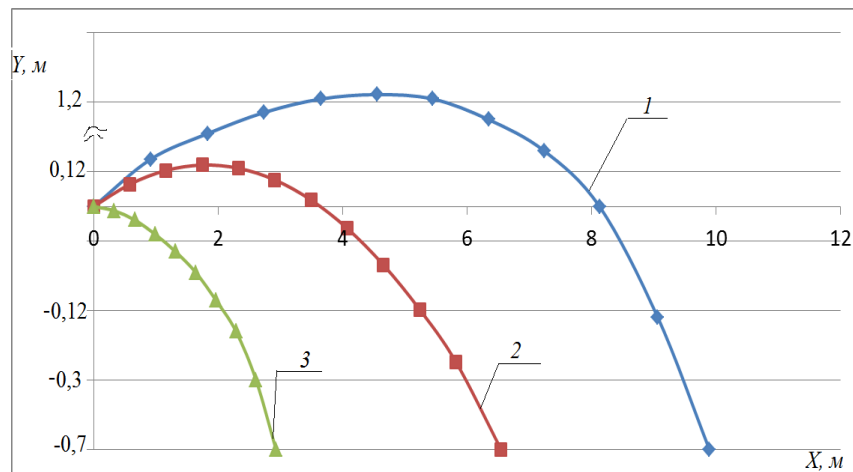


Fig. 10 - The trajectory of particles which escaped from designed working body

1 – trajectory of fertilizer particles which were launched from the blade, which is installed at angle 13°,
2 – at angle 8°, 3 – at angle 0°

For flight range of granules which was determined by formulas (12), the obtained value is 9.94 m and the maximum height is 1.2 m. While analyzing granule's motion which is speeded up by second scapula that has a length of 0.25 m, the inclination angle is $\alpha_2 = 8^\circ$, were obtained the granule escaping velocity $V_0 = 11.75$ m/s, launch angle – 7.5°. Under such conditions the flight distance was 6.35 m from the disk axis.

Trajectory of particle motion does not intersect with moving trajectory which is determined from the first scapula because of take-off height above disk, which in this case is 0.12 m.

Laboratory and field researches were performed using the most common granular fertilizers. They are: ammonia nitrate, superphosphate, mixtures NPK (complex fertilizers). Before work starting, their basic properties were determined in accordance with the methods, which count the great influence of mechanical and technological properties of the materials that were involved in the experiment for the final distribution by soil surface.

Figure 11 shows the effect of granules moisture on the maximum impact velocity by metal surface.

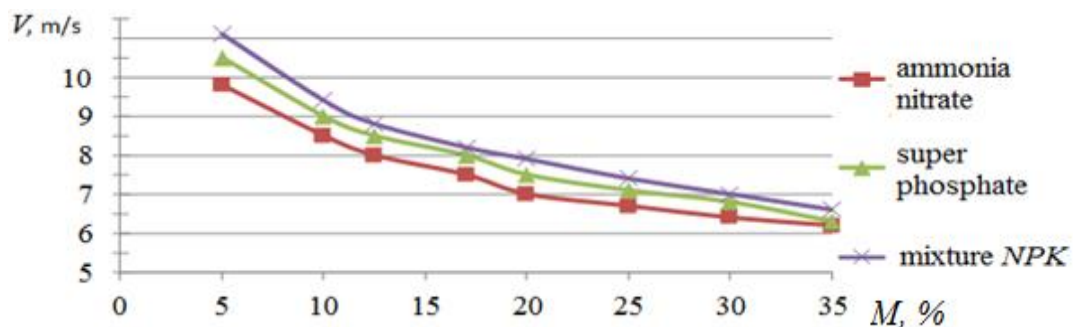


Fig. 11 - Influence of granules moisture on maximum velocity stroke to metal surface

The maximum permissible impact velocity by a metal surface with superphosphate – 11.3 m/s. If moisture of granules is from 5 to 12% then the speed reaches its maximum values in all researchable fertilizers (8-12 m/s). When the moisture rises from 12 to 35% an intense reduction of impact velocity by metal surface to 6.8 m/s was recorded. This is due to the destruction of the granules that hit and destruct. So this is the reason of acceptable impact velocity reduction.

Measured data of maximum impact velocity of fertilizers by metal are shown in Table 1.

Table 1

Physical and mechanical properties of the fertilizers used in the experiment

Type of fertilizer	Moisture	Bulk density	Angle of friction	Angle of internal friction	Impact velocity
	[%]	[t/m ³]	[degree]	[degree]	[m/s]
Ammonia nitrate	1.5 – 2.1	0.79 – 0.83	31 - 35	39 – 43	10.2
Superphosphate	4.4 – 4.9	1.13 – 1.19	26 - 34	31 – 35	12.3
Mixture NPK	5.8 – 6.7	1.03 – 1.12	30 - 35	40 - 44	9.7

Mechanical and technological properties of fertilizers, which affect the distribution process, were mainly determined experimentally. It has been established that the allowable impact velocity by metal surface is: superphosphate 12.3 m/s, ammonium nitrate - 10.2 m/s and a mixture NPK – 9.7 m/s, the optimal moisture is 12%.

The original methodology for determining critical impact velocity by metal surface with regard to granules moisture and wind influence on the final distribution has been developed. Methodology airflow influence research makes possible to determine the speed influence in laminar and turbulent modes.

Comparative laboratory tests proved that the proposed construction of a centrifugal spreader provides agro technical performance requirements for evenness of dispersion.

CONCLUSIONS

The developed methods of determining:

- parameters of granules distribution by the soil surface in laboratory condition;
- wind influence on the parameters of the granules distribution by the surface.

Methods of critical impact velocity by metal surface regarding moisture of granules and wind influence on the final distribution have been developed. The research methodology of air flow influence makes possible to determine the influence of the speed in laminar and turbulent modes.

Air flow that is directed at an angle from 45 to 135 degrees has the most negative impact on the fertilizer evenness distribution by the surface. Deviation in the wind direction should not exceed 45° from the movement direction of aggregate. Wind speed that exceeds 3 m/s is not desirable.

Constructive scheme of experimental installation have been developed and implemented in manufacture. The design of the centrifugal fertilizer spreader ensures the formation of multiple streams of fertilizers. It also leaves the disk at different speeds and different angles of flight.

It has been proved that the permissible impact velocity is from 8 to 12 m/s, depending on moisture.

Maximum resistance of granules to impact has been observed at their moisture of 9-12%.

ACKNOWLEDGEMENT

The work has been funded by the Ukrainian Ministry of Education and Science.

REFERENCES

- [1] Allaire S. E. and L. E. Parent, (2004), Physical Properties of Granular Organic-based Fertilisers, Part 1: Static Properties, *Biosystems Engineering*, 1, pp.79-87;
- [2] Antille D.L., Gallar-Redondo L., Godwin R.J., (2013), Determining the particle size range of organomineral fertilisers based on the spreading characteristics of the material, *ASABE Annual International Meeting*, Paper no. 13-1620197;
- [3] Biocca M., Gallo P., Menesatti P., (2013), Aerodynamic properties of six organo-mineral fertiliser particles. *Journal of Agricultural Engineering*, volume XLIV(s2):e83: pp.411-414;
- [4] Hofstee J. W., (1992), Handling and spreading of fertilizers: part 2, Physical properties of fertilizer, measuring methods and data. *Journal of Agricultural Engineering Research*, Vol. 53: pp.141–162;
- [5] Kravchuk V.I., Grytsigina M.I., Kovalya S.M., (2004), *Modern tendencies of construction development of agricultural technique (Сучасні тенденції розвитку конструкції сільськогосподарської техніки)*, Ed.Agrarian Science, 396 p.;
- [6] Ning S., Taosheng X., Liangtu S., Rujing W., & Yuanyuan, W, (2015), Variable rate fertilization system with adjustable active feed-roll length. *International Journal of Agricultural and Biological Engineering*, Vol. 8, Issue 4: pp.19–26;

- [7] Macmillan R.H., (2007), *The Mechanics of Fluid – Particle Systems*, with special reference to agriculture. Available at <http://eprints.unimelb.edu.au/archive/00001514/> (accessed on May, 2013);
- [8] Petcu A., Ștefan V., Popa L, Toderasc P., Ciupercă R., (2014), Factors influencing management granular fertilizers, *Tehnomarket* nr.2, pp.20-21;
- [9] Petcu A.S., Popa L., Ștefan V., et al., (2015), Theoretical research regarding the working process of the fertilizers managing systems by centrifugation. *Analele Universității din Craiova, seria Agricultură – Montanologie – Cadastru (Annals of the University of Craiova - Agriculture, Montanology, Cadastre Series)* Vol. XLV: pp.174-184;
- [10] Šima T., Nozdrovický L., Krupička J., Dubeňová M., Koloman K. (2013), Granulometric study of dasa 26/13 fertiliser. *MENDELNET*, pp.882-887;
- [11] Tijskens E., Van Liedekerke P., Piron E., Van Geyte J., Cointault F. et al., (2008), Recent results of experimental and Dem modeling of centrifugal fertilizer spreading. *Granular Matter, Springer Verlag*, 10 (4), pp.247–255;
- [12] Vasylieva N., (2016), Cluster models of the agrarian production's development in the households, *Economic annals - XXI. №. 3-4(2)*: pp.13–16;
- [13] Velychko O., (2015), Logistical system Fortschrittzahlen in the management of the supply chain of a multi-functional grain cooperative, *Economics and Sociology*, Vol. 8, No.1: pp.127-146;
- [14] ***Fertilizer Manual, (1998), *Fertilizer Manual (3rd ed.)*. Ed. United Nations Industrial Development Organization (UNIDO) and International Fertilizer Development Center (IFDC). Norwell, MA: Kluwer Academic.

PARTICLE MOTION OVER THE SURFACE OF A ROTARY VERTICAL AXIS HELICOID

/

РУХ ЧАСТИНКИ ПО ПОВЕРХНІ ГЕЛІКОЇДА, ЯКИЙ ОБЕРТАЄТЬСЯ НАВКОЛО ВЕРТИКАЛЬНОЇ ОСІ

Prof. Ph.D. Eng. Pylypaka S.F.¹⁾, Ph.D. Eng. Klendii M.B.²⁾, Ph.D. Eng. Klendii O.M.²⁾

¹⁾National University of Life and Environmental Sciences of Ukraine / Ukraine; ²⁾Separated Subdivision of National University of Life and Environmental Sciences of Ukraine Berezahny Agrotechnical Institute / Ukraine;
E-mail: alex_ks@mail.ru

Keywords: *vertical axis helicoid, rotary motion, relative particle motion, restrictive casing, differential equations of motion*

ABSTRACT

Particle relative motion over a rough surface of a rotary vertical axis helicoid has been considered. Differential equations of particle motion have been produced at its movement over the surface of a helicoid as well as at its contact with a restrictive cylindrical casing. The equations have been solved by numerical methods. The obtained results have been visualized.

РЕЗЮМЕ

Розглянуто відносний рух частинки по шорсткій поверхні гелікоїда, який обертається навколо вертикальної осі. Складено диференціальні рівняння руху частинки поверхнею гелікоїда, а також при її зустрічі з обмежувальним циліндричним кожухом. Рівняння розв'язані чисельними методами. Зроблено візуалізацію отриманих результатів.

INTRODUCTION

Helicoids, including screws, are wide-spread operating elements of the conveying units of agricultural machinery. In addition, they are used for well-drilling in construction. When in rotary helicoid motion, the particles of process material slide on the operating surface of a helicoid, thus executing a relative motion.

A particle or a material point executes a compound motion with the trajectory of relative sliding on the surface of a helicoid being its component. The investigation of such a motion by the example of a separate particle provides the insight into the nature of particle motion and the influence of the parameters of a helicoid on its behaviour. The most wide spread helicoids are screws, of which rectilinear generator of the surface is perpendicular to the axis. It has been of our interest to investigate particle motion over the helical surface, which rectilinear generator gets off the normal direction of the axis through a certain angle. At zero value of this deviation we will have a special case of a helicoid – a screw.

Investigation of the compound motion of the particles of process materials over moving surfaces has been covered in fundamental monographs (Vasylenko, 1960; Zaika, 1992). The movement of soil particles along moldboard is considered in monograph (Gyachev, 1961). Scientific papers (Pylypaka and Nesvidomyn, 2010 and 2011) are concerned with the most simple particle motion over the slant. Papers (Babka, 2013; Veselovski, 2013) consider slanting motion of the particles, which interact, namely form incompressible resilient strip.

The determination of the trajectory of a particle, which is moving over a cylindrical surface under the influence of buttress force, is covered in article (Voitiuk, Pylypaka, 1999). There is a group of articles, which consider particle movement over rough surfaces under gravity, that is to say gravity surfaces (Sysoev, 1949; Voitiuk and Pylypaka, 2002 and 2003).

A compound particle motion over an oscillating plan is represented in papers (Pylypaka and Klendii, 2013; Adamchuk et.al., 2014; Blehman and Dzhenalidze G.Ju., 1964). Particle motion over a rotary surface of a circular cylinder at various axel positions is considered. These works cover particle motion over a horizontal cylindrical blade of a centrifugal dispersive element with a vertical axis of rotation (Babka V.M. et.al., 2013; Pylypaka and Adamchuk 2012; Bulgakov et.al., 2010), over a spinning oblique cylinder (Grishhenko I.Ju et.al., 2010; Klendii M.B. and Klendii O.M., 2016) and over a spinning horizontal cylinder (Linnik and Pylypaka, 2009). The paper (Klendii M. and Pylypaka, 2015) considers relative particle motion over the inner rough surface of a rotary cone with a vertical axis of rotation.

MATERIAL AND METHODS

Parametric equations of a helicoid are of the following form:

$$\begin{aligned} X &= u \cos \beta \cos \alpha \\ Y &= u \cos \beta \sin \alpha \\ Z &= u \sin \beta + b\alpha \end{aligned} \tag{1}$$

where β – an angle of inclination of rectilinear generators of a helicoid to a horizontal plane – constant; u and α – independent variables of the surface, while u – the length of a rectilinear generator relative to the axis of a helicoid, α – angle of rotation of a surface point about a helicoid axis; b – helix parameter, in terms of which surface pitch B is determined: $B=2\pi b$.

Fig.1 represents the surface of a helicoid at $\beta=0$, which has been constructed using equation (1). It is called a right or screw conoid, which is referred to as a screw in technology. The surface is limited by a cylindrical shaft of radius r and its peripheral part - by a cylindrical casing of radius R (it is not shown in the Figure). If $\beta \neq 0$, it is a skew helicoid (Figure 1, c, d).

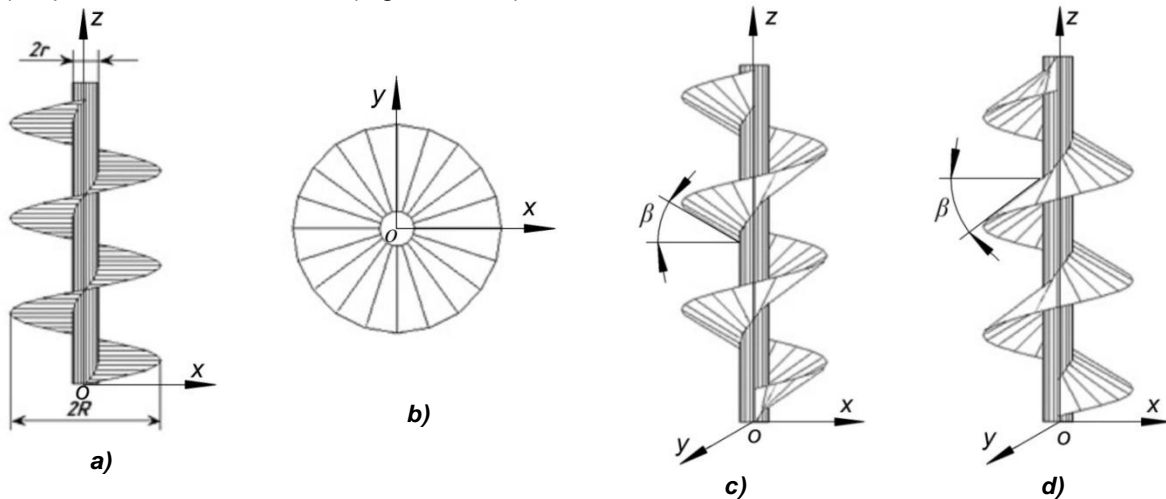


Fig. 1 - Right helicoid (the screw)

a) front view; b) side view; c) oblique helicoid with $\beta=30^\circ$; d) oblique helicoid with $\beta=-30^\circ$

Side views of the represented helicoids are the same (Fig. 1, b). When constructing the surface, variable u changes from r to R for a right helicoid and from $r/\cos\beta$ to $R/\cos\beta$ for a skew helicoid.

When determining the relation between variables u and α , a line on the surface of a helicoid is described. We assume that such a relation is determined by means of a parameter t – the time during which a particle slides on the surface of a helicoid. Then an intrinsic equation relative to the trajectory of particle motion can be described by the following dependences: $u=u(t), \alpha=\alpha(t)$. In order to determine the path (trajectory) of such particle motion and other kinematic characteristics, it is necessary to work out and solve differential equations.

The trajectory of relative particle motion is represented by equations (1) providing that $u=u(t), \alpha=\alpha(t)$. Using differentiation (1) with this provision, relative velocity V projections are obtained (since variables u and α are related to one another through a parameter t and equations (1) describe not a surface but a line on it, the derivatives are symbolized by lowercase letters):

$$\begin{aligned} x' &= \cos \beta (u' \cos \alpha - \alpha' u \sin \alpha) \\ y' &= \cos \beta (u' \sin \alpha + \alpha' u \cos \alpha) \\ z' &= u' \sin \beta + b\alpha' \end{aligned} \tag{2}$$

Its value is the geometrical sum of projections (2):

$$V = \sqrt{x'^2 + y'^2 + z'^2} = \sqrt{(u^2 \alpha'^2 + u'^2) \cos^2 \beta + (u' \sin \beta + b\alpha')^2} \tag{3}$$

When spinning at angular velocity ω , all the points of the conoid (1) turn through angle $\varphi = \omega t$.

Using turn formulas, parametric equations of a helicoid, which represent its position after the turn through angle φ are written:

$$\begin{aligned} X &= u \cos \beta \cos \alpha \cos \varphi - u \cos \beta \sin \alpha \sin \varphi \\ Y &= u \cos \beta \cos \alpha \sin \varphi + u \cos \beta \sin \alpha \cos \varphi \\ Z &= u \sin \beta + b\alpha \end{aligned} \tag{4}$$

After simplifications with regard to $\varphi=\omega t$, the equations (4) take the following form (due to the specified reasons, the equations (4) also represent a line, but it is the trajectory of absolute particle motion, that is why we pass on to lowercase letters):

$$\begin{aligned}x &= u \cos \beta \cos(\alpha + \omega t) \\y &= u \cos \beta \sin(\alpha + \omega t) \\z &= u \sin \beta + b\alpha\end{aligned}\quad (5)$$

The differential equation of particle motion over the surface of a helicoid is set up as $m\bar{w} = \bar{F}$, where m – mass of particle, \bar{w} - absolute acceleration vector, \bar{F} - resultant vector of the forces exerted upon a particle. These forces are: weight force of a particle mg ($g=9.81 \text{ m/s}^2$), surface reaction \bar{N} of a helicoid and friction force $F_f=fN$, which exhibits resistance to a particle sliding on its surface (f – friction coefficient). The given vector equation is broken down in projections on the coordinate axis, which results in obtaining a set of three differential equations.

Absolute acceleration is achieved by successive differentiation of the absolute path equation (5) with respect to time t . The first-order derivative of the equation (5), that is absolute acceleration vector of a particle, is given by:

$$\begin{aligned}x' &= \left[\begin{array}{l} u' \cos(\alpha + \omega t) - \\ -u(\alpha' + \omega) \sin(\alpha + \omega t) \end{array} \right] \cos \beta \\y' &= \left[\begin{array}{l} u' \sin(\alpha + \omega t) + \\ +u(\alpha' + \omega) \cos(\alpha + \omega t) \end{array} \right] \cos \beta \\z' &= u' \sin \beta + b\alpha'\end{aligned}\quad (6)$$

Differentiation (6) results in absolute acceleration vector projection on the coordinate axis:

$$\begin{aligned}x'' &= - \left[\begin{array}{l} (\alpha''u + 2u'(\alpha' + \omega)) \sin(\alpha + \omega t) + \\ +(-u'' + u(\alpha' + \omega)^2) \cos(\alpha + \omega t) \end{array} \right] \cos \beta \\y'' &= \left[\begin{array}{l} (\alpha''u + 2u'(\alpha' + \omega)) \cos(\alpha + \omega t) - \\ -(-u'' + u(\alpha' + \omega)^2) \sin(\alpha + \omega t) \end{array} \right] \cos \beta \\z'' &= u'' \sin \beta + b\alpha''\end{aligned}\quad (7)$$

The first exerted force is particle mass mg . Since a weight vector is down-directed, its projections on the coordinate axis are written as:

$$\{0; \quad 0; \quad -mg\} \quad (8)$$

The second exerted force is surface reaction \bar{N} of a helicoid directed normal to the surface. Normal direction N to the surface is determined from a vector product of two vectors, which pass through the point on the surface and line tangents to the coordinate curves of the surface. These two vectors are partial derivatives of the equations (1):

$$\begin{aligned}\frac{\partial X}{\partial \alpha} &= -u \cos \beta \sin \alpha; & \frac{\partial X}{\partial u} &= \cos \beta \cos \alpha \\ \frac{\partial Y}{\partial \alpha} &= u \cos \beta \cos \alpha; & \frac{\partial Y}{\partial u} &= \cos \beta \sin \alpha \\ \frac{\partial Z}{\partial \alpha} &= b; & \frac{\partial Z}{\partial u} &= \sin \beta\end{aligned}\quad (9)$$

After vector multiplication of the two vectors (9) and the reduction of the resulting vector to a unit one, its projections are written as:

$$\left\{ \begin{array}{l} \frac{b \sin \alpha - u \sin \beta \cos \alpha}{\sqrt{b^2 + u^2}} \\ \frac{b \cos \alpha + u \sin \beta \sin \alpha}{\sqrt{b^2 + u^2}} \\ \frac{u \cos \beta}{\sqrt{b^2 + u^2}} \end{array} \right\}. \quad (10)$$

A vector (10) is attached to the surface at the point of particle location. It has been determined without taking into account the turn of a helicoid, that is why the vector (10) must be turned through angle $\varphi=\omega t$, so as it corresponds to the point of the location of a particle on the surface. After its turn through angle $\varphi=\omega t$ the vector (10) takes the following form:

$$\left(\begin{array}{c} \frac{b \sin(\alpha + \omega t) - u \sin \beta \cos(\alpha + \omega t)}{\sqrt{b^2 + u^2}} \\ \frac{b \cos(\alpha + \omega t) + u \sin \beta \sin(\alpha + \omega t)}{\sqrt{b^2 + u^2}} \\ \frac{u \cos \beta}{\sqrt{b^2 + u^2}} \end{array} \right) \quad (11)$$

Finally, friction force $F_{fr}=fN$ points in the direction opposite to relative velocity V of particle motion, that is to say at a tangent to a relative path.

The projections of a unit vector, along which particle velocity is directed, are obtained by dividing velocity components (2) by its absolute value (3) with further turning through angle $\varphi=\omega t$:

$$\left(\begin{array}{c} \frac{\cos \beta (u' \cos(\alpha + \omega t) - \alpha' u \sin(\alpha + \omega t))}{\sqrt{(u^2 \alpha'^2 + u'^2) \cos^2 \beta + (u' \sin \beta + b \alpha')^2}} \\ \frac{\cos \beta (u' \sin(\alpha + \omega t) + \alpha' u \cos(\alpha + \omega t))}{\sqrt{(u^2 \alpha'^2 + u'^2) \cos^2 \beta + (u' \sin \beta + b \alpha')^2}} \\ \frac{u' \sin \beta + b \alpha'}{\sqrt{(u^2 \alpha'^2 + u'^2) \cos^2 \beta + (u' \sin \beta + b \alpha')^2}} \end{array} \right) \quad (12)$$

Differential equations can then be written relative to particle motion and taking into consideration exerted weight forces (8), surface reaction N and friction force $F_{fr}=fN$, which are vectored by unit vectors (11) and (12). The vector equation $m\bar{w} = \bar{F}$ is given by projections on the coordinate axis, taking into account that the projections of absolute acceleration vector \bar{w} are set out as (7):

$$\begin{aligned} m x'' &= N \frac{b \sin(\alpha + \omega t) - u \sin \beta \cos(\alpha + \omega t)}{\sqrt{b^2 + u^2}} - fN \frac{\cos \beta (u' \cos(\alpha + \omega t) - \alpha' u \sin(\alpha + \omega t))}{\sqrt{(u^2 \alpha'^2 + u'^2) \cos^2 \beta + (u' \sin \beta + b \alpha')^2}} \\ m y'' &= -N \frac{b \cos(\alpha + \omega t) + u \sin \beta \sin(\alpha + \omega t)}{\sqrt{b^2 + u^2}} - fN \frac{\cos \beta (u' \sin(\alpha + \omega t) + \alpha' u \cos(\alpha + \omega t))}{\sqrt{(u^2 \alpha'^2 + u'^2) \cos^2 \beta + (u' \sin \beta + b \alpha')^2}} \\ m z'' &= -mg + N \frac{u \cos \beta}{\sqrt{b^2 + u^2}} - fN \frac{u' \sin \beta + b \alpha'}{\sqrt{(u^2 \alpha'^2 + u'^2) \cos^2 \beta + (u' \sin \beta + b \alpha')^2}}. \end{aligned} \quad (13)$$

We substitute expressions of the second derivatives of absolute acceleration from (7) into (13) and solve the set (13) relative to the second derivatives of the unknown functions $u=u(t)$ and $\alpha=\alpha(t)$, as well as $N=N(t)$. After simplification we obtain:

$$\begin{aligned} \alpha'' &= -\frac{bg + 2uu'(\alpha' + \omega) + bu(\alpha' + \omega)^2 \sin \beta}{b^2 + u^2} - \frac{Af \alpha' \cos \beta}{\sqrt{(u^2 \alpha'^2 + u'^2) \cos^2 \beta + (u' \sin \beta + b \alpha')^2}} \\ u'' &= u \frac{(\alpha' + \omega)^2 (b^2 + u^2 \cos^2 \beta)}{b^2 + u^2} + \frac{2bu'(\alpha' + \omega) - gu}{b^2 + u^2} \sin \beta - \frac{Afu' \cos \beta}{\sqrt{(u^2 \alpha'^2 + u'^2) \cos^2 \beta + (u' \sin \beta + b \alpha')^2}} \end{aligned} \quad (14)$$

$$N = mA \cos \beta$$

Where $A = \frac{gu - 2bu'(\alpha' + \omega) + u^2(\alpha' + \omega)^2 \sin \beta}{\sqrt{b^2 + u^2}}$

Providing $b=0$ in the equations (1), they depict a cone surface. Accordingly, at $b=0$ the set of differential equations (14) coincide completely with a similar set, obtained in the paper (Klendii M. and Pylypaka, 2015).

RESULTS

The set (14) is solved by numerical methods. Depending on the direction of helicoid rotation, a particle in relative motion over its surface can go either upward or downward (as opposed to a cone, where the direction of rotation does not matter). In order to make a particle move upward, it is necessary to take on a positive value of a helical parameter b and a negative value of the angular velocity of rotation ω , or vice versa. The result of the set integration will be the same, where in one case it corresponds to a helicoid of a right-hand motion and in the second case - to a left-hand motion one. In order to make a particle move downward, it is necessary to reverse the sign of angular velocity. The equation of the relative path of particle sliding over the surface is found by substituting the dependencies $u=u(t), \alpha=\alpha(t)$, which are obtained as a result of numerical integration of the set (14), into the surface equations (1). An absolute path is routed with the help of the substitution of the same dependencies into the equations (5).

Paper (Klendii M. and Pylypaka, 2015) shows that the pattern of particle sliding over the inner surface of a cone is the same for various slope angles β of generators: a particle traces out a helical trajectory having constant upward conical motion. The same result is obtained when solving the set (14) at $b=0$ (Fig. 2). There is no motion stabilization: a particle either moves upwards or falls down at inefficient angular velocity of rotation ω .

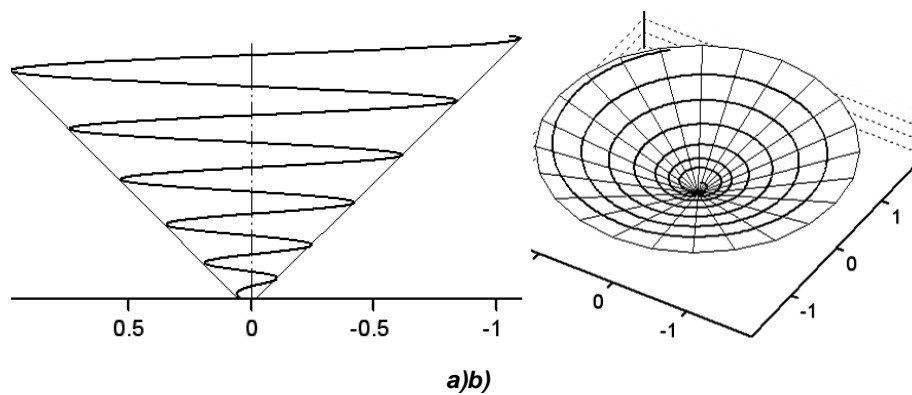


Fig. 2 - Trajectory of sliding of a corpuscle on an interior surface of a cone ($b=0, \omega=25\text{rad/s}, f=0.3$):
a) forming angle $\beta=45^\circ$; b) forming angle $\beta=20^\circ$

Let us consider relative particle motion over a helicoid without a restrictive casing. Fig.3–5 show relative paths of particle sliding over the surface of a helicoid (denoted by figure 1) and their absolute paths (denoted by figure 1) over a period of 1 second after a particle gets onto the surface near the shaft, which has been constructed in projections. For all the cases $b=0.03; r=0.025\text{ m}; f=0.3$ has been assumed.

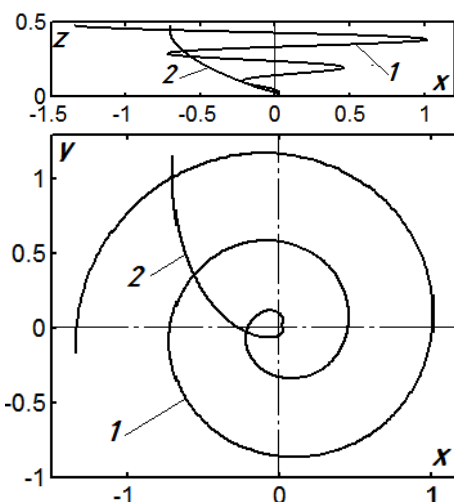


Fig. 3 - Trajectories of movement of a particle at $\beta=0; \omega=-20\text{ rad/s}$

Fig. 3 represents paths for a right helicoid (Fig.1, a), constructed when it rotates in such a way that a particle moves upward over the surface, and Fig.4 – when it counter-rotates and moves downward. It moves a longer way downward compared to moving upward and at that it moves much closer to the axis

of a helicoid. At the upward slope of generators (Fig.1,c) a particle moves a longer distance up than it does without a slope, at that it moves much closer to the axis of a helicoid.

Fig.3 shows, that if a particle moves upward when sliding on the surface of a right helicoid over a period of 1 second, it moves away from its axis for more than 1 m. Hence, if there is a restriction of the surface by a cylindrical casing, split seconds are needed so that a particle contacts it. Relative paths and the period of time, over which a particle reaches a cylindrical casing of radius $R=0.15\text{ m}$ at various angular velocities of rotation ω and slope angles β of generators have been investigated. Design parameters of a helicoid $b=0.03$; $r=0.025\text{ m}$; $R=0.15\text{ m}$ and friction coefficient $f=0.3$ are the same. In all the cases a particle gets onto the surface of a helicoid on a contact line with a shaft and has angular initial velocity, which is equal in value ω but opposite in sign. This condition is met at setting an initial value α' at numerical integration of the set (14).

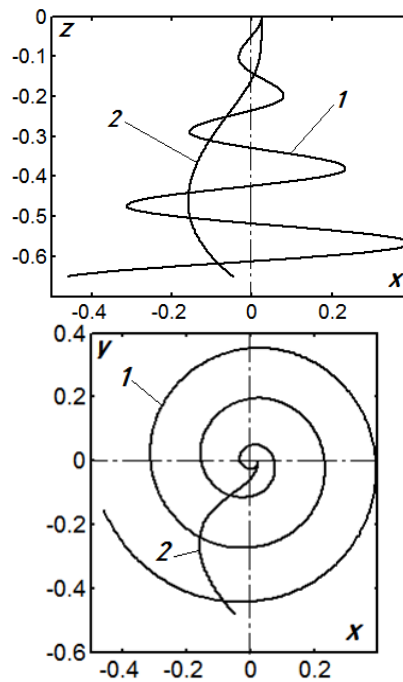


Fig. 4 - Trajectories of movement of a particle at $\beta=0^\circ$; $\omega=20\text{ rad/s}$

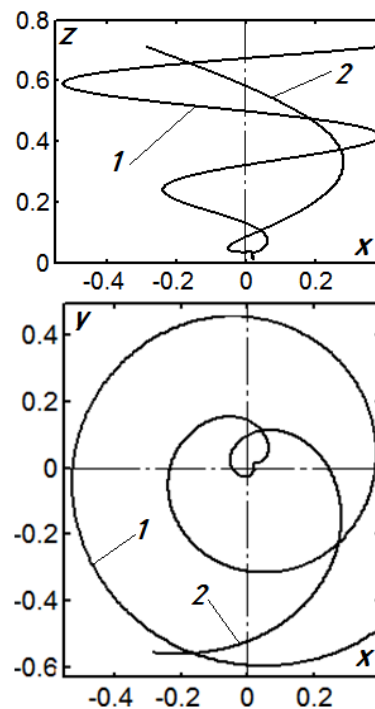


Fig. 5 - Trajectories of movement of a particle at $\beta=30^\circ$; $\omega=-20\text{ rad/s}$

Fig.6 represents relative paths of a right helicoid ($\beta=0$). For the specified angular velocities of rotation the period of time needed to reach the casing is 0.28 s, 0.25 s and 0.24 s (the time periods are ordered corresponding to the increasing velocity of rotation ω).

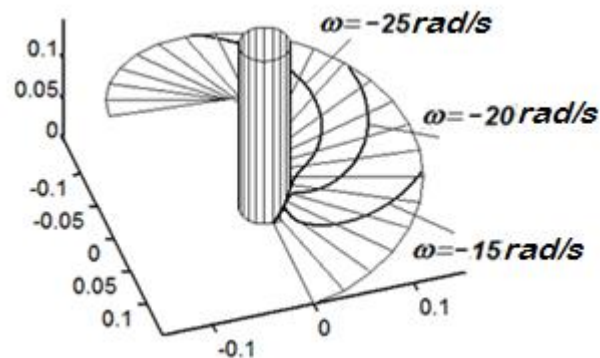


Fig. 6 - Trajectory of sliding of a particle at $\beta=0$ and different values of an angular velocity ω

Figs. 7, 8 show the paths of particle sliding on the surface of a skew helicoid, the rectilinear generators of which are sloped upward (Fig.7) and downward (Fig.8).

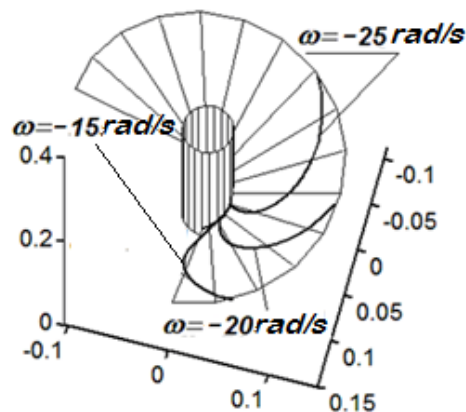


Fig. 7 -Trajectory of a particle sliding at $\beta=30^\circ$ and different values of an angular velocity ω

Corresponding to the increasing velocity of rotation ω , the time needed to reach the casing is 0.41 s, 0.325 s and 0.28 s for a skew helicoid (Fig. 7) and 0.22 s, 0.1 s and 0.2 s for a skew helicoid (Fig.8). Thus, a particle reaches a casing the fastest on the surface of a skew helicoid with the generators sloped downwards.

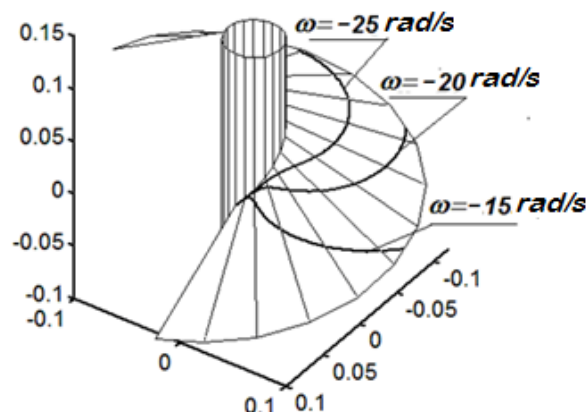


Fig. 8 - Trajectory of a particle sliding at $\beta=-30^\circ$ and different values of an angular velocity ω

Fig. 9 a) shows a change in height H , through which a particle rises when reaching a casing at $\omega=-20 \text{ rad/s}$ for the three surfaces presented: 1 – a right helicoid ($\beta=0$), 2 – a skew helicoid, the generators of which are sloped upward ($\beta=30^\circ$), 3 – a skew helicoid, the generators of which are sloped downward ($\beta=-30^\circ$), and Fig. 9 b) – graphs of behaviour for the rates of rise.

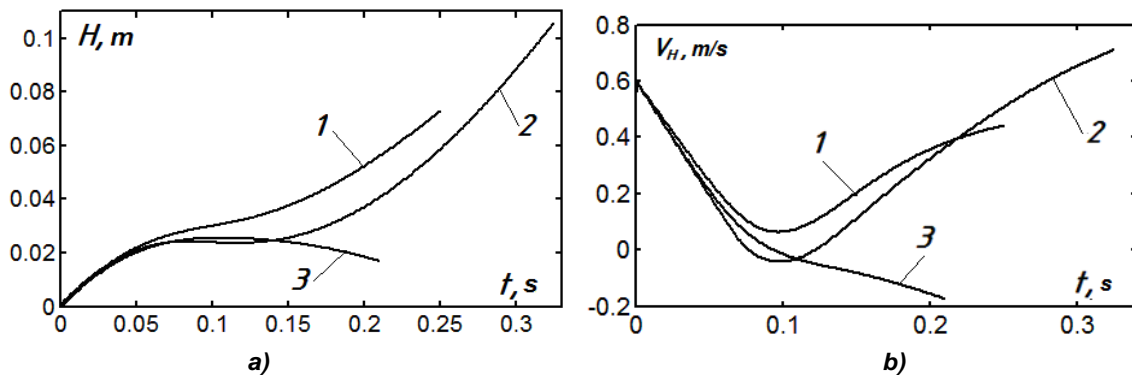


Fig. 9 - The graph of a modification of height (a) and velocities of lifting (b)

It appears to be interesting to consider in greater detail particle sliding on the surface of a skew helicoid, the generators of which are sloped upward. As it has been previously discussed, in a cone a particle can fall down at inefficient angular velocity of rotation ω . A particle behaves this way on a helicoid. When a helicoid with parameters $\beta=30^\circ$, $b=0.03$ and friction coefficient $f=0.3$ is rotating, a particle moves upward over its surface at angular velocity of rotation $\omega > 8 \text{ rad/s}$. At $\omega = 8 \text{ rad/s}$ particle starts sliding, but stops with time and begins to rotate together with a helicoid (Fig.10). When a helicoid is fixed ($\omega=0$), a particle begins to move downward and its motion is stabilized and it continues to move in a helix. Within the range of angular velocities $0 < \omega < 8 \text{ rad/s}$ particle moves downward and with time it enters the trajectory, along which it slides at $\omega=0$.

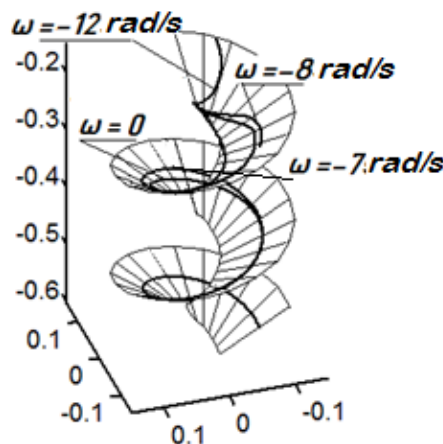


Fig. 10 - Trajectory of sliding of a particle at $\beta=30^\circ$ and different values of an angular velocity ω

Finally, let us investigate the influence of a helicoid pitch on particle sliding on the surface of a helicoid. Fig. 11 illustrates a side view of a right helicoid, where there are relative paths for various values of a helix parameter shown (a side view of the surface and of the paths are the same for various values b). A helicoid ($\beta=0$, $f=0.3$) rotates at constant angular velocity $\omega=-20 \text{ rad/s}$.

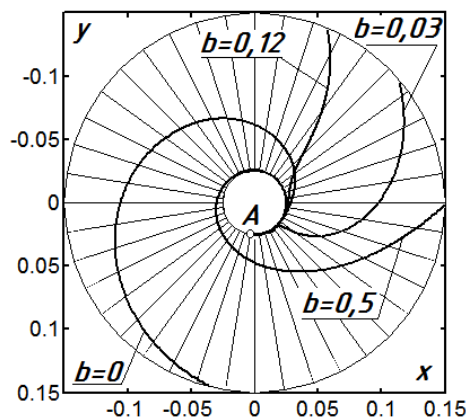


Fig. 11 - Trajectory of a particle sliding at different values of screw parameter b

In all the cases a particle gets onto the surface at point A. Visually, path projections are not much different from one another (that includes at $b=0$, when the surface of a helicoid transforms into a flat disc). Moreover, there is a minor difference in the time needed to reach a casing (0.44 s, 0.25 s, 0.29 s and 0.54 s corresponding to the increasing helix parameter b). However, the difference in the height H , through which a particle rises, is great. Fig.12 shows the graphs of a change in height corresponding to approaching a casing by a particle.

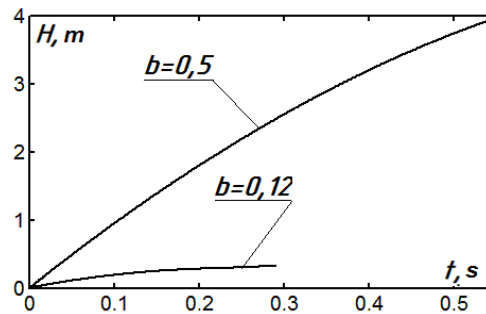


Fig. 12 - The graph of a particle lifting height modification for different values b

The graphs are constructed only for two greater values of helix parameter b , since for smaller values these heights are incommensurable and close to zero. Theoretically, it turns out that at helix parameter $b=0.5$ a particle can move upwards for about 4 m before it contacts a casing. Fig. 11 illustrates that it makes nearly a complete turn about a shaft and only then it begins to move to the periphery. In actual practice it may be not exactly the same, as it is, for example, in a known problem of rotating disc particle scattering. According to theoretical results, it is possible to attain any high rate of scattering by means of increasing angular velocity of disc rotation; however, experience has shown the advisability of certain limitations.

In order for a particle to move upwards, it is necessary to supply a proper angular velocity of rotation of a helicoid. For example, combination of $b=0.5$ and $\omega=-20$ rad/s results in particle rise for about 4 m and at $\omega=-10$ rad/s this rise is a bit more than 1 m, then it is followed by a particle downward motion (Fig.13). At $\omega=0$ a particle begins to move downward instantaneously.

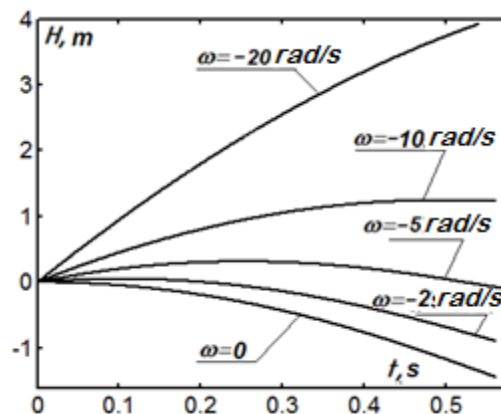


Fig. 13 - The graph of a particle lifting height modification for different values ω ($b=0.5$)

Thus, particle sliding on the surface of a helicoid till it contacts a casing takes split seconds; that is to say, the main time of upward material transportation is on its contact with the surface of a cylindrical restrictive casing. It restricts further slipping of the material to the periphery of the surface and makes particles move in a helix – an outer edge of the restricted module of a helicoid. Let us consider particle motion for this case.

Since particle motion takes place at $u = const$, then $u' = u'' = 0$. Taking that into account, projection expressions of absolute acceleration vector (7) are simplified. Besides, reaction force of a cylindrical casing \bar{N}_c appears, from which the force of particle friction on the surface of a casing $f_c N_c$ arises, where f_c – coefficient of particle friction over a casing. Reaction vector \bar{N}_c is directed inside the casing normal to its surface, that is why, its projections are written as follows:

$$\{-\cos \alpha; -\sin \alpha; 0\} \quad (15)$$

As in the previous case, it is turned through angle $\varphi = \omega t$, so that it corresponds to the point of the position of a particle on a helical line – an outer edge of a helicoid:

$$\{-\cos(\alpha + \omega t); -\sin(\alpha + \omega t); 0\} \quad (16)$$

The expression of a vector (11) of normal to a surface does not include the derivatives of $u=u(t)$, that is why, it remains unchanged. The forces of particle friction on a casing side and a helicoid surface are directed along the tangent to a relative path, the direction of which can be obtained if $u' = u'' = 0$ is substituted into (12):

$$\left\{ \begin{array}{l} \frac{u \cos \beta \sin(\alpha + \omega t)}{\sqrt{u^2 \cos^2 \beta + b^2}} \\ \frac{u \cos \beta \cos(\alpha + \omega t)}{\sqrt{u^2 \cos^2 \beta + b^2}} \\ \frac{b}{\sqrt{u^2 \cos^2 \beta + b^2}} \end{array} \right\} \quad (17)$$

Force of friction on the side of a casing $f_c N_c$ in our case is the force that makes a particle move upward on a helical line. If a casing is rotating together with a helicoid, a particle does not slide on its surfaces along a helical line at all. This case can be compared to the one, when a man has a ride on a merry-go-round and a centrifugal force presses his back against the wall, which is rotating together with him. If the back wall (a cylinder) was fixed, friction force on the man's back would try to get him moving. It is the same with a particle on a helical line of a little rise (less than that of a friction angle). That is why friction force $f_c N_c$ has a positive direction, which coincides with the direction of particle sliding. Taking this into account, it is possible to work out a set of differential equations of particle sliding:

$$\begin{aligned} mx'' &= N \frac{b \sin(\omega t + \alpha) - u \sin \beta \cos(\omega t + \alpha)}{\sqrt{b^2 + u^2}} + (fN - f_c N_c) \frac{u \cos \beta \sin(\alpha + \omega t)}{\sqrt{u^2 \cos^2 \beta + b^2}} - N_c \cos(\alpha + \omega t) \\ my'' &= -N \frac{b \cos(\alpha + \omega t) + u \sin \beta \sin(\alpha + \omega t)}{\sqrt{b^2 + u^2}} - (fN - f_c N_c) \frac{u \cos \beta \cos(\alpha + \omega t)}{\sqrt{u^2 \cos^2 \beta + b^2}} - N_c \sin(\alpha + \omega t) \\ mz'' &= -mg + N \frac{u \cos \beta}{\sqrt{b^2 + u^2}} - (fN - f_c N_c) \frac{b}{\sqrt{u^2 \cos^2 \beta + b^2}} \end{aligned} \quad (18)$$

Let us substitute the projections of absolute accelerations into (18), taking into account that $u' = u'' = 0$. After solving the set (18) for variables α'' , N , N_c , we obtain:

$$\begin{aligned} \alpha'' &= -\frac{bg}{b^2 + u^2 \cos^2 \beta} - \frac{gu \cos \beta (f \sqrt{b^2 + u^2} + u f_c \sin \beta)}{(b^2 + u^2 \cos^2 \beta)^{3/2}} + \frac{u f_c (\alpha' + \omega)^2 \cos \beta}{\sqrt{b^2 + u^2 \cos^2 \beta}} \\ N &= \frac{gmu \sqrt{b^2 + u^2} \cos \beta}{b^2 + u^2 \cos^2 \beta} \\ N_c &= mu \cos \beta \left[(\alpha' + \omega)^2 - \frac{gu \sin \beta}{b^2 + u^2 \cos^2 \beta} \right] \end{aligned} \quad (19)$$

When analysing expression α'' in (19), it is possible to conclude, that it includes all the constant values, except α' . It means, that provided $\alpha' = \text{const}$, $\alpha'' = 0$, that is to say we can equate this expression to zero and solve it for α' . It will be the value of constant angular velocity of particle sliding on a helical line (helicoid periphery) about its axis after the motion becomes steady. Because of the awkwardness this expression is not presented, and the necessary calculations will be made at $\beta = 0$, that is for a right screw conoid, known as a screw in technology. At that the expressions (19) are significantly simplified:

$$\begin{aligned} \alpha'' &= -\frac{g(b + fu)}{b^2 + u^2} + \frac{u f_c (\alpha' + \omega)^2}{\sqrt{b^2 + u^2}} \\ N &= \frac{mg u \sqrt{b^2 + u^2}}{b^2 + u^2} \\ N_c &= mu (\alpha' + \omega)^2 \end{aligned} \quad (20)$$

Having equated the expression (20) to zero and having solved it for α' , we obtain angular velocity of particle sliding on a rotating helical line – a screw periphery:

$$\alpha' = \omega_c = \sqrt{\frac{g(b+uf)}{uf_c \sqrt{b^2+u^2}}} - \omega \tag{21}$$

Formula (21) allows defining angular velocity of sliding ω_s at the set design parameters of a screw, angular velocity of its rotation ω and friction coefficients f and f_c . For example, at $b=-0.03$; $u=0.15$; $f=0.3$; $f_c=0.3$; $\omega=20$ rad/s angular velocity of particle sliding is $\omega_s=-15$ rad/s. Fig. 14 shows relative – 1 and absolute – 2 paths of particle motion at the specified parameters during one second. According to the last expression (6), the rate of particle rise (at $u=const$) is the following: $z' = b\alpha'$. In our case it is 0.45 m/s. During one second there is a particle rise of 0.45 m (Fig.14,a). It is obvious, that at small angular velocities of screw rotation a particle does not move upward, that is to say, angular velocity of particle sliding is zero. Having equated the expression (21) to zero, we obtain a critical value of angular velocity of screw rotation, at which a particle rise is possible:

$$\omega_{cr} > \sqrt{\frac{g(b+uf)}{uf_c \sqrt{b^2+u^2}}} \tag{22}$$

At the set parameters, critical angular velocity of screw rotation must be more than -5 s⁻¹, in absolute magnitude (the minus sign means that angular velocities of screw rotation and particle sliding are oppositely directed). Since we take a helix parameter b with a negative sign, it is possible that the expression in parentheses in (21) equals to zero. It corresponds to the case, when the angle of helix (screw periphery) is equal to the angle of particle friction on the surface of a screw. Then, according to (22) $\omega_s > 0$, that is to say, at minimum speed of screw rotation a particle moves upward and its angular velocity is maximum, in other words it equals to angular velocity of screw rotation as exemplified by (21). It means that in absolute motion a particle moves upward in a straight line (Fig. 14, b).

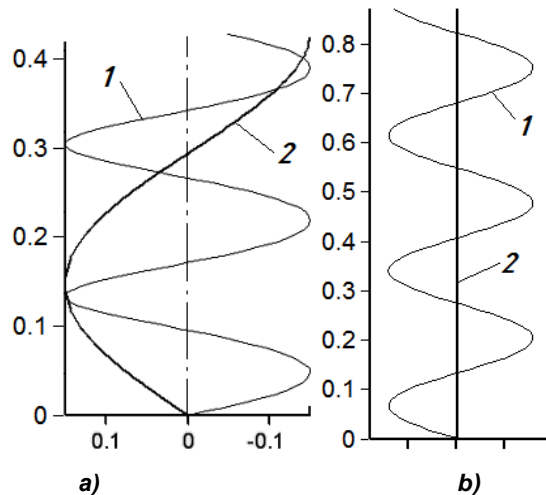


Fig. 14 - Relative -1 and absolute – 2 trajectories of movement of a particle at $u=0.15$ m; $f=0.3$; $f_c=0.3$; $\omega=20$ rad/s: a) $b=-0.03$; b) $b=-0.045$

The behaviour of a particle, when the angle of helix is equal to the angle of friction can be illustrated by the example of a fixed screw. If we assume, that the surface of a casing is absolutely smooth, that is $f_c=0$, a particle can either be at rest or move downward in a helix with constant speed, in other words, the forces exerted on it are balanced. At $f_c > 0$, a particle can be only at rest, because friction on the casing prevents its downward sliding, and in case of screw rotation, friction force, which arises, makes a particle slide in a helix and move upward. At that, balance of forces is set up as well, but taking into account the arisen force of friction on the casing, which is a driving force for a particle. If the angle of helix is higher than the angle of particle friction on the surface of a screw, then at $f_c=0$ and a fixed screw a particle slides in a helix and moves in downward direction with constant acceleration. At $f_c > 0$ the arising force of particle friction on the casing acts as a braking force, which remains the same in the case of screw rotation, that is to say at the rotating screw a particle slides in a helical line and moves downward.

Thus, the maximum rate of particle rise is in the case, when the angle of helix (screw periphery) is equal to the angle of particle friction on the surface of a screw. If the angle of helix is higher than the angle of friction, an inverse process begins – a particle slides downward in a helix. Hence, there is a restriction on the numerical value of a helix parameter b – in absolute magnitude it must be less than a numerical value uf : $b \leq uf$. For the given example, the maximum rate 0.9 m/s of particle rise is at $b = -0.045$ (Fig. 15,b). At $b = -0.03$ the rate of rise is twice less and equals 0.45 m/s (Fig. 15,a). The less if friction coefficient f , the less is the boundary value of a helix parameter b according to the expression $b \leq uf$. This means, that in the case of absolutely smooth surface of a screw, particle rise is impossible at any values of a helix parameter b . For the existing design of a screw (at $b = -0.03$ and $u = 0.15 \text{ m}$) the decrease in friction coefficient f from 0.3 to 0.2 results in the increase of the rate of rise from 0.45 m/s to 0.6 m/s at angular velocity of screw rotation $\omega = 20 \text{ rad/s}$. However, at further decrease in friction coefficient f particle rise is impossible, because the condition $b \leq uf$ is not met. Value $b = -0.03$ at $f = 0.2$ and $u = 0.15 \text{ m}$ becomes a boundary one for a particle rise in the version illustrated in Fig. 15,b. Thus, the maximum rate of rise is higher for a particle with a greater coefficient of friction on the surface of a helicoid (in our variant 0.9 m/s at $f = 0.3$ and 0.6 m/s at $f = 0.2$) and for a helix parameter b must have a boundary value $b = uf$.

Coefficient of particle friction on the casing f_c has insignificant influence on the rate of its rise. With the increase of value f_c the rate slightly increases and when there is a decrease – it reduces. There is a limit minimum value of friction coefficient f_c , at which a particle rise is possible. We obtain it by having equated (21) to zero and having solved it for f_c :

$$f_c > \frac{bg + fgu}{u\omega^2 \sqrt{b^2 + u^2}} \quad (23)$$

For $b = -0.03$; $u = 0.15 \text{ m}$; $f = 0.3$; $\omega = 20 \text{ rad/s}$ the value for the friction coefficient of a particle about the casing must be $f_c > 0.016$.

CONCLUSIONS

A rough surface of a rotary vertical axis helicoid can move a particle over its surface and as a result of sliding, it moves upward.

A slope angle of rectilinear generators of a helicoid influences a rate of rise in a certain way, but does not change the process regularity significantly.

If a pitch of a helicoid increases, the rate of rise increases as well at proper angular velocity of rotation of a helicoid. When rising, a particle moves a long distance away from the axis. If a restrictive cylindrical casing is used, the process of particle sliding on the surface is sort-term. Further particle rise is carried out by its sliding on a rotating helical line – helicoid periphery. At that, restrictions are placed on the angle of helix depending on the coefficient of particle friction on the surface of a helicoid and the radius of a restrictive cylindrical casing.

Coefficients of particle friction on the surface of a helicoid and that of a casing influence the rate of its rise in different ways. However, if at least one of them is equal to zero, a particle rise is impossible.

REFERENCES

- [1] Adamchuk V.V., Bulgakov V.M., Pylypaka S.F., Klendii M.B., (2014), Investigation of compound material particle motion over the inclined surface, which performs oscillating motion (Дослідження складного руху матеріальної точки по похилій площині, що здійснює коливальні рухи), *Herald of Zhytomyr National Agroecological University (Вісник Житомирського національного агроекологічного університету)*, No. 2(45), Vol. 4, Part.1, pp.54–63, Zhytomyr;
- [2] Babka V.M., Pylypaka S.F., Adamchuk O.V., (2013), Theoretical investigation of mass point motion over a cylindrical-shaped blade (Теоретичне дослідження руху матеріальної точки по лопатці циліндричної форми), *Oscillation in Process and Technology (Вібрації в техніці та технологіях)*, Vol.1 (69), pp.42–50, Vinnytsia;
- [3] Babka V.N., Pylypaka S.F., Zaharova T.N., (2013), Form of axis of a flexible resilient strip at its pushing on an inclined rough plane at constant speed (Форма оси гибкой несгибаемой полосы при её толкании по наклонной шероховатой плоскости с постоянной скоростью), *MOTROL. Motorization and Power Engineering of Plant Cultivation*, Vol.15, No.4, pp. 198–205, Lublin;
- [4] Blehman I.I., Dzhenalidze G.Ju. (1964), *Oscillatory displacement (Вибрационное перемещение)*, Nauka (Наука), 410 p., Moscow;

- [5] Bulgakov V., Pylypaka S., Pristupa V., (2010), Theory of particle motion in a centrifugal spinning apparatus (Теория движения частицы в центробежном высевающем аппарате), *MOTROL. Motorization and Power Engineering of Plant Cultivation*, Vol.12, pp.122–131, Lublin;
- [6] Grishhenko I.Ju, Pylypaka S.F., Pilipaka T.S., (2010), Investigation of particle motion over the inner surface of a spinning oblique cylinder (Исследование движения частицы по внутренней поверхности наклонного цилиндра, вращающегося вокруг собственной оси), *MOTROL, Motorization and Power Engineering of Plant Cultivation*, Vol.12., pp.115–121, Lublin;
- [7] Gyachev L.V., (1961), Theory of plow bottom surface (Теория лемешно – отвальной поверхности), *Azov, Chornomorsky Institut Agricultural Mechanization (Азово – чорноморський інститут механізації сільськогосподарського господарства)*, 317 p., Zernograd;
- [8] Klendii M.B., Klendii O.M., (2016), Interrelation between incidence angle and roll angle of concave disks of soil tillage implements, *INMATEH: Agricultural Engineering*, vol.49, no.2, pp.13-20, Bucharest;
- [9] Klendii M., Pylypaka S., (2015), Particle motion over the inner rough surface of a vertical axis rotary cone (Движение частицы по внутренней шероховатой поверхности ротационного конуса с вертикальной осью), *MOTROL. Motorization and Power Engineering of Plant Cultivation*, Vol.17, no.3, pp.73–83, Lublin;
- [10] Linnik M.K., Pylypaka S.F., (2009), Investigation of mass point motion over the inner surface of a horizontal cylinder (Дослідження руху матеріальної частинки по внутрішній поверхні горизонтального циліндра), *Herald of Agrarian Science (Вісник аграрної науки)*, Vol.2, pp.52–56, Kyiv;
- [11] Pylypaka S.F., Adamchuk O.V., (2012), Investigation of relative mass point motion over the surface of a horizontal cylinder, which rotates about a vertical axis (Дослідження відносного руху матеріальної частинки по поверхні горизонтального циліндра, який обертається навколо вертикальної осі форми), *Collection of Scientific Papers of Vinnytsia National Agrarian University. Series: Technical Sciences (Збірник наукових праць Вінницького національного аграрного університету. Серія: Технічні науки)*, Issue 11, Vol. II (66), pp.43–54, Vinnytsia;
- [12] Pylypaka S.F., Klendii M.B., (2013), Interaction between the inclined plane, all the points of which describe an ellipse at translation oscillation, and particles of material (Дослідження відносного руху матеріальної частинки по поверхні горизонтального циліндра, який обертається навколо вертикальної осі форми), *Mechanization and Electrification of Agriculture. Interdepartmental Collection of Subject Scientific Papers (Взаємодія похилої площини, всі точки якої при поступальному коливанні описують еліпси, із частинками матеріалу)*, Issue 98, Vol. 1, pp. 574–587, Glevaha;
- [13] Pylypaka S.F., Nesvidomyn A.V., (2010), Computer-designed modeling of particle motion over gravity surface by the example of an inclined plane in Maple system (Автоматизація моделювання руху частинки по гравітаційних поверхнях на прикладі похилої площини в системі Maple), *Applied Geometry and Engineering Graphics (Прикладна геометрія та інженерна графіка)*, Issue 86, pp.64–69, Kyiv;
- [14] Pylypaka S.F., Nesvidomyn A.V., (2011), Paths of particle motion over a rough inclined plane (Траєкторії руху частинок по шорсткій похилій площині при їх боковій подачі), *Applied Geometry and Engineering Graphics (Прикладна геометрія та інженерна графіка)*, Issue 87, pp.36–41;
- [15] Sysoev N.I., (1949), Theoretical basis and calculation for a sorting device “Zmeika” (Теоретические основы и расчет сортировки «Змейка»), *Agricultural Machinery (Сельхозмашина)*, Vol.8, pp.5–8, Kyiv;
- [16] Vasylenko P.M. (1960), Theory of particle motion over rough surfaces of agricultural machinery (Теория движения частицы по шероховатым поверхностям сельскохозйственных машин), *Publishing house of Ukrainian Academy of Agricultural Sciences (Издательство Украинской академии сельскохозйственных наук)*, p.283, Kyiv;
- [17] Veselovski M., Pylypaka S., Novak Ja., Voitiuk D., (2013), Form of axis of a slice when it is pushed over the plane of a sloping wedge at constant speed (Форма осі скиби при її штовханні по площині косоного клина зі сталою швидкістю), *Mechanization and Electrification of Agriculture. Interdepartmental. Collection of Subject Scientific Papers (Механізація та електрифікація сільськогосподарства. Міжвідомчий тематичний науковий збірник)*, Issue 98, Vol.1, pp.558–574, Glevaha;

- [18] Voitiuk D.G., Pylypaka S.F., (2002), Determination of a path of mass point motion over gravity ruled surfaces with a horizontal generatrix (Знаходження траєкторії руху матеріальної частинки по гравітаційних лінійчастих поверхнях із горизонтальними твірними), *Collection of Scientific Papers of National Agrarian University «Mechanization of Agricultural Production»* (Збірник наукових праць Національного аграрного університету «Механізація сільськогосподарського виробництва»), Vol.12, pp. 58–69, Kyiv;
- [19] Voitiuk D.G., Pylypaka S.F., (1999), Determination of a path of soil particle motion over cylindrical surfaces of the operating elements of soil tilling devices (До визначення траєкторії руху частинок ґрунту по циліндричних поверхнях робочих органів ґрунтообробних знарядь), *Collection of Scientific Papers of National Agrarian University «Mechanization of Agricultural Production»* (Збірник наукових праць Національного аграрного університету «Механізація сільськогосподарського виробництва»), Vol.5, pp.242–251, Kyiv;
- [20] Voitiuk D.G., Pylypaka S.F., (2003), Determination of a path of mass point motion over a gravity developed surface by the example of a developed helicoid (Знаходження траєкторії руху матеріальної точки по гравітаційній розгорнутій поверхні на прикладі розгортного гелікоїда), *Mechanization and Power Engineering in Agriculture. IV International Scientific and Technical Conference MOTROL. National Agrarian University* (Механізація і енергетика сільського господарства. IV міжнародна науково – технічна конференція MOTROL. Національний аграрний університет), Vol.6, pp. 113–126, Kyiv;
- [21] Voitiuk D.G., Pylypaka S.F., (2003), Peculiarities of mass point motion over gravity ruled surfaces (Особливості руху матеріальної частинки по гравітаційних лінійчастих поверхнях), *Herald of Kharkiv State Technological University of Agriculture. “Mechanization of Agricultural Production”* (Вісник Харківського державного технічного університету сільського господарства «Механізація сільського господарства»), Issue 21, pp.75–88, Kharkiv;
- [22] Zaika P.M., (1992), Selected tasks of agricultural mechanics (Избранные задачи земледельческой механики), *Publishing house of Ukrainian Academy of Agricultural Sciences* (Издательство Украинской академии сельскохозяйственных наук), p.507, Kyiv.

THEORETICAL ANALYSIS OF THE TECHNOLOGICAL FEED OF LIFTED ROOT CROPS

/

ТЕОРЕТИЧНИЙ АНАЛІЗ ТЕХНОЛОГІЧНОЇ ПОДАЧІ ВИКОПАНОГО ВОРОХУ КОРЕНЕПЛОДІВ

Dr. Prof. Baranovsky V.M.¹⁾, P.G. Potapenko M.V.²⁾

¹⁾ Ternopil Ivan Pul'uj National Technical University, Ternopil / Ukraine;

²⁾ Berezghany Agrotechnical Institute, Berezghany / Ukraine

E-mail: baranovskyvm@rambler.ru

Keywords: *vibrating lifter, root crop pile, root crops, impurities, feed per second, separation factor, loss factor.*

ABSTRACT

Based on the theoretical analysis of root crops lifting process, the simulation models are shown describing the relation of the feed per second of root crops coming to the cleaners, or the change of the cleaner required throughput capacity depending on the vibrating lifter design parameters, agro-biological characteristics of chicory root crops and working conditions of root-gathering machine.

РЕЗЮМЕ

На основі теоретичного аналізу процесу викопування коренеплодів наведено розрахункові математичні моделі, які характеризують взаємозв'язок секундної подачі вороху коренеплодів до очисників, або зміну необхідної пропускної здатності очисника залежно від конструктивних параметрів вібраційного копача, агробіологічних характеристик коренеплодів цикорію и умов роботи коренезбиральної машини.

INTRODUCTION

Separation of chicory root crops, which is dug by the working parts and subsequently enters the cleaning transport technology systems, is one of the most important and complex operations in the work of a root-gathering machine. The separation of soil, free and adhering to the surface of root crops, as well as plant impurities, is a priority in the general context of compliance with agronomic requirements for impurities purification process, namely with the quality of raw materials and final products of its processing (Voytyuk et al., 2015).

In addition to their separating abilities, root crops cleaners are also characterized by operational and technological criteria, including technological throughput capacity, or feed per second of root crops regulates the cleaning performance of root-gathering machine working parts, or the ability to handle root crops components without their *loading* on the working surfaces while minimizing overall damage and loss of root crops (Baranovsky V.M., 2008).

MATERIALS AND METHODS

To justify the rational constructive-kinematic parameters of the combined chicory root crops cleaner (Ramsh et al., 2011), respectively, to minimize its parameters under satisfactory technical indicators and performance parameters, the first priority is the theoretical study of the final cleaner's capacity based on analysis of the feed per second of dug crops to its working parts.

The purpose of this research is the further development of the theoretical aspects of root crop cleaners' parameters and operating modes optimization.

RESULTS

The criterion for the calculation of a root crop cleaner operation process is based on the condition that the throughput capacity of a cleaner working parts within a time interval $t = 1$ sec must be equal to or greater than the total feed per second of the crop feeding to them from the previous transport systems of a root-gathering machine, so the following condition should be provided:

$$dW_o / dt \geq dW_c / dt , \text{ or } W_o \geq W_c \tag{1}$$

Where:

W_o – throughput capacity (or performance) of a cleaner, [kg/s];

W_c – total feed per second of the crop, [kg/s].

To calculate the total feed per second of the crop W_{ck} , which is dug by the lifter of a root-gathering machine from n -th root rows and further theoretical substantiation of the crop cleaner parameters, consider the design scheme of digging root crops using vibrating lifter shown in fig. 1.

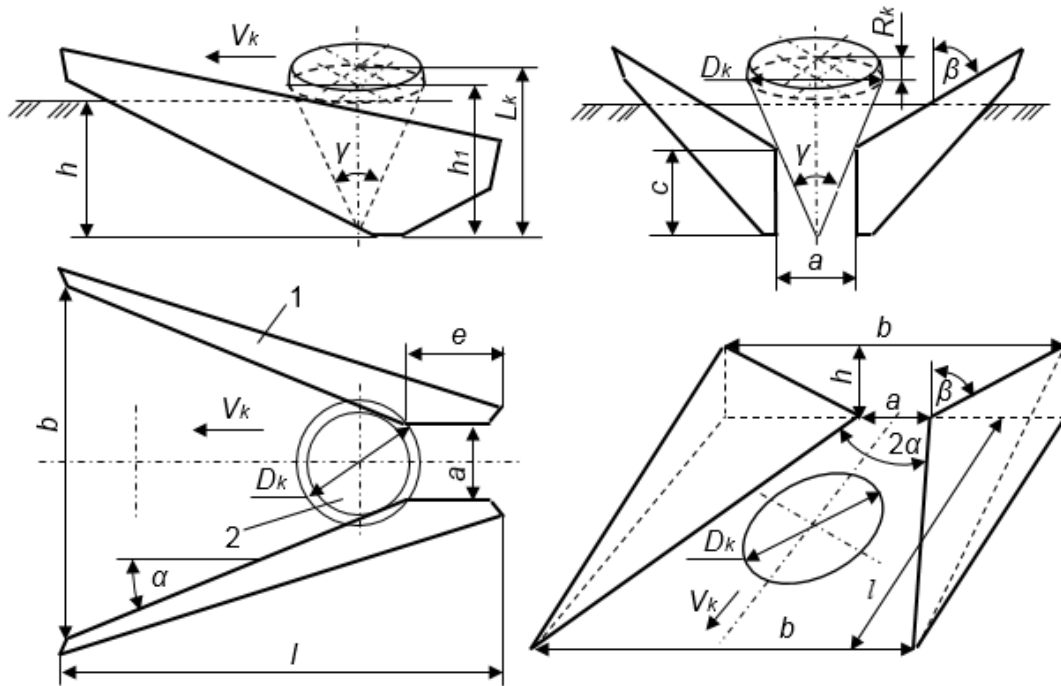


Fig. 1 - Scheme for calculating the crop feed using share-type lifter

1 - lifter; 2 – root crop

The total crop feed dW_c / dt , which will be supplied to the cleaner after lifter digging, except for the main operating factors (number of root crop rows being dug, lifter velocity, lifter running depth, level of root crop yield, agro-physical state of the soil, etc.) also depends on the separating capacity of the subsequent separating systems after the lifter, namely, on the value of free impurities separation factor.

Given (1) and assuming that there is no loss of root crops during the crops transfer by the transport systems to the cleaner, we can calculate (Baranovsky V., 2014):

$$dW_o / dt \geq (dW_{ck} / dt)\lambda , \text{ or } W_o \geq W_{ck}\lambda \tag{2}$$

where W_{ck} – the total feed per second of the root crops, [m/s];

λ – separation factor of free impurities on their path to the cleaner.

The feed of dug crops by vibrating lifter from one root crops row dW'_{ck} / dt is the feed sum of every j -th composite components of the crops: root crops dW'_1 / dt , soil dW'_2 / dt , plant impurities dW'_3 / dt , and:

$$\frac{dW'_{ck}}{dt} = \sum_{j=1}^3 \frac{dW'_{ckj}}{dt} = \frac{dW'_1}{dt} + \frac{dW'_2}{dt} + \frac{dW'_3}{dt} \tag{3}$$

where $\frac{dW'_{ck}}{dt}$ – feed of root crops from a single row, [kg/s];

$\frac{dW'_1}{dt}$, $\frac{dW'_2}{dt}$, $\frac{dW'_3}{dt}$ – feed of root crops, soil, plant impurities from a single row, respectively, [kg/s];

$j = 3$ – number of components of the crops: root crops, soil, plant impurities.

The total crop feed dW_c / dt from n -th root crops rows, which are dug simultaneously, equals the crop feed amount of each n -th row, or in accordance with (3) – the total feed amount of crop individual components of each n -the row: roots, soil and plant impurities:

$$\frac{dW_{ck}}{dt} = \left(\frac{dW_{11}}{dt} + \frac{dW_{12}}{dt} + \dots + \frac{dW_{1n}}{dt} \right) + \left(\frac{dW_{21}}{dt} + \frac{dW_{22}}{dt} + \dots + \frac{dW_{2n}}{dt} \right) + \left(\frac{dW_{31}}{dt} + \frac{dW_{32}}{dt} + \dots + \frac{dW_{3n}}{dt} \right) \quad (4)$$

where :

$\frac{dW_{11}}{dt}$, $\frac{dW_{21}}{dt}$, $\frac{dW_{n1}}{dt}$ – feed of root crops by the lifter from the first, second, ..., n -th row, respectively, [kg/s];

$\frac{dW_{21}}{dt}$, $\frac{dW_{22}}{dt}$, $\frac{dW_{2n}}{dt}$ – feed of groundwater impurities by the lifter from the first, second, ..., n -th row, respectively, [kg/s];

$\frac{dW_{31}}{dt}$, $\frac{dW_{32}}{dt}$, $\frac{dW_{3n}}{dt}$ – feed of plant impurities by the lifter from the first, second, ..., n -th row, respectively, [kg/s].

To calculate the feed of crop components by the lifter from a single row, that is, root crops, soil and plant impurities that are dug directly by the lifter working body, consider the process of lifting chicory root by the working body of ploughshare type lifter and further transportation of excavated crops by the transport systems of the machine to the combined root crops cleaner.

Based on the postulate that the feed of any material is the mass of an object (body), which is dug in the time interval t [s], and the mass of a solid body in general is $m = V\rho$, where V – body volume [m^3]; ρ – specific weight [kg/m^3] (Byrd J., 2008), then and taking into account (4) we can write:

$$\begin{aligned} \frac{dm_{ck}}{dt} = & \left(\frac{dV_{11}}{dt} + \frac{dV_{21}}{dt} + \dots + \frac{dV_{n1}}{dt} \right) \rho_1 + \left(\frac{dV_{12}}{dt} + \frac{dV_{22}}{dt} + \dots + \frac{dV_{n2}}{dt} \right) \rho_2 + \\ & + \left(\frac{dV_{13}}{dt} + \frac{dV_{23}}{dt} \rho_2 + \dots + \frac{dV_{n3}}{dt} \right) \rho_3 \end{aligned} \quad (5)$$

where V_{11} , V_{21} , V_{n1} – volume of root crops, which are dug by the lifter from the first, second, ..., n -th row, respectively, [m^3];

V_{12} , V_{22} , V_{n2} – volume of soil, which is dug by the lifter from the first, second, ..., n -th row, respectively, [m^3];

V_{13} , V_{23} , V_{n3} – volume of plant impurities, which are dug by the lifter from the first, second, ..., n -th row, respectively, [m^3];

ρ_1 , ρ_2 , ρ_3 – specific mass of root crops, soil, plant impurities, respectively, [kg/m^3].

To determine the appropriate amount of roots, soil and plant impurities, consider the equivalent scheme, which is shown in fig. 2.

During the movement of the vibrating lifter 1 (fig. 1), with forward speed V_k , in the time Δt , it passes the way $S_k = V_k \Delta t$ [m] and cuts a groove in the soil at a depth of plowshares stroke h , which is limited by the spatial shape contour $ABCDD_1C_1B_1A_1$ (fig. 2). In this space of the groove formed by plowshares in the time Δt , there are crop components: roots, soil and plant impurities, the amount of which constitutes the general crop feed dW_{ck}/dt , or adequate mass dm_{ck}/dt of the dug root crop, which is dug by the lifter from n -th rows in the time Δt .

In addition to it, the lifting process of root crop and its subsequent transportation by the transport systems has the following technological features:

- in the process of the mass of lifting root crop dm_{ck}/dt , which is inside the groove $ABCDD_1C_1B_1A_1$, part of the soil dm_2/dt and plant impurities dm_3/dt is extensively dressed, and some of the root crops dm_1/dt is not lifted, or is lost in the course of its movement through the working bodies to the subsequent lifter transporting systems of the root-gathering machine (Iamkov O.V., 2006);

- then, in the process of transporting the lifted soil and plant impurities, primary separated by the lifter, to the cleaner, their secondary separation is also performed on the working surfaces of the respective root-gathering machine transport systems.

The impurities separated and moved to the cleaner, together with supplied root crops, will compose the total crop dW_c/dt , which comes to the combined cleaner.

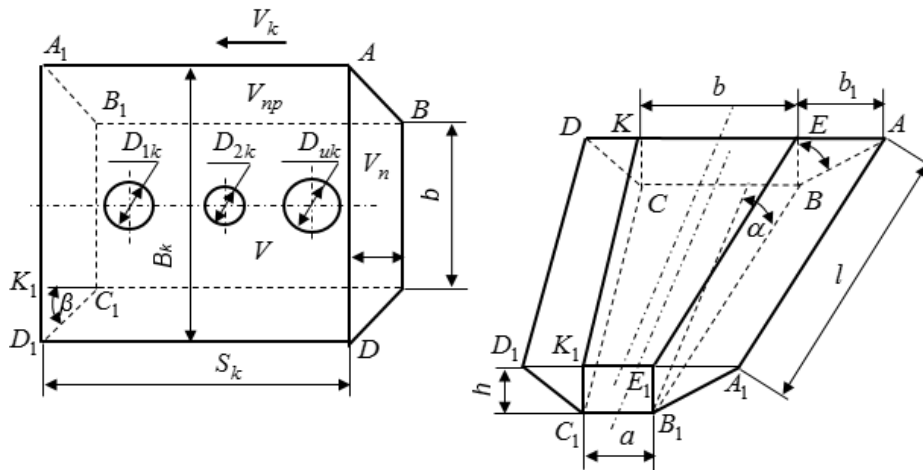


Fig. 2 – Scheme for calculating the groove volume

Then, to the specified pattern of the operation analysis of the lifter working bodies and root-gathering machine transport systems, we can write:

$$\begin{aligned} \frac{dW_c}{dt} = \frac{dm_c}{dt} = & \left(\frac{dV_{11}}{dt} k_{1k} + \frac{dV_{21}}{dt} k_{2k} + \dots + \frac{dV_{n1}}{dt} k_{nk} \right) \rho_1 + \\ & + \left(\frac{dV_{12}}{dt} \lambda_{1p} + \frac{dV_{22}}{dt} \lambda_{2p} + \dots + \frac{dV_{n2}}{dt} \lambda_{np} \right) \rho_2 \lambda_2 + \\ & + \left(\frac{dV_{13}}{dt} \lambda_{1p} + \frac{dV_{23}}{dt} \lambda_{2p} + \dots + \frac{dV_{n3}}{dt} \lambda_{np} \right) \rho_3 \lambda_3 \end{aligned} \quad (6)$$

where $k_{1k}, k_{2k}, \dots, k_{nk}$ – accordingly, the loss factor of root crops by vibrating share-type lifter from the first, second, ..., n -th rows;

$\lambda_{1p}, \lambda_{2p}, \dots, \lambda_{np}$ – respectively, soil separation factor by vibrating share-type lifter from the first, second, ..., n -th rows;

$\lambda_{1p}, \lambda_{2p}, \dots, \lambda_{np}$ – respectively, separation factor of free plant impurities by vibrating share-type lifter from the first, second, ..., n -th rows;

λ_2, λ_3 – respectively, separation factor of soil and free plant impurities of root crops after their lifting and moving by root-gathering machine transport systems on the way to the combined cleaner.

Thus, in a first approximation, we can write that the total root crops feed going to the working bodies of the combined cleaner is:

$$\frac{dW_c}{dt} = \frac{dm_c}{dt} = \sum_{i=1}^n \frac{dW_{1i}}{dt} k_k + \sum_{i=1}^n \frac{dW_{2i}}{dt} \lambda_p \lambda_2 + \sum_{i=1}^n \frac{dW_{3i}}{dt} \lambda_p \lambda_3 \quad (7)$$

where $k_k, \lambda_p, \lambda_2$ – accordingly, the total loss factor of root crops, soil separation and free plant impurities from n -th rows.

To use the characteristics of plantations and root crops as a stationary random sequence for the analysis of lifters operation processes, they are reduced to the argument, which is adopted in dynamic problems: the time and the speed by converting the correlation rate and the corresponding spectral density (Pogorely and Tatianko, 2004).

By the nature of auto- and inter correlation functions, it is found that the correlations of dimensional characteristics of adjacent root crops have a specific feature: close to a major root crop, there is often a small, and behind it - an average one (Bulgakov et al., 2009).

On this basis, the root crop feed from a single line dW'_1/dt will be the sum of every root crop feed dimensional of every j -th dimensional parameters, that are inside the groove $ABCDD_1C_1B_1A_1$, while the functional dependence of root crops from one line takes the following form:

$$\frac{dW'_1}{dt} = f_1 \left(\sum_{j=1}^u \frac{dW'_{1j}}{dt} \right) = f_1 \left(\sum_{k=1}^{N_1} \frac{dW'_{1k}}{dt} + \sum_{k=1}^{N_2} \frac{dW'_{2k}}{dt} + \dots + \sum_{k=1}^{N_u} \frac{dW'_{uk}}{dt} \right) \quad (8)$$

where $\sum_{k=1}^{N_1} \frac{dW'_{1k}}{dt}$, $\sum_{k=1}^{N_2} \frac{dW'_{2k}}{dt}$, ..., $\sum_{k=1}^{N_u} \frac{dW'_{uk}}{dt}$ – the total root crops feed of j -th dimensional parameter from a single line, respectively, [kg/s];

u – number of parametric root crops rows with the same dimension values, lifted from a single line;

N_1, N_2, \dots, N_u – number of identical root of j -th dimensional parameter lifted from a single line, respectively, [pcs.].

The total root crops feed $\sum_{i=1}^n dW_i' / dt$ consists of the sum of root crops feeds dW_i' / dt from every n -th row, and its functional relation is of the form:

$$\begin{aligned} \frac{dW_1}{dt} &= f_1 \left(\sum_{i=1}^n \sum_{j=1}^u \frac{dW'_{1j}}{dt} \right) = f_1 \left(\sum_{j=1}^u \frac{dW'_{1j}}{dt} + \sum_{j=1}^u \frac{dW'_{2j}}{dt} + \dots + \sum_{j=1}^u \frac{dW'_{nj}}{dt} \right) = \\ &= f_1' \left(\sum_{k=1}^{N_{11}} \frac{dW'_{1k}}{dt} + \sum_{k=1}^{N_{21}} \frac{dW'_{2k}}{dt} + \dots + \sum_{k=1}^{N_{u1}} \frac{dW'_{uk}}{dt} \right) + f_2' \left(\sum_{k=1}^{N_{12}} \frac{dW'_{1k}}{dt} + \sum_{k=1}^{N_{22}} \frac{dW'_{2k}}{dt} + \dots + \sum_{k=1}^{N_{u2}} \frac{dW'_{uk}}{dt} \right) + \dots + \\ &+ f_n' \left(\sum_{k=1}^{N_{1n}} \frac{dW'_{1k}}{dt} + \sum_{k=1}^{N_{2n}} \frac{dW'_{2k}}{dt} + \dots + \sum_{k=1}^{N_{un}} \frac{dW'_{uk}}{dt} \right) = \frac{dm_1}{dt} \end{aligned} \quad (9)$$

where $N_{11}, N_{21}, \dots, N_{u1}; N_{12}, N_{22}, \dots, N_{u2}; \dots; N_{1n}, N_{2n}, \dots, N_{un}$ – number of root crops with the same j -th dimensional parameters of each n -th row, [pcs.].

After transformation and simplification, let's write the relation (9) in the following form:

$$\frac{dW_1}{dt} = f_1' \left(\sum_{k=1}^{N_{11}+N_{12}+\dots+N_{1n}} \frac{dW'_{1k}}{dt} + \sum_{k=1}^{N_{21}+N_{22}+\dots+N_{2n}} \frac{dW'_{2k}}{dt} + \dots + \sum_{k=1}^{N_{u1}+N_{u2}+\dots+N_{un}} \frac{dW'_{uk}}{dt} \right). \quad (10)$$

The volume of root crop V_k (fig. 1) equals the sum of the volumes of a root crop head and body:

$$V_1 = \frac{1}{12} \pi D_k^2 h_1 + \frac{1}{12} \pi D_k^3 = \frac{1}{12} \pi D_k^2 (L_k - 0,5D_k) \quad (11)$$

where $h_1 = L_k - 0,5D_k$ – length of the root crop body, [m];

L_k, D_k – total length and diameter of the root crop head, respectively, [m].

Assume that:

$$\begin{aligned} N_{11} &= N'_{11} \frac{dS_k}{dt}; N_{21} = N'_{21} \frac{dS_k}{dt}; N_{u1} = N'_{u1} \frac{dS_k}{dt}; N_{12} = N'_{12} \frac{dS_k}{dt}; N_{22} = N'_{22} \frac{dS_k}{dt}; N_{u2} = N'_{u2} \frac{dS_k}{dt}; \\ N_{1n} &= N'_{1n} \frac{dS_k}{dt}; N_{2n} = N'_{2n} \frac{dS_k}{dt}; N_{un} = N'_{un} \frac{dS_k}{dt} \end{aligned} \quad (12)$$

where $N'_{11}, N'_{21}, \dots, N'_{u1}; N'_{12}, N'_{22}, \dots, N'_{u2}; \dots; N'_{1n}, N'_{2n}, \dots, N'_{un}$ – number of root crops with the same j -th dimensional parameters on one running meter of each n -th row, [pcs.];

dS_k / dt – number of linear meters run by the lifter in the time Δt , [r m/sec].

To simplify the problem, we take the basic assumption that the number of root crops of j -th dimensional parameter on one running meter in each n -th row is the same, that is $N'_{11} = N'_{21} = \dots = N'_{n1} = N_1$, $N'_{12} = N'_{22} = \dots = N'_{n2} = N_2$, $N'_{1u} = N'_{2u} = \dots = N'_{nu} = N_u$ we obtain the dependence for determining the total root crops feed dW_1 / dt , coming to the screws of the cleaner from n -th rows:

$$\frac{dW_1}{dt} = \frac{1}{12} \pi \rho_1 n k_k \frac{dS_k}{dt} \left[D_{1k}^2 N_1 (L_{1k} + 0,5D_{1k}) + D_{2k}^2 N_2 (L_{2k} + 0,5D_{2k}) + \dots + D_{uk}^2 N_u (L_{uk} + 0,5D_{uk}) \right] = \frac{dm_1}{dt} k_k. \quad (13)$$

The total soil feed dW_2 / dt , dug by the lifter, is the sum of the soil feeds dW_2' / dt from every n -th row.

With that said, the soil feed V_2' , inside the groove bounded by spatial figure $ABCDD_1C_1B_1A_1$ (fig. 2) immediately dug by the share-type lifter from a single row in the time Δt , equals the difference between the soil feed volume inside the groove dV / dt and the sum of underground parts volumes $d \sum_{j=1}^u V_{kj} / dt$ of j -th dimensional parameters of root crops 2 (fig. 1) from the n -th row, inside the groove $ABCDD_1C_1B_1A_1$, that is:

$$\frac{dW_2'}{dt} = \left(\frac{dV}{dt} - \frac{d \sum_{j=1}^u V'_{k_j}}{dt} \right) \rho_2 = \left(\frac{dV}{dt} - \frac{d \left(\sum_{k=1}^{N_1} V_{1k} + \sum_{k=1}^{N_2} V_{2k} + \dots + \sum_{k=1}^{N_u} V_{uk} \right)}{dt} \right) \rho_2 \quad (14)$$

where:

V – volume of the groove of spatial shape $ABCDD_1C_1B_1A_1$ of a single row, [m³];

$\sum_{j=1}^u V'_{k_j}$ – sum of underground parts volumes of root crops that are in the space of the groove $ABCDD_1C_1B_1A_1$ of a single row, [m³];

$V_{1k}, V_{2k}, \dots, V_{uk}$ – volume of one root crop underground part of j -th dimensional parameter, in a single row, respectively, [m³].

The sum of underground parts volumes of root crops from a single row in the area of the groove $ABCDD_1C_1B_1A_1$ equals:

$$\sum_{j=1}^u V'_{k_j} = \frac{1}{12} \pi \left[D_{1k}^2 N_1 (L_{1k} - 0,5D_{1k}) + D_{2k}^2 N_2 (L_{2k} - 0,5D_{2k}) + \dots + D_{uk}^2 N_u (L_{uk} - 0,5D_{uk}) \right] \quad (15)$$

where:

$\sum_{j=1}^u V'_{k_j}$ – sum of underground parts volumes of root crops from a single row in the area of the groove $ABCDD_1C_1B_1A_1$, [m³].

Given (14), (15), the total feed of the soil dug directly by the lifter from n -th rows of root crops is determined by the formula:

$$\frac{dW_2}{dt} = \left\{ \frac{dV}{dt} - \frac{1}{12} \pi \frac{dS_k}{dt} \left[D_{1k}^2 N_1 (L_{1k} - 0,5D_{1k}) + D_{2k}^2 N_2 (L_{2k} - 0,5D_{2k}) + \dots + D_{uk}^2 N_u (L_{uk} - 0,5D_{uk}) \right] \right\} n \rho_2. \quad (16)$$

The volume of the spatial figure groove bounded by $ABCDD_1C_1B_1A_1$, is the sum of the parallelepiped volume V_n and prism double volume V_{np} (fig. 2), and:

$$V = V_n + 2V_{np} = bhS_k + hb_1S_k = hS_k (b + b_1) = hS_k (b + htg\beta) \quad (17)$$

where:

h – average running depth of share-type lifter, [m];

b – front socks gap of plowshares at soil surface level, [m];

S_k – path run by the lifter Δt , [m];

β – tilting angle of plowshare lateral plane to a vertical plane parallel to the velocity attitude of the lifter movement, [degrees].

Given (14) (16) (17) and with the assumption that $\lambda_{1\rho} = \lambda_{2\rho} = \dots = \lambda_{n\rho} = \lambda_\rho$, we obtain the dependence for determining the total feed of soil dW_2/dt , coming on the screws of the cleaner from n -th rows:

$$\frac{dW_2}{dt} = \left\{ \frac{dS_k}{dt} h(b + htg\beta) - \frac{1}{12} \frac{dS_k}{dt} \pi \times \left[D_{1k}^2 N_1 (L_{1k} - 0,5D_{1k}) + D_{2k}^2 N_2 (L_{2k} - 0,5D_{2k}) + \dots + D_{uk}^2 N_u (L_{uk} - 0,5D_{uk}) \right] \right\} \rho_2 \lambda_\rho \lambda_2 n = \frac{dm_2}{dt} \lambda_\rho \lambda_2. \quad (18)$$

Similarly, the total feed of plant impurities dW_3/dt , dug by the lifter, is the sum of plant impurities feeds dW_3'/dt from every n -th row.

Plant impurities feed dW'_3/dt , dug by the lifter from a single root crop row, according to assumption, is made up of the feed of free tops lost by tops-gathering machine, residues of tops on the heads of root crops and feed of weeds that are inside the upper area of the figure A_1ADD_1 (fig. 2), formed by the groove $ABCDD_1C_1B_1A_1$, that is:

$$\frac{dW'_3}{dt} = \frac{dW'_{3v}}{dt} + \frac{dW'_{3b}}{dt} + \frac{dW'_{3z}}{dt} \quad (19)$$

where

$\frac{dW'_{3v}}{dt}$, $\frac{dW'_{3b}}{dt}$, $\frac{dW'_{3z}}{dt}$ – feed of lost tops, weeds and tops residues on the heads dug by the lifter from a single root crop row, [kg/s].

According to the agronomic requirements to tops-gathering machine, the loss of free tops, cut by the machine working bodies and tops residues on root crops heads must not exceed 10%, respectively 8% of its yield and weed weight - no more than 0,1 kg/m² (Bulgakov et al., 2009, Baranovsky and Potapenko, 2016).

Then, taking the maximum values of these parameters and using (19), the feed of plant impurities dW'_3/dt , directly dug by vibrating lifter from a single root crops row, is determined by the formula:

$$\frac{dW'_3}{dt} = 0,1U_g \frac{dF_k}{dt} + 0,08U_g \frac{dF_k}{dt} + 0,1 \frac{dF_k}{dt} = 0,1 \frac{dF_k}{dt} (U_g + 1) + 0,08U_g \frac{dF_k}{dt} \quad (20)$$

where:

U_g – tops yield, [kg/m²];

$F_k = S_k B_k = S_k (b + 2htg\beta)$ – area of top base of the figure AA_1D_1D of the groove $ABCDD_1C_1B_1A_1$, [m²];

B_k – coverage width of plowshares of vibrating lifter, [m].

Assuming $\lambda_{1p} = \lambda_{2p} = \dots = \lambda_{np} = \lambda_p$, we obtain the dependence for determining the total feed of plant impurities dW_3/dt , coming on the cleaner screws from n -th rows:

$$\frac{dW_3}{dt} = \left[0,1 \frac{dS_k}{dt} (b + 2htg\beta) \right] \left[(U_g + 1) \lambda_p \lambda_3 + 0,08U_g \right] n = \frac{dm_3}{dt} \lambda_p \lambda_3. \quad (21)$$

Thus, given (13), (18), (21), the dependence for determining the total feed dW_c/dt of dug root crops from n -th rows, coming on the cleaner screws has the following form:

$$\begin{aligned} \frac{dW_c}{dt} &= \frac{dm_1}{dt} k_k + \frac{dm_2}{dt} \lambda_p \lambda_2 + \frac{dm_3}{dt} \lambda_p \lambda_3 = \frac{dm_c}{dt} = \\ &= \frac{1}{12} \pi \rho_1 n k_k \frac{dS_k}{dt} \left[D_{1k}^2 N_1 (L_{1k} + 0,5D_{1k}) + D_{2k}^2 N_2 (L_{2k} + 0,5D_{k_2}) + \dots + D_{uk}^2 N_u (L_{uk} + 0,5D_{uk}) \right] + \\ &+ \rho_2 \lambda_p \lambda_2 n \left\{ \frac{dS_k}{dt} h(b + htg\beta) - \frac{1}{12} \pi \frac{dS_k}{dt} \times \right. \\ &\left. \left[D_{1k}^2 N_1 (L_{1k} - 0,5D_{1k}) + D_{2k}^2 N_2 (L_{2k} - 0,5D_{k_2}) + \dots + D_{uk}^2 N_u (L_{uk} - 0,5D_{uk}) \right] \right\} + \\ &+ n \left[0,1 \frac{dS_k}{dt} (b + 2htg\beta) \right] \left[(U_g + 1) \lambda_p \lambda_3 + 0,08U_g \right] \end{aligned} \quad (22)$$

After simplifying equation (22) and taking, in accordance with (2) $\lambda_2 = \lambda_3 = \lambda$ and denoting components $D_{1k}^2 N_1 (L_{1k} - 0,5D_{1k}) + D_{2k}^2 N_2 (L_{2k} - 0,5D_{k_2}) + \dots + D_{uk}^2 N_u (L_{uk} - 0,5D_{uk}) = \Theta_{V_{k_1}}$, $b + 2htg\beta = \Omega_{VF}$, $D_{1k}^2 N_1 (L_{1k} + 0,5D_{1k}) + D_{2k}^2 N_2 (L_{2k} + 0,5D_{k_2}) + \dots + D_{uk}^2 N_u (L_{uk} + 0,5D_{uk}) = \Theta_{V_k}$, we obtain the dependence characterizing the relation of change of root crops feed to the screws of combined cleaner or change of the cleaner required throughput capacity according to the vibrating lifter plowshares design parameters, agrophysical characteristics of root crops plantations and machine conditions:

$$W_c = n \lambda_\rho \lambda \rho_2 V_k \left\{ \frac{1}{12} \pi D_k^2 N \left(\frac{\rho_1 k_k (h + D_k)}{\lambda_\rho \lambda \rho_2} - 1 \right) + [a + 2(l \sin \alpha + htg\beta)] \times \right. \\ \left. \times \left[h \left(1 - \frac{htg\beta}{[a + 2(l \sin \alpha + htg\beta)]} \right) + 0,1 \left[(U_g + 1) \lambda_p + \frac{0,08 U_g}{\lambda} \right] \right] \right\} \quad (23)$$

Where:

- $dS_k / dt = P_k \cong V_k$, where P_k – number of running meters run by the lifter in the time of 1 s;
- V_k – forward speed of the lifter [m/s], but in this case, dimension V_k , can be written as [r m/s] because of matching the symmetric difference of sets (Husak and Brichkina, 2012);
- $N_1 + N_2 + \dots + N_u = N$, where N – average number of chicory root crops per 1 r m;
- $D_{1k} = D_{2k} = \dots = D_{uk} = D_k$, where D_k – average diameter of root crops head, [m];
- $L_{1k} + 0,5D_{1k} = L_{2k} + 0,5D_{2k} = \dots = L_{uk} + 0,5D_{uk} = L_{ck} + 0,5D_k = (h + 0,5D_{ck}) + 0,5D_k = h + D_k$, where L_k – average total length of sugar beet root crops, [m];
- $L_{1k} - 0,5D_{1k} = L_{2k} - 0,5D_{2k} = \dots = L_{uk} - 0,5D_{uk} = L_k - 0,5D_k = h$; $b = a + 2l \sin \alpha$, where a – rear plowshares gap, [m];
- l – coulter blade length, [m];
- α – half angle of plowshares noses, [degrees].

In addition, formulas (13), (18) and (21) will have the form:

$$W_1 = \frac{\pi}{12} n_k \rho_1 k_k V_k D_k^2 N (h + D_k); \quad (24)$$

$$W_2 = n_k \rho_2 \lambda_\rho \lambda V_k h \left[(a + 2l \sin \alpha + htg\beta) - \frac{1}{12} \pi D_k^2 N \right]; \quad (25)$$

$$\frac{dW_3}{dt} = \left[0,1 \frac{dS_k}{dt} [a + 2(l \sin \alpha + htg\beta)] [(U_g + 1) \lambda_p \lambda + 0,08 U_g] \right] n_k. \quad (26)$$

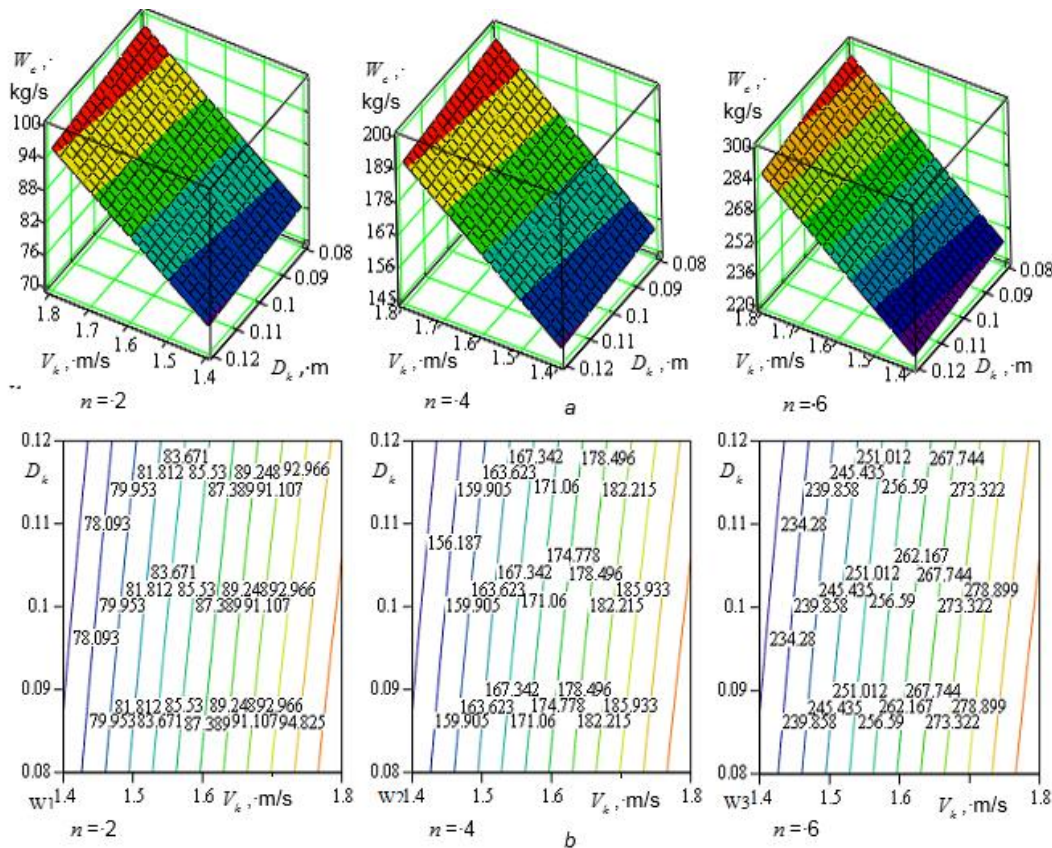


Fig. 3 – Dependence area between change of root crops feed per second W_c , lifter operating velocity V_k and root crops diameter D_k (a); 6 – dimensional section W_c

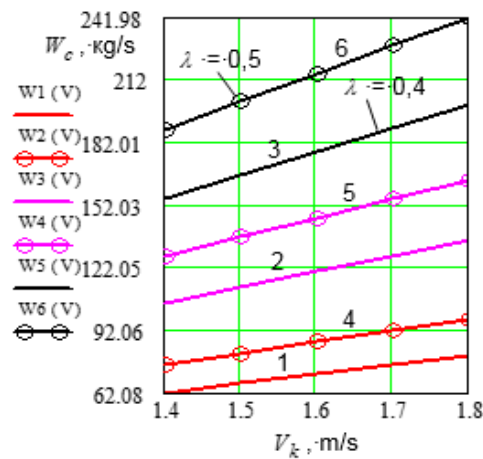


Fig. 4 – Dependence of change W_c and lifter operating velocity V_k

$$1, 2, 3 - n_k = 2, 4, 6; \lambda = 0,4; 4, 5, 6, - n_k = 2, 4, 6; \lambda = 0,5$$

At initial conditions, when $N = 6$ [pcs.]; $a = 0.07$ [m]; $l = 0.2$ [m]; $\alpha = 30$ [degrees]; $h = 0.09$ [m]; $\beta = 12$ [degrees]; $\lambda_\rho = 0.4$; $\lambda_p = 0.7$; $\lambda = 0.4$; $\rho_2 = 1500$ [kg/m³]; $U_g = 3.0$ [kg/m³]; $\rho_1 = 550$ [kg/m³]; $k_k = 0.015$ and according to formula (23), we constructed the dependence area between change of root crops feed per second W_c , coming to the combined cleaner screws and vibrating lifter operating velocity V_k and root crops average diameter D_k (fig. 3a) and its dimensional section (fig. 3b) for corresponding values for the number of rows n .

The analysis of the characteristic curve shows that changing the root crops feed per second W_c depending on the machine velocity V_k and the number of rows n , being collected at the same time, is directly proportional. With the increase V_k from 1,4 to 1.8 m/s the root crops feed per second W_c , coming to the cleaner screws when gathering 2 rows of root crops with average diameter $D_k = 0.12$ m increases from 76 to 96 kg/s, that is approximately 1.3 times (fig. 3). Accordingly, for the 4 and 6 rows - from 150 to 195 kg/s and 225 to 295 kg/s, that is also about 1.3 times, that is also characteristic to the analysis of straight proportional change of dependences W_c , which resulted in fig. 4, with the increase of rows number from 2 to 6, the root crops feed per second W_c coming to the cleaner screws increases by about 3 times.

Second serve lots W_c depending on the increase of diameter D_k of root crop from 0.08 to 0.12 (m) grows in insignificant limits – an average of 3.4 kg/s.

CONCLUSIONS

The obtained dependence is the simulation mathematical model which describes the relation between the changes of root crops feed per second W_c to the cleaner screws or change of the cleaner required throughput capacity W_o according to the design parameters of the vibrating lifter plowshares, agrophysical characteristics of root crops plantations and machine operating conditions.

This model is the optimization dependence in the context of further substantiation of constructive-kinematic parameters and operating modes of cleaning working bodies of root crops gathering machines.

REFERENCES

- [1] Baranovsky V.M., (2008), Results of theoretical and experimental studies of feed per second of root crops (Аналіз тенденцій розвитку робочих органів для сепарації вороху коренеплідів), *Mechanization of agricultural production (Механізація сільськогосподарського виробництва)*, Vol 1, Issue 75, pp. 111-120, Kharkiv/Ukraine;
- [2] Baranovsky V., (2014), Methodological and structural-technological aspects of development of adapted root crop machinery (Методологічні та конструктивно-технологічні аспекти розробки адаптованих коренезбиральних машин), *Science journal. Journal of TNTU (Науковий журнал. Вісник ТНТУ)*, Том 2 (74), pp. 106-113, Ternopil/Ukraine;

- [3] Baranovsky V.M., Potapenko M.V., (2016), Perfection of the cleansing systems the lots of root crops of chicory (Вдосконалення очисних систем вороху коренеплодів цикорію), *Scientific journal. Innovative solutions in modern science*, no 1(1), pp. 138-146, Dubai/OAE;
- [4] Byrd J., (2008). *Engineering Mathematics (Инженерная математика)*, Dodeka-XXI, Moskva/Russia;
- [5] Bulgakov V.M., Chernovol, M.I., Sviren N. A., (2009), *Theory beet-lifting machines : monograph (Теория свеклоуборочных машин)*, Kirovograd, ISBN 978-966-1508-01-08, Kirovograd/Ukraine;
- [6] Husak A.A., Brichkina E.A., (2012), *Bases of higher mathematics: manual for the students of institutes of higher (Основы высшей математики: пособие для студентов вузов)*, Minsk: TetraSistems (Минск: ТетраСистемс), Minsk/ Belorusiya;
- [7] Iamkov O.V., (2006), Defining the minimum energy consumption profile of working surface of plowshare of vibrating sugar beet lifter (Визначення профілю мінімальної енергоємності робочої поверхні лемеша коливного копача цукрових буряків), *APK Technics (Техніка АПК)*, no. 9-10, pp. 55-57, Kijv/Ukraine;
- [8] Pogorely L.V., Tatianko M.V., (2004), *Beetroot-lifting machine: history, design, theory, forecast (Свеклоуборочные машины: история, конструкция, теория, прогноз)*, K. : Phoenix (К. : Феникс), ISBN 966-651-166-5, Kijv/Ukraine;
- [9] Ramsh V.Y., Baranovsky V.M., Pankiv M.R, Gerasimchuk G.A., (2011), Analysis of trends of development of working bodies for root crops separation (Аналіз тенденцій розвитку робочих органів для сепарації вороху коренеплодів), *Scientific notes (Наукові нотатки)*, Vol. 31, pp 298-305, Lutsk/Ukraine;
- [10] Voytyuk D.G., Aniskevych L.V., Baranowsky V.M., et al., (2015), *Agricultural machines: textbook (Сільськогосподарські машини : підручник)*, Ahroosvita, ISBN 978-617-7283-06-4, Kijv/Ukraine.

MECHANICAL BEHAVIOR OF CORN STALK PITH: AN EXPERIMENTAL AND MODELING STUDY

玉米秸秆内瓢的力学特性试验与模拟研究

Lect.Ph.D. Stud. Lixian Zhang ¹⁾, Prof. Ph.D. Zhongping Yang ^{*1)}, Prof. Ph.D. Eng. Qiang Zhang ²⁾,
Prof. Xinhua Zhu ¹⁾, Lect.Ph.D.Haijun Hu ³⁾

¹⁾ Department of Mechanical and Electronic Engineering, Northwest A&F University, Shaanxi/China;

²⁾ Department of Biosystems Engineering, University of Manitoba, Manitoba /Canada;

³⁾ College of Water Resources and Architectural Engineering, Northwest A&F University, Shaanxi/China

Tel: +8613384943185; E-mail: zhanglixian031229@126.com

Keywords: corn stalk pith, mechanical properties, discrete element model (DEM), tensile strength

ABSTRACT

Corn stalk pith (CSP) is porous and highly elastic, which makes it an excellent renewable packaging material with good cushioning properties. This paper investigated some important mechanical properties of corn stalk pith. The effects of moisture content, internodal position and variety on corn stalk pith's tensile strength and the Young's modulus were experimentally determined. A discrete element model (DEM) was developed to simulate the tensile testing process. It was found that the mechanical properties of corn stalk pith were highly variable, with a tensile strength in the range of 0.2-1.35MPa, and Young's modulus 0.02-0.19GPa. The tensile strength of CSP increased with moisture content, while the Young's modulus showed the opposite tendency. From the DEM simulations of the load-displacement curve of CSP, the values of key mechanical properties in the DEM were determined: the normal stiffness coefficient $k_n = (0.5-3) \times 10^6$ N/m; the tangent stiffness coefficient $k_s = 1.0 \times 10^6$ N/m; the normal bonding coefficient $n\text{-bond} = (5-50)$ N/m³; and the tangential bonding coefficient $s\text{-bond} = (10-50)$ N/m³. These values provided important and necessary data for further analysing the mechanical properties of packaging materials made of CSP.

摘要

玉米秸秆内瓢细胞疏松多孔、弹性大，是缓压减震包装材料的一种主要原材料，其力学特性对包装材料的强度等性能指标具有重要影响。本文对玉米秸秆内瓢的拉伸特性进行深入探究；测试了含水率、节间位置及品种对玉米秸秆内瓢抗拉强度和弹性模量的影响；建立离散元模型模拟了拉伸过程中的力学行为。研究表明：随含水率增加秸秆内瓢的抗拉强度增大，而弹性模量减小；秸秆内瓢抗拉强度为 0.2-1.35MPa，弹性模量为 0.02-0.19GPa。在设定的含水率下，模拟得到了玉米秸秆内瓢拉伸变形图和载荷位移曲线，获得了离散元模型的主要力学特性参数：法向刚度系数 $K_n = (0.5-3) \times 10^6$ N/m，切向刚度系数 $K_s = 1.0 \times 10^6$ N/m，法向粘合系数 $n\text{-bond} = (5-50)$ N/m³，切向粘合系数 $s\text{-bond} = (10-50)$ N/m³。上述研究结果为分析和确定基于秸秆内瓢的包装材料性能指标提供理论参考。

INTRODUCTION

Corn stalk is an important renewable resource. A lot of research and exploration of the potential usage of corn stalk have been conducted (Husseien M. et al., 2009; Igathinathane C. et al., 2010; Li Zhiyong et al., 2012). Corn stalk has complex mechanical properties, due to its inhomogeneous compositions and structures. For example, corn stalk rind has high lignin content and strength, which makes it a good raw material for making paper and biocomposites (Speck Thomas et al., 2011). In contrast, corn stalk pith (CSP) is porous and highly deformable, and thus uniquely suited as a good cushioning packaging material (Rousserie F et al., 1997). To fully explore the potential of corn stalk pith as a "green" material for industrial usage, the knowledge of mechanical properties of CSP is critical, such as the strength and elasticity. These properties dictate the performance of final products derived from CSP, as well as equipment design for processing CSP. For example, damages of pith structure during processing may affect the packaging material's effectiveness. Limited information exists in the literature on the mechanical properties of CSP. The objectives of this study were to: (1) determine several critical mechanical property parameters, such as the tensile strength and Young's modulus, as affected by moisture content, intermodal position for different corn varieties; and (2) develop a discrete element model (DEM) to simulate mechanical behaviour of CSP.

Many studies of the mechanical properties of corn stalk have been conducted to explore the potential use of this renewable material. Reddy, et al. (Reddy Narendra et al., 2005) investigated the structure of corn stalk rind fibre using a tensile tester, X-ray diffraction and a scanning electron microscope. Their tensile test results showed that the tensile strength range was 1.5-4.5g per denier. Rodriguez, et al. (Panthapulakal Suhara et al., 2007; Rodriguez Manuel et al., 2010) derived the intrinsic tensile strength of the polypropylene composites that constitute the corn stalk; The tensile tests conducted in their study showed corn stalks strength to be 460-670 MPa. Von, et al. (Von Forell Greg et al., 2015) studied the influence of structure and moisture content on the mechanical properties of corn stalk and determined the ultimate strength and the Young's modulus. Their study was based on simulations of a finite element model (FEM), and the results revealed that the diameter of the corn stalk had a significant impact on the bending strength. The results also suggested a new strategy for breeding and developing maize varieties for producing bioenergy, specifically, counterbalancing tissue weaknesses by relatively small increases (e.g. 5%) in stalk diameter that reduced structural stresses. Hu, etc. (Hu H. et al., 2013; Peiffer Jason A et al., 2013; Zhong-Zhen Sun et al., 2013) conducted three and four points bending tests to measure the bending strength and Young's modulus of corn stalk and developed a viscoelastic model. They concluded that the viscoelasticity of corn stalks was closely related to the corn stalk variety, moisture content and intermodal position. Zhang, et al. (Zhang L. et al., 2016) measured the average values of Young's modulus and tensile strength of corn stalk rind to be 122.26 MPa and 19.31 GPa, respectively. Chen, et al. determined the tensile strength of corn stalk rind to be 67.2MPa (Chen Zhengguang et al., 2012). Huang, et al. (Liao Na. et al. 2011) measured corn stalk pith's viscoelastic coefficient in a transverse compression experiment and developed a FEM model to simulate the compression and stress relaxation processes.

Corn stalk pith is porous and voids in the structure frequently occur after the material is dried. Studies (Wang Donghai et al., 2002) have shown that the mechanical properties of corn stalk pith are highly related to its microstructure. This means that the models for porous materials, such as DEM, would be better suited for capturing the effect of microstructure of corn stalk pith. The DEM models have been utilized to model the mechanical behaviours of porous materials, such as soil, rock and concrete (Cundall Peter A, 1988; Hart R. et al., 1988; Qin Chuan et al., 2013). Based on an intensive literature review, we know that corn stalk pith may be approximated by bonding discrete spherical particles that represent the porous corn stalk pith. This paper focuses on the development of a discrete dynamic model for corn stalk pith using commercial DEM software and an experimental validation of the simulation results by means of a tensile testing experiment. The remainder of this paper is organized as follows. Section 3 describes the corn stalk pith tensile tests, presents the tensile test method and process. Section 4 focuses on the development of the DEM model. It explains discrete element contacting theory; introduces the setup of the model, including the creation of the geometry model and mechanical parameters; Section 5 presents the tensile test results, analyses the influence of related parameters on the results, and compares both the simulation and the experimental results. The final section summarizes our findings from the comparison of the simulation and experimental results.

MATERIAL AND METHODS

Tensile tests

The corn stalk samples were obtained from an experimental plot at the Northwest A&F University, Yangling, China. This plot was planted in June, 2013 and harvested in October, 2013. The plant height was approximately 180-220 cm. Each plant had at least nine internodes that were fully grown and was representative of all corn stalks in the same plot. The leaves were removed from the corn stalks and the rinds were peeled off. The dumb-bell shaped specimens were cut out of corn stalks manually. All tensile specimens had an overall dimension of 90 mm x 2 mm x 15 mm (length x thickness x width); the width at the narrow section in the middle was 5 mm, and there was a 50-mm test section between the grips (Fig. 1).

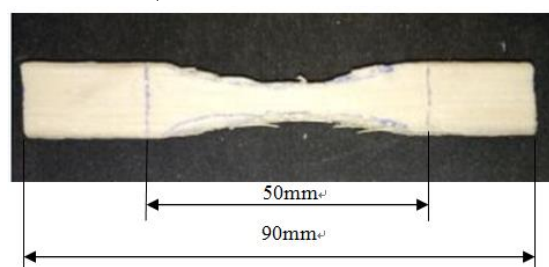


Fig. 1 - Corn stalk pith specimen for tensile test

The conditions of specimens, such as moisture content, would have significant impact on the mechanical properties of CSP. Three important sample conditions were considered in this study, as summarized in Table 1 (Nazari Galedar M. et al., 2008; Tavakoli H et al., 2009). The samples from two corn varieties, SD9 and SD12, were tested.

Table 1

Conditions of CSP test specimens

Factor	Level	Details
Moisture content	10%(dry)	Natural drying > 3 month
	70%(fresh)	Less than 3 hours after being cut
Internodes position	1—9	9 internodes from root to top

Tests were conducted using a biomechanical testing machine (Fig.2, Changchun Machinery Research Institute, Changchun, Liaoning China). The test machine had a capacity of 10 KN, with a force measurement accuracy of $\pm 0.5\%$, and movement accuracy of $\pm 0.02\%$. The specimen was installed on the test machine by using a pair of grips (Fig.2). A computer data acquisition system recorded the magnitude of the applied load to the specimen and elongation of the specimen.



Fig. 2 - Biomechanical testing machine

The tests were conducted following the ASTM Standards (Astm, 2014) (Tensile strength, Young's modulus, stress-strain measurement method for steel material). The moisture content was measured according to the ASABE standard (Asbe, 2006). A loading speed of 5 mm/min was used for all tests to minimize the loading rate effect (Wright Christopher T et al., 2005).

The stress-strain curve was plotted directly from the data post-processing software associated with the biomechanical tensile tester. From the stress-strain curve, the maximal stress (strength) σ_{max} in was identified and Young's modulus E was determined from the linear section of the stress-strain curve.

DEM analysis

Corn stalk pith consists of spongy parenchyma and vascular bundles (Thamae Timothy et al., 2008). The vascular bundles embedded into the parenchyma have a small percentage of volume and weight. The external load is carried mostly on the spongy parenchyma. Therefore, CSP could be considered as an isotropic porous material. A discrete spherical particle contacting mechanics model was used to simulate the CSP behaviour. The tissue was represented by spherical particles and the bio-bonding forces between tissues were represented through the contact, friction and damping forces between the particles (Fig.3). The advantages of using the DEM model were to simulate the "porous" nature of CSP and to handle large deformations that CSP might experience in various applications, such as packaging.

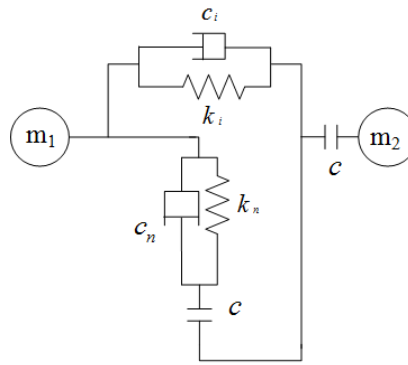


Fig. 3 - Sphere contact model for CSP

Note: k_n and k_s are normal and shear stiffness between two particles (N/m)

c_n and c_s are the normal and shear damping. C is the coupling relation

In the proposed model, inter-particle forces (torques) satisfied the following equilibrium equations (Itasca, 2008):

$$\vec{F} = F_n \vec{n}_n + F_s \vec{n}_s \quad [\text{N}] \quad (1)$$

$$\vec{M} = M_n \vec{n}_n + M_s \vec{n}_s \quad [\text{Nm}] \quad (2)$$

$$F_n = K_n A U_n \quad [\text{N}] \quad (3)$$

$$F_s = K_s A U_s \quad [\text{N}] \quad (4)$$

$$M_n = K_n J \theta_n \quad [\text{Nm}] \quad (5)$$

$$M_s = K_n J \theta_s \quad [\text{Nm}] \quad (6)$$

In which:

\vec{F} , \vec{M} are the inter-particles contacting force and moment;

\vec{n}_n , \vec{n}_s are the normal and tangent unit vectors;

F_n , F_s are the normal and tangent forces;

M_n , M_s are the normal and tangent moments;

K_n , K_s are particle normal and tangent stiffness;

U_n , U_s are the normal and tangent displacements, (m);

A is the constraint cross section area, (m²);

J is the contact surface polar moment of inertia, (m⁴);

I is the constraint cross section moment of inertia about axis through contacting point, (kg.m²);

θ_n , θ_s are the normal and tangent angular displacements, (rad).

The parameters in the DEM model could not be directly determined from experiments. Therefore, the DEM model was used to simulate the tensile tests and the simulated results were then compared with the experimental results to generate the best-fit DEM model parameters. The simulated CSP had the same geometry and dimensions of the test specimen (Fig. 4).



Fig. 4 - Tensile specimen model of CSP

In order to develop a DEM model that closely represented CSP, some critical physical parameters, such as density, had to match the measured value. The corn stalk pith density was determined to be 160-1100 kg/m³ based on the measured mass and volume. The porosity was calculated as:

$$n = \frac{V_p}{1 - V_p} \quad (7)$$

where n is porosity, and V_p is volume of void, m^3 . The simulated density was derived from:

$$\rho = \frac{\rho_1}{n + 1} \quad (8)$$

where ρ is simulated particle density, and ρ_1 is the measured pith density.

RESULTS

Experimental results

Figure 5 shows a typical failure pattern of CSP specimens in tensile test. The fracture surface was flat with little shrinkage in the cross-sectional area, which is of typical brittle failure.



Fig. 5 - The broken specimen

The measured load-deformation curves showed four distinct stages before the occurrence of failure: initial defatation; linear increase; yield, and fracture. During the initial defatation, elongation was significant at low stress level. This “flat” portion of the load-deformation curve might not reflect the behaviour of CSP; rather, it was due to slip between the specimen and the grips. In the second stage, elongation increased linearly with load. Yielding was identified by a small dip in load. Load continued to increase after yielding until the peak was reached. Finally, fracture occurred and the load began to decrease. The load decreased to zero when the sample was broken completely.

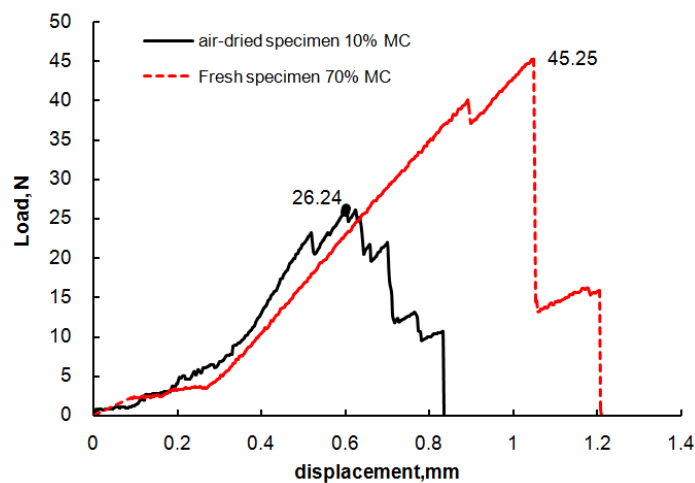


Fig. 6 - Load-displacement curve

The load-deformation curves were noticeably different for CSP specimens of different moisture contents (Fig.6). The fresh specimens at higher moisture content exhibited greater strength and elasticity than did the dried specimens (Fig.6). In the dried specimens, internal voids began to appear

due to shrinkage as the moisture content decreased. Thus, failure could have begun to initiate near the large voids and quickly propagate to the neighbouring areas. This explained why dried CSP specimens were weaker than the fresh specimens.

The tensile strengths of CSP calculated from the measured peak loads are summarized in Figure 7. Analysis of variance showed that dried corn stalk pith had a significantly lower tensile strength than the fresh CSP ($P \leq 0.05$). On the other hand, the internodal position and variety did not have any significant influence on tensile strength ($P > 0.05$). On average, fresh and dry specimens had an average tensile strength of 1.09 MPa and 0.86 MPa, respectively. The tensile strengths for the two varieties (SD9 and SD 12) of corn stalks were 1.00 MPa and 0.95 MPa, respectively.

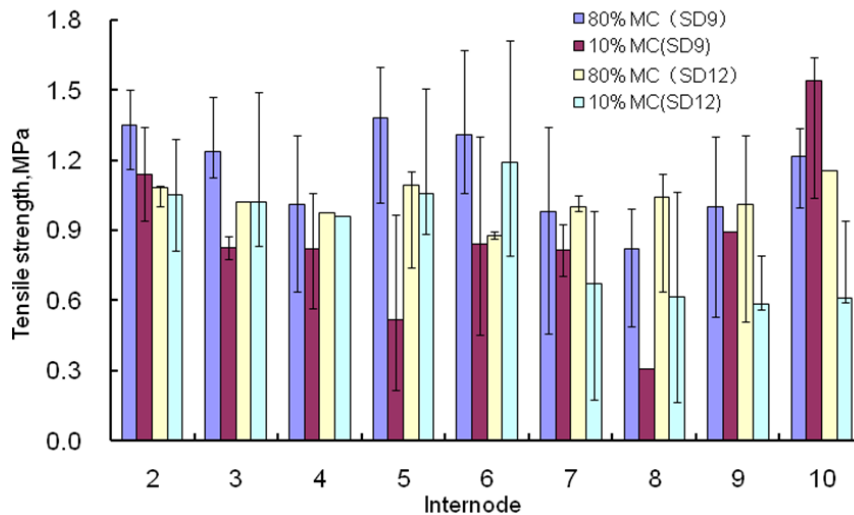


Fig. 7 - Variation of tensile strength of corn stalk pith for different varieties, moisture contents and internodes

Figure 8 summarizes the measured values of Young's modulus for different varieties, moisture contents and internodes. Dried corn stalk pith had a significantly higher Young's modulus (0.12 GPa) than did the fresh samples (0.06 GPa) ($P < 0.05$). The internodes position and corn variety did not have any significant influence on the Young's modulus ($P > 0.05$).

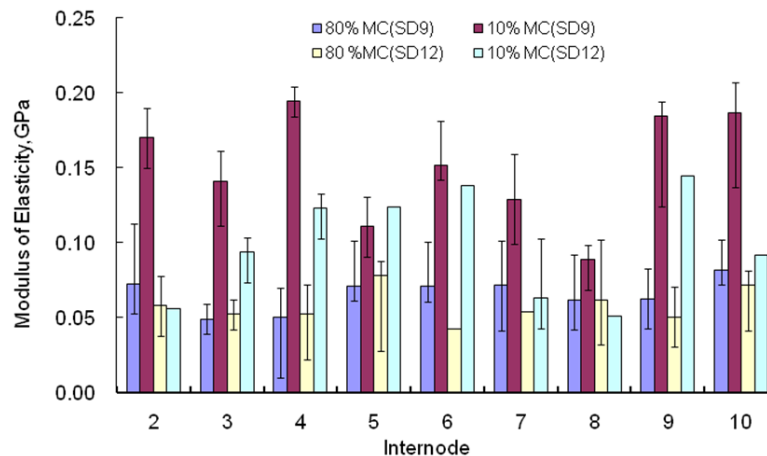


Fig. 8 - Variation of elastic of modulus of corn stalk core for different varieties, moisture contents and internodes

Simulation results

After running simulations for all the conditions of tensile test considered in the study, it was found that the particle density had little impact on the simulated mechanical behaviour of CSP in tensile tests. This was attributed to the fact that the gravitational force and applied tensile force were perpendicular to each other in the DEM simulations. The particle radius and porosity significantly impacted the failure pattern (the shape of fracture surface) and computational time. The simulated fracture surface agreed with experimental observations when the number of particles exceeded 5000. When the particle radius and porosity were small ($R < 0.43\text{mm}$, $n < 0.35$), the time of model run time was over 40 hours. The range

of particle radius and porosity were optimized based on trial runs of simulation to keep the run time below 24 hours (Table 2).

To determine DEM model mechanical property parameters, including inter-particle normal stiffness coefficient K_n , tangential stiffness coefficient K_s , normal bonding coefficient, tangential bonding coefficient and friction coefficient μ , simulations were conducted for a range of parameter values and the correlations between the these parameters and the simulated strength were developed in Equation (9):

$$\left. \begin{aligned} y_1 &= 18.247x_1^3 - 102.13x_1^2 + 171.26x_1 + 51.52 (R^2 = 1) \\ y_2 &= 181.59e^{-0.233x_2} (R^2 = 0.9202) \\ y_3 &= 2.9147x_3 - 3.2878 (R^2 = 0.9882) \\ y_4 &= -0.0051x_4^3 + 0.442x_4^2 - 10.77x_4 + 209.9 (R^2 = 1) \end{aligned} \right\} \quad (9)$$

Where:

- x_1 is the tangential stiffness coefficient;
- x_2 is the normal stiffness coefficient;
- x_3 is the normal bonding coefficient;
- x_4 is the tangent bonding coefficient;
- y_i is the ultimate strengths.

Simulation shows that normal bonding coefficient x_3 had a significant influence ($R > 0.05$) to strength, while the other factors had no impact ($R < 0.05$). The model's macro-mechanical behaviours (e.g., cross section shape, location and number of overflow particles) also would be change with the parameters value. The optimized range of x_1 , x_2 , x_3 and x_4 were determined by comparing the model's macro-mechanical behaviours and the experimental phenomenon:

$$\left. \begin{aligned} x_1, x_2 &\in (0.5E+06, 3E+06) \\ x_3 &\in (5, 50) \\ x_4 &\in (10, 50) \end{aligned} \right\} \quad (10)$$

The obtained numerical values of the best-fit DEM model parameters are summarized in Table 2. It was impossible to match the simulated results with the experimental data with a single set of DEM model parameters. Therefore, the ranges of parameters values were determined, and two simulation models were then created – Model 1 was based on the lower limits of parameter ranges, and Model 2 on the upper limits (Table 2).

Table 2

Numerical range of particles' mechanical parameters	
Parameter	value
Sphere particle density/kg·m ⁻³	753
Sphere particle radius/mm	0.43-0.5
Porosity/kg·m ⁻³	0.35-0.65
$k_n / N \cdot m^{-1}$	0.5E+06-1.5 E+06 (model 1) 2 E+06-3.0 E+06 (model 2)
$k_s / N \cdot m^{-1}$	1.0 E+06
n-bond/ $N \cdot m^{-3}$	5-30 (model 1) 35-50 (model 2)
s-bond/ $N \cdot m^{-3}$	10-20 (model 1) 40-50 (model 2)
Friction coefficient	1

The simulated responses of CSP (e.g. contacting force chain and fracture lines) are visualized in Fig.9. The left end was the fixed boundary and the right end was moved at a speed of 5 mm/min (the loading rate used in the tensile tests). It was visible that voids occurred as the loading progresses. The lines in the diagram represent the force chains. It is interesting to note that forces (stresses) were not transmitted uniformly in the simulated CSP. The maximum stress and fracture would occur in the area where force transmission lines were intensely populated.

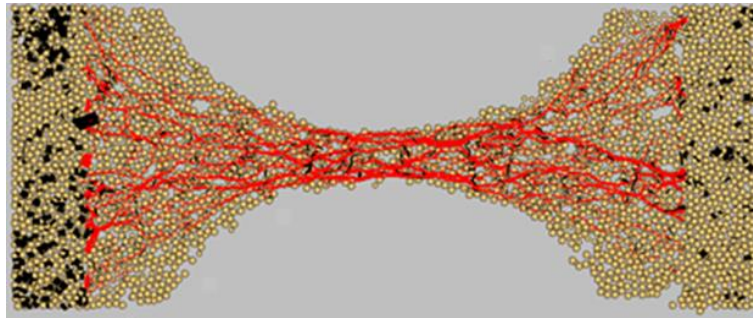


Fig. 9 - Simulated force transmission in a specimen of tensile test

As the load was increasing, the voids became larger, causing reductions in the actual cross-sectional area for carrying the load; the specimen was broken when the stress at a critical location exceeded the ultimate bonding strength between particles. The fractured cross section tended to be flat, as shown in Figure 10, which was similar to that observed in the experiments (Fig. 5).

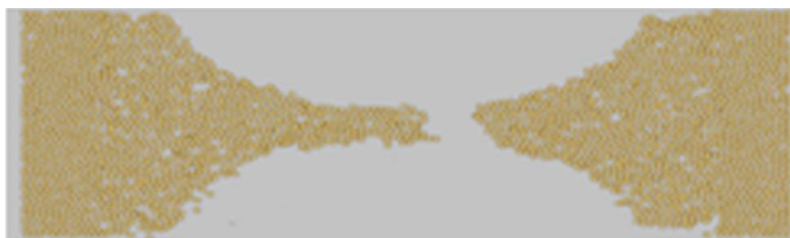


Fig. 10 - Simulated fracture surface of CSP specimen

Simulated load-displacement curves similar to the measured curves (Figs.11 and 6). However, the strength results differed – the simulated strength was found to be approximately 2.3-17.9 times the real strength. For example, an ultimate load 138.48 N was predicted by Model 1 (Fig.10), whereas a load of 45.25 N was measured for the fresh specimen (Fig.3). The parameters of the micro mechanical properties correspond to the macro parameters, which indicate that the micro mechanical properties matched well with the properties of corn stalk pith.

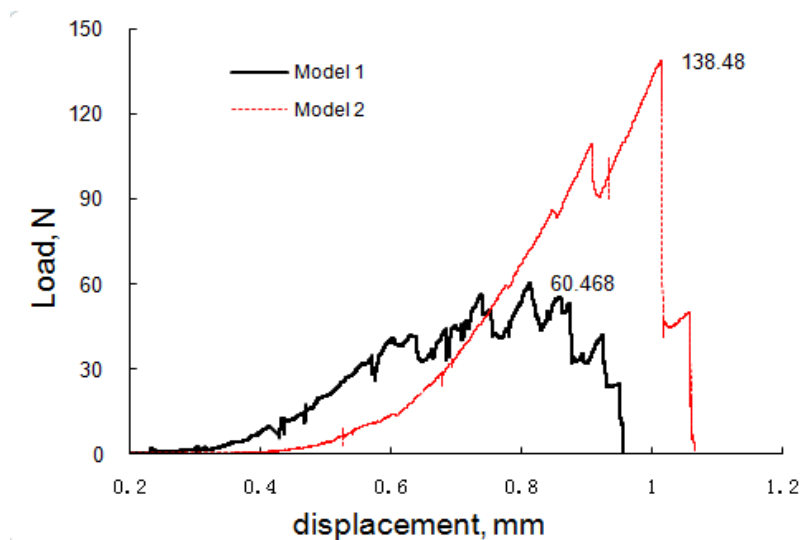


Fig. 11 - Load-displacement curves simulated with DEM model

Using smaller values of model parameters (Table 3), Model 1 resulted in lower strength and stiffness, which led to further local failure and dramatic stress changes, in comparison with Model 2, which used greater values of property parameters.

Table 3

The value of particles' mechanical parameters in model 1 and model 2

Parameter	model 1	model 2
Sphere particle density / $N \cdot m^3$	753	753
Sphere particle radius / mm	0.5	0.5
Porosity / $N \cdot m^3$	0.65	0.65
$k_n / N \cdot m^{-1}$	1.50E+06	2.00E+06
$k_s / N \cdot m^{-1}$	1.00E+06	1.00E+06
n-bond / $N \cdot m^{-3}$	10	50
s-bond / $N \cdot m^{-3}$	10	50

CONCLUSIONS

A tensile test and DEM simulation were conducted to investigate the tensile strength and Young's modulus for different varieties of corn stalk pith under various conditions. The influence of moisture content, internodal position and variety on corn stalk pith's tensile strength and Young's modulus was analysed. The main conclusions in this paper are:

(1) Load-displacement curves in tensile tests indicated that both fresh and dry corn stalk pith fractured as a brittle material.

(2) Fresh corn stalk pith had greater tensile strength, but lower Young's modulus than the dry corn stalk.

(3) The internodes position and corn variety had insignificant effect on either the tensile strength or Young's modulus of fresh and dry corn stalk pith.

(4) The optimized DEM model parameters for dry corn stalk pith were: $K_n = (0.5-1.5) \times 10^6$ N/m, $K_s = 1.0 \times 10^6$ N/m, n-bond=(5-30) N/m^3 and s-bond=(10-20) N/m. For fresh stalk they were: $K_n = (2.0-3.0) \times 10^6$ N/m, $K_s = 1.0 \times 10^6$ N/m, n-bond = (35-50) N/m^3 and s-bond = (40-50) N/m^3 .

(5) The shape of load-displacement curves simulated with the DEM was similar to the measured curves; The simulated ultimate strength was approximately 2.3-17.9 times that of the measured values.

The corn stalk pith material model developed by utilizing both tensile test results and DEM analysis was simplified and found to match the real material; therefore, in our opinion, this model is capable of providing valuable data for further investigation.

ACKNOWLEDGEMENT

This work was supported in part by The Public Welfare and Industry Special Fund Project of the Ministry of Agriculture of China: Crop straw substrate utilization (201503137).

REFERENCES

- [1] Asbe A., (2006), S358. 2: *Moisture Measurement-Forages*. ASAE Standards, USA;
- [2] Chen Z., (2012), Experiment on tensile and shearing characteristics of rind of corn stalk. *Transactions of the Chinese Society of Agricultural Engineering*, Beijing/China, Vol. 28, Issue 21, pp. 59-65;
- [3] Cundall P. A., (1988), Formulation of a three-dimensional distinct element model—Part I. A scheme to detect and represent contacts in a system composed of many polyhedral blocks. *Paper presented at the International Journal of Rock Mechanics and Mining Sciences & Geomechanics Abstracts*, Oxford/England, Vol. 25, Issue 3, pp.107-116;
- [4] Hart R., (1988), Formulation of a three-dimensional distinct element model—Part II. Mechanical calculations for motion and interaction of a system composed of many polyhedral blocks. *International Journal of Rock Mechanics & Mining Science & Geomechanics Abstracts*, Oxford/England, Vol. 25, Issue 3, pp.117-125;
- [5] Hu H., (2013), QTL mapping of stalk bending strength in a recombinant inbred line maize population. *Theor Appl Genet*, Beijing/China, Vol. 126, Issue 9, pp. 2257-2266;
- [6] Hussein M., (2009). A comprehensive characterization of corn stalk and study of carbonized corn stalk in dye and gas oil sorption. *Journal of Analytical and Applied Pyrolysis*, Amsterdam/Netherlands, Vol. 86, Issue 2, pp. 360-363;

- [7] Igathinathane C., (2010), Corn stalk orientation effect on mechanical cutting. *Biosystems Engineering*, San Diego/USA ,Vol. 107, Issue 2, pp. 97-106;
- [8] Itasca, (2008), *PFC3D particle flow code in 3 dimensions, theory and background*. Inc. Minneapolis.
- [9] Li Z., (2012). Cell morphology and chemical characteristics of corn stover fractions. *Industrial Crops and Products*, Amsterdam/Netherlands, Vol. 37, Issue 1, pp. 130-136;
- [10] Liao Na, (2011), Structure Modeling and Radial Compression Simulation of Corn Stalk Cores *Transactions of the Chinese Society for Agricultural Machinery*, Beijing/China, Vol. 42, Issue 6, pp. 117-121;
- [11] Nazari Galedar M. et al., (2008). *Effects of moisture content and level in the crop on the engineering properties of alfalfa stems*. *Biosystems Engineering*, San Diego/USA, Vol. 101, Issue 2, pp.199-208;
- [12] Panthapulakkal S., (2007), Agro-residue reinforced high-density polyethylene composites: Fibre characterization and analysis of composite properties. *Composites Part A: Applied Science and Manufacturing*, Oxford/England, Vol. 38, Issue 6, pp. 1445-1454;
- [13] Peiffer J. A., (2013), The genetic architecture of maize stalk strength. *PLoS One*, Cambridge/United Kingdom Vol. 8, Issue 6, pp.66-67.
- [14] Qin C., (2013), Impact splitting tensile experiments of concrete and numerical modeling by meso-scale discrete elements. *Journal of Hydroelectric Engineering*, Beijing/China, Vol. 32, Issue 1, pp.196-205;
- [15] Reddy N., (2005), Structure and properties of high quality natural cellulose fibres from cornstalks. *Polymer*, Oxford/England, Vol. 46, Issue 15, pp. 5494-5500;
- [16] Rodriguez M., (2010), Determination of corn stalk fibres' strength through modeling of the mechanical properties of its composites. *BioResources*, Raleigh/USA, vol. 5, Issue. 4, pp. 2535-2546;
- [17] Rousserie F., (1997), Characterization of corrugated board panels: an experimental study. *Journal of pulp and paper science*, Montreal/Canada, Vol. 23, Issue 7, pp. 330-334;
- [18] Speck T., (2011), Plant Stems: Functional Design and Mechanics. *Annual Review of Materials Research*, Palo Alto/USA, Vol. 41, Issue 1, pp.169-193;
- [19] Standard test methods and definitions for mechanical testing of steel products. (2014). Astm. http://xueshu.baidu.com/s?wd=paperuri%3A%28dad744dd4d6f60d54b4bd89236f0fd16%29&filter=sc_l_ong_sign&tn=SE_xueshusource_2kduw22v&sc_vurl=http%3A%2F%2Fcds.cern.ch%2Frecord%2F2031231&ie=utf-8&sc_us=16224858868936973418
- [20] Tavakoli H., (2009), Physical and mechanical properties of wheat straw as influenced by moisture content. *Int. Agrophysics*, Lublin/Poland, Vol. 23, Issue 2, pp.175-181;
- [21] Thamae T., (2008), Developing and characterizing new materials based on waste plastic and agro-fibre. *Journal of Materials Science*, New York/USA ,Vol. 43, Issue 12, pp. 4057-4068;
- [22] Von Forell G., (2015), Preventing lodging in bioenergy crops: a biomechanical analysis of maize stalks suggests a new approach. *Journal of experimental botany*, Oxford/England, Vol. 66, Issue 14, pp.4367;
- [23] Wang D., (2002), Low density particleboard from wheat straw and corn pith. *Industrial Crops & Products*, Amsterdam/Netherlands, Vol.15, Issue 1, pp. 43-50;
- [24] Wright C.T., (2005), Biomechanics of wheat/barley straw and corn stover. *Applied biochemistry and biotechnology*, Totowa/USA, Vol. 121, Issue 1-3, pp. 5-19;
- [25] Zhang L., (2016), Tensile Properties of Maize Stalk Rind. *BioResources*, Raleigh/USA, Vol. 11, Issue 3, pp. 6151-6161.
- [26] Zhong-Zhen S., (2013), The Viscoelasticity Model of Corn Straw under the Different Moisture Contents. *Mathematical Problems in Engineering*, Totowa/USA, Vol. 2013, Issue 6, pp. 14-26.

FEASIBILITY STUDY OF MIXTURE TRANSPORTATION AND STIRRING PROCESS IN CONTINUOUS-FLOW CONVEYORS

/

ТЕХНІКО-ЕКОНОМІЧНЕ ОБГРУНТУВАННЯ ПРОЦЕСУ ТРАНСПОРТУВАННЯ ТА ЗМІШУВАННЯ СУМІШЕЙ ТРУБЧАСТИМИ КОНВЕЄРАМИ

Prof. Ph.D. Eng. Hevko R.B.¹⁾, Prof. Ph.D. Eng. Yazlyuk B.O.¹⁾, Assoc. Prof. Ph.D. Eng. Liubin M.V.²⁾,
Assoc. Prof. Ph.D. Eng. Tokarchuk O.A.²⁾, Ph.D. Eng. Klendii O.M.³⁾, Eng. Pankiv V.R.⁴⁾

¹⁾Ternopil National Economical University / Ukraine; ²⁾ Vinnitsa National Agrarian University / Ukraine; ³⁾Separated Subdivision of National University of Life and Environmental Sciences of Ukraine Berezahany Agrotechnical Institute / Ukraine;

⁴⁾Ternopil Ivan Pul'uj National Technical University
E-mail: alex_ks@mail.ru

Keywords: *continuous-flow conveyor, loose material, beaded scrapers, load weight, pilot plant, mixture heterogeneity*

ABSTRACT

The article presents a research technique on the process of simultaneous transporting and stirring of mixture components by a continuous-flow conveyor. Kinematic motion parameters of loose materials in the main characteristic route segments have been substantiated. Experimental studies have been conducted in order to determine the drag force in set route segments and the stirring rate of mixture components. The obtained results provide a mean of choosing cost-effective operating modes of a conveyor-mixer, whereby the specified quality of mixtures is achieved.

РЕЗЮМЕ

В статті представлена методика дослідження процесу транспортування та одночасного змішування компонентів сумішей трубчастим скребковим конвеєром. Проведено обґрунтування кінематичних параметрів руху сипкого матеріалу на основних характерних ділянках траси. Виконані експериментальні дослідження для виявлення сил опору на встановлених ділянках траси та ступеня змішування компонентів сумішей. Отримані результати дають можливість обирати економічно доцільні робочі режими конвеєра-змішувача, за яких досягається задана якість сумішей.

INTRODUCTION

Continuous-flow conveyors are widely applied when transporting loose materials. Considering their power inputs and ecological safety (*Dziadykevych Y.V., 2016*), these conveyors are the most effective, since they transport materials in closed environments. They are widely applied for feeding, but there are certain difficulties providing simultaneous transporting and stirring of loose components, especially on a large scale. In addition, it is advantageous to make sectional traction elements and beaded operating elements with a central opening in order to provide spillage and stirring of feed mixture.

The analysis of recent researches (*Hryshova and Lebedev, 2015; Hevko M.R. and Vitrovyyi A.O., 2016; Hevko R.B. and Klendiy O.M., 2014; Hevko R.B. et.al., 2016; Loveikin et.al., 2010; Loveikin and Rogatynska, 2011; Lyashuk O.L. et.al., 2015; Pylypaka S.F. and Klendiy M.B., 2016; Rogatynska, 2010; Rogatynska O. et.al., 2015; Rohatynskiy et.al., 2016; Shynkaryk et.al., 2014*) shows that the main disadvantages of the existing traction elements and operating elements of continuous-flow conveyors are the following: their high material capacity and low maintenance ability as well as limited functionality, which provides only transporting of loose materials without providing mixture homogeneity.

MATERIAL AND METHODS

In order to improve the effectiveness of continuous-flow conveyor operation, a flow sheet of simultaneous transporting and stirring of mixture components which can provide their transporting and the attainment of the required homogeneity has been developed.

The technological lane of a continuous-flow conveyor is spatial and consists of certain set segments: rectilinear, curvilinear concave, vertical, curvilinear convex and so on.

Figure 1 shows the technological lanes of such segments.

The procedure of transporting and stirring is the following. In the first stage (Fig.1a) a conveyor casing is fed with the first mixture component with a certain filling coefficient of inter-scraper space, which is picked by scrapers with a central opening and is transported along the route.

In the second stage, a certain batch of the second component is fed through a special hopper (Fig.1b). As a rule, this component is situated on the surface of a load layer, which is to be transported.

In the third stage (Fig.1c), a load placed between continuous scrapers, when being transported along the route, begins to spill through central openings of beaded scrapers.

In the fourth stage (Fig.1d), when transporting the load, which is situated between continuous scrapers, in vertical route segments there is effective spillage and stirring of mixture components.

In the fifth stage (Fig.1e), the load is transported in a curvilinear vertical segment, where mixture fills certain space between beaded scrapers and load is stirred in continuous flow.

In the sixth stage (Fig.1f), mixture is unloaded and when it is spilled into a container, the mixture is entirely stirred.

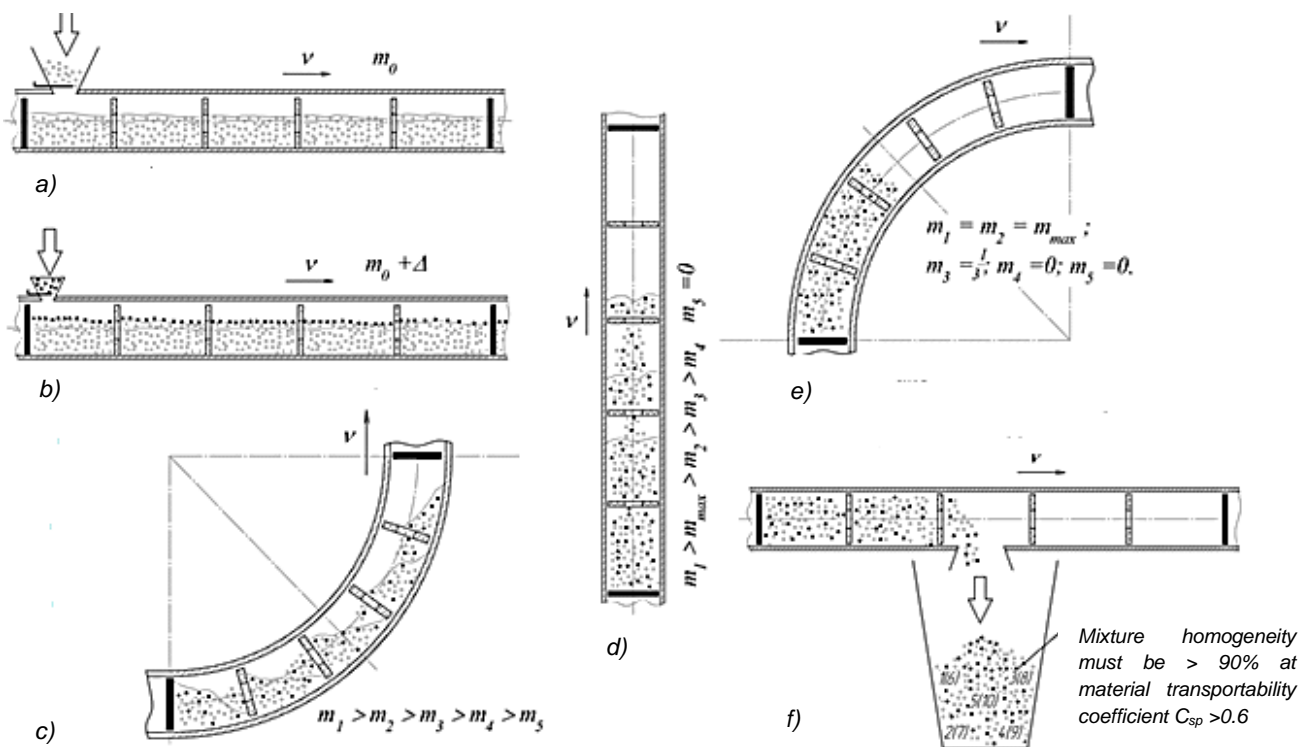


Fig. 1 - Flow sheets of simultaneous transporting and stirring of mixture components

a – I stage – feed of the main component; b – II stage – feed of the second component;

c – III stage – partial stirring of components; d – IV stage – main stirring of components;

e – V stage – transportation of components; f – VI stage – unloading with entire stirring of components

In order to provide proper homogeneity, it is necessary to determine the influence of technical and design parameters, namely: speed of transportation, diameter of a pipe-line, pitch of scrapers, diameter of scrapers, diameter of an opening etc. on load parameters of the process and mixture homogeneity.

In order to substantiate kinematic motion parameters of loose material with elementary mass dm_c in vertical segments of a technological lane, possible cases of the motion of a variable-mass body vertically upwards (Fig. 2a) have been considered:

- separation from a scraper surface 1 of elementary mass particle Δdm_c ;
- simultaneous attachment to a scraper surface 2 and separation from its surface of elementary mass particle Δdm_c ;
- attachment to a scraper surface 3 of elementary mass particle Δdm_c .

A change in elementary mass dm_i on operational surfaces of relative scrapers over a period of time Δt_c is determined using the following system of equations:

$$\left. \begin{aligned} \Delta dm_C &= dm_C(t_c) - dm_C(t_c + \Delta t_c); \\ \Delta dm_M &= dm_M(t_c) + \Delta dm_C - dm_M(t_c + \Delta t_c); \\ \Delta dm_L &= dm_L(t_c) + \Delta dm_M(t_c + \Delta t_c) \end{aligned} \right\} \quad (1)$$

where Δdm_C – separated or attached elementary mass particle Δdm_M ; Δt_c – period of time for separation and attachment of elementary mass particle Δdm_C and Δdm_M .

Based on energy conservation law, momentum Q_C of elementary mass particle dm_C in case of separation, simultaneous attachment and separation, attachment of elementary mass particle Δdm_C at instant of time t_y , respectively, equals:

$$Q_C(t_y) = (dm_C + \Delta dm_C)g_y - \Delta dm_C g_1, \quad Q_M(t_y) = dm_M g_c + \Delta dm_C g_1 - \Delta dm_M g_2, \quad Q_L(t_y) = (dm_L + \Delta dm_M)g_y + \Delta dm_M g_2.$$

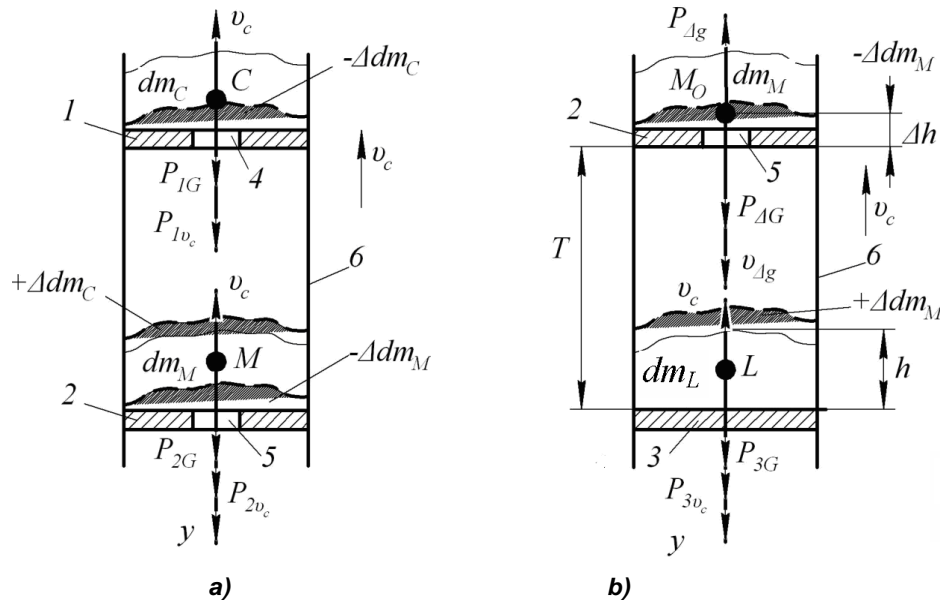


Fig. 2 - Design diagrams of kinematic motion parameters of loose materials

Applying Meshchersky's equation with regard to (1) and resultant force exerted on elementary mass dm_i , we have obtained a differential equation for the motion of loose material in a vertical route segment of an operating element for the three cases of behaviour at instant of time t_y taking into account the aerodynamic drag force of aerial environment:

$$dV_C \psi \frac{d^2 y_C}{dt_c^2} = dV_C \psi \left[g + p \left(\frac{dy_C}{dt_c} \right)^2 \right] + \frac{d(dV_C \psi)}{dt_c} \left(\frac{dy_1}{dt_c} - \frac{dy_C}{dt_c} \right) \quad (2)$$

$$dV_M \psi \frac{d^2 y_M}{dt_c^2} = dV_M \psi \left[g + p \left(\frac{dy_M}{dt_c} \right)^2 \right] - \frac{d(dV_C \psi)}{dt_c} \left(\frac{dy_1}{dt_c} - \frac{dy_C}{dt_c} \right) + \frac{d(dV_M \psi)}{dt_c} \frac{dy_2}{dt_c} \quad (3)$$

$$dV_L \psi \frac{d^2 y_L}{dt_c^2} = dV_L \psi \left[g + p \left(\frac{dy_L}{dt_c} \right)^2 \right] + \frac{d(dV_L \psi)}{dt_c} \left(\frac{dy_3}{dt_c} - \frac{dy_L}{dt_c} \right) \quad (4)$$

where dV_C , dV_M , dV_L – voluntary unit of elementary mass dm_C , dm_M , dm_L ; ψ – specific load weight; y_C , y_M , y_L – C, M, L point coordinates of the mass centre of constant elementary mass dm_C , dm_M , dm_L ; y_1 , y_2 , y_3 – point coordinates of the mass centre of variable elementary mass dm_C , dm_M , dm_L .

A differential equation of elementary mass motion Δdm_M (Fig. 2b) vertically downward under gravity and taking account of aerodynamic drag force of aerial environment is the following:

$$\Delta dm_M \frac{d^2(T-h+\Delta h)}{dt_c^2} = \Delta dm_M g - p \Delta dm_M g_{\Delta g}^2 = \Delta dm_M (g - p g_{\Delta g}^2) \quad (5)$$

where T – pitch of scrapers; h – initial height of loose material hopper relative to the work surface of a scraper; Δh – height, which takes into account scraper thickness 3 and centre-of-mass coordinate M relative to work surface of a scraper.

In order to determine the speed or obtain the equation of elementary mass downward motion Δdm_M it is necessary to eliminate time t_c , applying a substitute method (5). Then, the differential equation (5) becomes the following:

$$\frac{d(T-h+\Delta h)}{dt_c} = \int_0^{t_c} \left(g - 2p \frac{g_{\Delta g}}{dt_c} \right) dt_c = g t_c - 2p g_{\Delta g} \quad \text{or} \quad \int_0^{g_{\Delta g}} \frac{d(T-h+\Delta h)}{\frac{g t_c}{p} - 2g_{\Delta g}} = p \int_0^{t_c} dt_c \quad (6)$$

In order to eliminate random time integration constant we shall take the defined integral, remaining upper and lower limits of variable integration. For lower limits $t_c = 0$, $g_{\Delta g} = 0$. After the separation of variables, integration and transformation (6), the following can be deduced:

$$\int_0^{T-h+\Delta h} d(T-h+\Delta h) = \sqrt{g/p} \int_0^{t_c} \ln(t_c \sqrt{gp}) dt_c; \quad y_{\Delta M} = T-h+\Delta h = \frac{1}{p} \ln(t_c \sqrt{gp}) \quad (7)$$

The dependence (7) describes a law of vertical downward motion of elementary mass particle Δdm_M taking into account aerodynamic drag force of aerial environment, and can be used for the substantiation of the parameters of an operating element by determining the time and the distance needed to fill the inter-scraper space volume of the last scraper and their pitch to capacity.

A pilot plant used for the determination of the drag force in set route segments and the stirring rate of mixture components (Fig.3) contains horizontal 5 and 14, curvilinear 9 and 11 and vertical 10 segments, where there is a traction operating element with scrapers 6. In loading and unloading area there is a hopper 7, component additives feeder 8, an unloading port 12 and a load tank 13.

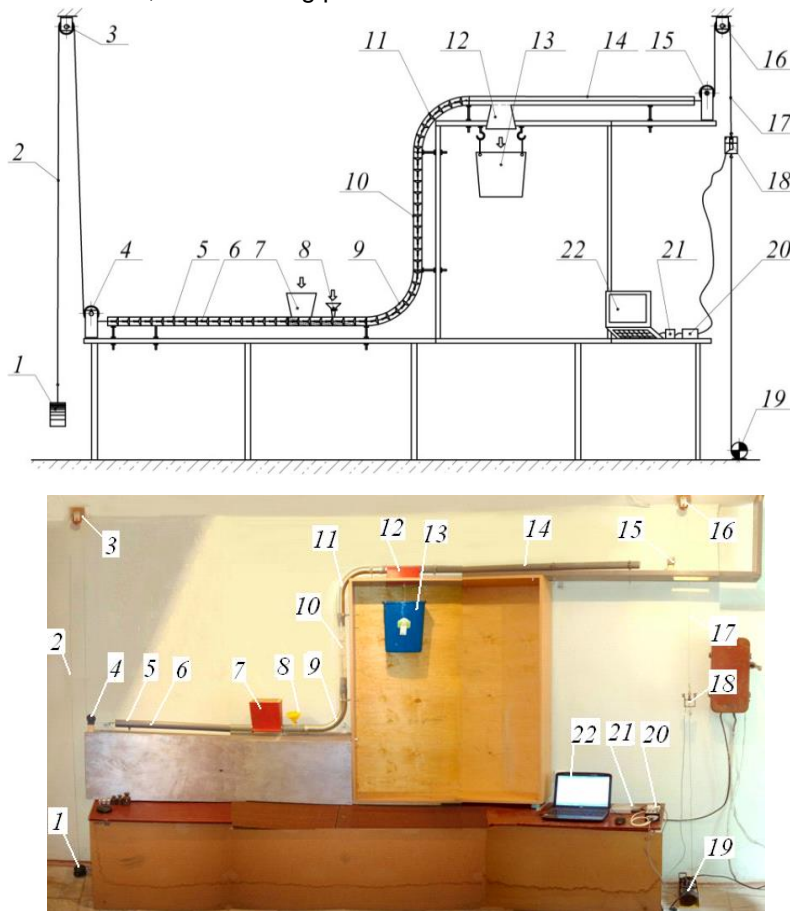


Fig. 3 - Installation diagram and overview of a pilot plant of a continuous-flow conveyor with the designed scrapers

A traction operating element interacts with cables 2 and 17, which are weighted by load 1 via guide blocks 3,4,15 and 16 and are coupled to an electric drive 19. The tension force of a driving part of a cable 17 was recorded on PC monitor 22 via an inductive sensor 18 (JA12SSVD10/N2P), a switch and a power supply unit of a measuring system 20, an analog-to-digital adaptor 21 (ADA-1406).

The length of a cable from a sensor 18 to an electric drive 19 was divided into segments, which corresponded to a horizontal segment of a casing in the area of hoppers arrangement, a curvilinear segment and a vertical segment as well as a curvilinear area, which transforms into a horizontal one in the area of loose mixture unloading.

The change of a drag force was recorded on a PC monitor in each segment of the technological lane.

RESULTS

Experimental studies in order to determine the spillage rate of loose materials in a curvilinear route segment through the openings in beaded scrapers were conducted using a test stand. A curved bend, which had 5 sections, was fed with loose material with the weight of 100...150 g, which corresponded to space filling coefficient $\psi = 0.6...0.9$. After opening a flap, the flow of loose materials pressed a lever pedal, which turned the timer on. The flow quantity was weighed by an electronic balance. Bend sections with beaded scrapers arranged at angles of $\alpha_1=75^\circ$, $\alpha_2=6^\circ$, $\alpha_3=45^\circ$, $\alpha_4=3^\circ$ were used. The diameter of the central openings of beaded scrapers was 12, 14, 16, 20 and 24 mm, and the outside diameter of washers was $d_w = 45$ mm.

The overview of the process of transporting and stirring of mixed fodder in a transparent guide pipe in a vertical route segment is shown in Figure 4.



Fig. 4 - A beaded operating element and the process of transporting and stirring of mixed fodder in a vertical route segment of a technological lane

The rate (coefficient) k_{tr} of the transported material, which was unloaded into the tank, was determined with the help of the dependence $k_{tr} = (m_{tr} / m_{\Sigma}) \cdot 100\%$, where m_{tr} is the mass of the material transported; m_{Σ} is the total mass of the material, which was picked by five scrapers.

It has been stated that the greatest force increment P_d (Fig. 5) for the transportation of materials in all the route segments is observed during transporting corn seeds at $\psi = 0.8$. In a curvilinear segment, the friction coefficient in scraper-guide pipe pair has the maximum influence on the force P_d (steel-steel – solid lines, steel-polycarbonate – cross hatching lines).

As a result of data processing for a complete factorial type experiment CFE 3^2 we have obtained the regression equations in actual values, which specify the change in the mass m of loose materials spilled by washers in a curvilinear segment of the lane depending on the diameter of the opening d_{op} and the washer angle α relative to the horizon:

$$\left. \begin{aligned} m_{mf} &= -35.61 + 4.71d_{op} + 2.81\alpha - 0.42 \cdot 10^{-2} d_{op} \alpha - 0.04d_{op}^2 - 0.05\alpha^2; \\ m_w &= 130.78 + 1.29d_{op} - 1.35\alpha + 0.12d_{op} \alpha - 0.11d_{op}^2 - 0.02\alpha^2; \\ m_m &= 488.76 + 0.73d_{op} - 47.58\alpha - 0.13d_{op} \alpha + 0.01d_{op}^2 + 1.67\alpha^2 \end{aligned} \right\} \quad (8)$$

where m_{mf}, m_w, m_m is the mass of spilled mixed fodder, wheat, millet.

Statistical significance evaluation of the coefficients of the regression equation and model validity for actual experimental data file was conducted using Student's test and Fisher's test. According to (8) the response surface of the mass-change of spilled material from d_{op} and α has been defined, Fig. 6.

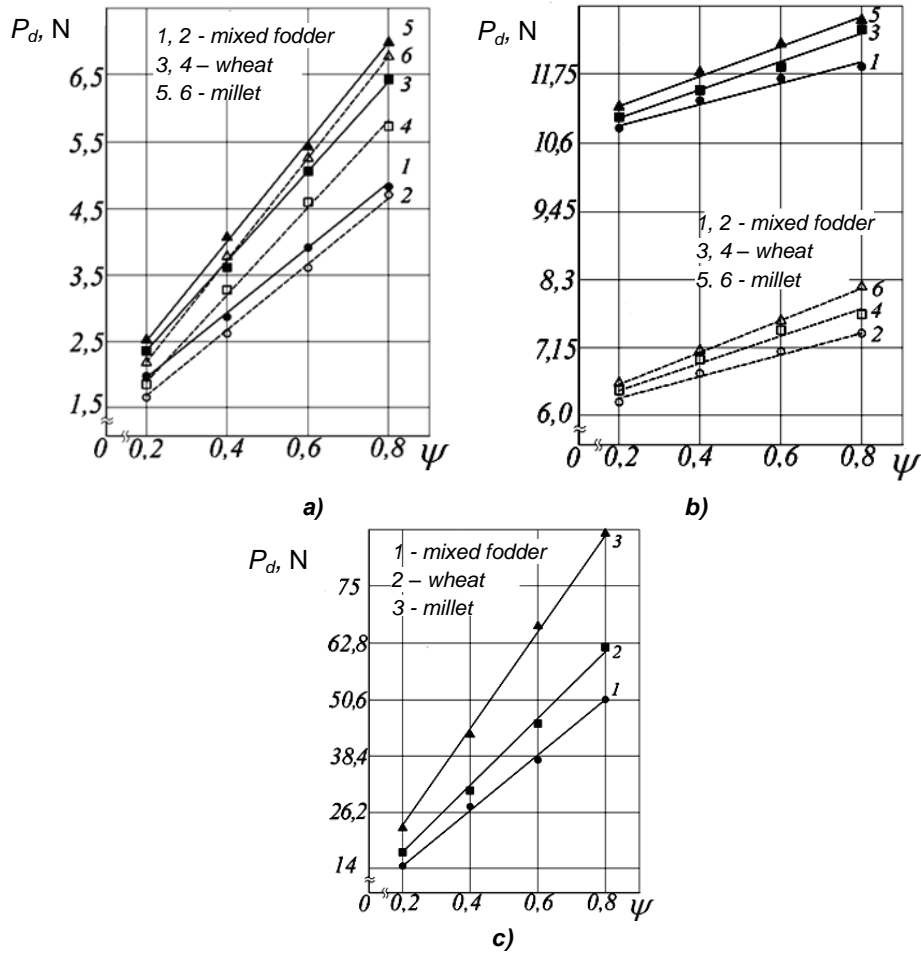


Fig. 5 - The dependence on the change of the force P_d , needed to transport materials with the help of ten scrapers (1 rm) on loading coefficient of the guide pipe ψ :
 a) horizontal; b) curvilinear; c) vertical route segment

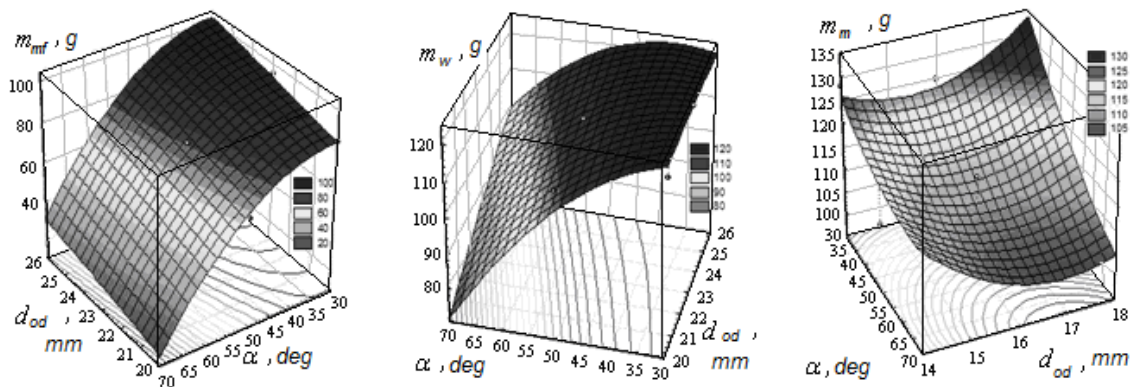


Fig. 6 - Response surface of spilled material mass from d_{op} and α

It has been determined that the change in the diameter of a washer opening from 10 up to 25 mm causes an increase in the mass of spilled material m_i , and the increase of a washer angle α relative to the horizon is of the opposite pattern.

A regression equation of the dependence of the change in the coefficient of transported material k_{tr} on the speed of scraper movement ($0.1 \leq V \leq 0.5$ m/s), the diameter of the internal opening ($20 \leq d_{od} \leq 26$ mm) and a cone angle ($14 \leq \chi \leq 42$ degrees) have been obtained:

$$k_{tr} = 576.749 - 23.020V - 40.118 \cdot d_0 - 0.217\chi + 0.875Vd_0 + 0.305V\chi + 1.079 \cdot 10^{-2} d_0\chi + 2.425 \cdot V^2 + 0.756d_0^2 - 3.128 \cdot 10^{-3} \chi^2. \quad (9)$$

It has been determined that the dominant factor, which influences the coefficient of the transported material k_{tr} is the diameter of the internal opening d_{op} of scraper washers (Fig.7). The change in the speed of movement V and the cone angle χ of a washer within the limits of 14-28 (degrees) does not influence the increase of the coefficient k_{tr} significantly, but the increase of the angle χ to 42 degrees causes the decrease of the coefficient k_{tr} due to material jamming.

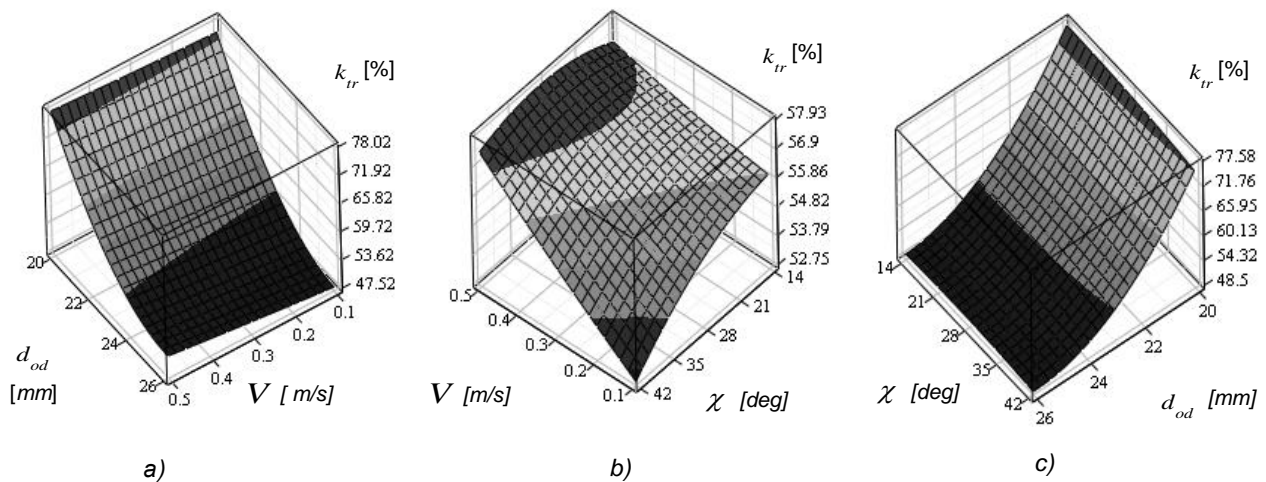


Fig. 7 - Response surface of change the coefficient k_{tr} as functionality

a) $k_{tr} = f(V, d_{od})$; b) $k_{tr} = f(V, \chi)$; c) $k_{tr} = f(d_{od}, \chi)$

For the in-process testing, which is connected with the determination of the productivity of the scraper conveyor-mixer, the quality of the process and simultaneous stirring of the components of microgranulated mixed fodder depending on the design and kinematic parameters of the operating elements, a pilot plant has been designed and constructed. Its general view is shown in Fig.8.

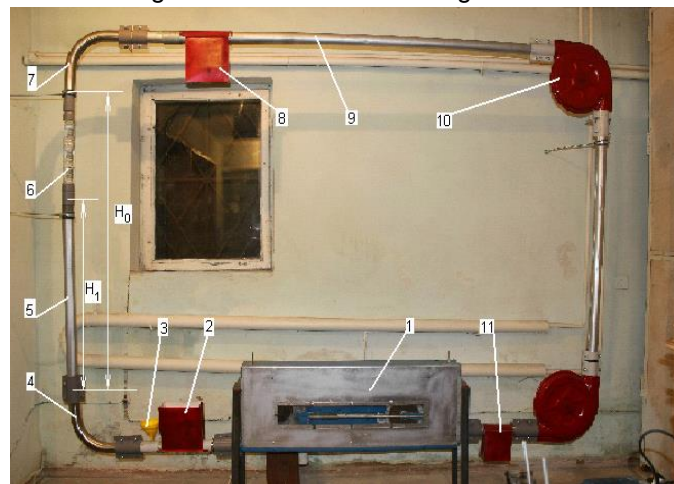


Fig. 8 - Pilot plant

1 – power-drive station; 2 – loading hopper; 3 – bunker for micro additives; 4 – concave curvilinear route segment; 5 – vertical route segment; 6 – vertical transparent route segment; 7 – convex vertical segment; 8 – unloading port; 9 – horizontal segment; 10 – swivel block; 11 – unloading port for material remains

The plant contains a power-drive station 1, where there are horizontal 9, vertical 5, curvilinear (concave 4 and convex 7) sections of pipe technological lanes attached about a closed path. Inside the lanes there are the designed scraper operating elements arranged. In the left side of the vertical lane there is a section 6 of a vertical transparent route segment mounted. Its length is $H_0 - H_1 = 0.5$ m, which corresponds to five scraper sections of the operating element connected with each other.

In the area of the material intake there is a loading hopper 2 for the main component of microgranulated mixed fodder and a hopper 3 for the control component.

During the in-process testing, the efficiency of a scraper conveyor-mixer depending on variable design and kinematic parameters of the operating element as well as on the stirring quality of feed components was determined.

When determining the effectiveness of the scraper conveyor-mixer, microgranulated mixed fodder was applied. Forward speed of the operating element of the conveyor changed within the range of $V = 0.1 \dots 0.5$ m/s. In the process of the investigation, scrapers with skid-washers with the internal diameter $d_{in} = 18, 20$ and 23 mm were used. The results of the conducted experiments are shown in Table 1.

Table 1

Forward speed of the operating element V , m/s	Effectiveness of a conveyor-mixer E , t/h		
	$d_{in} = 18$ mm	$d_{in} = 20$ mm	$d_{in} = 23$ mm
0.1	0.392	0.365	0.338
0.2	0.785	0.733	0.637
0.3	1.172	1.098	1.026
0.4	1.561	1.469	1.362
0.5	1.998	1.838	1.711

The investigation aimed at defining the dependence of mixture heterogeneity H_m on the coefficient of the transported material k_{tr} . For the experimental studies microgranulated mixed fodder with bulk density being 500 kg/m^3 and with particle size being $1 \dots 1.5$ mm and rape seeds with bulk density being 654 kg/m^3 were chosen. A rape seed was chosen to be the control component and it was stirred with microgranulated mixed fodder at the ratio of 1:8. The indicated component was fed from the side of the loading branch pipe. Mixture quality was determined from the degree of distribution of the control component in the mass of microgranulated mixed fodder.

In the process of experimental studies the spot sampling method was applied. Sampling from the container was done at regular intervals with the help of a special sampler.

The minimum sample mass is calculated using the following formula:

$$G_M = \frac{10^4 \pi d^3 \rho}{c_0 + 1.5c_0} \approx \frac{1.26 \cdot 10^4 d^3 \rho}{c_0} = \frac{1.26 \cdot 10^4 \cdot 0.1^3 \cdot 0.5}{0.125} = 50.4 \text{ g} \quad (10)$$

where d – diameter of mixture particles, [cm];

ρ – bulk density of mixture particles, [g/cm^3];

c_0 – value of the specified concentration of the main component.

Thus, let us assume sample mass $G \geq G_M \geq 50$ g.

The number of samples is 9; the repetition of the testing is triple. The main component content of rape seeds in the samples was determined using a quantitative analysis of samples. In order to do this, they were weighed using a second type balance like compensatory analytical balance VLKT-500g-M and they were consecutively separated on sieves, since the use of a gravimetric method is possible when all the particles of the control component form a fraction without any particles of other components. After their separation on sieves, the seed mass of the main component (rape seeds) and its concentration in a sample were determined. Having obtained a number of concentration values of the main component in samples c_i , the coefficient of mixture heterogeneity (variations) H_m for a certain coefficient value of the transported material k_{tr} is defined applying the following formula:

$$V_c = \frac{100}{\bar{c}} \sqrt{\frac{1}{n-1} \sum_{i=1}^n (c_i - \bar{c})^2}, \% \quad (11)$$

where \bar{c} – arithmetic mean value of the main component in the samples, [%]; c_i – value of the main component concentration in the i -sample, [%]; n – a number of samples analysed.

Based on the obtained experimental data by means of the regression analysis in Microsoft Office Excel environment, the empirical data were approximated by theoretical curves, the results of which are shown in Fig. 9.

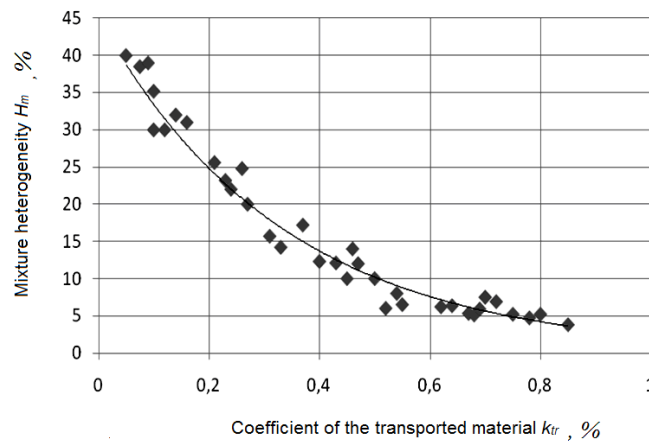


Fig. 9 - The dependence of mixture heterogeneity H_m on the coefficient of the transported material k_{tr}

The obtained results enable to choose such operating modes of the conveyor-mixer at which the specified mixture quality can be attained.

In order to determine economic efficiency, an experimental example of a continuous-flow conveyor-mixer has been designed and has undergone in-process testing.

We have suggested the methodology for determining economic results of the application of the designed conveyor-mixer compared to the basic example, which was taken from the best foreign prototype (that is the decrease of the material capacity of the operating element as well as the decrease of power inputs into the process of transportation). Besides, in the process of transportation, stirring of mixture components of loose materials takes place.

CONCLUSIONS

Having analysed scientific researches, a new flow sheet of simultaneous transportation and stirring of loose material components has been suggested.

The dependencies which define a motion law of an elementary mass particle vertically downward in the process of attachment and separation of loose material or its stirring have been obtained, the analysis of which enables to determine the time and the way needed for filling to capacity inter-scrapers space volume, scraper pitch and the amount of transported loose material.

Test stands have been designed and constructed in order to conduct experimental studies.

It has been determined that the greatest force increment P_d needed for material transportation in all the route segments is observed during transporting corn seeds at loading coefficient being $\psi = 0.8$ for steel scrapers, the force P_d is 12.4 and 6.8 greater than in a rectilinear route segment and in a curvilinear one.

Maximum demand of traction force F_D change when the block of beaded scrapers is moved can be observed in a vertical route segment, where F_D for solid scrapers is in 1.1...1.15 times greater than for scrapers with openings and the change in motion speed within the limits of 0.15...0.3 m/s does not influence the force F_D significantly.

Based on the conducted laboratory research, it has been determined that the change in the diameter of a scraper opening from 20 to 25 mm causes the decrease in the time of mixed fodder spillage from 3.3 to 2.25 s, if the angle of washer arrangement is $\alpha = 30^\circ$; in the process, there is spillage of 84.6% and 96.1% of mixed fodder out of the loaded mass respectively. If the angle is $\alpha = 75^\circ$ the time of mixed fodder spillage decreases from 4.9 to 3.2 s, the spillage of mixed fodder is 17.3% and 30.8% respectively.

The dominant factor, which influences a coefficient value of transported material k_{tr} , is the diameter of the internal opening d_{op} of scraper washers and the change in the speed of movement and the cone angle of an operating surface within the limits of $0.1 \leq V \leq 0.5$ (m/s). $14 \leq \chi \leq 28$ (degrees) does not cause a significant increase of the coefficient k_{tr} , but further increase of the angle χ to 42 degrees causes the decrease of the coefficient k_{tr} . It has been determined that the effectiveness of the conveyor-mixer, when the internal opening of a washer is changed from 18 to 23 mm, decreases from 2.0...1.7 t/h at forward speed of the operating element being 0.5 m/s and the best homogeneity of mixed fodder mass is achieved at the coefficient k_{tr} from 0.55...0.6 and above.

REFERENCES

- [1] Dziadykevych Y.V. and others, (2016), *Environmental and Natural Resources Economics: monograph (Економіка довкілля і природних ресурсів: монографія)*, (Астон), p.392, Ternopil;
- [2] Nevko M.R., Vitrovyi A.O., (2016), *Results of Experimental Investigations for Determination of Energy and Power Parameters of Hinged Operating Elements of Flexible Screw Conveyors (Результати експериментальних досліджень з визначення енерго-силових параметрів шарнірних робочих органів гнучких гвинтових конвеєрів)*. Bulletin of Engineering Academy of Ukraine (Вісник інженерної академії України). Vol.1. pp.148-154, Kyiv/Ukraine;
- [3] Nevko R.B., Klendiy M.B., Klendii O.M., (2016), Investigation of a transfer branch of a flexible screw conveyor, *INMATEH-Agricultural Engineering*, vol.48. no.1, pp.29-34, Bucharest/Romania;
- [4] Nevko R.B., Klendiy O.M., (2014), The investigation of the process of a screw conveyor safety device actuation, *INMATEH-Agricultural Engineering*, vol.42, no.1, pp.55-60, Bucharest/Romania;
- [5] Nevko R.B., Zalutskiy S.Z., Tkachenko I.G., Klendii O.M., (2015), *Development and investigation of reciprocating screw with flexible helical surface*. INMATEH: Agricultural engineering, vol.46, no.2. pp. 133-138, Bucharest/Romania;
- [6] Hryshova I.Y., Lebedev V.V., (2015), Development of Transport and Logistic Services Market in the Context of Enterprise Management (Розвиток ринку транспортно-логістичних послуг в контексті менеджменту підприємств), *Bulletin of Sumy National Agrarian University. Series "Economics and Management" (Вісник Сумського національного аграрного університету. Серія "Економіка та менеджмент")*, vol.12 (66), pp.11-15, Sumy/Ukraine;
- [7] Loveikin V., Rogatynska O., Rogatynska L., Dudun Y., (2010), Dynamics of Screw Conveyors (Динаміка гвинтових конвеєрів), *Bulletin of I.Pyliui Ternopil National Technical University (Вісник Тернопільського національного технічного університету ім. І.Пулюя)*, Vol.15, pp.100-105, Ternopil/Ukraine;
- [8] Loveikin V., Rogatynska L., (2011), *A Model of Loose Material Transportation by Means of High-Speed Conveyors with Elastic Operating Devices (Модель транспортування сипкого вантажу швидкохідними гвинтовими конвеєрами з еластичними робочими органами)*. (Вісник Тернопільського національного технічного університету ім. І.Пулюя), Vol.16, pp.66-70, Ternopil;
- [9] Lyashuk O.L., Rogatynska O.R., Serilko D.L., (2015), *Modelling of the vertical screw conveyor loading*, INMATEH-Agricultural Engineering, vol.45, no.1, pp.87-94, Bucharest/Romania;
- [10] Pylypaka S.F., Klendiy M.B., (2016), Analytical Model of Installation of Concave Coulters for Definition Geometrical and Technological Characteristics (Аналітична модель установки ґрунтообробних сферичних дисків для визначення геометричних та технологічних характеристик), *Scientific Journal of National University of Life and Environmental Sciences of Ukraine series «Technology and Energy AIC" (Науковий вісник НУБіП України: Серія «Техніка та енергетика АПК»)*, Vol.241, pp.140-150, Kyiv/Ukraine;
- [11] Rogatynska L.R., (2010), Evaluation of Stress-Strained State of Elastic Helixes of Screw Conveyors when Loading (Оцінювання напружено-деформованого стану еластичних спіралей гвинтових конвеєрів при навантаженні), *Bulletin of I. Pyliui Ternopil National Technical University (Вісник Тернопільського національного технічного університету ім. І.Пулюя)*, Vol.15, pp.131-137. Ternopil/Ukraine;
- [12] Rogatynska O., Liashuk O., Peleshok T., Liubachivskiy R., (2015), Investigation of the Process of Loose Material Transportation by Means of Inclined Screw Conveyors (Дослідження процесу транспортування сипкого вантажу похилими гвинтовими конвеєрами), *Bulletin of I.Pyliui Ternopil National Technical University (Вісник Тернопільського національного технічного університету ім. І.Пулюя)*, Vol.79, pp.137-143, Ternopil/Ukraine;
- [13] Rohatynskiy R.M., Diachun A.I., Varian A.R., (2016), Investigation of Kinematics of Grain Material in a Screw Conveyor with a Rotating Casing (Дослідження кінематики зернового матеріалу у гвинтовому конвеєрі із обертовим кожухом), *Bulletin of Kharkiv Petro Vasylenko National Technical University of Agriculture, №168, (Вісник Харківського національного технічного університету сільського господарства імені Петра Василенка №168)*. p.24-31, Kharkiv/Ukraine;
- [14] Shynkaryk M.I., Nevko R.B., Klendii O.M., (2014), Dynamic calculation of a safety device of screw conveyor (Динамічний розрахунок запобіжного пристрою шнекового транспортера), *Bulletin of Engineering Academy of Ukraine (Вісник інженерної академії України)*, Vol.2, pp. 163-168, Kyiv.

INVESTIGATION OF CONSTRUCTIVE GEOMETRICAL AND FILLING COEFFICIENTS OF COMBINED GRINDING SCREW CONVEYOR

/

ДОСЛІДЖЕННЯ КОНСТРУКТИВНОГО ГЕОМЕТРИЧНОГО КОЕФІЦІЄНТА ТА КОЕФІЦІЄНТА ЗАПОВНЕННЯ КОМБІНОВАНОГО ГВИНТОВОГО ТРАНСПОРТЕРА-ПОДРІБНЮВАЧА

P.G. Pankiv V.R.¹⁾, Ph.D. Eng. Tokarchuk O.A.²⁾

¹⁾ Ternopil Ivan Pul'uj National Technical University, Ternopil / Ukraine;

²⁾ Vinnitsa National Agrarian University, Vinnitsa / Ukraine

E-mail: vitalijpankiv25@gmail.com

Keywords: grinding screw conveyor, worm conveyor, spiral curl, knife-chopper, coefficient, volume, screw diameter, varied pitch of the screw.

ABSTRACT

This paper presents the structure and technological processes of combined grinding screw conveyor. The theoretical dependencies, which describe the nature of the geometric factor of screw conveyor and load factor of combined grinding screw conveyor, depending on its design parameters, are also substantiated here.

РЕЗЮМЕ

Наведено будову та технологічний процесу роботи комбінованого гвинтового транспортера-подрібнювача. Обґрунтовано теоретичні залежності, які описують характер зміни геометричного коефіцієнта шнекового конвеєра та коефіцієнта заповнення комбінованого гвинтового транспортера-подрібнювача залежно від його конструктивних параметрів.

INTRODUCTION

Further development of the agricultural sector of Ukraine is possible through the use of progressive mechanization means for agricultural products production processes. Improving the technical and economic performance of processing enterprises is achieved through the development and introduction of energy saving technologies and technical facilities that are designed for preparation and processing of agricultural raw materials (Baranovsky V.M., 2014, Hevko R.B., Klendiy O.M., 2014).

Screw conveyors (augers, conveyors) have gained wide acceptance in various industries. In particular, in the agricultural sector, screw conveyors are designed for horizontal, slope and vertical continuous moving of stream at considerable distances of agricultural products, such as root crops, grains, meal mixture. In addition, screw conveyors due to their design features also can simultaneously perform related functions - mixing of materials, grinding or crushing of materials, dosage, etc. (Hevko Iv.B., 2013).

The combination of performing one or more technological operations, along with the transportation of materials, which is inherent for the combined screw conveyor, is their defining feature.

Improvement of existing designs of screw transport mechanisms can significantly increase the performance and reliability of technological operations and contributes to the further development of production. Screw conveyors are part of comprehensive mechanization and automation. According to various estimates, their share in cargo handling operations is 40-45% (Baranovsky V.M., Potapenko M.V., 2016).

Purpose of work is to improve technological process parameters of simultaneous grinding and transportation of roots through the development and justification of working bodies' parameters of combined grinding screw conveyor. Investigation of transportation process technological parameters is based on the analysis of combined grinder conveyor design features.

MATERIAL AND METHODS

Screw conveyors, as separate technical element of transport mechanisms, are widely used in layout schemes of machines for reloading or moving materials due to their simple design, of maintenance service and the ability to load and partial unload the material at any location of the processing line.

Screw transport mechanisms are widely used in the construction of agricultural machinery - grain harvesters, beet and potato harvesters, fertilizers, grinders, seed disinfectant, etc. (Voytyuk D.G., et al., 2015; Hevko R.B., Zalutskyi S.Z., et al., 2015).

Also screw conveyors are used for the mechanization of loading and unloading processes of bulk and large-size materials, such as corn and different kinds of root crops - wheat, corn, sugar and fodder beet, rape plant, chicory. For this purpose, as transportation means for the mechanization of livestock farms, bakeries use mobile assembled augers, trucks and transporters.

Combined grinding screw conveyors are widely used in agriculture production sector, processing and food branches of industry which are specified due to the wide range of technological processes of products collecting and recycling.

Therefore, during their designing should be taken into account the specific technical requirements and functional performances of machines to carry out the relevant work, and also the features of transport-technological processes, agrobiological, physical and mechanical properties of the products to be transported (Hevko Iv.B., 2008).

Investigation of transportation process technological parameters is based on the analysis of combined grinder conveyor design features.

RESULTS

Analysis of the current state of screw transport mechanisms functioning showed that there are significant preconditions for further research, aimed at the development and application of energy-saving, high technology for combined screw conveyors. They will ensure effective implementation of various functions of related operations for simultaneously transporting and grinding agricultural crop in their processing.

Based on the given analysis of technological parameters for materials transportation of agricultural production, we have offered constructive scheme of the improved combined grinding screw conveyor, fig. 1.

Combined grinding screw conveyor (combined SGC) consists of a loading bunker 1 and 2 and the guide tube. In the guide tube 2 is installed the screw conveyor, which is designed as a drive shaft 3 on which is installed the drum 4. On the drum of drive shaft, along separate helical lines, fixed spiral turns 5 and plate knife-grinders 6 are installed on the drum between the spiral turns and at an angle to the cross-section of the drum. Screw lines of spiral turns and grinder blades are made with variable step, concurrently step of spiral turns and step of plate grinder blades with a constant lifting angle of spiral line towards the unloading part of the guide tube.

The material, for example root crops, fed into the loading bunker 1, which later moved to the guide tube 2 to the screw conveyor, or to the plate grinder knives 6. During the rotation of the drive shaft 3 and, accordingly, the drum 4 and the plate grinder knife occurs simultaneous grinding of root crops and transportation (movement) of root crops milled particles by the related installation of plate grinder knives at an angle to the cross-section of the drum and its attachment to the drum along the spiral line. In addition, simultaneously with the movement of root crops milled particles by plate grinder knives also occurs their transportation as spiral turns towards unloading part of the guide tube.

By increasing the speed of the axial movement of root crops milled particles, increased performance of combined SGC was generated.

The main criteria that characterize the technological and economic efficiency of any transport vehicles or mechanisms, which move or deliver materials to a given point, is the productivity of their performance, consumption of power inputs during materials transportation process, reliability and stability, performance of the process, work resource and others (Rogatinsky R., 2012).

Combined SGC (fig. 1) has its own specific technological and structural elements and processes that significantly distinguish it from the traditional basic screw mechanisms. Simultaneous presence of technological operations, grinding and transporting of the material (root crops), or the presence of grinder blades 6, which are installed in interterm space of screw conveyor along helical lines, make significant adjustments to existing techniques and calculating methods for the screw mechanisms.

In this respect, one of the priorities and the special factors, which will regulate the calculated productivity of combined SGC, is an index that characterizes volumetric filling factor of screw conveyor working space (Hevko R.B., Dzyura V.O., Romanovsky R.M., 2014). In turn, filling factor of screw conveyor working space depends not only on the amount of material that goes into it, but also on the design of the screw conveyor main transporting element (Hevko R.B., Zalutskyi S.Z., Tkachenko I.G., et al., 2015).

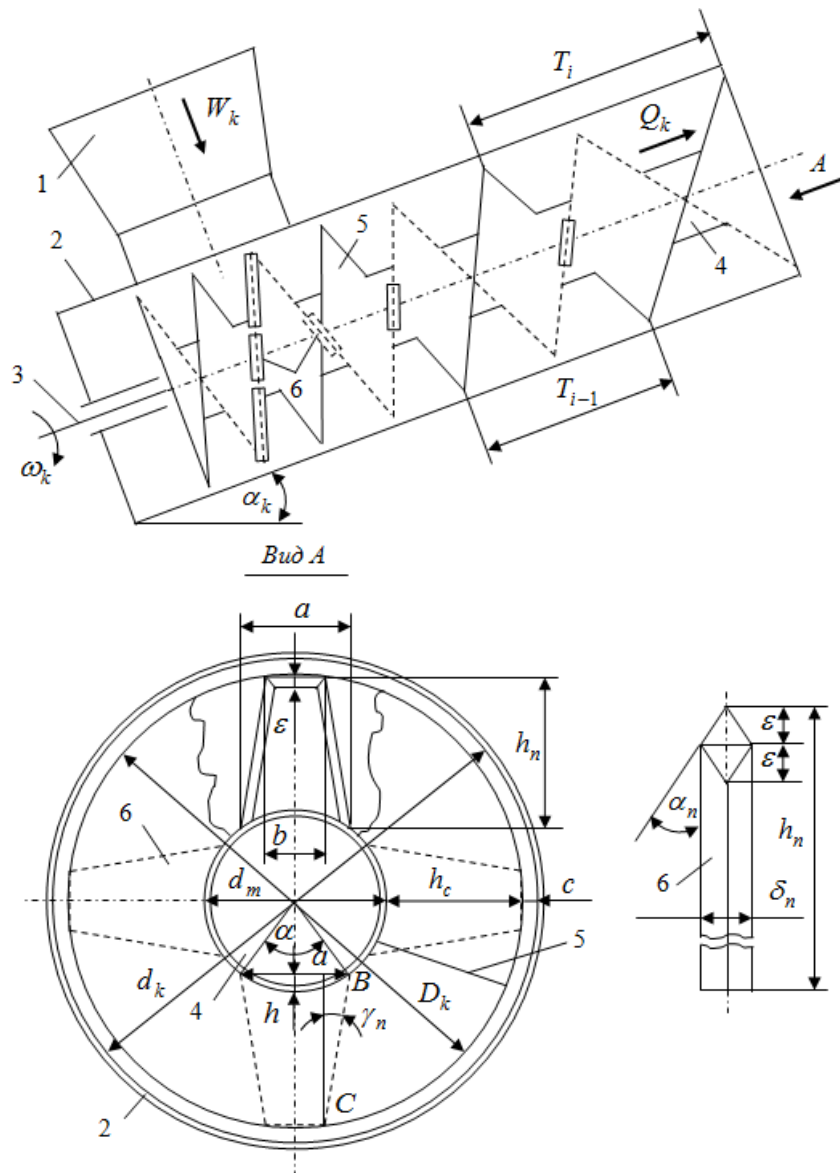


Fig. 1 - Construction scheme of combined grinding screw conveyor
 1 – loading bunker; 2 – guide tube; 3 – drive shaft; 4 – drum; 5 – spiral turn;
 6 – grinder knife

In the general context, filling factor of screw conveyor working space shows, which is the part of useful volume filled with material that moves along the turns of the screw.

Then, taking into account known provisions (Hevko R.B., Zalutskyi S.Z., Tkachenko I.G., et al., 2015) we represented the filling factor of combined SGC (hereinafter - filling factor k_z) as the ratio of the interterm space volume of screw conveyor, which is filled with grinded root crops, and the total volume of combined SGC, as follows:

$$k_z = V_{zk} / V_z \tag{1}$$

where

V_{zk} – filled volume of screw conveyor space, m^3 ;

V_z – total amount of combined SGC, space, m^3 .

To determine the set volume V_{zk} , V_z and ultimately filling factor k_z and calculate performance let's consider the composite structural and design scheme to determine the technological indicators of combined SGC, which is shown in fig. 1.

We initiate indication of the first helical turn step by alphabetic expression T_1 , second helical turn – T_2 , and last i - helical coil - T_i .

According to fig. 1, total volume V_z of combined SGC space consists of internal volume of the guide tube 2, or the volume of straight hollow cylinder:

$$V_z = 0,25\pi d_k^2 L_k = 0,25\pi (D_k + 2c)^2 (T_1 n_1 + T_2 n_2 + \dots + T_i n_j), [\text{m}^3] \quad (2)$$

where

d_k – inner diameter of the covering, m;

L_k – working height of the guide tube, or the length of screw conveyor, m;

D_k – outside diameter of screw conveyor, m;

c – the gap between the external edge of the spiral turn and the inner diameter of the guide tube, m;

T_1, T_2, \dots, T_i – the step of first, second, i -th spiral coil, m;

n_1, n_2, \dots, n_j – the total number of spiral turns per one step, m.

Filled volume of screw conveyor space V_{zk} by the grinded root crops will be determined according to the following considerations. V_{zk} , essentially, is a useful volume where root crops are placed loaded and grinded during the transportation.

The useful volume of screw conveyor V_{zk} consists of volume difference of screw conveyor total volume V_k and the total volume, occupied by the working elements of screw conveyor V_e , or the amount of drum volume V_{dm} , the volume of spiral turns V_c and the volume V_n knives-grinders, as follows:

$$V_{zk} = V_k - V_e; \quad V_e = V_{dm} + V_c + V_n; \quad V_{zk} = V_k - V_{dm} - V_c - V_n, [\text{m}^3] \quad (3)$$

where

V_{dm} – total volume of the screw conveyor, m^3 ;

V_{dm} – the volume of the tube drum of the screw conveyor, m^3 ;

V_e – total volume, occupied by the working elements of the screw conveyor, m^3 ;

V_c – volume occupied by the spiral turns, m^3 ;

V_n – volume occupied by knife-grinders, m^3 .

After substituting (2) and (3) in (1), we obtain:

$$k_z = \frac{1 - \frac{V_e}{V_k}}{0,25\pi (D_k + 2c)^2 (T_1 n_1 + T_2 n_2 + \dots + T_i n_j)} \quad (4)$$

Let's designate in (4) the ratio $V_e/V_k = k_n$, where the symbol k_n is the definition of constructive geometric factor of combined SGC (hereinafter – constructive geometric factor k_n), only during one configured constructive cycle of combined SGC technological process.

Then, the relation (4) will have the following form:

$$k_z = \frac{(1 - k_n) V_k}{0,25\pi (D_k + 2c)^2 (T_1 n_1 + T_2 n_2 + \dots + T_i n_j)} \quad (5)$$

To set the limits of structural changes of geometric factor k_n determine the total volume of screw conveyor V_k , total volume occupied by the working elements of the screw conveyor V_e which consists of the volume of the screw conveyor tube drum V_{dm} , the volume occupied by the spiral turns V_c , the volume

occupied by knife-grinders V_n .

However, according to fig. 1 and (Berd J., 2008) we have:

$$V_k = 0,25\pi D_k^2 L_k, [\text{m}^3]; \quad V_{d_m} = 0,25\pi d_m^2 L_k, [\text{m}^3]; \quad V_c = F_n l_c z, [\text{m}^3]; \quad V_n = V_{1n} \theta_n, [\text{m}^3] \quad (6)$$

where

d_m – diameter of the screw conveyor tube drum, m;

F_n – cross sectional area of screw conveyor card bales turn $F_n = \delta_c h_c, \text{m}^2$;

δ_c – thickness of the spiral turn card bales, m;

h_c – height of the spiral turn card bales $h_c = 0,5(D_k - d_m), \text{m}$;

l_c – total length of the spiral line by the average diameter of the screw conveyor, m;

z – number of the screw conveyor activities, units;

V_{1n} – volume of one knife-grinder, m^3 ;

θ_n – the amount of knife-grinders, units.

Or:

$$V_k = 0,25\pi D_k^2 (T_1 n_1 + T_2 n_2 + \dots + T_i n_i), [\text{m}^3] \quad (7)$$

$$V_{d_m} = 0,25\pi d_m^2 (T_1 n_1 + T_2 n_2 + \dots + T_i n_i), [\text{m}^3] \quad (8)$$

$$V_c = 0,5\delta_c z (D_k - d_m) \left(n_1 \sqrt{T_1^2 + 0,25(D_k + d_m)^2} + n_2 \sqrt{T_2^2 + 0,25(D_k + d_m)^2} + \dots \right), [\text{m}^3] \quad (9)$$

The volume V_n , occupied by knife-grinders 6 can be determined according to the following considerations. Each knife-grinder made in straight prism form, which is based on equilateral trapezium, with this three working side edges of the prism from two sides sharpen with the grinding angle α_n , and side edge, which relies on a large basis b of the trapezium has the shape of a segment whose radius is the radius of the tube drum r_m of the screw conveyor.

Then the volume V_n , occupied by knife-grinder will be equal:

$$V_n = (V_{np} - V_z - V_{cn}) \theta_n, [\text{m}^3] \quad (10)$$

where

V_{np} – volume of direct prism, m^3 ;

V_z – total volume of direct prisms that are cut during the sharpening of side edges with basis BC , m^3 ;

V_{cn} – volume of straight prism, which is cut out of side edge with basis b , m^3 .

In such case (Shipachev V.S., 2003):

$$V_{np} = F_{mp} \delta_n = \frac{a+b}{2} h_n \delta_n, [\text{m}^3]; \quad V_z = 2V_{1z} + 4V_{2z}, [\text{m}^3]; \quad V_{cn} = F_c L_k, [\text{m}^3] \quad (11)$$

$$V_{1z} = 0,125\delta_n^2 b t g \alpha_n, [\text{m}^3]; \quad V_{2z} = 0,125\delta_n^2 h_n / \cos \gamma_n, [\text{m}^3] \quad (12)$$

$$V_z = 0,25\delta_n^2 b t g \alpha_n + \frac{0,5\delta_n^2 h_n}{\cos \gamma_n}, [\text{m}^3] \quad (13)$$

$$F_c = r_m^2 [(\pi\alpha / 180) - \sin \alpha] / 2, [\text{m}^2] \quad (14)$$

where

F_{mp} – area of main prism (trapezoid area) m^2 ;

a, b – base of trapezoid, m;

V_{1z} – volume which is cut out from one side of side edge with the base b , $V_{1z} = 0,5\delta_n b / 2, \text{m}^3$;

ε – triangle height $\varepsilon = 0,5\delta_n \operatorname{tg} \alpha_n$, m;

α_n – skew angle of side edge, grade;

V_{2z} – volume which is cut out from one side of side edge with the base BC , $V_{2z} = 0,5\delta_n \varepsilon BC$, m³;

$BC = h_n / \cos \gamma_n$ – length of the side edge $BC = h_n / \cos \gamma_n$, m;

γ_n – the angle between the knife height and trapeze edge, grad;

F_c – segment area with height h , tighten by chord a and a central angle α , m²;

r_m – the radius of the screw conveyor drum tube (m), with this $a = 2r_m \sin(\alpha/2)$, from where $\sin(\alpha/2) = a/2r_m$, $\alpha/2 = \arcsin(a/2r_m)$.

Then according to (11), (14) we will have:

$$V_{cn} = 0,25d_m^2 \left[\left(\pi \arcsin \frac{a}{d_m} \right) / 180 - \frac{a}{d_m} \cos \arcsin \frac{a}{d_m} \right] (T_1 n_1 + T_2 n_2 + \dots + T_i n_j), \text{ [m}^3\text{]} \quad (15)$$

Substituting the values of the components from (11) (13) (15) in equation (10) we obtained a formula for determining the volume V_n , which is occupied by knives-grinders:

$$V_n = \left((a+b)h_n \delta_n - 0,5\delta_n^2 \left(\operatorname{btg} \alpha_n + \frac{h_n}{\cos \gamma_n} \right) - 0,5d_m^2 \times \right. \\ \left. \times \left[\left[\left(\pi \arcsin \frac{a}{d_m} / 180 \right) + \frac{a}{d_m} \cos \arcsin \frac{a}{d_m} \right] (T_1 n_1 - T_2 n_2 - \dots - T_i n_j) \right] \right) \frac{\theta_n}{2}, \text{ [m}^3\text{]} \quad (16)$$

Then, the total volume V_e of the screw conveyor, according to (3), (8), (9) and (16), is defined by the formula:

$$V_e = 0,25\pi d_m^2 (T_1 n_1 + T_2 n_2 + \dots + T_i n_j) + 0,5\delta_c z (D_k - d_m) \times \\ \times \left(n_1 \sqrt{T_1^2 + 0,25(D_k + d_m)^2} + n_2 \sqrt{T_2^2 + 0,25(D_k + d_m)^2} + \dots + n_j \sqrt{T_j^2 + 0,25(D_k + d_m)^2} \right) + \\ + 0,5\theta_n \left((a+b)h_n \delta_n - 0,5\delta_n^2 \left(\operatorname{btg} \alpha_n + \frac{h_n}{\cos \gamma_n} \right) - 0,5d_m^2 \times \right. \\ \left. \times \left[\left[\left(\pi \arcsin \frac{a}{d_m} / 180 \right) + \frac{a}{d_m} \cos \arcsin \frac{a}{d_m} \right] (T_1 n_1 - T_2 n_2 - \dots - T_i n_j) \right] \right) \text{ [m}^3\text{]} \quad (17)$$

However, according to (4), the constructive geometric factor k_n of the screw conveyor will be determined by applying the formula:

$$k_n = \frac{0,5\pi d_m^2 (T_1 n_1 + T_2 n_2 + \dots + T_i n_j) + \delta_c z (D_k - d_m) \times \\ \times \left(n_1 \sqrt{T_1^2 + 0,25(D_k + d_m)^2} + n_2 \sqrt{T_2^2 + 0,25(D_k + d_m)^2} + \dots + n_j \sqrt{T_j^2 + 0,25(D_k + d_m)^2} \right) + \\ + \theta_n \left((a+b)h_n \delta_n - 0,5\delta_n^2 \left(\operatorname{btg} \alpha_n + \frac{h_n}{\cos \gamma_n} \right) - 0,5d_m^2 \times \right. \\ \left. \times \left[\left[\left(\pi \arcsin \frac{a}{d_m} / 180 \right) + \frac{a}{d_m} \cos \arcsin \frac{a}{d_m} \right] (T_1 n_1 - T_2 n_2 - \dots - T_i n_j) \right] \right)}{\pi D_k^2 (T_1 n_1 + T_2 n_2 + \dots + T_i n_j)} \quad (18)$$

Thus, according to (5), the filling factor k_z is determined by dependence:

$$k_z = \frac{D_k^2}{(D_k + 2c)^2} - \frac{0,5\pi d_m^2 (T_1 n_1 + T_2 n_2 + \dots + T_i n_j) + \delta_c z (D_k - d_m) \times \left(\sqrt{T_1^2 + 0,25(D_k + d_m)^2} + n_2 \sqrt{T_2^2 + 0,25(D_k + d_m)^2} + \dots \right) + \dots}{\pi (D_k + 2c)^2 (T_1 n_1 + T_2 n_2 + \dots + T_i n_j)} + \theta_n \left(\frac{(a+b)h_n \delta_n - 0,5\delta_n^2 \left(b \operatorname{tg} \alpha_n + \frac{h_n}{\cos \gamma_n} \right) - 0,5d_m^2 \times \left[\left(\frac{\pi \arcsin \frac{a}{d_m}}{180} \right) + \frac{a}{d_m} \cos \arcsin \frac{a}{d_m} \right] \times (T_1 n_1 - T_2 n_2 - \dots - T_i n_j)}{\pi (D_k + 2c)^2 (T_1 n_1 + T_2 n_2 + \dots + T_i n_j)} \right) \quad (19)$$

For practical application of obtained dependences (18) and (19) let's simplify them through the formalization of constructive execution of combined screw conveyor SGC.

For this, let's accept the assumption that:

– the number of turns n_1, n_2, \dots, n_j of each n -th T_i step is the same, which means $n_1 = n_2 = \dots = n_j = n_z$;

– each next step of turns starts with the first increases in constant value ΔT , thus: $T_2 = T_1 + \Delta T; \dots; T_i = T_{i-1} + \Delta T$;

– the number of knife-grinders that are installed on the screw conveyor tube drum between one pair of two adjacent spiral turns is the same and equal θ_1 .

In this case:

– the sum of $T_1 n_1 + T_2 n_2 + \dots + T_i n_i$ n -th steps of spiral turns, which is equal to the screw conveyor length L_k , can be represented as dependence:

$$T_1 n_1 + T_2 n_2 + \dots + T_i n_j = \frac{n_z n}{2} [T_1 + \Delta T (n-1)], \text{ [m]} \quad (20)$$

where

n_z – number of turns of each T_i -th step;

n – number of T_i -th steps;

– total number of knives θ_n , that are installed on the screw conveyor tube drum will be equal:

$$\theta_n = \theta_1 (n_z n - 1), \text{ [units]} \quad (21)$$

In addition, also accept the assumption that each knife-grinder designed as straight prisms whose height is equal to δ_n and the basis of the prism is an equilateral trapezium, whose height is equal to h_n , we can notice that the height of the trapezoid will be approximately equal to the height of the spiral coil, or $h_n \cong h_c \cong 0,5(D_k - d_m)$, three working side edges of the prism on both sides will have sharpening angle α_n .

In this case, the volume V'_n which is occupied by knives-grinders will be equal:

$$V'_n = (V_{np} - V_z) \theta_1 (n_z n - 1) = \frac{\theta_1 (n_z n - 1) [(a+b)(D_k - d_m) \delta_n \cos \gamma_n - \delta_n^2 (b \operatorname{tg} \alpha_n + 0,5(D_k - d_m))]}{\cos \gamma_n}, \text{ [m}^3\text{]} \quad (22)$$

Then, equations (18) and (19) will have a final form:

$$k_n = \frac{d_m^2}{2D_k^2} \left[1 + \frac{4\Omega\delta_c z(D_k - d_m)}{\pi m D_k^2 [2T_1 + \Delta T(n-1)]} + \frac{\theta_1(n_z n - 1)\delta_n}{\pi} \times \left(\frac{2(a+b)(D_k - d_m)\cos\gamma_n - \delta_n [btg\alpha_n \cos\gamma_n + 0,5(D_k - d_m)]}{n d_m^2 [2T_1 + \Delta T(n-1)]\cos\gamma_n} \right) \right] \quad (23)$$

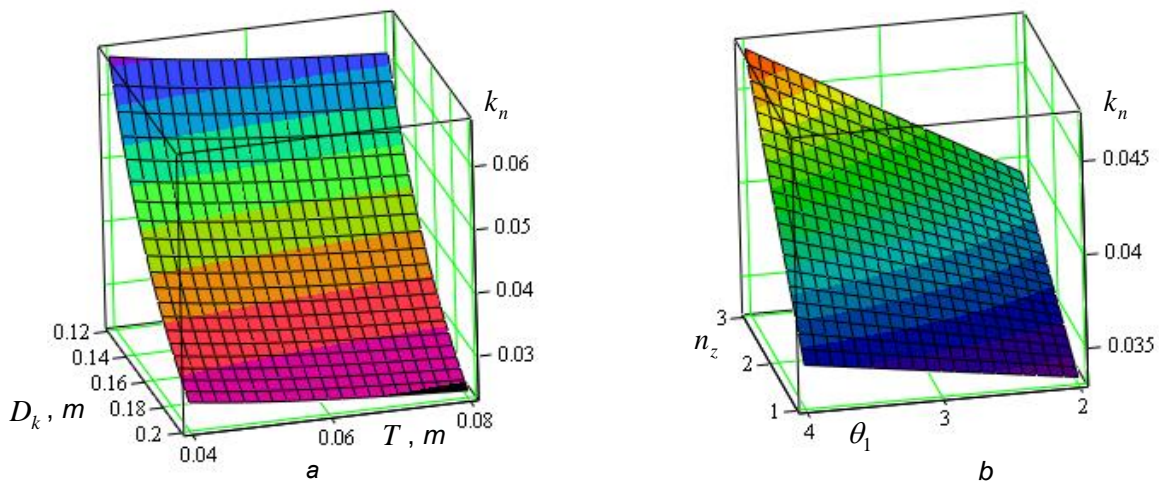
$$k_z = \frac{D_k^2 - \frac{d_m^2}{2}}{(D_k + 2c)^2} \left[1 + \frac{4\Omega\delta_c z(D_k - d_m)}{\pi m D_k^2 [2T_1 + \Delta T(n-1)]} + \frac{\theta_1(n_z n - 1)\delta_n}{\pi} \times \left(\frac{2(a+b)(D_k - d_m)\cos\gamma_n - \delta_n [btg\alpha_n \cos\gamma_n + 0,5(D_k - d_m)]}{n d_m^2 [2T_1 + \Delta T(n-1)]\cos\gamma_n} \right) \right] \quad (24)$$

where

$$\Omega = \sqrt{T_1^2 + 0,25(D_k + d_m)^2} + \sqrt{T_2^2 + 0,25(D_k + d_m)^2} + \dots + \sqrt{T_i^2 + 0,25(D_k + d_m)^2} = \sqrt{T_1^2 + 0,25(D_k + d_m)^2} + \sqrt{(T_1 + \Delta T)^2 + 0,25(D_k + d_m)^2} + \dots + \sqrt{[T_i + \Delta T(n-1)]^2 + 0,25(D_k + d_m)^2}; \Theta = \left[\left(\pi \arcsin \frac{a}{d_m} / 180 \right) + \frac{a}{d_m} \cos \arcsin \frac{a}{d_m} \right].$$

According to initial conditions $d_m = 0.04$ m; $\Delta T = 0.01$ m; $\delta_n = 0.002$ m; $n_z = 2$; $n = 3$; $\alpha_n = \pi / 6$ grad.; $a = 0.03$ m; $b = 0.02$ m; $c = 0.002$ m, according to equation (23) results the built dependence of constructive geometric factor k_n , and according to (24) – the filing factor k_z .

Analysis of the dependence (fig. 2) showed that constructive geometric factor k_n depends on the diameter changes D_k and step T of the screw conveyor is in the range 0.025...0.07 on a number of variables T_i -th steps that are equal to $n = 3$, number of spiral turns of the same T_i -th step – $n_z = 2$ and the



number of knife-grinders, installed between one pair of two adjacent spiral turns $\theta_1 = 4$ units.

Fig. 2 - Dependence on change of constructive geometric factor k_n as functionality

a – $k_n = f_n(D_k; T)$ with $\theta_1 = 3$ units; b – $k_n = f_n(n_z; \theta_1)$ with $D_k = 0.16$ m; $T = 0.05$ m

With this change, k_n , which is defined as a functional dependence $k_n = f_n(D_k; T)$ is reversible - with increasing of the diameter D_k and step T of the screw conveyor constructive geometric factor k_n decreases by parabolic function. We established that with increasing the number of knife-grinders θ_1 , which are installed between a pair of two adjacent spiral turns and the number of spiral turns n_z of one T_i -th step,

the constructive geometric factor k_n increases in direct proportion to the θ_1 i n_z , thus, the average growth value of k_n is in the range 0.002...0.0025 and 0.003...0.005.

In this regard, we can say that structural change in the number of blade-grinders θ_1 and the number of spiral turns n_z of one T_i -th step do not significantly affect the structural change of the factor k_n .

Three-dimensional graphical interpretation of filling factor changes depending on k_z as functional $k_z = f_z(D_k; T)$ and $k_z = f_z(D_k; \Delta T)$ given, respectively, on fig. 3 and fig. 4.

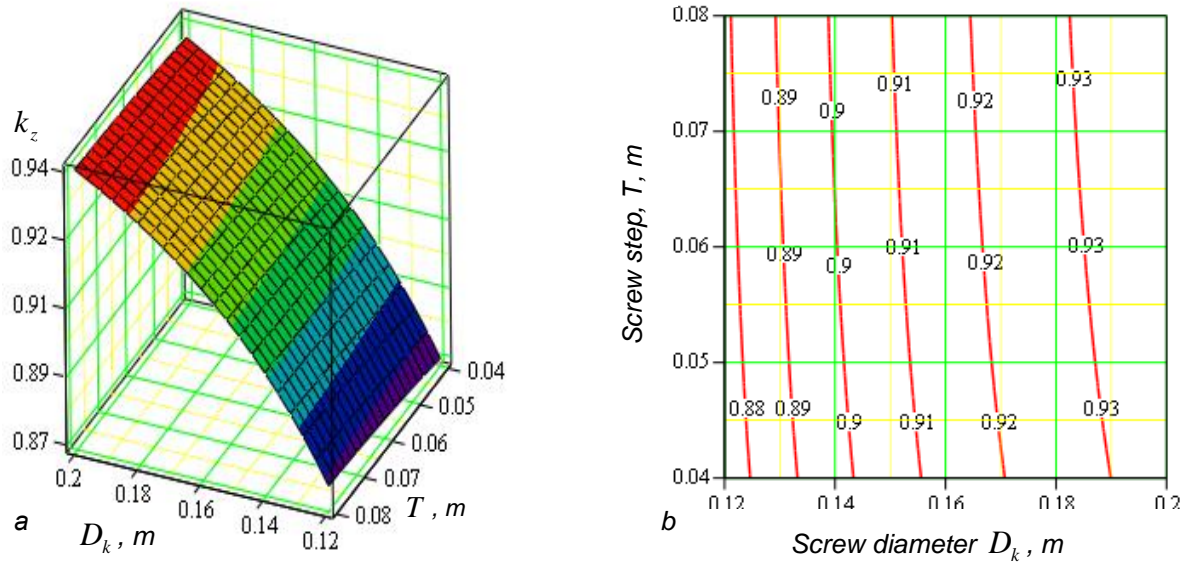


Fig. 3 - Dependence of change of filling coefficient k_z as functional $k_n = f_n(D_k; T)$ on $\theta_1 = 3$
 a – three-dimensional surface; b – two dimensional surface cross section

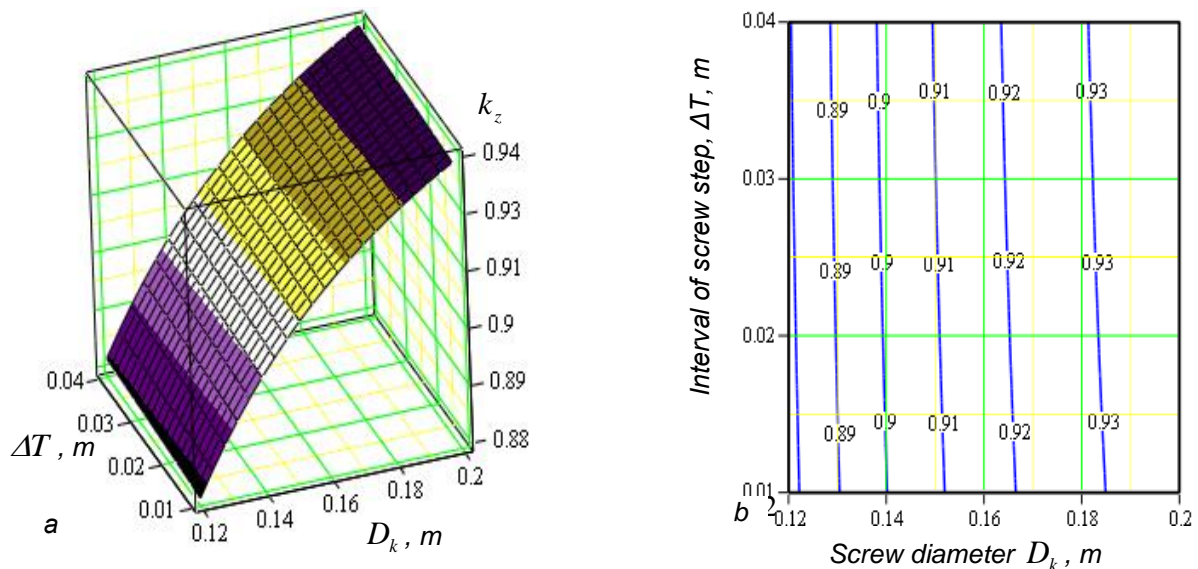


Fig. 4 - Dependence of change of filling coefficient k_z as functional $k_n = f_n(D_k; \Delta T)$ on $\theta_1 = 3$
 a – three-dimensional surface; b – two dimensional surface cross section

It was established that the functional change of filling factor k_z depending on the diameter changes D_k and step T of the screw conveyor (fig. 3, fig. 4), in contrast to the structural changes of geometric coefficient k_n of combined SGC has reversible type - with increasing D_k and T filling factor k_z and also growing in the range 0.87...0.94. In this case dominant factor that largely regulates the quantitative value of

filling factor k_z , is the diameter D_k of the screw conveyor, and a significant increase of k_z occurs when the value $D_k \geq 0.12$ m - in the range of change D_k from 0.12 to 0.16 (m) filling factor k_z growing on 0.05. Step change T and increasing of interval ΔT of the screw conveyor has insignificant impact on the quantitative value k_z by increasing step T from 0.04 to 0.08 (m) and increasing the step interval ΔT from 0.01 to 0.04 (m) filling factor k_z increases, respectively, on 0.004 and 0.001.

CONCLUSIONS

The obtained values of filling factor $k_z = 0.87...0.94$ by its analytical nature, is the most-possible technological parameters of the transporting process of chopped root crops by working bodies of combined SGC and characterizes its maximum degree of workspace filling i.e. it can be stated that the maximum value of filling factor k_z ranges within $k_{z,max} = 0.87...0.94$.

Thus, we established at analytical level, the numerical value of the maximum filling factor $k_{z,max} = 0.87...0.94$, is a further step for research of technological and energy parameters of chopped roots transporting process justification of combined SGC productivity and energy costs that are necessary for the simultaneous grinding and transportation, which ultimately will lead directly to a rational justification of structural and kinematic parameters of combined SGC working bodies.

REFERENCES

- [1] Baranovsky V., (2014), Methodological and structural-technological aspects of development of adapted root crop machinery (Методологічні та конструктивно-технологічні аспекти розробки адаптованих коренезбиральних машин), *Science journal. Journal of TNTU (Науковий журнал. Вісник ТНТУ)*, том 2 (74), pp.106-113, Ternopil/Ukraine;
- [2] Baranovsky V.M., Potapenko M.V., (2016), Improvement of the clearing of systems of chicory root heaps. (Вдосконалення очисних систем вороху коренеплодів цикорію), *Scientific journal. Innovative solutions in modern science*, # 1(1), pp.138-146, Dubai/OAE;
- [3] Byrd J., (2008). *Engineering Mathematics (Инженерная математика)*, Dodeka-XXI, Moskva/RF;
- [4] Hevko Iv.B., (2008), *Spiral transport and technological mechanisms, calculation and design (Гвинтові транспортно-технологічні механізми: розрахунок і конструювання)*, Ternopil, TNTU Ivan Pul'uj, Ternopil/Ukraine;
- [5] Hevko Iv.B., (2013), *Scientific and applied basis for the creation of screw transport and technological mechanisms: dissertation thesis (Науково-прикладні основи створення гвинтових транспортно-технологічних механізмів)*, Doctor. Sc. Sciences, National University "Lviv Polytechnic, Lviv/Ukraine;
- [6] Hevko R.B., Dzyura V.O., Romanovsky R.M., (2014), Mathematical model of the pneumatic-screw conveyor screw mechanism operation, *INMATEH, Agricultural Engineering*, vol.44, no.3, pp.103-110, Bucharest/Romania;
- [7] Hevko R.B., Klendiy O.M., (2014), The investigation of the process of a screw conveyer safety device actuation, *INMATEH, Agricultural Engineering*, vol.42, no.1, pp.55-60, Bucharest/Romania;
- [8] Hevko R.B., Zalutskyi S.Z., Tkachenko I.G., et al., (2015), Development and investigation of reciprocating screw with flexible helical surface, *INMATEH Agricultural Engineering*, vol.46, no.2, pp.133-138, Bucharest/Romania;
- [9] Rogatinsky R., (2012), Model of construction and choice of screw conveyors with advanced technological capabilities (Модель конструювання і вибору гвинтових конвеєрів з розширеними технологічними можливостями), *Science journal. Journal of TNTU (Науковий журнал. Вісник ТНТУ)*, том 3 (67), pp.197-210, Ternopil/Ukraine;
- [10] Shipachev V.S., (2003), *Book of problems in higher mathematics (Задачник по высшей математике)*, 3-rd ed., Moskva/Russia;
- [11] Voytyuk D.G., Aniskevych L.V., Baranowsky V.M., et al., (2015), *Agricultural machines (Сільськогосподарські машини)*, Ahrosvita, Kijv/Ukraine.

INVESTIGATION OF DYNAMICAL IMPACT LOADS IN SCREW CONVEYER DRIVES WITH SAFETY CLUTCHES

ДОСЛІДЖЕННЯ ДИНАМІЧНИХ НАВАНТАЖЕНЬ В ПРИВОДАХ ГВИНТОВИХ КОНВЕЄРІВ З ЗАПОБІЖНИМИ МУФТАМИ

Prof.Ph.D.Eng. Lutsiv I.V, Prof. Ph.D. Eng. Hevko I.B., Prof. Ph.D. Eng. Lyashuk O.L., Dubynyak T.S.
 Ternopil Ivan Pul'uj National Technical University, Ternopil / Ukraine
 E-mail: d_taras@ukr.net

Keywords: *impact loadings, screw conveyers, drives, safety clutches*

ABSTRACT

Elastic-conical SCI design for decreasing of impact loadings in half-couplings of screw conveyer safety clutches at the moment of their wearing is offered. Analytical dependence of impact loadings determination at direct and torque shocks in the investigated clutch with gap S of spring installation and certain safety clutch without gap is given. Graphic dependences of these relations on gap S and spring tension C and graphs of axial and rotational velocities dependences on impacts from inclination angle of nonworking limit β are shown.

РЕЗЮМЕ

Запропонована конструкція пружно-конусної ЗМ для зменшення ударних навантажень в півмуфтах ЗМ ГК в момент їх спрацьовування. Приведені аналітична залежність визначення ударних навантажень при осьовому та крутильних ударах в досліджуваній муфті з зазорами S установки пружини і певною запобіжною муфтою без зазору. Наведені графічні залежності цих відносин від зазору S і жорсткості пружини C і графічні залежності осьової і окружної швидкості при ударі від кута нахилу неробочої межі β .

INTRODUCTION

The creation of new and improvement of existing designs of transport and technological mechanisms are favourable for further production development and increase in labour productivity. Screw mechanisms (SM) are integrated parts of production complex mechanization and automation. During transport and technological processes operation with screw conveyers (SC) overloadings caused by technological processes of operations performance as well as stochastic phenomena often occur in their drives. These overloadings result in significant deformations and breakages of screw working parts. It is possible to prevent overloadings of technological character providing efficient filling of SC screw interturn space by transporting material or improving chargers (bins, heads). It is difficult to predict stochastic overloadings but they can be prevented using specially designed safety clutches (SCI) in SC drives constructions.

The problem of the improvement of SM and their safety devices design is investigated by (Zenkov, 1987; Ivashkov, 1987; Kolobov, 1987; Hryhoryev, 1972; Hevko B.M. et al., 1993; Rohatynskiy et al., 2014; Nahornyak et al., 1992).

The researches of some authors (Holybentsev, 1959; Komarov, 1979; Loveykin, 2002; Nesterov, 2002 and other scientists), deal with dynamic processes in machines.

Machine drives are investigated by Malashchenko V.S. (2006); Polyakov V.S. and others (1974); Tepynkycheyev V.K. (1964); Hevko R.B. (2014). At the same time the problem of dynamic behaviour of machine drives with safety mechanisms still remains unsearched hence scientific-practical problem is vital.

MATERIAL AND METHODS

Safety friction, jaw, ball-type clutches, combined elastic-safety clutches (SCI) (Hryhoryev, 1972; Nahornyak, 1992; Malashchenko, 2006; Polyakov et al., 1974), are widely used in SC structures. However not all SCI structures meet the requirements concerning effective kinematic chain interruption in a case when overloading occur in SC. Thus for SC drives protection from overloading the spring-jaw and spring-ball type safety clutches are used at low speeds, small torque moment values and rotating masses of fittings. In a case of high speeds and large masses such clutches form frequent overloadings at the moment of chain reclosing. Mentioned above loadings cause quick wearing of cams and balls surfaces and unstability of rotational torque.

To decrease dynamical impact loadings in half-couplings of screw conveyer safety clutches at the moment of their actuation and increase of their operating life, elastic-conical SCI design represented in Fig. 1 is proposed.

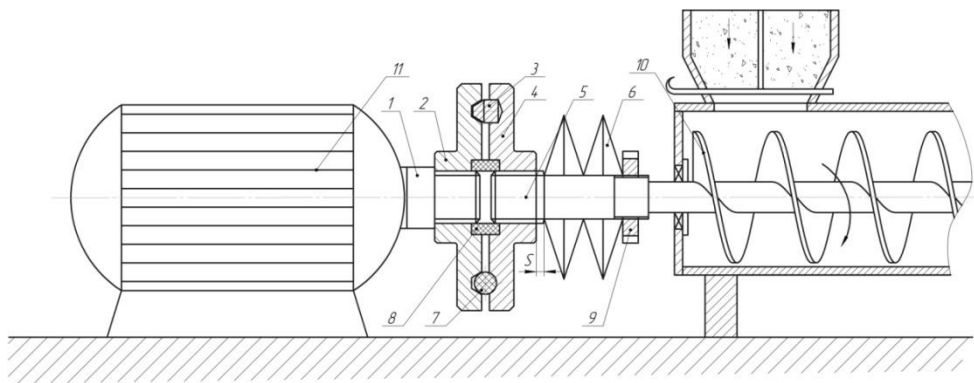


Fig. 1 - Screw conveyor with elastic-conical safety clutch

1 – drive shaft; 2, 4 – driving and driven half couplings; 3 – coupling engagement components (conical pins); 5 – driven shaft; 6 – spring; 7 – holes with balls made of elastic material; 8 – elastic ring; 9 – nut; 10 – screw; 11 – electric motor

Torque moment from electric motor 11 through the driving half coupling 2 and coupling engagement components 3 (pins) of conical shape is transferred to the driven half coupling 4 moving in axial direction and from it to the screw 10 of the screw conveyer. Half couplings are joined by compression spring 6 one end of which rests upon nut end 9 and another upon driven shaft shoulder 5. Thus if no external force is applied to the clutch, the S-sized gap is formed between the driven clutch face and the spring. In such a case at the starting impact moment during actuation time the spring elastic force 6 does not act on the driven half coupling. Besides balls 7 made of elastic materials are located in the grooves on half coupling faces 2 and 4 and elastic ring 8 is mounted in the circular grooves. They cushion axial and radial impacts after actuation.

In a case of the screw overloading and its emergency shutdown the driven shaft 5 stopping takes place. This provides conical pins 3 and balls 7 recession with the holes of driving half coupling 2 and axial movement of driven half coupling 4 with spring 6 compression. SCI restore its engagement when the loading is to decrease to the specified. The computation model of the screw conveyor with elastic-conical SCI is given in Fig.2. Since the equation of connection between driving and driven half couplings in elastic-conical SCI can be considered like in jaw one with identical jaw profiles then the computation model of elastic-conical SCI is reduced to the jaw SCI model.

The clutch dynamic model is the mechanical system consisting of two torque masses 1 and 2 with half couplings at the ends. The given inertia mass moments are equal to I_1 and I_2 correspondingly. Half coupling is freely installed on the shaft of the driven torque mass and is spring-loaded in axial direction by spring of C rigidity with previous compression. Under unloaded conditions acting upon the given mechanical system the gap S is formed between the driven half coupling and the spring.

The moment produced by the motor T_{dr} and the moment transmitted by the clutch T_{act} upon the driving clutch rigidly mounted with torque mass 1. The motion resistant moment produced by the screw T_{sh} and the moment transmitted by the clutch T affect the driven mass 2. The axial force F_{ax} from the driven half coupling side and the spring elastic force F_{el} act upon the moving half coupling.

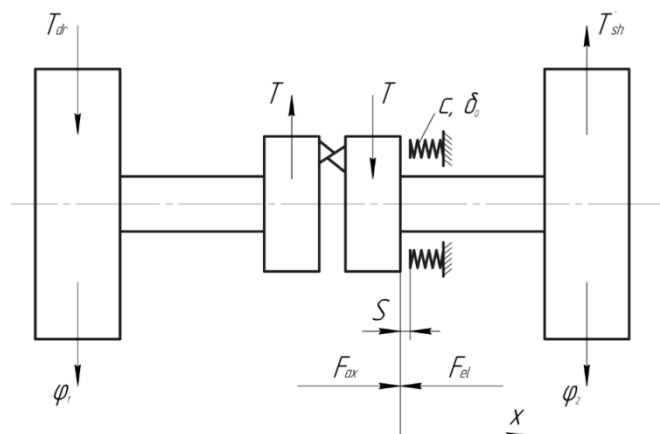


Fig. 2 - The computation model of the screw conveyor with elastic-conical safety clutch

In common case the torque moment produced by the driving mechanism T_{dr} is the function of the rotary speed ω_1 of the driving mass $T_{dr} = f(\omega_1)$. In the given problem definition it is considered to be constant in time: $T_{dr} = const.$

The torque T'_{sh} can be represented as the one consisting of two parts: constant and variable.

$$T'_{sh} = T_{sh} + T_T \quad (1)$$

where: $T_T = f(t - t_1)$ – is its variable component as time function;

t – time;

t_1 – certain time value, starting from action upon the system which changes in time of resistant moment component produced by the driven mechanism.

Longitudinal movement of movable half coupling up to half coupling release equals:

$$x = \frac{D}{2 \cdot \operatorname{tg} \alpha} \psi, \quad (2)$$

where:

D – is the mean diameter of conical pins;

α – is the inclination of holes active faces;

ψ – is the turning angle of rotating mass 1 relatively to rotating mass 2.

The axial force acting from the driving half coupling side on the driven one under the constant contact of conical pins surfaces with holes in half couplings (Polyakov V. S., and others, 1974) is:

$$F_a = \frac{2T}{D} \left[\operatorname{tg}(\alpha - \rho_1) - \frac{D}{d} f_1 \right] \quad (3)$$

where:

ρ_1 – is friction angle between the conical pins and the holes;

d – is shaft diameter with mounted movable half coupling;

f_1 – is coefficient of friction in spline joint.

Spring elastic force affecting the driven movable half coupling equals:

$$F_{el} = c[\delta_0 + x - S] \quad (4)$$

Let us assume that the clutch transmits definite moment. Hence the driven half coupling contacts with the spring one. Thus the movement of the clutch mechanical system is performed providing that $S \leq x \leq h_K$ and is described by the following equation system. (Presented equation system does not consider the vibration damping and rotating mass a 1 and 2 torsional rigidity).

$$\begin{aligned} I_1 \ddot{\varphi}_1 &= T_{dr} - T \\ I_2 \ddot{\varphi}_2 &= T - T_{sh} - T_T \\ m\ddot{x} &= -c(\delta_0 + x - S) + \frac{2T}{D} \left[\operatorname{tg}(\alpha - \rho_1) - \frac{D}{d} f_1 \right] \\ x &= \frac{D}{2 \cdot \operatorname{tg} \alpha} (\varphi_1 - \varphi_2); \quad \psi = \varphi_1 - \varphi_2 \end{aligned} \quad (5)$$

where:

h_K – is the maximum driven clutch move (conical pins height);

φ_1 – is the rotation angle of torsion mass 1;

φ_2 – is the rotation angle of torsion mass 2.

Let us assume that at the time starting moment only the constant resistant moment of motion acts upon the driving rotating mass, i.e. motion takes place at the time moment t and corresponds to inequation $0 \leq t \leq t_1$ thus $T_T = 0$. Reducing the given above equation system we get the following equation:

$$\ddot{\psi} + \frac{chh_1}{I_{el}} \psi = \frac{T_{dr}}{I_{el}} I_2 + \frac{T_{sh}}{I_{el}} I_1 - \frac{ch}{I_{el}} (\delta_0 - S) \quad (6)$$

Here

$$I_{el} = \frac{I_1 \cdot I_2}{I_1 + I_2} + mhh_1; \quad i_1 = \frac{I_1}{I_1 + I_2}; \quad i_2 = \frac{I_2}{I_1 + I_2};$$

$$h_1 = \frac{D}{2 \cdot \operatorname{tg} \alpha}; \quad h = \frac{D}{2 \left[\operatorname{tg}(\alpha - \rho) - \frac{D}{d} f_1 \right]}$$

Symbolizing:

$$\frac{chh_1}{I_{el}} = \omega^2; \quad \frac{T_{dr}}{I_{el}} i_2 + \frac{T_{sh}}{I_{el}} i_1 = \frac{ch(\delta_0 - S)}{I_{el}} = a_1$$

and solving differential equation under initial conditions:

$$\psi|_{t=0} = \frac{a_1}{\omega^2}, \quad \dot{\psi}|_{t=0} = 0$$

we obtain:

$$\psi = \frac{a_1}{\omega^2}$$

or:

$$\psi = \frac{1}{chh_1} [T_{dr} i_2 + T_{sh} i_1 - ch(\delta_0 - S)]$$

Correspondingly:

$$x = \frac{1}{ch} [T_{dr} i_2 + T_{sh} i_1 - ch(\delta_0 - s)] \quad (7)$$

At a certain time moment t_1 the motion resistant moment T_T changing in time is applied to the driven part. Let us assume that this moment depends on time linearly, i.e. $T_T = h(t - t_1)$.

Then at $t \geq t_1$ and $x \leq h_K$ the system movement is described by equation

$$\ddot{\psi} + \frac{chh_1}{I_{el}} \psi = \frac{ki_1}{I_{el}} t + \frac{T_{dr} i_2 + T_{sh} i_1 - ch(\delta_0 - S) - hi_1 t_1}{I_{el}}. \quad (8)$$

Accepting previous symbols and assuming that $\frac{ki_1}{I_{el}} = a_2$ under initial conditions $\psi|_{t=t_1} = \frac{a_1}{\omega^2}$,

$\dot{\psi}|_{t=t_1} = 0$, we solve the equation in the form of:

$$\psi = -\frac{a_2}{\omega^3} \sin[\omega(t - t_1)] + \frac{a_2}{\omega^2} (t - t_1) + \frac{a_1}{\omega^2} \quad (9)$$

The movement according to the defined regulation is taking place until conical pins recession. Dynamic system behaviour after conical pins recession is described by the following equation system:

$$\begin{cases} I_1 \ddot{\phi}_1 = T_{dr}; \\ I_2 \ddot{\phi}_2 = -T_{sh} - k(t - t_1); \\ m\ddot{x} = -c(x + \delta_0 - S). \end{cases} \quad (10)$$

The solution of the given (10) equation system is:

$$\begin{cases} \psi = \left(\frac{T_{dr}}{I_1} + \frac{T_{sh}}{I_2} - \frac{kt_1}{I_3} \right) \frac{t^2}{2} + \frac{k}{I_2} \cdot \frac{t^3}{6} + C_{31} t + C_{32} \\ x = C_3 \cdot \sin \left(\sqrt{\frac{C}{m}} t + \gamma_3 \right) - (\delta_0 - S) \end{cases} \quad (11)$$

Constants C_{31} , C_{32} , C_3 , γ_3 are derived from the initial conditions determined by equation (10) at $x = h_K$.

After conical pins recession they contact again (now by their nonworking surfaces) and their mutual sliding occurs up to the moment of their working surfaces impact.

Conical pins contact following the recession takes place when:

$$x = \frac{2 \cdot h_1 h_k (tg\alpha + tg\beta)}{2 \cdot h_1 tg\beta + D} \quad (12)$$

where: β – inclination angle towards the vertical of conical pins nonworking surfaces.

The value of the axial force acting from the driving half coupling side upon the driven one after contact recovery under conical pins mutual sliding along the holes by nonworking surfaces is equal:

$$F_{ax} = \frac{2T}{D} \left[tg(\beta + \rho_1) - \frac{D}{d} f_1 \right] \quad (13)$$

and the axial displacement of the driven half coupling is:

$$x = h_k \left(1 + \frac{h_2}{h_1} \right) - h_2 \psi$$

where: $h_2 = \frac{D}{2 \cdot tg\beta}$

The equation system describing the process of conical pins sliding by their nonworking surfaces along the holes takes the form:

$$\begin{cases} I_1 \ddot{\phi}_1 = T_{dr} + T; \\ I_2 \ddot{\phi}_2 = -T - T_{sh} - T_T; \\ m\ddot{x} = F_{ax} - c(x + \delta_0 - S). \end{cases} \quad (14)$$

The initial conditions are determined at the moment of contact. Mathematical description of this process is approximate as it is unknown how speeds are distributed after the contact and if the mutual sliding of conical pins along the holes without failure actually occurs.

Within limits of the given problem set we consider that the contact of conical pins nonworking surfaces along the holes goes on “smoothly” without rebound and the impact is nonelastic i.e. relative speed of conical pins at the moment after the impact is equal to the projection of this speed before the impact on the axes coinciding with the direction of the conical pins nonworking surface (fig.3), that is:

$$v_{ai} = -\dot{x}_i \cos \beta + R\dot{\psi}_i \cdot \sin \beta \quad (15)$$

Consequently (15)

$$\dot{x}_{ai} = \dot{x}_i \cos^2 \beta - R\dot{\psi}_i \cdot \sin \beta \cdot \cos \beta; \quad \dot{\psi}_{ai} = -\frac{\dot{x}_i}{R} \sin \beta \cdot \cos \beta + \dot{\psi}_i \sin^2 \beta \quad (16)$$

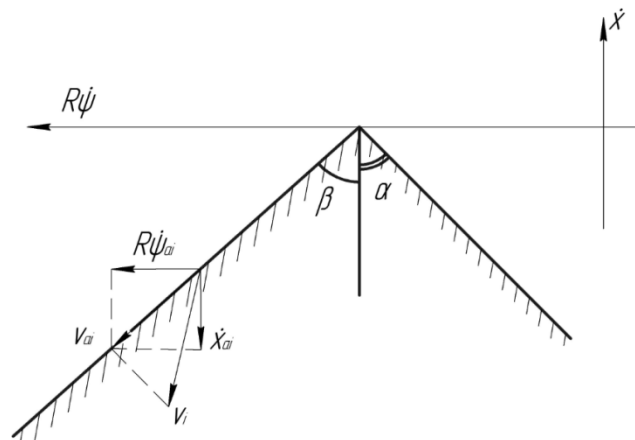


Fig. 3 – The calculation scheme of the conical pins nonworking surfaces contact along the holes

Here indexes i impact and ai after impact define the speeds at the moment of time that directly precedes the holes contact and moment of time that occurs directly after the moment of contact between nonworking surfaces of half coupling holes.

Equation system (14) can be reduced to the equation:

$$\ddot{\psi} + \frac{ch_2h_3}{I_{el}^*} \psi = T_{dr} \frac{i_2}{I_{el}^*} + \frac{T_{sh}}{I_{el}^*} i_1 + \frac{ki_1}{I_{el}^*} (t - t_1) + \frac{ch_3}{I_{el}^*} \left[\delta_0 - S + h_k \left(1 - \frac{h_2}{h_1} \right) \right] \quad (17)$$

where: $I_{el}^* = \frac{I_1 \cdot I_2}{I_1 + I_2} + mh_2h_3$; $h_3 = \frac{D}{2 \left[\text{tg}(\beta + \rho_1) - \frac{D}{d} f_1 \right]}$

Introducing symbols $\omega_2^2 = \frac{ch_2h_3}{I_{el}^*}$; $b_3 = \frac{k}{I_{el}^*} \cdot i_1$; $a_3 = \frac{1}{I_{el}^*} \left\{ T_{dr}i_2 + T_{sh}i_1 + ch_3 \left[\delta_0 - S + h_k \left(1 + \frac{h_2}{h_1} \right) \right] \right\}$,

and solving differential equation (17) we obtain:

$$\psi = C_4 \cdot \sin(\omega_2 t + \gamma_4) + \frac{b_3}{\omega_2^2} (t - t_1) + \frac{a_3}{\omega_2^2} \quad (18)$$

Constants C_4 and γ_4 are determined from the initial conditions.

The equation (18) describes the process until the moment when spring elastic force F_{el} affects the driven half coupling. The spring interrupts its action at $x < S$.

Equation describing the system motion after interruption of the spring action is:

$$\ddot{\psi} = \frac{1}{I_{el}^*} [T_{dr}i_2 + T_{sh}i_1 + k(t - t_1)i_1] \quad (19)$$

Taking into account the introduced symbol $a_4 = \frac{1}{I_{el}^*} (T_{dr}i_2 + T_{sh}i_1)$, the solution of this differential equation (19) takes the following form:

$$\psi = a_4 \frac{t^2}{2} + b_3 \frac{(t - t_1)^3}{6} + C_{41}t + C_{42}; \quad x = h_k \left(1 + \frac{h_2}{h_1} \right) - h_2\psi \quad (20)$$

Constants C_{41} and C_{42} are determined from the initial conditions at the moment of time when the spring interrupts its action that is $x = S$.

The impact of conical pins by their working surfaces occurs when $x = 0$. Dynamic loadings originated from conical pins of half couples impact by working surfaces result in increased wear of the impact surfaces and short clutch life (service time decrease). Dynamic loadings F_d on impact are determined from static ones F_{st} multiplying them by dynamic coefficient K_d :

$$F_d = F_{st} \cdot K_d \quad (21)$$

In the given case both axial impact of half couplings and torque impact by driving and driven rotating masses occur. That is why we should distinguish the axial impact loading F_d of axial impact and dynamic impact moment T_i of torque impact.

Thus dynamic coefficients K_{Fd} and K_{Td} are different. Let us consider the case of impact loadings effect on axial and torque impacts in the investigated clutch with spring installation gaps S and certain safety clutch without gap. All values related to the investigated clutch are indicated by index 1 and those related to the given clutch by index 2.

At the impact moment the static torque moments in both clutches are equal to:

$$\begin{aligned} T_{st1} &= T_{dr}i_2 + T_{sh}i_1 + ki_1(t - t_1); \\ T_{st2} &= T_{dr}i_2 + T_{sh}i_2 + ki_1(t - t_1) + ch_3\delta, \end{aligned} \quad (22)$$

where: δ - preload adjustment of the spring regulating the clutch transfer moment in the known clutch.

Static axial loadings are equal to:

$$F_{st1} = \frac{T_{st1}}{h_3}; F_{st2} = \frac{T_{st2}}{h_3}. \tag{23}$$

To compare dynamic impact loadings in the investigated and given clutches we should find the ratio of these loadings in the above mentioned clutches. As it is difficult to determine the values of dynamic coefficients because of complexity of occurred processes let us assume dynamic coefficients to be approximately proportional to the speed modules at the impact moment:

$$K_{Fd} = |\dot{x}_i| \cdot K_{F_0} \quad K_{Td} = |\dot{x}_i| \cdot K_{T_0} \tag{24}$$

where: K_{F_0}, K_{T_0} - are proportionality coefficients correspondently.

Then in a case of torque impact we have

$$\frac{T_{d1}}{T_{d2}} = \frac{\dot{\psi}_{i1}}{\dot{\psi}_{i2}} \cdot \frac{T_{st1}}{T_{st2}}, \tag{25}$$

or
$$\frac{T_{d1}}{T_{d2}} = \frac{\dot{\psi}_{i1}}{\dot{\psi}_{i2}} \cdot \frac{T_{st1}}{T_{st1} + ch_3\delta}$$

On axial impact (since $\dot{x}_1 = -h_2\dot{\psi}_i$ and $F_{st} = \frac{T_{st}}{h_3}$):
$$\frac{F_{d1}}{F_{d2}} = \frac{T_{d1}}{T_{d2}} = \frac{\dot{\psi}_{i1}}{\dot{\psi}_{i2}} \cdot \frac{T_{st1}}{T_{st1} + ch_3\delta}.$$

RESULTS

Computer investigation of dynamics of proposed and given safety clutches enables to determine axial and angular mass velocities at the moment of conical pins impact by their working surfaces and relative dynamic impact loadings.

The graph dependences on gap S and spring rigidity C and graph dependences of axial and rotational velocities on impacts from inclination angle of nonworking limit β are shown in Fig. 5 and Fig. 4.

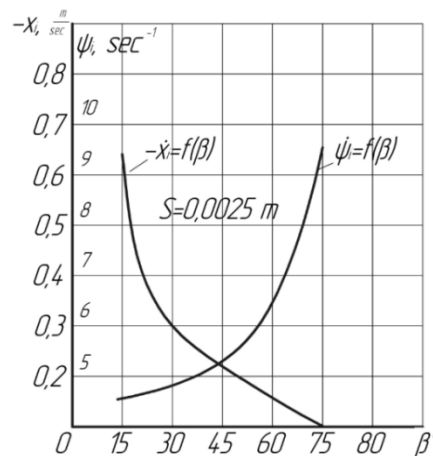


Fig. 4 – Dependences of axial and rotational velocities of half couplings on inclination angle of conical pins active faces (engagement elements)

It is evident from the graphs that the proposed safety clutch with the spring installed with the gap makes it possible to reduce impact loadings by 10–15%. in comparison with the given one. It is advantageous to use conical pins with active faces 45° inclination angle as in this case the axial and rotational velocities of half couplings on impacts are minimal (Fig. 4).

When the gap S increases, the dynamical impact loadings slightly decrease but the clutch loses its sensitivity and is unable to activating after the overload removal. That is why it is reasonable to make effective use of clutch designs with gaps $S = 1 \div 2$ mm.

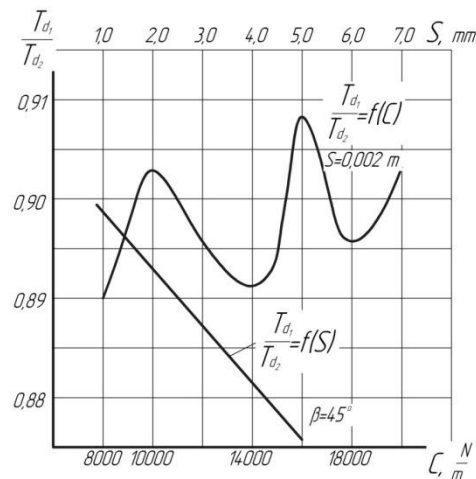


Fig. 5 – Dependences of axial and rotational velocities of half couplings on inclination angle of conical pins nonworking faces (engagement elements)

With the spring rigidity increase the dynamic impact loadings occurrence in compared clutches have zigzag-shaped changes but within small limits (Fig. 5). That is why it is advisable to use springs with 14000 N/m rigidity.

CONCLUSIONS

Carried out experiments proved that the offered elastic-conical safety clutch of screw conveyer provides significant reduction of dynamic impact loadings under screw overloadings, increases accuracy of automatic half couplings reconnection after loading removal and at the same time considerably increases reliability and service life of screw conveyer driving mechanisms.

REFERENCES

- [1] Hevko B.M. and others, (1993), *Mechanisms with screw devices (Механізми з гвинтовимй пристроями)*, Svit, p. 208, Lviv;
- [2] Hevko R.B., Klendiy O.M., (2013), Methodology of investigation of a screw conveyer with a safety device (Методика проведення досліджень шнекового транспортера із запобіжним пристроєм) *Agricultural Machinery: Scientific works. (Сільськогосподарські машини: Збірник наукових статей)*, No. 24, Edition of Lutsk NTU, pp. 67–75, Lutsk;
- [3] Hevko R.B., Klendiy O.M., (2014), The investigation of the process of a screw conveyer safety device actuation, *INMATEH: Agricultural Engineering*, vol.42, no.1, pp. 55-60;
- [4] Holubentsev A.N., (1959), Dynamics of transition processes in machines with multiple masses (Динамика переходных процессов в машинах со многими массами), *МАШНИЗ*, p.180, Moscow;
- [5] Нгуогуев А.М., (1972), Screw conveyers (Винтовые конвейеры), *Mechanical engineering*, p.184, Moscow;
- [6] Комаров М.С., (1979), Dynamics of machines (Динамика машин), *Machynostroyenie*, p.342, Moscow;
- [7] Loveykin V.S., Nesterov A.P., (2002), *Dynamic force of lifting machines optimization (Динамическая сила оптимизация подъемных машин)*, LNU Press, p. 387, Luhansk;
- [8] Malashchenko V.O., (2006), Drivers clutches, *Designs and calculation samples (Муфти приводів. Конструкції та приклади розрахунків)*, National University «Lvivska Polytechnika», p.196, Lviv;
- [9] Nahornyak S.H., and others, (1992), Safety mechanisms of metal machining equipment: Reference guide (Предохранительные механизмы металлообрабатывающего оборудования: Справочник), *Technika*, p. 72, Kyiv;
- [10] Polyakov V.S., and others, (1974), Reference guide on clutches (Справочник по муфтам), *Machynostroyenie*, p. 352, Moscow;
- [11] Rohatynskiy R.M., and others, (2014), *Scientific applied foundations of screw transport-technological mechanisms creation (Наукові прикладні основи створення гвинтових транспортно-технологічних механізмів)*, p.280, Ternopil;
- [12] Терункучуев V.K., (1964), Safety machinery from machine tools overloading (Предохранительные устройства от перегревки станков), *Machynostroyenie*, p. 157, Moscow;
- [13] Zenkov R.L., (1987), Stream-flow transportation machines (Машины непрерывного транспорта), *Mechanical engineering*, p.320, Moscow.

A SWITCHING CONTROL STRATEGY OF GREENHOUSE COOLING SYSTEM BASED ON TEMPERATURE PREDICTION MODEL FOR ENERGY SAVING

基于温度预测模型的温室降温系统的节能切换控制

Ph.D. Stud. Zhenfeng Xu¹⁾, Prof. Ph.D. Junjie Chen^{*1)}, Assoc. Prof. Ph.D. Gang Yu²⁾, Ms. Yahui Wang¹⁾

¹⁾ School of Instrument Science and Engineering, Southeast University / China;

²⁾ Jiangsu Academy of Agricultural Sciences / China

E-mail: inschenjj@seu.edu.cn

Keywords: switching control, prediction mode, energy saving, greenhouse, temperature

ABSTRACT

In order to reduce the energy consumption of greenhouse cooling in subtropical and tropical regions, we proposed a switching control strategy based on temperature prediction model. Due to the facilities driven by the on-off actuators in many greenhouses, the cooling system was treated as a hybrid system with discrete operating modes. When the indoor air temperature reaches the upper limit set by growers, the IARX model in each mode is used to predict the indoor air temperature over a specified horizon respectively. Then the energy consumption of each mode is pre-estimated and the mode with minimum estimation is selected. The control strategy was simulated. The energy saving potential of the proposed control strategy is related to a variety of factors. In this simulation, the results indicate that the control strategy saves 15.4% energy within the temperature range (20°C, 30°C); while it saves 24.6% energy within the temperature range (24°C, 30°C), compared with a reference with fixed switching rules. Finally, the main influencing factors of energy consumption were discussed. The conclusions are instructive for the future application of the control strategy.

摘要

为减少热带和亚热带地区温室降温能耗，提出了一种基于温度预测模型的切换控制策略。由于许多温室内的设备采用开关控制，因此把降温系统看作为带有离散运行模式的混杂系统。当温室内空气温度超过设定上限时，分别使用每种模式下的 IARX 温度预测模型预测未来有限时域内温度的变化。然后评估每种模型的能耗，并选择出能耗最小的那种运行模式。对该控制策略进行了仿真。其节能潜能与多种因素有关。在该仿真中，与一个使用固定切换规则的参考控制方法相比，当温度范围为时(20°C, 30°C)，该控制策略可以节能 15.4%；而当温度范围为(24°C, 30°C)，该控制策略可以节能 24.6%。最后讨论了影响能耗的最要因素。相关结论对于该控制策略的今后使用具有指导意义。

INTRODUCTION

A greenhouse is a plastic or glass building that can provide a suitable microclimate for plants, protecting them from severe and variable outdoor weather conditions. As a result, many greenhouses can operate all year round and produce much higher yields than the open land cultivation. However, the greenhouse production system consumes much more energy. The energy is consumed mainly for heating in cold regions (Sethi et al., 2008; Vadiiee et al., 2014), and for cooling in subtropical and tropical regions (Kumar et al., 2009; Sethi et al., 2007). South China is located in the subtropical region, so the greenhouses in this area usually need cooling in most time of a year. In order to reduce the consumption of electric energy and fossil fuels for greenhouse cooling, some researchers tried to use renewable energy, such as solar energy (Chungloo et al., 2007; Cuce et al., 2016;), geothermal energy (Ozgener et al., 2010; Sethi et al., 2007), etc. The use of renewable energy has a significant potential to reduce the consumption of conventional energy, but their systems are very complicated and the initial construction costs are very high, so that it is difficult to popularize these alternative methods. Another way to reduce the consumption of conventional energy is to design new control methods. Because the facilities in many greenhouses are driven by the on-off actuators (Teitel et al., 2004), it's difficult to use the conventional control methods, such as PID control (Hu et al., 2010), model predictive control (Blasco et al., 2007), fuzzy control (Nachidi et al., 2010), etc., and the operating mode of greenhouse cooling system can be divided into different sub-modes. The greenhouse control system is treated as a hybrid system in this paper, due to the interaction between discrete on-off control signals and continuous environmental factors (Lin et al., 2014).

At present, hybrid systems have been widely applied in many fields (Balluchi et al., 2013; Febbraro et al., 2016), but rarely used in the greenhouse control system. Yang et al. adopted hybrid automata and studied the modeling and control of the temperature system in a greenhouse with only one on-off ventilation window (Yang et al., 2011). Chu et al. also studied the temperature control system based on hybrid automata in a greenhouse with three facilities, i.e., a roof window, a fan and a wet pad (Chu et al., 2015). However, the energy-saving issue was not considered in their studies. Another problem is that the design of switching rules is very complicated when there are multiple facilities, because several environmental factors have to be taken into account, such as indoor and outdoor air temperature, solar radiation, etc.

We proposed a switching control strategy of different cooling modes based on temperature prediction model for energy saving, because some simple temperature prediction models have been developed for control purposes (Frausto et al., 2003; Xu et al., 2016). The rest of the article is organized as follows. In Material and Method section, the proposed switching control strategy for energy saving is described at first. Then the simulation experiments are designed and a mechanistic model is used to test the energy-saving effect of the proposed control strategy. In Results section, the simulation results are introduced at first. Then, the energy-saving potential of the proposed control strategy is analysed by comparison with a reference one with fixed switching rules. At last, the main influencing factors of energy consumption are also discussed. The paper is concluded at last.

MATERIAL AND METHODS

Switching control strategy for energy saving

In subtropical and tropical regions, there are usually multiple cooling facilities installed in a greenhouse. Four common kinds of facilities are considered in this research, i.e., roof windows, fans, a wet pad and external shading net. Assume that they are all driven by the on-off actuators, which is in accordance with the actual situation of many greenhouses. According to the first three kinds of facilities, the greenhouse operation is divided into three modes, i.e., natural ventilation mode, mechanical ventilation mode and pad-fan cooling mode. When all the facilities don't work, the operating mode is called passive mode in this paper. The operation process can be regarded as a switching one among the four modes, and the greenhouse is in only one of the four modes at any time. The shading net also affects the indoor air temperature, but it is not used to divide the operating modes, because it is folded or unfolded, mainly depends on the solar radiation intensity, having little containment relationship with the above four operating modes. Therefore, the shading net can be folded or unfolded, no matter that the greenhouse is in any of the operating modes. The switching control system of the greenhouse is shown in Fig.1. The outdoor environmental factors are used as input to the controller to facilitate the construction of indoor air temperature prediction model.

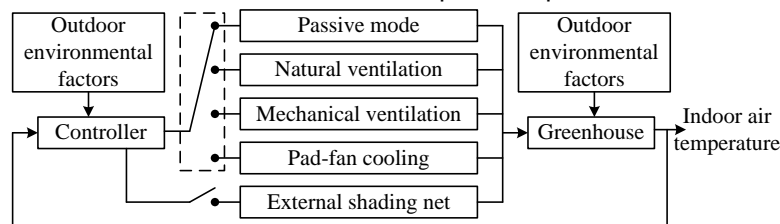


Fig.1 - The greenhouse cooling system

We proposed a new switching control strategy based on temperature prediction model to reduce the energy consumed for greenhouse cooling. At first, it's necessary to construct the prediction model of indoor air temperature in each cooling mode. At present, there are three kinds of prediction models, i.e., mechanistic model (Singh et al., 2006), ARX model (auto regressive prediction model with external variables) (Frausto et al., 2003) and neural network model (Frausto et al., 2004). The ARX model is simpler and has smaller computational burden than the other two kinds, so it is often used for control purposes. We have constructed the temperature prediction models in different operating modes based on the analysis of mechanistic models, called IARX (incremental ARX) model (Xu et al., 2016). The IARX models have fewer coefficients than typical ARX models, so they are more suitable for online identification in real-time control. The IARX prediction models of indoor air temperature in the natural ventilation mode and mechanical ventilation mode have the same form, shown as Eq.(1); while the prediction model in the pad-fan cooling mode is shown as Eq.(2).

$$\Delta T_i(k+1) = \alpha_1 \Delta T_{oi}(k) + \beta_1 R_{out}(k) + \varepsilon \quad (1)$$

$$\Delta T_i(k+1) = \alpha_1 \Delta T_{oi}(k) + \beta_1 R_{out}(k) + \gamma_1 \Delta T_{pi}(k) + \varepsilon \quad (2)$$

where $\Delta T_i(k+1)$ denotes the difference of indoor air temperature at the time instants $k+1$ and k ($^{\circ}\text{C}$); $\Delta T_{oi}(k)$ the difference of outdoor and indoor air temperature at the time instant k ($^{\circ}\text{C}$); $\Delta T_{pi}(k)$ the difference of indoor air temperature and that of the wet air that just passes through the pad at the time instant k ($^{\circ}\text{C}$); $R_{out}(k)$ the solar radiation intensity at the time instant k (W/m^2); α_1 , β_1 , γ_1 and ε are all coefficients.

When the models are used to predict temperature at the time instant $k+i$ ($i>1$), it is necessary to provide the data of relevant environment factors at time $k+i-1$. However, the environmental data at future time instants are unknown in the actual control process. We will adopt the lazy man weather prediction method (Tap et al., 1996), in which the environmental factors remain unchanged over a specified horizon. The prediction method is effective when the horizon is not too long.

Assume the greenhouse is in the passive mode and the shading net is folded at the beginning. When the indoor air temperature reaches the upper limit, the model in each cooling mode is used to predict the indoor air temperature over a specified horizon respectively. Natural ventilation is the first choice because it consumes very little energy. As long as the predicted temperature in the natural ventilation mode is within the set range, this mode is selected directly and it is not necessary to consider the other two cooling modes. If the natural ventilation mode cannot reduce the indoor air temperature below the upper limit, the other two cooling modes will be adopted. Different from the natural ventilation mode, the mechanical ventilation mode and pad-fan cooling mode both consume much more energy. Of course, their capacities for cooling are significantly enhanced. In particular, the pad-fan cooling mode can reduce the indoor air temperature lower than that outside. In order to forbid the two cooling modes to run for too long time, we set the selection and stopping criteria for the two modes. The mechanical ventilation mode is taken for example. When the indoor air temperature reaches the upper limit and the predicted temperature over a specified horizon in the natural ventilation mode is also higher than the upper limit, the temperature model in the mechanical ventilation mode is used to predict over a specified horizon. If the predicted temperature can reach the lower limit, the cooling mode may be selected. The cooling mode is stopped when the indoor air temperature reduces to the average of the upper and lower limits. The selection and stopping criteria can ensure that the running time of mechanical ventilation is not more than the prediction horizon. The selection of pad-fan cooling mode is the same. If only one of the two cooling modes meets the selection criterion, it will be selected. If both modes meet it, it's required to make further judgments between them. We pre-estimate the energy consumption of the two cooling modes based on the prediction results over a specified horizon respectively. The algorithm is shown in Eq.(3), and the cooling mode with the smaller estimation will be selected.

$$\begin{aligned} J &= P \cdot n \cdot \Delta t \\ \text{s.t. } T_{pred}(k+n|k) &\geq T_a \\ T_{pred}(k+n+1|k) &< T_a \\ 1 &< n < N \end{aligned} \quad (3)$$

where the letter J denotes the energy consumption (J); P denotes the operating power of cooling mode (W); Δt the sampling period (s); N the length of prediction horizon (measured by the number of sampling periods); n the length of the continuous operation of cooling mode; $T_{pred}(k+j|k)$ the prediction value of indoor air temperature at the time instant $k+j$ ($^{\circ}\text{C}$); T_L the lower limit ($^{\circ}\text{C}$); T_a the average of the upper and lower limits ($^{\circ}\text{C}$).

The selection process of cooling modes will be repeated every time when the indoor air temperature reaches the upper limit. Assume that the pad-fan cooling mode can meet the cooling requirements in any case, which is consistent with the real situations of many greenhouses. In the above control process, two thresholds are set for the shading net. When the solar radiation intensity exceeds the high threshold, the shading net is unfolded; while when the solar radiation intensity reduces to the low threshold, the shading net is folded. The difference between the two thresholds is helpful to avoid frequent switching of the shade net. The accuracy of temperature prediction models is very important to the switching control strategy. In order to obtain good accuracy, the receding horizon method is adopted to update the model coefficients in time (Tap et al., 1996). Therefore, the switching control of cooling modes can be implemented for energy saving.

Simulation experiments

We have constructed a mechanistic model of Venlo-type glass greenhouse microclimate to develop new control strategies and the discrete on-off control characteristics are fully considered (Xu et al., 2016).

The mechanistic model of greenhouse temperature system is shown as Eq.(4), and we will use it to simulate the proposed switching control strategy.

$$\begin{cases} \rho_a V_g C_a \frac{dT_{in}(t)}{dt} = Q_{radin}(t) - x_1 Q_{nv}(t) - x_2 Q_{mv}(t) - x_3 Q_{pf}(t) - Q_{exch}(t) - Q_{tran}(t) \\ s.t. \sum x_j \leq 1, x_j = 0, 1 (j=1, 2, 3) \end{cases} \quad (4)$$

where ρ_a denotes the air density (g/m^3); V_g the greenhouse volume (m^3); C_a the air specific heat ($\text{J}/(\text{g}^\circ\text{C})$); $T_{in}(t)$ the indoor air temperature ($^\circ\text{C}$); t time (s); $Q_{radin}(t)$ the solar radiation power received in the greenhouse (W); $Q_{nv}(t)$ the power loss caused by natural ventilation (W); $Q_{mv}(t)$ the power loss caused by mechanical ventilation (W); $Q_{pf}(t)$ the power loss caused by pad-fan cooling (W); $Q_{exch}(t)$ the power loss caused by the energy exchange through cover layer (W); $Q_{tran}(t)$ the power loss of crop transpiration (W); x_j ($j=1, 2, 3$) decision variables and have values of either 0 or 1 (0 denotes OFF and 1 ON). There is at most one decision variable with the value 1 at any time, according to the operating process of greenhouse described in above switching control strategy section.

Before simulation, the data of four outdoor environmental factors should be provided, i.e., outdoor air temperature, relative humidity, solar radiation intensity and wind speed. A sunny day, Apr. 22, 2014 in Nanjing area is selected. Because cooling is not necessary at night, the control experiments are only simulated in day time and the simulation period is set to 7:30-16:30. The four outdoor environmental factors during this period are shown in Fig. 2.

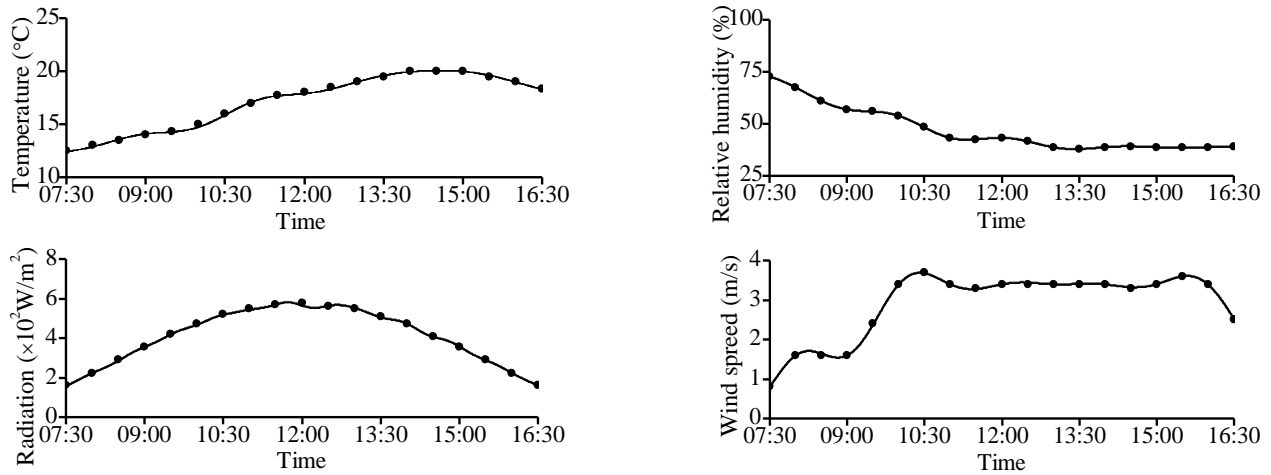


Fig. 2 - Four outdoor environmental factors

The facilities in simulation are consistent with that in the greenhouse which is used to verify the above mechanistic model. There are four ventilation fans, which are controlled by the same on-off drive signal. The greenhouse operates in mechanical ventilation mode when only the fans are switched on. The total area of roof windows is about tenth of the greenhouse area, with the maximal opening angle 30° . The greenhouse operates in mechanical ventilation mode when only the roof windows are switched on. There is a shade net above the greenhouse, the light transmission of which is about 50%. The thresholds for the shading net are set to 420 W/m^2 and 400 W/m^2 . The IARX model includes solar radiation intensity, so the working state of shading net will affect the prediction results. The IARX models expressed in Eq.(1) and Eq.(2) are revised based on the on-off characteristic of shading net, and the revised IARX models are as follows respectively.

$$\Delta T_i(k+1) = \alpha \Delta T_{oi}(k) + \beta(1 - x_4 \eta) R_{out}(k) + \varepsilon \quad (5)$$

$$\Delta T_i(k+1) = \alpha \Delta T_{oi}(k) + \beta(1 - x_4 \eta) R_{out}(k) + \gamma \Delta T_{pi}(k) + \varepsilon \quad (6)$$

where x_4 is the control signal of shading net (0 denotes OFF and 1 ON); η the light transmission (50%).

The operation powers of all facilities are required to calculate the energy consumption of greenhouse operation. The rated power of each fan is 1KW, and that of wet pad is 2KW. While compared with fans and wet pad, the energy consumption of roof windows and the shading net is very little, so they are neglected. It has been found that the indoor air temperature can reach a steady state within 10 minutes after the greenhouse entered into a new operating mode in actual tests (Xu et al., 2016), so the prediction horizon is set to 10 minutes. In order to study the influence of the upper and lower limits and the set range of temperature on the energy consumption, we set three temperature ranges. The butterfly orchid plant were

potted in greenhouse when the mechanistic model was verified (Xu *et al.*, 2016), so the temperature ranges are set as (20°C, 30°C), (24°C, 30°C) and (22°C,32°C), and they are numbered as case 1, 2 and 3, for easy identification. The above simulation experiments will be done in the three cases.

The IARX prediction models should be identified at first before use. For convenience, for the first three cooling requirements, the greenhouse is forced to enter into the three cooling modes successively. In order to obtain enough environmental data for model identification, the sampling period is set to 30s. After the first three cooling actions, the proposed control strategy is adopted for the greenhouse cooling system. As previously mentioned, the receding horizon method is adopted to update the model coefficients.

In order to explore the energy saving potential of the proposed control strategy, we designed a reference one without any temperature prediction model. The reference control strategy operates with fixed switching rules, which is described as follows. At the beginning, assume the greenhouse is in the passive mode and the shading net is folded. When the indoor air temperature reaches the upper limit, the natural ventilation mode is adopted at first. If the natural ventilation mode cannot meet the cooling requirement, the mechanical ventilation mode will be adopted. In order to prevent the fans from running for too long time, if the indoor air temperature cannot be reduced to the average of the upper and lower limits within five minutes, the greenhouse will be forced to transfer into the pad-fan cooling mode. When the indoor air temperature reaches the upper limit every time, the cooling mode adopted last time will be adopted at first. After unfolding the shading net, the switching process will repeat the above switching rules, and the natural ventilation mode is the first choice for cooling. Except for the switching rules, the other settings are the same as that in the proposed control strategy. The control strategies are programmed and simulated in MATLAB software.

RESULTS

The dynamic behaviours of indoor air temperature in the three cases are shown in Fig. 3 to Fig. 8. The simulation results indicate that the two switching control strategies can meet the cooling requirement. The operating times of three cooling modes are counted in the three cases for the two control strategies, and listed in Table 1. The energy consumption of the two control strategies is calculated and shown in Table 2. The results in case 1 and case 2 indicate that the proposed control strategy has a good potential for energy saving. The results in case 3 will be analysed specially below.

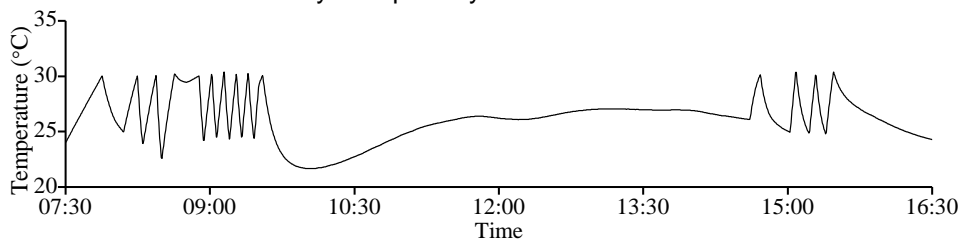


Fig.3 - The indoor air temperature of the proposed control strategy in case 1

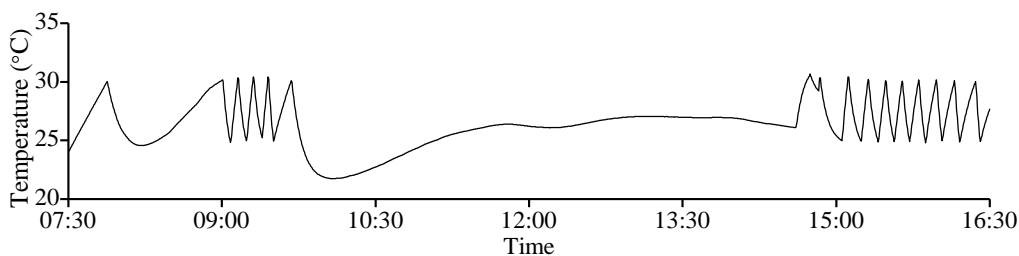


Fig.4 - The indoor air temperature of the reference control strategy in case 1

In case 1 and case 2, the dynamic behaviours of indoor air temperature simulated by the two control strategies are different, and the main difference appears in the later stage of the simulation process. The reason is as follows. For the proposed control strategy, the mode switch is based on the real-time prediction results. The prediction results of temperature models change with the outdoor environmental factors, so the proposed control strategy can choose the natural ventilation mode in time with the decrease of outdoor air temperature and solar radiation. Therefore, the proposed control strategy has a good adaptive ability,

compared with the reference one. The proposed control strategy can save energy about 15.4% compared with the reference in case 1; while it can save energy about 24.6% in case 2.

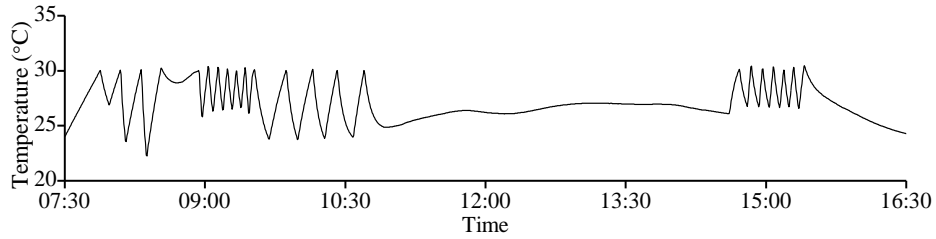


Fig.5 - The indoor air temperature of the proposed control strategy in case 2

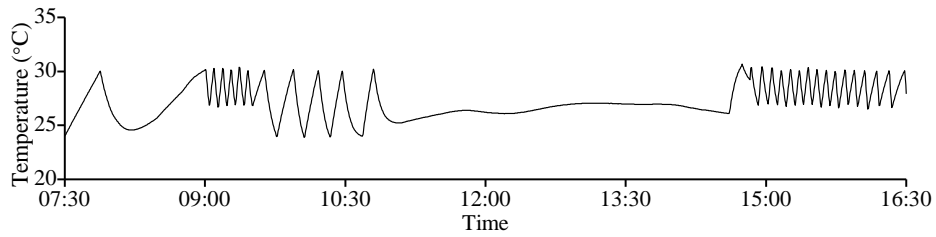


Fig.6 - The indoor air temperature of the reference control strategy in case 2

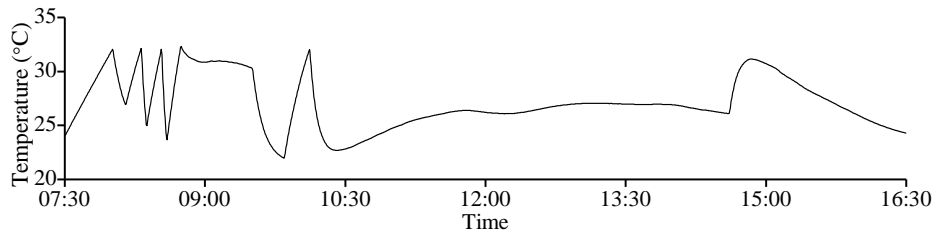


Fig.7 - The indoor air temperature of the proposed control strategy in case 3

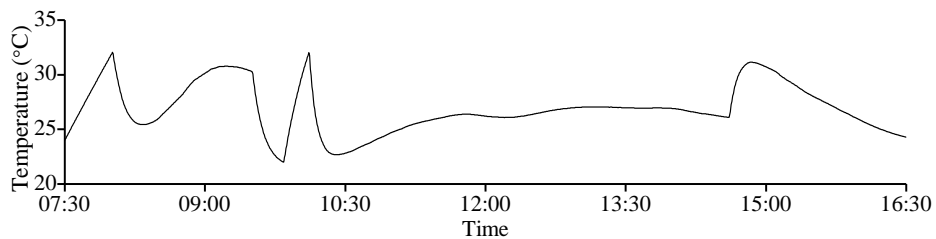


Fig.8 - The indoor air temperature of the reference control strategy in case 3

Table 1

The operating times of cooling modes in both control strategies

Case	Proposed control strategy (min)			Reference one (min)		
	NV	MV	PF	NV	MV	PF
1	400	3	53	371	20	52
2	371	15	33	340	22	42
3	458	3	3	493	0	0

Note: NV natural ventilation; MV denotes mechanical ventilation mode; PF pad-fan cooling mode.

Table 2

Comparison of energy consumption of two control strategies

Case	Proposed control strategy (kW.h)	Reference one (kW.h)	Energy saving [%]
1	5.5	6.5	15.4
2	4.3	5.7	24.6
3	0.5	0	--

The simulation results in case 3 are very different from that in the first two cases. The natural ventilation mode can meet the cooling requirement very well in case 3, so both the control strategies almost don't consume energy. The proposed control strategy consumes a little energy because of the first three fixed cooling actions. It can be seen that the upper limit has a great influence on the energy consumption for greenhouse cooling. The higher the upper limit is, the less the energy consumption will be. According to the temperature integration theory (Sigrimis *et al.*, 2000), a short-term high temperature has little effect on crops. Therefore, in some cases, allowing the indoor air temperature to exceed the upper limit briefly will be helpful for energy saving.

According to the results in case 1 and case 2, the different energy saving effect indicates that the set temperature bandwidth has influence on the energy saving potential. In case 2, the temperature bandwidth is narrower, while the energy consumption is less. According to previous studies (Gu *et al.*, 2001), the indoor air temperature changes in the form of a negative exponential function during the cooling process, and thus the energy for reducing 1°C is more and more as the indoor air temperature is reduced. Therefore, the narrow range is conducive to save energy. However, the simulation results also show that the indoor air temperature fluctuates more frequently in case 2. In fact, the narrow range leads to the frequent switch of operating modes, which means that the facilities are switched on and off frequently. It's important to compromise the above contradictions for growers, because the frequent switch is easy to damage the facilities.

We focussed on the switching control of the three common cooling modes for energy saving, so we didn't study the cooling effect of shading net quantitatively in this paper. The simulation results indicate that the shading net is effective to reduce the energy consumption. In case 1 and case 2, when the shading net is folded, the natural ventilation mode is unable to reduce the indoor air temperature below the upper limit; while when the shading net is unfolded, the natural ventilation mode can meet the cooling requirement well. The influence of shading net is also confirmed by the simulation results in case 3. Therefore, it's necessary to make full use of the shading net for cooling greenhouse in future practice. Before setting the thresholds for shading, the demand of light illumination must be fully considered for the photosynthesis of indoor crops.

CONCLUSIONS

In order to reduce the energy consumption of greenhouse cooling in subtropical and tropical regions, we proposed a switching control strategy based on temperature prediction model for the greenhouses with the facilities driven by the on-off actuators. The simulation results indicate that the control strategy has a good adaptive ability and a good energy saving potential. The control strategy is easy to implement without major revisions on the existing facilities. Even if there are more facilities, the control strategy is still applicable, as long as the operating modes are re-divided and the indoor air temperature prediction models in all modes are constructed. Therefore, the proposed control strategy has a good universality.

ACKNOWLEDGEMENT

This work was supported by the National Science and Technology Support Project (2014BAD08B03), the Science and Technology Special Fund of North Jiangsu province (BN2014085), the Agricultural Science and Technology Support Project of Jiangsu province (BE2014312) and the Sanxin Fishery Project of Jiangsu province (Y2016-3).

REFERENCES

- [1] Balluchi A., Benvenuti L., Benedetto M.D.D., Sangiovanni-Vincentelli A., (2013), The design of dynamical observers for hybrid systems: theory and application to an automotive control problem, *Automatica*, Vol.49, Issue 4, pp.915-925;
- [2] Blasco X., Martínez M., Herrero J.M., Ramos C., Sanchis J., (2007), Model-based predictive control of greenhouse climate for reducing energy and water consumption, *Computers and Electronics in Agriculture*, Vol.55, Issue 1, pp.49-70;
- [3] Chu Z., Qin L., Lu L., Ma G., Wu G., (2015), Hybrid controller design and analysis for experimental greenhouse temperature system (实验温室温度系统混杂控制器设计与分析), *Journal of University of Science and Technology of China*, Vol.45, Issue 4, pp.268-274;
- [4] Chungloo S., Limmeechokchai B., (2007), Application of passive cooling systems in the hot and humid climate: The case study of solar chimney and wetted roof in Thailand, *Building and Environment*, Vol.42, Issue 9, pp.3341-3351;

- [5] Cuce E., Harjunowibowo D., Cuce P.M., (2016), Renewable and sustainable energy saving strategies for greenhouse systems: A comprehensive review, *Renewable & Sustainable Energy Reviews*, Vol.64, pp.34-59;
- [6] Febbraro A.D., Giglio D., Sacco N., (2016), A deterministic and stochastic Petri net model for traffic-responsive signalling control in urban areas, *IEEE Transactions on Intelligent Transportation Systems*, Vol.17, Issue 2, pp.510-524;
- [7] Frausto H.U., Pieters J.G., Deltour J.M., (2003), Modelling greenhouse temperature by means of auto regressive models, *Biosystems Engineering*, Vol.84, Issue 2, pp.147-157;
- [8] Frausto H.U., Pieters J.G., (2004), Modelling greenhouse temperature using system identification by means of neural networks, *Neurocomputing*, Vol.56, pp.423-428;
- [9] Gu J., Mao H., (2001), A mathematical model on intelligent control of greenhouse environment (温室环境智能化控制数学模型的研究), *Transactions of The Chinese Society of Agricultural Machinery*, Vol.32, Issue 6, pp.63-65, 80;
- [10] Hu H., Xu L., Wei R., (2010), Nonlinear adaptive Neuro-PID controller design for greenhouse environment based on RBF network, *International Joint Conference on Neural Networks*, pp.1-7, Barcelona, Spain;
- [11] Kumar K.S., Tiwari K.N., Jha, M.K., (2009), Design and technology for greenhouse cooling in tropical and subtropical regions: A review, *Energy and Buildings*, Vol.41, Issue 12, pp.1269-1275;
- [12] Lin H., Antsaklis P.J., (2014), Hybrid Dynamical Systems: An Introduction to Control and Verification, *Foundations & Trends in Systems & Control*, Vol.1, Issue 1, pp.1-172;
- [13] Nachidi M., Rodríguez F., Tadeo F., Guzman J.L., (2010), Takagi-Sugeno control of nocturnal temperature in greenhouses using air heating, *Isa Transactions*, Vol.50, Issue 2, pp.315-320;
- [14] Ozgener L., Ozgener O., (2010), An experimental study of the energetic performance of an underground air tunnel system for greenhouse cooling, *Renewable Energy*, Vol.35, Issue 12, pp.2804-2811;
- [15] Sethi V.P., Sharma S.K., (2007), Experimental and economic study of a greenhouse thermal control system using aquifer water, *Energy Conversion and Management*, Vol.48, Issue 1, pp.306-319;
- [16] Sethi V.P., Sharma S.K., (2007), Survey of cooling technologies for worldwide agricultural greenhouse applications, *Solar Energy*, Vol.81, Issue 12, pp.1447-1459;
- [17] Sethi V.P., Sharma S.K., (2008), Survey and evaluation of heating technologies for worldwide agricultural greenhouse applications, *Solar Energy*, Vol.82, Issue 9, pp.832-859;
- [18] Sigrimis N., Anastasiou A., Rerras N., (2000), Energy saving in greenhouses using temperature integration: a simulation survey, *Computers and Electronics in Agriculture*, Vol.26, Issue 3, pp.321-341;
- [19] Singh G., Singh P.P., Lubana P.P.S., Singh K.G., (2006), Formulation and validation of a mathematical model of the microclimate of a greenhouse, *Renewable Energy*, Vol.31, Issue 10, pp. 1541-1560;
- [20] Tap R.F., Willigenburg L.G., Straten G.V., (1996), Receding horizon optimal control of greenhouse climate based on the lazy man weather prediction, *13th IFAC World Congress*, San Francisco, USA, pp. 387-392;
- [21] Teitel M., Zhao Y., Barak M., Bar-Lev E., Shmuel D., (2004), Effect on energy use and greenhouse microclimate through fan motor control by variable frequency drives, *Energy Conversion and Management*, Vol.45, Issue 2, pp. 209-223;
- [22] Vadié A., Martin V., (2014), Energy management strategies for commercial greenhouses, *Applied Energy*, Vol.114, Issue 2, pp. 880-888;
- [23] Xu Z., Chen J., Zhang J., Liu Y., Zhang Q., (2016), Incremental auto regressive prediction models with external variables of greenhouse air temperature for control purposes, *International journal of smart home*, Vol.10, Issue 9, pp. 45-58;.
- [24] Xu Z., Chen J., Zhang Q., Gu Y., (2016), Dynamic mechanistic modeling of air temperature and humidity in the greenhouses with on-off actuators, *TELKOMNIKA (Telecommunication Computing Electronics and Control)*, Vol.14, Issue 2a, pp.248-256;
- Yang B., Qin L.L., Gang W., (2011), Modeling and control for greenhouse temperature system based on hybrid automata, *30th Chinese Control Conference*, Yantai, China, pp. 1627-1631.

ENERGY BALANCE ANALYSIS AND MECHANIZATION INDEX FOR GREENHOUSE VEGETABLE PRODUCTION IN SOUTHERN OF ALGERIA. AN OVERVIEW OF BISKRA PROVINCE

تحليل الميزان الطاقوي ومؤشر المكننة لزراعة البيوت المحمية في الجزائر. نظرة عن ولاية بسكرة

Ph.D.Eng. Nourani A.*¹, As. Ph.D. Stud. Eng. Bencheikh A.

Scientific and Technical Research Centre on Arid Regions (CRSTRA), Biskra/Algeria

Tel: 00213797687297; E-mail: nourani83@gmail.com

Keywords: protected vegetable, greenhouse, energy analysis, mechanization, Biskra

ABSTRACT

This work aims to determine the energy use for greenhouse vegetable production and to estimate the mechanization index in Biskra province (Algeria). The results revealed that the total energy required for vegetable protected production is 119.68 GJ per hectare where the infrastructure was the highest energy consumer followed by the electricity and fertilizers with a share of 22%, 20% and 19%, respectively. The energy use efficiency was calculated as 0.82, showing the inefficiency use of energy in the protected vegetable production. The entire farmers use least machinery labour energy in hectare compared to the human energy and the itinerary crop is similar for all greenhouses.

ملخص

يهدف هذا العمل إلى تحديد استخدام الطاقة لإنتاج الخضار للزراعات المحمية وتقدير مؤشر المكننة في محافظة بسكرة (الجزائر). وكشفت النتائج أن إجمالي الطاقة اللازمة لإنتاج الخضار المحمية هي 119.68 جيجا جول في الهكتار الواحد حيث كانت البنية التحتية المستهلك الأعلى للطاقة يليه الكهرباء والأسمدة بحصة بلغت 22%، 20% و 19% على التوالي. تم احتساب كفاءة استخدام الطاقة وهي 0.82، والتبين عدم كفاءة استخدام الطاقة في إنتاج الخضار للزراعات المحمية. جل المزارعين يستخدمون طاقة ميكانيكية في الهكتار أقل مقارنة مع الطاقة البشرية والأعمال الزراعية هي متماثلة في جميع البيوت البلاستيكية.

INTRODUCTION

In the two last decades, Algeria has experienced a notable agricultural development driven by a prosperous trend in market gardening in plastic greenhouses due of the favourable climatic conditions and the government's policy. As results of this development, Biskra province becomes the first producer of early vegetables nationally (Allache et al., 2015) where, the surface occupied by the greenhouse has increased by 528.52% over the last 20 years (Belhadi et al., 2016).

Taking into account limited natural resources and the impact of using different energy sources on environment and human health; it is substantial to investigate energy use patterns in agriculture (Samavatean, 2011). Therefore, research efforts have emphasized energy and economic analysis of various agricultural productions for planning resources in the ecosystem (Singh et al., 2002). While several works across the world have been conducted to estimate the energy use in greenhouse vegetable production, such as: Ozkan et al. (2004), Elings et al. (2005), Campiglia et al. (2007), Djevic and Dimitrijevic (2009), Ozkan et al. (2011), Pahlavan et al. (2011), Heidari and Omid (2011), Bojacá et al. (2012), Baptista et al. (2012) and Hedau at al. (2014). However, no studies have been published on energy input–output analysis and the mechanization index analysis of greenhouse vegetable production in Algeria.

With these observations in mind, this study addresses the determining input-output energy use in greenhouse vegetable production in order to study the energy consumption efficiency. Furthermore, this study wishes to estimate the mechanization degree and the mechanization index for the greenhouse vegetable production in Biskra province, southern of Algeria.

MATERIAL AND METHODS

Study area

According to Rekibi (2015), Biskra province occupies over 32% of national production of protected crops which make it the first producer of early vegetable in Algeria. The vegetables produced most extensively are tomato, cucumber, eggplant and pepper. For this reason, this study has been carried out in this region. The study area is located in the south-eastern of the country, the gateway to the Sahara. The

height above sea level is 112 m which makes it one of the lowest cities. The chief town of the province is located at 400 km of the capital, Algiers. It has surface area of 21,671 km², divided into 12 administrative districts (Fig. 1). Biskra has a hot desert climate, with very hot and dry summers and mild winters with annual rainfall averaging between 120 and 150 mm/year. The average annual temperature is 20.9°C.

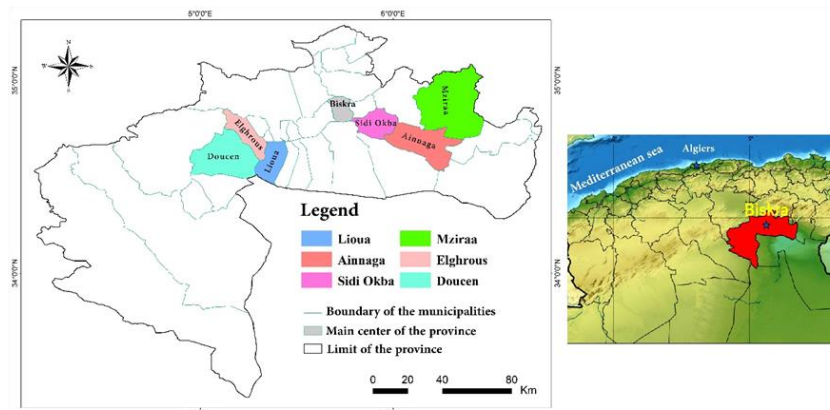


Fig. 1 - Situation of study area

Survey

An investigation was conducted in Biskra province during the season 2014-2015. The study employed face-to-face personal interviews using questionnaires which compound sections providing the economic characteristics, practices and management of the farm. The data have been collected from 65 farmers representing 5% of greenhouse vegetable growers from the six most productive municipalities, namely: M'ziraa, Ainnaga, Sidi Okba, Elghrous, Doucen and Lioua (Fig.1). In this area, the vegetables produced most extensively are tomato, cucumber, eggplant and pepper.

Energy input-output measurement

Energy requirements in agriculture are divided into two groups, direct and indirect (Samavatean, 2011). In this study, direct energy includes human labour, diesel, water for irrigation and indirect energy includes seeds, fertilizers, Farmyard manure, chemicals, machinery and infrastructure. Based on the energy equivalents of the inputs and outputs (Table 1), the metabolisable energy was calculated. Renewable energy (RE) consists of human labour, seed, manure and water for irrigation, whereas non-renewable energy (NRE) includes machinery, diesel fuel, electricity, infrastructure, fertilizers and chemicals.

To analyse the energy flow, energy ratio (energy use efficiency) (ER), energy net (EN) and energy productivity (EP) indexes were calculated as following:

$$\text{Output - input ratio (ER)} = \frac{\text{Energy output [MJ/ha]}}{\text{Energy input [MJ/ha]}} \quad (1)$$

$$\text{Energy productivity (EP) [kg/MJ]} = \frac{\text{Total output [kg/ha]}}{\text{Energy input [MJ/ha]}} \quad (2)$$

$$\text{Energy Net (EN) [MJ/ha]} = \text{Energy output [MJ/ha]} - \text{Energy input [MJ/ha]} \quad (3)$$

$$\text{Specific energy [MJ/kg]} = \frac{\text{Energy input [MJ/ha]}}{\text{vegetable output [kg/ha]}} \quad (4)$$

$$\text{Energy intensiveness} = \frac{\text{Energy Input [MJ/ha]}}{\text{Cost of cultivation [$/ha]}} \quad (5)$$

Table 1

Energy equivalent factors used to transform the inputs and the outputs yield of the greenhouse tomato production system in Biskra region

Energy source	Unit	Energy equivalent [MJ/unit]	Reference
Inputs			
Human labour	h	1.96	Singh et al. (2002)
Machinery	h	62.70	Singh et al. (2002)
Diesel oil	l	45.40	Bojacá et al. (2012)
Infrastructure	kg		

Energy source	Unit	Energy equivalent [MJ/unit]	Reference
Steel		33.00	Medina A, et al (2006)
Polyethylene		9.90	Medina A, et al (2006)
Synthetic fibre		1.20	Medina A, et al (2006)
PVC		11.60	Medina A, et al (2006)
Fertilizers	kg		
N		60.60	Ozkan et al. (2004)
P ₂ O ₅		11.10	Ozkan et al. (2004)
K ₂ O		6.70	Ozkan et al. (2004)
Farmyard manure	kg	0.30	Bojacá et al. (2012)
Pesticides	kg		
Fungicides		216	Mohammadi and Omid (2010)
Insecticides		101.20	Mohammadi and Omid (2010)
Plant materials			
Plantlets	unit	0.20	Bojacá et al. (2012)
Water for irrigation	m ³	0.63	Bojacá et al. (2012)
Electricity	kW h	3.60	Ozkan et al. (2004)
Output			
Tomato, cucumber, eggplant, pepper	kg	0.80	Ozkan et al. (2004)

Greenhouse production is more expensive than producing the same crop in the open field, the most important factors determining costs are depreciation of the structure and equipment, labour, energy and variable costs such as plant material, substrate and fertilizer (Peet and Welles, 2005). For this, the output/input analysis was also applied in economic benefits. The process was similar with energy balance analysis. The economic analysis of the investigated farmers was determined using the following indicators (Fadavi et al., 2011):

$$\text{Gross value } [\$/\text{ha}] = \text{vegetable yields } [\text{kg}/\text{ha}] \times \text{price } [\$/\text{kg}] \quad (6)$$

$$\text{Gross return } [\$/\text{ha}] = \text{Total production value } [\$/\text{ha}] - \text{Variable cost of production } [\$/\text{ha}] \quad (7)$$

$$\text{Net return } [\$/\text{ha}] = \text{Total production value } [\$/\text{ha}] - \text{Total production costs } [\$/\text{ha}] \quad (8)$$

$$\text{Benefit - Cost ratio} = \frac{\text{Total production value } [\$/\text{ha}]}{\text{Total production costs } [\$/\text{ha}]} \quad (9)$$

$$\text{Productivity } [\text{kg}/\$] = \frac{\text{Vegetable yield } [\text{kg}/\text{ha}]}{\text{Total production costs } [\$/\text{ha}]} \quad (10)$$

Mechanization index estimation

Mechanization index (IM): Singh (2006) presented a definition for mechanization index based on using living thing and machine in input energy which is calculated from the relationship.

$$IM = \frac{CEM}{CEH + CEA + CEM} [\%] \quad (11)$$

where: *IM*: mechanization index, *CEM*: Cost of using machine, *CEH*: Cost of manpower, *CEA*: Cost of using animal power.

Machinery energy ratio (machine index), the machinery energy ratio is an index which represents the fraction of the total energy inputs through the various tools and implements used in different operations for cultivation of the particular crop. The machinery energy was determined using the following equation.

$$MER = \frac{Ed}{Te} [\%] \quad (12)$$

Where *MER* is the ratio of the machinery energy to the total energy input; *Ed* is the energy input through the various machines/implements; *Te* is the total energy input from human labour, animals, machine/hand tools, seed, and farm yard manures for the vegetable greenhouse production.

RESULTS

The data were collected from 65 vegetable protection growers in Biskra province. The average size of greenhouses is around 2.1 ha with a range from 0.25 up to 12.75 ha. All of the surveyed greenhouses were the plastic houses and metallic structures. Also the data showed that almost all surfaces covered by greenhouse were irrigated using drip irrigation and about 73% of visited farms were privately owned and 27% rented.

Energy inputs – outputs used analysis

The summarized information on energy use pattern and yield value of vegetable production is presented in Table 2 and along with Fig.1 gives the percentage distribution of energy inputs.

Table 2

Amounts of inputs and output energy used in protected vegetable production.

Energy source	Quantity per unit area [ha]	Total Energy equivalent [MJ/unit]
Input		
Human labour [h]	3457.03	6775.78
Machinery [h]	31.38	1967.25
Diesel oil [l]	129.02	5857.41
Infrastructure [kg]		
Steel	146.68	4840.31
Polyethylene	2082.54	20617.14
Synthetic fibre	105.81	126.97
PVC	130.82	1517.46
Fertilizers [kg]		
N	278.86	16899.13
P ₂ O ₅	354.66	3936.76
K ₂ O	274.50	1839.16
Farmyard manure [kg]	47742.54	14322.76
Pesticides [kg]		
Fungicides	10.30	2224.12
Insecticides	96.47	9762.64
Plant materials		
Plantlets [units]	17232	3446.35
Water for irrigation [m ³]	3154.00	1987.02
Electricity [kW h]	6544.84	23561.42
Output		
Tomato, cucumber, eggplant, pepper [kg]	122095.24	97676.19

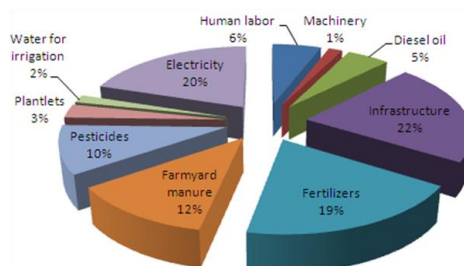


Fig. 2 - Percentage distribution of energy inputs

The results revealed that the total energy required for vegetable protected production is 119.68GJ per hectare. Compared to other study, in Turkey, the consumption of energy by cucumber, tomato, eggplants and pepper were 134.77, 127.32, 98.68 and 80.25 GJ/ha, respectively (*Ozkan et al., 2004*). In central of Italy, the total energy requirements for producing the greenhouse vegetable crops were found in the range of 64,232–142,835 GJ/ha (*Campiglia et al., 2007*). These results indicate that the energy consumption for vegetable greenhouse production is different from one region to another with light variation. Among the different energy sources the infrastructure was the highest energy consumer followed by the electricity and fertilizers with a share of 22%, 20% and 19%, respectively. This result is in accordance with that founded by *A. Medina, et al (2006)* where the highest portion of the energy use in Colombia comes from the greenhouse construction with 41.29% of the total energy use and the major part of this energy is attributed to the steel.

The proportion of energy input of farmyard manure, pesticides, human labour, diesel oil, plantlets, water and machinery used for protected vegetable (tomato, cucumber, eggplant, pepper) growing were 12%, 10%, 6%, 5%, 3%, 2% and 1%, respectively. In similar works, in Antalya (Turkey), the results indicated that the bulk of energy consumed for greenhouse winter crop tomato production was: fertilizer (38.22%), electricity (27.09%), manure (17.33%) and diesel-oil (13.65%) (Ozkan *et al.*, 2011), while, among input energy sources, diesel fuel and fertilizers contained highest energy with 54.17% - 49.02% and 21.64% - 24.01%, respectively (Heidari and Omid, 2011). This comparison shows that each region has specificity in terms of energy inputs sharing.

The fertilizers and manure required to fertilize the soil are 48650.56 kg/ha with nearly a third of total energy consumed (31%), this observation is a common belief that increased use of fertilizer and manure will increase the yield. 3457.03 h of human power and 31.38 h of machine power are required per hectare of vegetable production in the research area. The crop itinerary is mainly similar for all the greenhouses crops moreover it is carried out generally by human labour energy (6%) compared to machinery energy (1%). The source of human labour in the investigated farms is from either family members or mainly from hired (seasonal) labours. Also, 5857,41 MJ/ha of diesel fuel was consumed generally for machinery purposes and most of the machineries are mainly provided by rent.

Table 3 presents the energy use efficiency, energy productivity, specific energy, net energy and energy intensiveness of protected vegetable production.

Table 3

Energy input–output ratio in greenhouse vegetable production		
Items	Unit	Protected vegetable production
Energy input	MJ/ ha	119681,69
Energy output	MJ/ha	97676,19
Yield	Kg/ha	122095,24
Energy use efficiency	---	0.82
Specific energy	MJ/kg	0.98
Energy productivity	Kg/MJ	1,02
Net energy	MJ/ha	-22005,50
Energy intensiveness	MJ/\$	2.09

Energy use efficiency (energy ratio) was calculated as 0.82, showing the inefficiency use of energy in the protected vegetable production. Other results founded for protected vegetable, such as 0.66 for tomato (Pahlavan *et al.*, 2011), 0.76 for cucumber, 0.61 for eggplant, 0.99 for pepper (Ozkan *et al.*, 2004), 0.32 for tomato, 0.31 for cucumber, 0.23 for eggplant, 0.19 for pepper (Canakci and Akinci, 2006) have been reported for different crops, showing the inefficient use of energy, thus it is concluded that the energy ratio can be increased by raising the crop yield and/or by decreasing energy input consumption. Similar results such as 0.68 for tomato (Bojacá *et al.*, 2012), 0.69 and 1.48 for cucumber and tomato respectively (Heidari and Omid, 2011) 0.8 for winter crop tomato (Ozkan *et al.*, 2011) were calculated.

The average energy productivity of protected vegetable was 1.02 kg/MJ. This means that 1.02kg of tomato, cucumber, pepper or eggplant output was obtained per unit energy. The specific energy, net energy and energy intensiveness of protected vegetable production were 0.98 MJ/kg, -22005.50 MJ/ha and 2.09 MJ/\$, respectively. Net energy is negative (less than zero). Therefore, it can be concluded that in protected vegetable production, energy is being lost and this result similar to that was obtained by other researchers such as: Ozkan *et al.* (2004), Canakci and Akinci (2006) and Pahlavan *et al.* (2011). Parallel studies obtain 0.31 MJ/kg (Ozkan *et al.*, 2004), 12380.3 MJ/t (Hatirli *et al.*, 2006) and 0.94 kg/MJ (Ozkan *et al.*, 2011) for the specific energy of corn production.

Total mean energy input as direct, indirect, renewable and non-renewable forms are given in Table 4.

Table 4

Total energy input in the form of direct, indirect, renewable and non-renewable for vegetable production

Form of energy	[MJ/ha]	[%]
Direct energy	38181.63	31.90
Indirect energy	81500.06	68.10
Renewable energy	26531.92	22.17
Non-renewable energy	93149.77	77.83

The total energy input consumed could be classified as direct energy (31.90%), indirect energy (68.10%) and renewable energy (22.17%) and non-renewable energy (77.83%). A number of resultants, in same cultivation system, revealed that for tomato in Turkey indirect energy (41.54%) is less than that of direct energy (58.18%), and renewable energy (81.60 %) is greater than that of non-renewable energy (18.12 %) (*Ozkan et al., 2011*) while for the same crop and region, the results show that the share of direct input energy was 59% in the total energy input compared to 41% for the indirect energy. On the other hand, non-renewable and renewable energy contributed to 88 and 12% of the total energy input, respectively (*Hatirli et al., 2006*).

Economic analysis

In this section, the majority of studies worked on energy balance of protected vegetable and didn't take into account the economic feature. From our perspective, the costs of each input used and calculated gross production values for protected vegetable production are shown in Table 5.

Table 5

Economic analysis of greenhouse vegetable production

Economic index	Unit	Value
Yield	Kg/ ha	122095.24
Sale price	\$ /kg	0.47
Gross value	\$/ ha	57384.76
Variable cost	\$/ha	24842.28
Fixed cost	\$/ha	3907.09
Total cost	\$/ ha	28749.37
Cost of production	\$/ kg	0.24
Gross return	\$/ ha	32542.47
Net return	\$/ha	28635.39
Benefit to cost ratio		1.99
Productivity	kg /\$	4.25

The result reveal that, the gross value of production is 57384.76 \$/ha where the total mean costs for the production was 28749.37 \$/ha. About 86.40% of the total expenditure was variable costs, while 13.59 % was fixed expenditure. Several studies reported that the ratio of variable cost was higher than that of fixed cost in cropping systems (*Samavatean et al., 2011*). Starting from these results, the benefit-cost ratio from protected vegetable production in the farms was calculated to be 1.99. These results are consistent with the findings reported by *Canakci and Akinci (2006)* where the benefit/cost ratio for the tomato, pepper, cucumber and eggplant production were calculated at 1.57, 1.15, 1.29 and 1.10, respectively. On the other side, benefit/cost ratio was calculated for others crop such as 1.36 for Garlic production (*Samavatean et al., 2011*), 1.83 and 2.21 for greenhouse and open-field grape (*Ozkan et al., 2007*). Concerning the gross return, the calculation gave the result 32542.47 \$/ha while for the productivity, it is 4.25 kg/\$.

Mechanization index analysis

Different clusters of farm were determined basing on greenhouse area. Table 6 illustrate that Mechanization index (MI) of 0.119 is obtained for protected vegetable production in the visited region.

Table 6

Mechanization Index and Machinery energy ratio for different land size

	<1	1-<3	3-<5	>5	total
Mechanization index (MI)	0.119	0.124	0.111	0.112	0.119
Machinery energy ratio (MER)	0.008	0.012	0.007	0.017	0.010
Number of farmers	41	12	4	8	65

It seems that, the MI calculated for all clusters are almost equal with a small difference. All farmers use least machinery labour energy per hectare than the human energy labour, thus we could say that the itinerary crop is similar for all the greenhouses visited. These results could be explained by unavailability of the machine destined to greenhouse cultivation in the local market especially the planter machine, also due the finical situation of the farmer. Previous work has showed that the MI at all-India level was only 14.5% and it varied from 8.2% in sorghum and paddy to a highest value of 29.00% in wheat (*Singh, 2006*).

CONCLUSIONS

This work aimed to analyse the energy balance for the protected vegetable in Biskra province (Southern of Algeria), also to make economic analysis and determination of the mechanization index for this sector. For this reason, a survey has been conducted with 65 farmers.

The results revealed from this study could be presented as follows:

- The total energy required for vegetable protected production is 119.68 GJ per hectare which is close to that reported in previous researches (*Ozkan et al., 2004*).
- Among the different energy sources the infrastructure was the highest energy consumer followed by the electricity and fertilizers with a share of 22%, 20% and 19%, respectively.
- Each region has specificity in terms of energy inputs sharing.
- Energy use efficiency (energy ratio) was calculated as 0.82, showing the inefficiency use of energy in the protected vegetable production.
- The gross value of production is 57384.76 \$/ha where the total mean costs for the production was 28749.37 \$/ha. About 86.40 % of the total expenditure was variable costs, while 13.59 % was fixed expenditure.
- All farmers use least machinery labour energy per hectare compared to the human energy labour, thus we could say that the itinerary crop is similar for all the greenhouses visited.

As recommendations, the below propositions could enhance the control of energy flow in protected vegetable production and also allow the farmer to improve their financial situation, namely:

- Providing a formation, by a qualified employer, to farmers for changing their wrong behaviours and the controlled input;
- Improving the pest management using an integrated fighting method (IPM);
- Elaboration of a strategy to introduce the machine for carrying out the farm operation and to promote the farm machinery.

ACKNOWLEDGEMENT

This research was financially supported by the Scientific and Technical Research Centre for Arid Areas (CRSTRA), Biskra, Algeria. Special thanks are extended to the farmers who contributed to this survey.

REFERENCES

- [1] Allache F., Bouta Y., Demnati F., (2015), Population development of the tomato moth *Tuta absoluta* (*Lepidoptera: Gelechiidae*) in greenhouse tomato in Biskra, Algeria, *Journal of Crop Protection*, Vol. 4, issue 4, pp. 509-517, Faculty of Agriculture, Tarbiat Modares University, Tehran/Iran;
- [2] Baptista F.J., Silva A.T., Navas L.M., Guimarães A.C., Meneses J.F., (2012), Greenhouse Energy Consumption for Tomato Production in the Iberian Peninsula Countries. *Proc. IS on GreenSys2011. Acta Horticulturae*. 952, ISHS 2012: p.409, International Society for Horticultural Science, Leuven/Belgium;
- [3] Belhadi A., Mehenni M., Reguieg L. and Yekhlif H., (2016), Plasticulture contribution to agricultural dynamism in the Ziban region (biskra). *Revue Agriculture*. Numéro spécial (1), pp. 93–99, Setif university/Algeria;
- [4] Bojacá C.R., Casilimas H. A., Gil R., Schrevens E., (2012), Extending the input-output energy balance methodology in agriculture through cluster analysis, *Energy*, vol.47, pp. 465-470, Ed.Elsevier, London/U.K;
- [5] Canakci M., Akinici I., (2006), Energy use pattern analyses of greenhouse vegetable production. *Energy*, vol.31, pp.1243-1256, Ed.Elsevier, London/U.K.;
- [6] Campiglia E., Colla G., Mancinelli R., Roupheal Y., Marucci A., (2007), Energy Balance of Intensive Vegetable Cropping Systems in Central Italy. *Proc. VIIIth IS on Protected Cultivation in Mild Winter Climates. Acta Horticulturae*, 747, ISHS 2007: pp. 185-192, International Society for Horticultural Science, Leuven/Belgium;
- [7] Djevic M., Dimitrijevic A., (2009), Energy consumption for different greenhouse constructions. *Energy*, vol. 34, pp. 1325–1331, Ed. Elsevier, London/U.K.;
- [8] Elings A., Kempkes F.L.K., Kaarsemaker R.C., Ruijs M.N.A., van de Braak N.J., Dueck T.A., (2005), The Energy Balance and Energy-Saving Measures in Greenhouse Tomato Cultivation. *Proc. IC on*

- Greensys, *Acta Horticulturae*, 691, ISHS 2005, pp. 67-74, International Society for Horticultural Science, Leuven/Belgium;
- [9] Fadavi R., Keyhani A., Mohtasebi S.S., (2011), An analysis of energy use, input costs and relation between energy inputs and yield of apple orchard, *Research in Agricultural Engineering*, vol.57, issue 3, pp. 88-96, Czech Academy of Agricultural Sciences, Praha/Czech Republic;
- [10] Hatirli S.A., Ozkan B., Fert C., (2006), Energy inputs and crop yield relationship in greenhouse tomato production, *Renewable Energy*, vol.31, pp. 427–438, Ed.Elsevier, London/U.K;
- [11] Heidari M.D., Omid M., (2011), Energy use patterns and econometric models of major greenhouse vegetable productions in Iran, *Energy*, vol.36, pp. 220-225, Ed. Elsevier, London/U.K.;
- [12] Hedau N.K., Tuti M. D., Stanley J., Mina B.L., Agrawal P.K., Bisht J.K., Bhatt J.C., (2014), Energy-use efficiency and economic analysis of vegetable cropping sequences under greenhouse condition. *Energy Efficiency*, vol. 7, issue 3, pp. 507-516, Ed. Springer, Berlin/Germany,
- [13] Medina A., Cooman A., Parrado C.A., Schrevens E., (2006), Evaluation of Energy Use and Some Environmental Impacts for Greenhouse Tomato Production in the High Altitude Tropics, *Proc. IIIrd IS on HORTIMODEL2006, Acta Horticulturae*, 718, ISHS 2006, pp. 415-422, International Society for Horticultural Science, Leuven/Belgium;
- [14] Ozkan B., Figen Ceylan R., Kizilay H., (2011), Comparison of energy inputs in glasshouse double crop (fall and summer crops) tomato production, *Renewable Energy*, vol. 36, pp. 1639-1644, Ed. Elsevier, London/U.K.;
- [15] Ozkan B., Kurklu A., Akcaoz H., (2004), An input-output energy analysis in greenhouse vegetable production: a case study for Antalya region of Turkey, *Biomass Bioenergy*, vol.26, pp. 189-195;
- [16] Pahlavan R., Omid M., Akram A., (2011), Energy use efficiency in greenhouse tomato production in Iran. *Energy* 36: pp. 6714-6719, Ed. Elsevier, London/U.K.;
- [17] Peet M.M., Welles G., (2005), Greenhouse tomato production, Tomatoes, *Centre for Agriculture and Biosciences International*, Chp.9, pp. 275-304, Oxford/U.K.;
- [18] Rafiee S, Mousaviavval S.H., Mohammadi A., (2010), Modelling and sensitivity analysis of energy inputs for apple production in Iran, *Energy*, vol.35(8), pp. 3301-3306, Ed. Elsevier, London/U.K.
- [19] Rekibi F., (2015), *Analyse compétitive de la filière tomate sous serre, Cas de la Wilaya de Biskra*. Magister Thesis, Mohamed Kheider University, Biskra/Algeria;
- [20] Singh H., Mishra D., Nahar N.M., (2002), Energy use pattern in production agriculture of a typical village in arid zone India-Part I. *Energy Conversion Manage*, vol.43, pp. 2275-2286, Ed. Elsevier, London/U.K.;
- [21] Singh G., (2006), Estimation of a Mechanization Index and Its Impact on Production and Economic Factors - a Case Study in India, *Biosystems Engineering*, vol. 93(1), pp. 99-106, Ed. Elsevier, London/U.K.;
- [22] Mohammadi A., Omid M., (2010), Economical analysis and relation between energy inputs and yield of green house cucumber production in Iran, *Energy*, vol.87, pp.191-196, Ed. Elsevier, London/U.K.;
- [23] Samavatean N., Rafiee S. and Mobli H., (2011), An Analysis of Energy Use and Estimation of a Mechanization Index of Garlic Production in Iran, *Journal of Agricultural Science*, Vol.3, issue 2, pp. 198-205; Canadian Centre of Science and Education, Toronto/Canada;
- [24] Zarini R.L., Ghasempour A., Mostafavi S.M., (2013), A comparative study on energy use of greenhouse and open-field cucumber production systems in Iran, *International Journal of Agriculture and Crop Sciences*, vol.5 (13), pp. 1437-1441, Science Explorer Publications, London/U.K.

INTEGRATED USE OF BIOENERGY CONVERSION TECHNOLOGIES IN AGROECOSYSTEMS

/

КОМПЛЕКСНЕ ВИКОРИСТАННЯ ТЕХНОЛОГІЙ БІОЕНЕРГЕТИЧНОЇ КОНВЕРСІЇ У АГРОЕКОСИСТЕМАХ

Doctor of technical sciences Golub G.A.¹⁾, Doctor of technical sciences Kukharets S.M.²⁾,
Ph.D. Eng. Yarosh Y.D.²⁾, Ph.D. Econ. Kukharets V.V.²⁾

¹⁾National University of Life and Environmental Sciences of Ukraine / Ukraine, ²⁾Zhytomyr National Agroecological University / Ukraine
Tel: +380676653548, E-mail: saveliy_76@ukr.net

Keywords: *agro-ecosystems, energy, conversion, straw, biodiesel, biogas*

ABSTRACT

The paper substantiates the mechanical and technological principles of formalizing the structure of agroecosystems on the basis of optimizing the interdependence between the elements of the agroecosystem within a specified range of conditions. The equipment for the production of bioenergy resources is improved by means of minimizing its energy capacity with all qualitative indices of the technological processes preserved.

РЕЗЮМЕ

У статті обґрунтовано механіко-технологічні основи для формалізації структури агроєкосистем на основі оптимізації взаємозв'язків між елементами агроєкосистеми у визначеному діапазоні умов. Удосконалено обладнання для виробництва біоенергоресурсів шляхом мінімізації його енергоємності при збереженні якісних показників технологічних процесів.

INTRODUCTION

There is no doubt that every measure proposed for implementation in agroecosystems should not only provide soil fertility, but favour the expanded fertility renewal. Therefore, the important task is to determine the amount of plant biomass, which can be used in heating without any harm to soil fertility recovery. It should also be taken into account that the use of technological processes with high mechanization level does not always lead to higher economic production indices because of increased deductions in production costs for technical servicing and repair of technical equipment, as well as deductions for depreciation, which are not compensated by additional production profits.

Oil-bearing crop production takes one of the leading positions in the structure of plant growing and in the whole system of agricultural production in Ukraine. In the structure of total agricultural output, 35% of total production volumes in all farm categories are due to these crops. The main producers of these products manufacture 60% of oilseed products (****Agricultural Ukraine, 2015*). In terms of food security, the volumes of domestic production fully satisfy domestic demands in these products, leaving some bulk for export and raw materials for biofuels.

The experience of using biogas plants was completely analysed by the Agency for renewable resources in Germany (****Guide to biogas, 2012*). The authors of the analysis indicate that in the absence of biomass mixing in the reactor, after a while there is a separation of biomass with layer forming due to the difference in density of certain mineral and organic components, as well as to flotation of particles while yielding gas. Thus, the biggest part of the anaerobic bacteria biomass is situated at the bottom of the reactor and the organic part of the biomass substrate accumulates at the top of the reactor. As a result, the contact zone of anaerobic bacteria with biomass substrate is limited by a boundary layer of mentioned parts of the reactor. Floating crust of solid organic substances also blocks biogas yield. Facilitation of anaerobic bacteria contact with substrate biomass is provided by mixing the substrate, but intensive mixing should be avoided because it can cause stopping of anaerobic fermentation at the expense of disturbance of acetogenic and methanogenic bacteria symbiosis. In practice, a compromise is achieved by slow rotation of agitators or by their work within a short period of time. Part of the solid mineral inclusions contained in substrates based on manure is released in the process of biological decomposition inside the reactor. Mineral sediment reduces the useful volume of the reactor (*Gouxa X. et al, 2016; Satjaritanuna P. et al, 2016*).

MATERIALS AND METHODS

Structural diagram for the biological conversion of organic material in agricultural ecosystems with production of outputs and biofuels was developed on the basis of typical crop rotation for intensive farming in the Forest-Steppe zone using the calculation of the balance of humus and compost mixture formulation through agrochemical balances. The amount of straw for combustion was calculated as the difference between the total quantity of straw and the priority needs of its use. Heat generation ability of different types of straw was calculated on the basis of DSTU 3581-97 Energy efficiency. We used the methods of measurement and calculation of combustion heat. Biodiesel production resources were determined on the basis of statistical indicators of Ukrainian agricultural sector. Estimated volume of the produced biogas was determined on the basis of the intensity of organic biomass decomposition during its fermentation.

RESULTS

Biological energy conversion

With due regard to well-known regularities and research results it is developed the structural diagram and simulation model of diversified manufacturing of products with biological energy conversion of organic raw materials for 6-field crop rotation with a total area of 300 hectares (fig. 1).

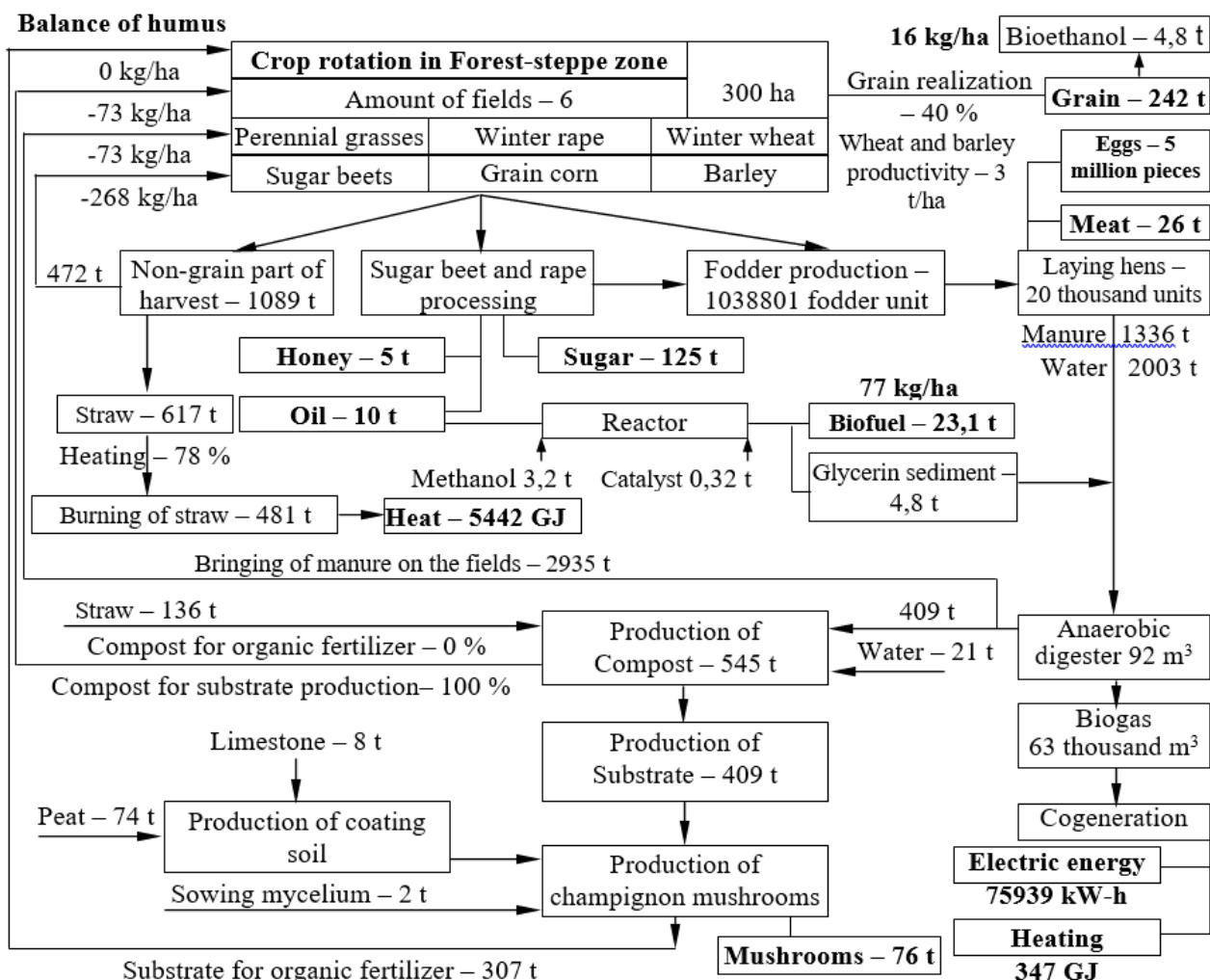


Fig. 1 – Structural diagram for the manufacturing of production and energy on the basis of biofuels

Structural diagram of diversified manufacturing of agricultural products and energy envisages: growing of rotation field crops with production of grain and sugar beets; harvesting of crop straw and rape stalks; leaving of shredded corn stalks in the field as mulch; feed production for poultry; manufacturing of poultry products; methane (anaerobic) fermentation of poultry manure with production of heat and electric power from biogas; the preparation and use of grain crop straw and rape stalks for heating needs in the form of briquettes, rolls or chaff; usage of grain crop straw, rape stalks and fermented manure for compost production; production of substrate for champignon growing in compost and champignon production;

production of biodiesel from rape seeds; use of glycerine residue for heating needs or its anaerobic fermentation.

On the basis of the introduced scheme it was defined the balance of humus in crop rotation using the well-known equation:

$$B = \frac{1}{\sum_{i=1}^n S_i} \left[-\sum_{i=1}^n S_i M_i + \sum_{i=1}^n S_i U_i k_{DWi} k_{Hi} + \sum_j^m OB_j \left(1 - \frac{W_j}{100} \right) k_{Hj} \right], \quad (1)$$

where:

B – the annual balance of humus in crop rotation, kg/ha;

S_i – the area under the i rotation crop, ha; M_i – mineralization of humus by the i rotation crop, kg/ha;

U_i – the productivity of the i rotation crop, kg/ha;

k_{DWi} , k_{Hi} – output coefficients of dry weight of residues and their humification for the i rotation crop, rel. units.;

OB_j – annual organic biomass volume of the j species (non-seed biomass of agricultural crops remaining in the fields, manure, compost, substrate and biomass of weeds, green manure, etc.), which enters the field during a year, kg;

W_j – relative humidity of organic biomass of the j species, %;

k_{Hj} – humification coefficient of dry organic biomass of the j species, rel. units.;

n , m – the number of rotation fields and the number of organic biomass species respectively, units.

Computer simulation model allows determining the quotient of straw, which can be used for heating needs individually for separate farm. Thus, under the conditions shown in the figure, it can be reserved 78 % of straw for heating needs, and the part of the gathered straw in amount of 136 tons should be used for humus deficiency compensation in order to compensate humus losses completely. This can be done by two methods – either to leave some chopped straw in the fields or to develop on its basis compost or substrate for growing champignons.

Straw combustion

On the basis of existing indicators, which characterize agricultural production in Ukraine during recent years in general, there were also made the calculations on defining the straw volume limits used for heating needs. This dependence defined as a percentage of the total amount of straw is as follows:

$$C^{\%} = -0,57D + 48,66 \quad (2)$$

where:

$C^{\%}$ is the straw amount limit from the total amount which can be used for heating needs, %;

D – annual humus deficiency, kg/ha.

It should be mentioned, that in the case of the total humus deficiency in the range of 80 to 90 kg/ha, the use of straw for heating needs is impossible because of soil fertility preserving terms. The maximum amount of straw which can be used for heating needs with zero humus balance is about 50%.

To ensure use of corn and sunflower tops for heating needs, as well as of rape stems, there remain unsolved technical issues of this plant biomass storage, that's why nowadays it is usually crushed and left in the fields.

When summarizing the data of chemical composition of straw it was assumed that the nitrogen-sulphur ratio in cereal straw is 5 units (in legume straw – 10 units), and the hydrogen-sulphur ratio is 56 units, which correspond to the averaged data according to (Barotfy I., Rapan P., 1988). The carbon-nitrogen ratio was taken as medium in volume, according to the data in (Shkarada M., 1985). On the basis of the generalized data, introduced in table 1, were received empirical calculation dependences for determination of heat of different straw combustion types.

While calculations performed to prove the use of plant biomass for specific region or whole country, the heat of straw combustion should be determined by the equation which takes into account the importance of the volumes of a particular straw type. For example, it is known that the main volumes of grain crop straw in Ukraine are presented by wheat straw (from 40 to 60%), barley straw (from 20 to 30%), rye straw (from 3 to 6%) and legume straw (from 2 to 8%). In recent years, it began to increase specific weight of rape straw, which reached values from 4 to 6%.

It is well-known that grain crops, vegetative mass major producers, traditionally occupy from 40 to 55% in the structure of sowed crops. It should also be mentioned that with livestock decrease straw consumption

for feeding and litter decreased as well, and the surplus straw is usually burned in fields. Using straw in existing volumes would allow natural gas saving in the range from 4.5 to 14.3 billion m³.

Table 1

Field crop – the straw producer	Content of dry weight, %								Calculation formula, MJ/kg
	Ash	Organic matter	Nitrogen, N	Carbon, C	Hydrogen, H	Oxygen, O	Sulphur, S	C/N	
Wheat	4.65	95.35	0.52	44.43	5.86	44.43	0.11	85	$Q_H^p = 16.261 - 0.1876W$
Rye	4.65	95.35	0.43	45.02	4.80	45.02	0.09	105	$Q_H^p = 15.309 - 0.1781W$
Barley	4.65	95.35	0.59	44.03	6.58	44.03	0.12	75	$Q_H^p = 16.914 - 0.1941W$
Oats	6.98	93.02	0.51	43.35	5.71	43.35	0.10	85	$Q_H^p = 15.865 - 0.1836W$
Corn	4.65	95.35	0.63	43.80	7.01	43.80	0.13	70	$Q_H^p = 17.304 - 0.1980W$
Rape	5.88	94.12	0.66	42.96	7.40	42.96	0.13	65	$Q_H^p = 17.520 - 0.2002W$
Grain legumes	6.98	93.02	1.64	41.02	9.19	41.02	0.16	25	$Q_H^p = 18.915 - 0.2141W$

It is necessary to mention the appropriateness and availability of rolled straw storage, because this technology allows quick removal of straw from fields and is realized by means of simple and reliable technical equipment.

According to our estimations, while annual volume of straw combustion at the rate of 30 million tons, the total amount of natural gas yielded will be 10.9 billion m³. In these conditions, additional investments for preparation and combustion of straw will be 14.6 billion UAH, and their payback period will be from 1.2 to 1.3 years.

The effectiveness of straw combustion on the basis of comparison to heat generation by natural gas burning dependence from the heat production efficiency of straw when compared to gas heating and changing of straw cost.

Biodiesel

In Ukraine there are many cases of usage by agricultural producers of rapeseed oil in mixture with diesel for diesel tractors which have exceeded their service life.

We found that rapeseed oil production for usage as biodiesel can be economically reasonable in terms of agricultural production, when compared to rapeseed selling if the total cost of production is high and close to the average selling price of rapeseeds, or if the price of realization is low and similar to the total cost of rapeseeds.

Using biodiesel to replace diesel, it is necessary to heat biodiesel in the fuel lines of low pressure up to the temperature which provides the determined level of biodiesel filtration (Man X. et al, 2015; Corsini A. et al, 2015). To increase efficiency and temperature range of biodiesel use, we have designed and made a two-stage heating system, which allows using biodiesel under any values of environment temperature and provides an increase in completeness of fuel combustion. The second stage of fuel heating is made in the fuel pump-injector section for its better spraying and increase of speed and combustion completeness.

Fuel prices are constantly increasing, and faster than those for agricultural products, which significantly affects production cost, realization price and farmers' profit. The analysis shows (fig. 2) that in 2000 farmers had to sell 4.6 tons of wheat to buy 1 ton of diesel, in 2006 it was necessary to sell 8.1 tons of wheat, in 2008 – 9.1 tons. Over the past 11 years the price of wheat increased 2.74 times and of diesel – 4.73 times.

On the basis of statistical data about consumption of diesel in agriculture and rape gross harvest, we have evaluated the capacity of replacing diesel to biodiesel while processing of whole rape harvest.

The largest consumption of diesel in agriculture for the observed period was noticed in 2001, 2002, 2000, and the lowest – in 2006, 2007, 2008; in 2011 it was observed the tendency of diesel use increase when compared to 2010 from 1201.4 thousand tons to 1349.7 thousand tons. Rape gross yield increase is being observed since 2004, and in 2009 was noticed production decline. The volume of biodiesel production while processing the whole rape harvest was to be the highest for the investigated period in 2008 – 900.6

thousand tons of biodiesel, in 2009 – 587.3 thousand tons, in 2010 – 460.8 thousand tons, in 2011 – 387.9 thousand tons, and the lowest – in 2003 – 15.8 thousand tons, as well as in 2002 – 19.1 thousand tons. The quotient of diesel which can be substituted to biodiesel while processing whole rape harvest was the largest in 2008 – 64.7%. At the same time, as it is predicted, production and use of biofuel in 2020 will not exceed 100 thousand tons per year (Geletukha G.G., Zheleznaya T.A., 2012).

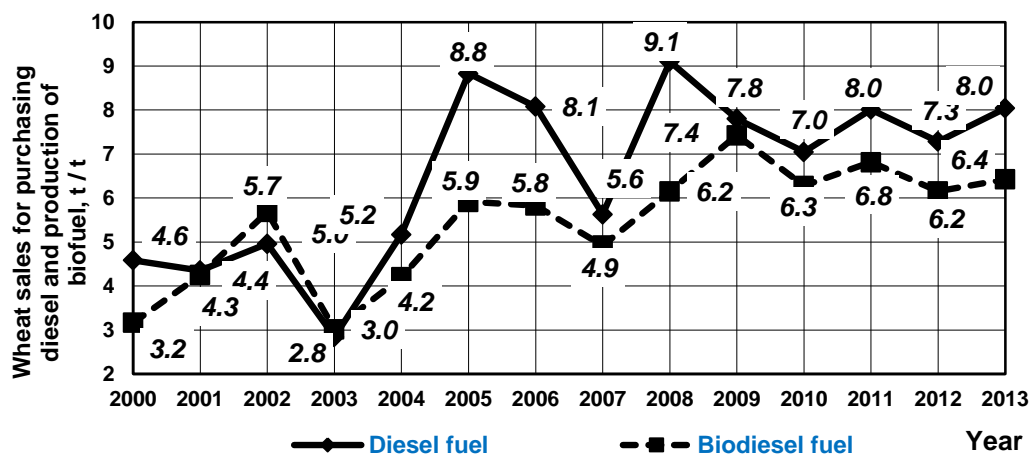


Fig. 2 – Change dynamics of required wheat sale volumes to buy diesel or produce biodiesel

Farms can produce biodiesel after harvesting oilseeds, i.e. in autumn. In autumn-winter period diesel is limitedly used in agricultural production – in animal husbandry only (Ivanova B., Stoyanov S., 2016; Baskar G., Aiswarya R., 2016). The produced biodiesel is stored in warehouses for oil products till the beginning of spring field work. When stored in sealed containers, biodiesel does not lose its properties during the year, unlike rapeseeds and rape oil. Prices for fossil diesel are constantly increasing, especially at the beginning of spring, but the cost of produced biofuels in the previous year remained unchanged, that is one of the cost saving provisions in agriculture.

The profitability of production of rapeseeds, rapeseed oil and based on it biodiesel is affected by a number of factors including: the cost and selling price of rapeseeds, production capacity of equipment which was used for production of oil and biofuels, the price situation in the diesel market. Profitability of rapeseed oil production was higher than the one of rapeseed production for the entire studied period, except of 2001, 2002 and 2010. Profitability of biodiesel production was lower than the one of oil and rapeseeds in 2000-2004, 2006, 2008, 2009, 2011 and 2012. Profitability of biodiesel production in 2005, 2007, 2010 and 2013 was greater than the one of rapeseed production, which can be explained by reducing of rapeseed realization cost.

Stable high demands, formed by the world market, and high prices provide highly profitable rapeseed production and are very attractive to investors. Profitability of rapeseed production was increasing till 2004 and reached 69%, and starting from 2005 up to 2007 it tended to decrease, and stabilized at 17-35%. Profitability of rapeseed oil production was increasing till 2004 and reached 81%, from 2005 to 2010 – it was decreasing (except in 2008, when there was the highest index – 86%) and stabilized at the level of 8-17%. Analysing the profitability of biodiesel production, it should be mentioned, that by 2002 biodiesel production was not profitable, due to the relatively high cost of its production and a fairly low price of diesel. However, with the rising cost of fossil fuels, the profitability of biodiesel production has significantly increased, and from 2004 to 2007 exceeded even the profitability of crop production, confirming the effectiveness of investment and the need to develop the biofuel production branches.

The analysis of interest rates on deposits of banks of Ukraine shows that for the 2000-2011 the interest rate for individuals ranged from 12.6 to 20.4%, for legal entities – from 6.6 to 13.8% (National Bank of Ukraine). However, investing money into biodiesel production, investor derives much greater profit. So, in 2004 the average interest rate on bank deposits for individuals was 15.7%, for entities – 8.9%, while the profitability of biofuel production was 40%, in 2007 respectively – 14.1 and 8.9%, and biofuel profitability – 38%, in 2010, rates of banks – 18.8% and 13.7%, while biofuel production – 27%. Raising funds to produce biodiesel is probable not only to improve the efficiency of invested capital, but also to make contribution for improving the environmental situation of the country and for ensuring power independence industry, as well as the country as a whole.

BIOGAS

Experience of using biogas reactors showed that there are reactors already half-filled with mineral sediment, which can be removed only with an excavator after total stopping of fermentation process. Floating layers, especially based on fibrous substrates, often form a crust and if it is not mixed, the reactor must also be stopped to remove it.

Thus, the improvement of biogas reactor work to ensure the mixing of biomass substrate layers requires new technical solutions, one of which is mixing by rotation of the suspended reactor submerged into water. We have developed and patented several designs of modular anaerobic digesters of rotational type (Patent Ukraine №110077, 2015); the design of one of those is shown in fig. 3.

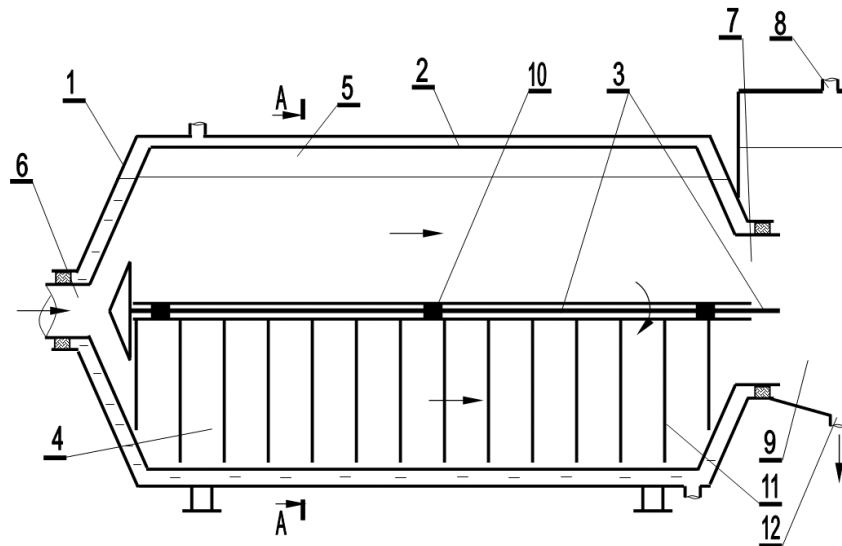


Fig. 3 – Construction of anaerobic digester immersed into thermostatic liquid

1 – horizontal outer casing, 2 – cylindrical reactor 3 – longitudinal bulkhead, 4, 5 – fermentation chambers, 6, 7 – tubes for cart and removal of organic matter, 8 – pipe for biogas runoff, 9 – unloading camera, 10 – joints
11 – mixing fingers, 12 – pipe for organic matter removing

Our calculations showed that the microbiological decomposition while anaerobic fermentation of 1 kg of organic matter is accompanied by about 0.4 kg of methane yield and by 0.7 kg of carbon dioxide yield. Assuming that the volume of produced biogas is determined by the intensity of organic matter decomposing during organic biomass fermentation, biogas yield while fermentation in terms of normal conditions can be defined as follows:

$$V_{BG} = \rho_{BM} \left(1 - \frac{W_{BM}}{100} \right) k_{OM} k_{OM}^D \frac{m_{BG}}{\rho_{BG}^N}, \quad (3)$$

where:

V_{BG} is a specific biogas yield from the reactor under normal conditions, m^3_{BG}/m^3_{BM} per day;

ρ_{BM} – biomass density, kg_{BM}/m^3_{BM} ;

W_{BM} – biomass humidity, %;

$\left(1 - \frac{W_{BM}}{100} \right)$ – dry matter content in relation to the total biomass, kg_{DM}/kg_{BM} ;

k_{OM} – organic matter content in relation to the volume of the total dry weight in fermenting biomass, kg_{OM}/kg_{DM} ;

k_{OM}^D – the number of decomposed organic matter per day in relation to the total organic mass, kg_{DOM}/kg_{OM} per day;

M_{BG} – biogas yield per unit of decomposed organic matter, kg_{BG}/kg_{DOM} ;

ρ_{BG}^N – biogas density under normal conditions, kg_{BG}/m^3_{BG} .

Table 2

Calculation of the specific release of biogas and biomethane		
Indicator	Measurement	Values
Manure density	$\text{kg}_{\text{BM}} / \text{m}^3_{\text{BM}}$	1062
Humidity	%	90
Water content	$\text{kg}_W / \text{kg}_{\text{BM}}$	0.9
Dry weight	%	10
	$\text{kg}_{\text{DM}} / \text{kg}_{\text{BM}}$	0.1
Organic matter content	%	80
	$\text{kg}_{\text{OM}} / \text{kg}_{\text{DM}}$	0.8
The intensity of organic matter decomposing	% per day	3.0
	$\text{kg}_{\text{DOM}} / \text{kg}_{\text{OM}}$ per day	0.03
	$\text{kg}_{\text{DOM}} / \text{m}^3_{\text{BM}}$ per day	2.55
Biogas yield from decomposed organic matter under normal conditions	$\text{kg}_{\text{BG}} / \text{kg}_{\text{DOM}}$	1.1
	$\text{m}^3_{\text{BG}} / \text{kg}_{\text{DOM}}$	0.92
Biogas yield from the reactor under normal conditions	$\text{m}^3_{\text{BG}} / \text{m}^3_{\text{BM}}$ per day	2.34
Biomethane yield under normal conditions	$\text{m}^3_{\text{CH}_4} / \text{m}^3_{\text{BM}}$ per day	1.666
The maximum level of organic biomass decomposing	%	38
	$\text{kg}_{\text{POM}} / \text{m}^3_{\text{BM}}$	32.5
Fermentation time	days	12.74

At the same time, specific biomethane yield will be:

$$V_{\text{CH}_4} = V_{\text{BG}} k_{\text{CH}_4}, \quad (4)$$

where:

V_{CH_4} – is specific biomethane yield from the reactor under normal conditions, $\text{m}^3_{\text{CH}_4} / \text{m}^3_{\text{BM}}$ per day;

k_{CH_4} – volume of biomethane content in biogas, $\text{m}^3_{\text{CH}_4} / \text{m}^3_{\text{BG}}$.

With the parameters introduced in table 2, the relations between the intensity of organic matter decomposing and specific biomethane and biogas yields, and fermentation time, will take the form shown in fig. 4.

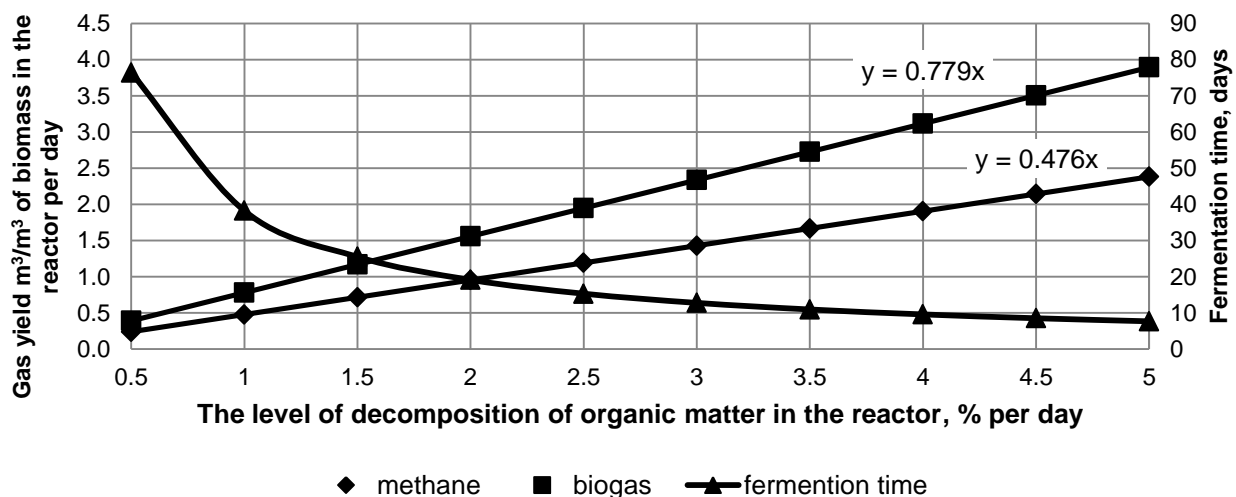


Fig. 4 – The effect of organic matter decomposing intensity on the specific yield of biomethane, biogas and fermentation time

Biogas and biomethane yields increase proportionally with increasing the level of organic biomass decomposing in the reactor, and the fermentation time decreases exponentially until it reaches 38% fermentation level.

CONCLUSIONS

Biological and energetic conversion of organic agroecosystem raw materials with energy production can ensure energy autonomy of agroecosystems in total energy balance. Though, it is impossible to do it according to the types of fuels and energy, since there is a limit on the possibility of autonomous production of electric power and gasoline. However, production of biodiesel and heat energy can be redundant. The source of raw materials that would meet the needs of agricultural production under centralized bioethanol production is sufficient. At the same time, to implement such systems, first of all, it is necessary to change the basic principles of society existence, regarding manufacturing of environmentally friendly production and biological diversity preserving.

The heat of straw combustion reduces down to 0.18 to 0.21 MJ/kg for each percent of its humidity increase. Energy efficiency is increased while burning straw in the compressed form (briquettes, pellets). Baled straw should be burned in boilers equipped with cameras for post-combustion of volatile compounds. Non-pressed straw should be burned in crushed form by using eddy chambers.

The main direction in manure fermentation process intensification is the increase of organic matter decomposition at the cost of creation of appropriate conditions for the development of anaerobic microflora. This can be achieved by creating stable fermentation temperature conditions and, what is more important, by providing quality biomass mixing, which, on the one hand, must not disturb the symbiosis of acetogenic and methanogenic bacteria, and, on the other hand, prevent the exfoliation of biomass in the reactor to mineral sediment and floating organic layer.

REFERENCES

- [1] Barotfy I., Rapan P., (1988), *Energy saving technology and aggregates in livestock farms. (Энергосберегающие технологии и агрегаты на животноводческих фермах)*, p. 228, Agropromizdat, Moscow;
- [2] Baskar G., Aiswarya R., (2016), Trends in catalytic production of biodiesel from various feedstocks, *Renewable and Sustainable Energy Reviews*, Vol. 57, pp. 496–504, Colorado/USA;
- [3] Corsini A., Marchegiani A., Rispoli F., et al., (2015), Vegetable Oils as Fuels in Diesel Engine. Engine Performance and Emissions, *Energy Procedia*, Vol. 81, pp. 942–949, Sweden;
- [4] Geletukha G.G., Zheleznaya T.A., (2012), The place of bioenergy in development updated energy strategy of Ukraine until 2030 (Место биоэнергетики в проекте обновленной энергетической стратегии Украины до 2030 года. Аналитическая записка), *Electronic resource*, <http://www.qclub.org.ua/wp-content/uploads/>;
- [5] Golub G.A., Kukharets S.M., (2015), Patent № 110077. Ukraine, *Methanetanks (Метантенк) Digest №21*, p.5;
- [6] Gouxa X., Calusinskaa M., Fossépréa M., et al., (2016), Start-up phase of an anaerobic full-scale farm reactor – Appearance of mesophilic anaerobic conditions and establishment of the methanogenic microbial community, *Bioresource Technology*, Vol. 212, pp. 217–226, Punjab/India;
- [7] Ivanova B., Stoyanov S., (2016), A mathematical model formulation for the design of an integrated biodiesel-petroleum diesel blends system, *Energy*, Vol. 99, pp. 221–236, Aalborg/Denmark;
- [8] Man X., Cheung C, Ning Z. (2015), Effect of Diesel Engine Operating Conditions on the Particulate Size. Nanostructure and Oxidation Properties when Using Wasting Cooking Oil Biodiesel, *Energy Procedia*, Vol. 66, pp. 37-40, Sweden;
- [9] Satjaritanuna P., Khunatorna Y., Vorayosa N., et al., (2016), Numerical analysis of the mixing characteristic for napier grass in the continuous stirring tank reactor for biogas production, *Biomass and Bioenergy*, vol 86, pp. 53–64, Aberdeen/U.K.;
- [10] Shkarada M., (1985), Production and Application of organic fertilizers (Производство и применение органических удобрений) p. 364, *Agropromizdat*, Moscow/USSR;
- [11] *** Agricultural Ukraine. Stat. Coll.; eds. O.M. Prokopenko, (2015), p. 360, *State Statistics Service of Ukraine*, Kyiv/Ukraine;
- [12] *** DSTU 3581-97, Energy efficiency, *Methods of measuring and calculating the heat of combustion (Энергосбережения. Методи вимірювання і розрахунку теплоти згорання палива)*, Kyiv/Ukraine;
- [13] *** Guide to biogas. From obtain to using / Renewable resources Agency (FNR). 5th edition, (2012), (Руководство по биогазу. От получения до использования / Специальное агентство возобновляемых ресурсов (FNR). 5-е издание.), p. 213, Hyultsov/Germany;
- [14] ***National Bank of Ukraine, Electronic resource, <http://www.bank.gov.ua>;

STABILITY OF EPS SYSTEM OF AGRICULTURAL VEHICLES UNDER VIBRATION ENVIRONMENT

农用车辆振动环境下电动助力转向系统的稳定性研究

Ph.D. Zhipeng Li, M.S. Songzhuo Shi¹⁾

School of Transportation, Northeast Forestry University, Harbin, Heilongjiang / China

Tel: +86-0451-82191847; E-mail: sisongzhuo@126.com

Keywords: road surface input; power steering; global fast terminal sliding mode control; steering stability

ABSTRACT

Agricultural towing vehicles are driven under poor road conditions. The impact of rough road surface seriously affects the driving safety of agricultural towing vehicles. The mechanism of vibration of agricultural towing vehicles caused by rough roads is explored to reduce the adverse effects of road surface impact on the handling stability of agricultural towing vehicles and to improve the handling and steering stability of vehicles. First, the adverse effects of rough road input conditions on the handling stability of electric power steering (EPS) system were considered, and the kinetic model of the EPS system and the eight degree-of-freedom models of the whole vehicle were established. Second, tire and road surface impact models were introduced. Finally, the stability of the steering system under rough road input conditions was analyzed. Results show that the current following accuracy of the proposed motor control system is increased by 5%, and the final return-to-center residual angle of the steering wheel is 15 degrees. This study indicates that the vehicle vibration caused by road surface impact affects not only the driving stability of vehicles but also the smooth return of the steering system. The motor control system designed in this study effectively reduces the adverse effects of road surface impact on the steering system. The analysis and research process and the results are suitable for the investigation on the return-to-center performance of the EPS system for passenger and freight cars and the response of vehicle handling stability under different vibration sources.

摘要

农用牵引车辆行驶路面条件恶劣，路面不平产生的冲击严重影响了农用牵引车辆的行驶安全性。为了降低路面冲击对农用牵引车辆操纵稳定性造成的不良影响，本文研究了路面不平引起的农用牵引车辆振动的产生机理，以提高车辆转向时的操纵稳定性。首先，针对不平路面输入状况对电动助力转向系统操纵稳定性产生的不良影响，建立了电动助力转向系统动力学模型与整车 8 自由度模型，同时引入了轮胎和路面冲击模型，分析了不平路面输入状况下转向系统的稳定性。结果显示，本文设计的电机控制系统的电流跟随准确性提升了 5%，转向盘的最终回正残留角度为 15 度。研究表明，路面冲击产生的车辆振动不仅对车辆的行驶稳定性产生影响，同时会影响转向系统转向回正平顺性，本文设计的电机控制系统有效降低了路面冲击对转向系统性能造成的不良影响。本文的分析和研究过程适用于研究乘用车及货运车电动助力转向系统回正性能和车辆操纵稳定性在不同振源下的响应，研究结论可以应用在不同路面激励下，电动助力转向系统转向盘回正响应的理论研究中。

INTRODUCTION

Agricultural towing vehicles have complex working conditions because roads in the wild field are rough, and these vehicles are prone to making lateral and yaw motion when steering. When the steering wheel of agricultural towing vehicles returns to center, road surface impact also affects the accuracy of the return-to-center angle of the steering wheel, thereby causing the vehicle to deviate from the safe travel path. The EPS system is combined with the active front-wheel steering system in which the damping compensation algorithm is used to control the power motor in the EPS system, to effectively reduce the negative effect of road surface impact on the steering system (Fan lu and Zhou bing, 2014). The vibration sources of vehicles, such as the jitter that occurs when the engine is running, and the low-frequency vibration of the steering system itself, affect the steering stability of vehicles (He Ren and Miao Lidong, 2009). In the research on road vibration, the road surface input model is divided into random and non-random road surface input models; currently, research on the road surface input model mainly focuses on

non-random road surface input model (Hu Jianjun, et al., 2008). Scholars generally believe that the high-precision control algorithm of motor current tracking and the simulation technology of computer-based road vibration play a unique role in suppressing road vibration and improving EPS steering stability (Hamada H. et al., 2006; Anthony J, 2000). Other scholars have also conducted considerable research to explore the improvement of the response speed and precision of motor used in the EPS system and to reduce the adverse effect of vehicle vibration on the motor tracking performance. Zhao and Bei (Bei Shaoyi et al., 2011) applied the fuzzy PID control algorithm to the return-to-center control to improve the return-to-center stability of the EPS system, and the experimental results indicated that the algorithm improves the insufficient and overshoot return-to-center situations of the steering system. Borowiec et al. (Sen A. et al., 2010) collected data on the vertical acceleration speed of left and right suspension racks of a vehicle under three road conditions, namely, asphalt, stone, and imitation railway crossroads; their analysis results of the collected data values showed that the vertical vibration of the suspension rack caused by roads is a low-frequency vibration. Múčka (Múčka P, 2016) used the “road surface vehicle driver” as a carrier and established the relationship between the international flatness index and road roughness impact response to improve the driving comfort and vehicle safety of the driver. This study analyzes the kinetic model of the EPS system, the road surface input model, and the eight degree-of-freedom (DOF) whole vehicle model, and investigates the effect of road surface impact on the steering stability of the EPS system.

MATERIAL AND METHODS

Eight DOF model of agricultural towing vehicles

Based on the yaw, lateral, and pitching motion of vehicles, the vehicle longitudinal dynamics of the four DOF mathematical model was established. Formulas 1-3 are the kinetic equation of the vehicle in the yaw, lateral, and pitching DOFs (Xiao Hansong et al., 2014; Guo Konghui, 1991), respectively.

$$I_z \ddot{Y}_{aw} = \frac{B_1}{2} [(-F_{x11} + F_{x12}) \cos \delta - (-F_{y11} + F_{y12}) \sin \delta] + \frac{B_2}{2} (-F_{x12} + F_{x22}) + a[(F_{x11} + F_{x12}) \sin \delta + (F_{y11} + F_{y12}) \cos \delta] - b(F_{y21} + F_{y22}) \quad (1)$$

Where Y_{aw} is yaw angular velocity of vehicle (rad/s), δ is steering angle of front wheel ($^\circ$), a is distance between vehicle centroid and front wheels (mm), b is distance between vehicle centroid and rear wheels (mm), B_1 and B_2 is distance between front wheels and between rear wheels respectively (mm), I_z is vehicle yaw moment of inertia (kg/m^2), $F_{x11}, F_{x12}, F_{x21}$ and F_{x22} is lateral force of left front, left rear, right front, and right rear tire, respectively (N), $F_{y11}, F_{y12}, F_{y21}$ and F_{y22} is longitudinal force of left front, left rear, right front, and right rear tire, respectively (N).

The pitch motion equation of vehicles is as follows:

$$J_y \ddot{\theta} + m_s D_0 (\dot{u} - v \dot{Y}_{aw}) - F_{s11} a - F_{s12} a + F_{s21} b + F_{s22} b = 0 \quad (2)$$

Where m_s is mass of the whole vehicle (kg), J_y is the pitch moment of inertia of the vehicle body (kg/m^2), $F_{s11}, F_{s12}, F_{s21}$ and F_{s22} is suspension force (N), v is vehicle horizontal velocity (m/s), θ is vehicle pitch angle ($^\circ$), u is vehicle lateral velocity (m/s^2), D_0 is coefficient of body roll.

The lateral motion equation of vehicles is as follows:

$$J_x \ddot{f} - m_s e_0 (\dot{v} + u \dot{Y}_{aw}) = -F_{s11} \frac{1}{2} B_{11} + F_{s12} \frac{1}{2} B_{11} - F_{s21} \frac{1}{2} B_{22} + F_{s22} \frac{1}{2} B_{22} \quad (3)$$

Where: J_x is vehicle lateral moment of inertia (kg/m^2), f is the roll angle of the vehicle, e_0 is coefficient of body pitch.

The vertical displacement caused by random road excitations will change the vertical force of vehicles. The vertical motion equation of vehicles is shown in Formulas 4-7.

$$m_{t1} \ddot{x}_{t1} = k_{t1} (x_{r1} - x_{t1}) + k_{s1} (x_{s1} - x_{t1}) + c_{s1} (\dot{x}_{s1} - \dot{x}_{t1}) \quad (4)$$

$$m_{t2} \ddot{x}_{t2} = k_{t2} (x_{r2} - x_{t2}) + k_{s2} (x_{s2} - x_{t2}) + c_{s2} (\dot{x}_{s2} - \dot{x}_{t2}) \quad (5)$$

$$m_{t3} \ddot{x}_{t3} = k_{t3} (x_{r3} - x_{t3}) + k_{s3} (x_{s3} - x_{t3}) + c_{s3} (\dot{x}_{s3} - \dot{x}_{t3}) \quad (6)$$

$$m_{t4} \ddot{x}_{t4} = k_{t4} (x_{r4} - x_{t4}) + k_{s4} (x_{s4} - x_{t4}) + c_{s4} (\dot{x}_{s4} - \dot{x}_{t4}) \quad (7)$$

where m_{i1}, m_{i2}, m_{i3} and m_{i4} is suspension mass (kg), x_{r1}, x_{r2}, x_{r3} and x_{r4} is Roda surface stimulus input (mm). x_{s1}, x_{s2}, x_{s3} and x_{s4} is suspension mass and displacement at the connection of suspension (mm), c_{s1}, c_{s2}, c_{s3} and c_{s4} is equivalent damping coefficient of left front wheel, left rear wheel, right front wheel and right wheel, k_{s1}, k_{s2}, k_{s3} and k_{s4} is suspension stiffness coefficient, k_{t1}, k_{t2}, k_{t3} and k_{t4} is tire stiffness.

The longitudinal displacement of vehicles will cause the change in vehicle suspension force. Formulas 8–11 are used to calculate the suspension force.

$$F_{s11} = K_1(x_{t1} - a\theta + \frac{1}{2}B_{11}\dot{f}) + C_1(x_{t1} - a\dot{\theta} + \frac{1}{2}B_{11}\dot{f}) \tag{8}$$

$$F_{s12} = K_1(x_{t2} - a\theta - \frac{1}{2}B_{11}\dot{f}) + C_1(x_{t2} - a\dot{\theta} - \frac{1}{2}B_{11}\dot{f}) \tag{9}$$

$$F_{s22} = K_2(x_{t3} - b\theta + \frac{1}{2}B_{22}\dot{f}) + C_2(x_{t3} - b\dot{\theta} - \frac{1}{2}B_{22}\dot{f}) \tag{10}$$

$$F_{s21} = K_2(x_{t4} - b\theta + \frac{1}{2}B_{22}\dot{f}) + C_2(x_{t4} - b\dot{\theta} + \frac{1}{2}B_{22}\dot{f}) \tag{11}$$

where x_{i1}, x_{i2}, x_{i3} and x_{i4} is sprung mass displacement (mm).

Formula 12 expresses the conversion relationship between the steering and the front-wheel angle.

$$\delta = \frac{\theta_s}{n} - \frac{M_{l1} + M_{l2}}{k} \tag{12}$$

where M_{l1} and M_{l2} is positive moments of left and right front wheels (kg), k is stiffness of steering system, n is total transmission ratio of steering system.

The DOF of the whole vehicle model is illustrated in Fig.1.

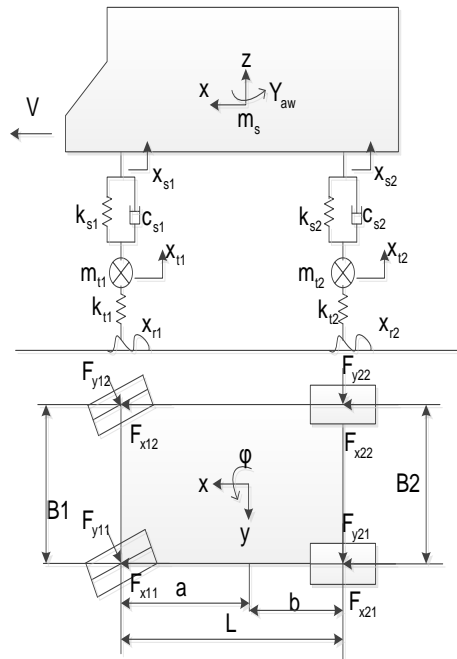


Fig.1 - Whole vehicle model

Kinetic model of EPS system

The EPS system is a steering column EPS system (Lin Yi et al., 2007; Mohammadi H and Kazemi R, 2003), and the established kinetic equation of the EPS steering system is expressed as Formulas 13–17.

$$\text{Steering column : } J_s \ddot{\theta}_s + B_s \dot{\theta}_s + k_s (\theta_s - \frac{x_r}{r_p}) = T_d \tag{13}$$

$$\text{Output shaft: } J_e \ddot{\theta}_e + B_e \dot{\theta}_e = k_s (\theta_s - \frac{x_r}{r_p}) + \frac{k_m i_m}{r_p} (\theta_m - \frac{x_r}{r_p}) \tag{14}$$

$$\text{Rack: } m_r \ddot{x}_r + b_r \dot{x}_r + F_r = \frac{k_s}{r_p} (\theta_s - \frac{x_r}{r_p}) + \frac{k_m i_m}{r_p} (\theta_m - \frac{x_r}{r_p}) \tag{15}$$

$$\text{Motor: } J_m \ddot{\theta}_m + B_m \dot{\theta}_m = T_m - \frac{T_a}{G} \quad (16)$$

$$\text{Motor current: } i_m = \frac{u - k_m \theta_m}{R} \quad (17)$$

where J_e is deceleration mechanism inertia (kg/m^2), J_m is motor moment of inertia (kg/m^2), B_s is damping coefficient of steering column, B_e is damping coefficient of deceleration mechanism, B_m is motor damping coefficient, k_s is stiffness coefficient of torque sensor, k_m is motor torque coefficient, T_m is motor electromagnetic torque (N.m), T_a is power torque of motor (N.m), T_d is input torque of steering wheel (N.m), x_r is rack displacement (mm), r_p is pinion radius (mm), i_m is motor current (A), m_r is total mass of pinion and rack (kg), b_r is sticking coefficient of the rack; G is transmission ratio of deceleration mechanism; U is motor voltage (V), F_r is force of tire on the road (N), J_s is moment of inertia of steering column (kg/m^2).

Tire Model

The conversion between steering and the front wheel angle requires using the return-to-center torque of the tire; thus, introducing the tire mechanics model is necessary. The establishment of a relatively perfect tire model is difficult because the force of the tire is influenced by many factors, such as tire material, pressure, and positioning parameter. This study quotes a mature tire model, namely, the tire magic formula model (Li Songyan et al., 2009).

In formula 18, F_r is the force between tire and road surface. If the tire sideslip angle is less than 3° , then the lateral force is linearly proportional to the transverse displacement of the rack x_r .

$$F_r = D \sin\{C \arctan[Bx - E(Bx - \arctan Bx)]\} \quad (18)$$

where Y is a longitudinal force, lateral force, or return-to-center torque; x is the tire sideslip angle or longitudinal slip rate; D is the peak factor; C is the shape factor; B is the stiffness factor and E is the curvature factor.

Under pure rolling conditions, the lateral force applied on the tire is expressed as follows:

$$F_y = D \sin\{C \arctan[BX_1 - E(BX_1 - \arctan BX_1)]\} + S_v \quad (19)$$

where S_v is the vertical displacement of the tire lateral force curve. Road surface conditions affect the smooth driving of vehicles, and the dynamic load of the tire is closely related to road excitation.

Road time-domain model of four-wheel input

The road-surface input model (Lu Shifu and Zhao Heng, 1999) acting on the tire is expressed as follows:

$$\dot{x}_r(t) = F_w x_0(t) + B_0 w_1(t) \quad (20)$$

where $x_r = [x_{r1}, x_{r2}, x_{r3}, \text{ and } x_{r4}]^T$ is the road excitation input of four wheels. $w_1(t)$ is the white noise input of the left front wheel. F_w is the product of vehicle speed V and road roughness coefficient a .

Determination of return-to-center status of EPS system

The torque sensor used in the designed EPS system integrates the function of detecting the steering wheel angle. Therefore, the return-to-center conditions of the EPS system can be judged by the steering wheel angle and the change rate of angle. The judgment bases are demonstrated as follows:

Power control conditions: $\theta_s > 0, \dot{\theta}_s > 0$;

Return-to-center control conditions: $\theta_s > 0, \dot{\theta}_s < 0$;

Design of variable structure controller of global fast terminal sliding mode

A global fast terminal sliding mode control (SMC) can make the system (Liu Jinkun, 2000) state converge to zero within a finite time, whereas an ordinary sliding mode control gradually converges under the linear sliding mode surface. The dynamic performance of the system is better than the ordinary sliding mode control.

Design of sliding mode surface

The EPS system is a two-order system, and the sliding mode surface equation of the sliding mode controller is $s = \alpha e + \dot{e} + \beta e^{q/p}$, where $e = \theta_s - x_r$, $\dot{e} = \dot{\theta}_s - \dot{x}_r$, where e is the error signal, θ_s is the steering wheel angle, the state variable x_r is the displacement of gear, and α is the constant larger than zero and satisfies the Hurwitz polynomial. $b > 0$, p and $q (p > q)$ are positive odd number, in which $F(t)$ represents the non-linear part, $F(t) = f(t)\beta e^{q/p}$. The sliding mode surface equation satisfies the following conditions: (1) $s(0) = \alpha e(0) + \dot{e}(0) + F(t)$; (2) $t \rightarrow \infty, s(0) = 0$; (3) $s = \alpha e + \dot{e} + \beta e^{q/p}$ and can be differentiable. Condition (1) ensures that the initial condition of the system is on a sliding mode surface. Condition (2) ensures the gradual stability of the system. Condition (3) ensures the occurrence of sliding mode motion.

Verifying the stability of sliding mode controller

The high-order single-input single-output nonlinear state equation of the global fast terminal sliding mode controller is expressed in the following formulas:

$$\dot{x}_i = x_{i+1} \quad (21)$$

$$\dot{x}_n = f(x) + g(x)u(t) \quad (22)$$

According to the sliding mode surface equation, the recursive expression for the sliding mode surface of the global fast sliding mode is expressed as follows:

$$s_{n-1} = \dot{s}_{n-2} + \alpha_{n-2}s_{n-2} + \beta_{n-2}s_{n-2}^{q_{n-2}/p_{n-2}} \quad (23)$$

According to formula 23,

$$\dot{s}_{n-1} = \ddot{s}_{n-2} + \alpha_{n-2}\dot{s}_{n-2} + \beta_{n-2}\frac{d}{dt}s_{n-2}^{q_{n-2}/p_{n-2}} \quad (24)$$

$$\dot{s}_{n-1} = f(x) + g(x)u(t) + \sum_{k=0}^{n-2} \alpha_k s_k^{(n-k-1)} + \sum_{k=0}^{n-2} \beta_k \frac{d^{n-k-1}}{dt^{n-k-1}} s_k^{q_k/p_k} \quad (25)$$

After substituting formula 2 into formula 25,

$$\dot{s}_{n-1} = -\varphi s_{n-1} - \gamma s_{n-1}^{q/p} \quad (26)$$

According to Lyapunov function,

$$V = \frac{1}{2} s_{n-1}^2 \quad (27)$$

Then, $\dot{V} = s_{n-1}\dot{s}_{n-1} = -\varphi s_{n-1}^2 - \gamma s_{n-1}^{(q+p)/p}$, $p+q$ is an even number; thus, when $\dot{V} < 0$, the system is stable.

Design of sliding mode control rule

If $x = \theta_s$, then the EPS system model can be represented by a high-order single-input single-output nonlinear system:

$$\begin{aligned} \ddot{x} &= f(x) + g(x)u(t) + d(t) \\ f(x) &= \left(\frac{k_m^2 G_m}{R} + \frac{k_m^2 p G_m}{J_s r_p} \right) x - \left(B_s + \frac{k_m^2 G_m^2}{R} \right) \dot{x}; \quad g(x) = -\frac{k_m G_m}{R} x - \frac{k_m x_r}{J_s r_p} \\ d(t) &= \frac{T_d}{J_s} - \frac{r_p}{J_s} (m_r \ddot{x}_r + b_r \dot{x}_r + k_r x_r) \end{aligned} \quad (28)$$

The control rule of the global time-varying sliding mode, $u = u_{eq} + u_{vss}$, $\ddot{x} = f(x) + g(x)u(t) + d(t)$ is substituted into $\dot{s} = 0$. Then,

$$u = \frac{\alpha \dot{e} + \beta q e + p \left[\frac{k_m G_m}{R} x - \left(B_s + \frac{k_m^2 G_m^2}{R} \right) \dot{x} \right] + \frac{k_m^2 p \theta_m^2 - \frac{r_p}{J_s} (m_r \ddot{x}_r + b_r \dot{x}_r + k_r x_r)}{\frac{k_m G_m}{R} x + \frac{k_m x_r}{J_s p}} + K \text{sign}(t) \quad (29)$$

RESULTS

In this study, an LH-UTV-400 low-energy-consumption agricultural towing vehicle is used as the research object. Fig.2(a) depicts the real vehicle.

Table 1 displays the measurement parameters of the vehicle.



Fig. 2(a) - Picture of vehicle

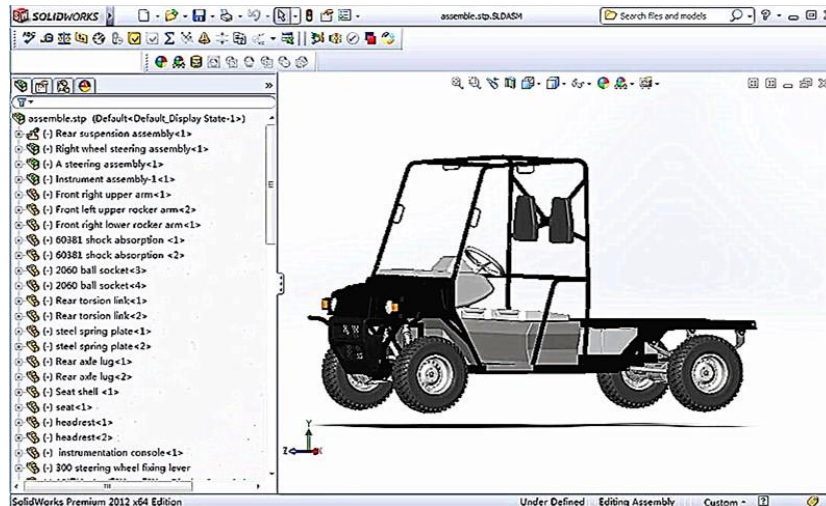


Fig.2(b) - Picture of vehicle model

Fig.2(b) illustrates the vehicle simulation model established in SolidWorks software based on the measurement parameters of the vehicle.

Table 1

Vehicle parameters

Name of parameters	Parameter value
Mass of vehicle, (m/kg)	3021
Mass of suspension, (m _s /kg)	2687
Lateral inertia moment of body, ($J_y/kg/m^2$)	1960
Distance between front wheels, B_1 (mm)	1320
Distance between rear wheels B_2 (mm)	1330
Distance between vehicle centroid and front axle, a (m)	1.24
Distance between vehicle centroid and rear axle b (m)	1.28
Body yaw rotation inertia I_x (kg/m^2)	10437
Mass of front wheel non-suspension, m_{t1}, m_{t2} (kg)	55
Mass of rear wheel non-suspension, m_{t3}, m_{t4} (kg)	58
Stiffness of front suspension k_{s1}, k_{s2} (N/m)	17000
Stiffness of rear suspension k_{s3}, k_{s4} (N/m)	2000
Total transmission ratio of steering system, n	18
Stiffness of left-front tire and left rear-tire k_{t1}, k_{t2} (N/m)	192000
Stiffness of left-front tire k_{t3} and left-rear tire k_{t4} (N/m)	192000
The total stiffness of the steering system k (N/m)	2317
The damping coefficients of left-front wheel and left-rear wheel $c_{s1} c_{s2}$ (Ns/m)	2048
The damping coefficients of right-front wheel and right-rear wheel c_{s3} and c_{s4} (Ns/m)	2048

Comparison between accuracy of motor target current tracking through the variable structure control algorithm of the global fast terminal sliding mode and PID algorithm

The preconditions for the variable structure controller of the global fast terminal sliding mode to reach the steady state include the following: (1) The sliding mode surface moves on the surface $s = 0$ from $t = 0$. (2) The phase trajectory of the system finally converges to 0. In Fig.3, the sliding mode surface selected by global fast terminal sliding mode control has a position displacement of -0.1 near $s = 0$ at the initial stage of the system motion, which lasts for approximately 0.25 s, and the state variable selected from the system moves on the sliding mode surface $s = 0$. In Fig.4, the phase plane of the sliding mode controller is convergent, indicating that the sliding mode control is stable. The motion trajectory of the state variable selected by the sliding state controller has been on the sliding mode surface, and the system has strong robustness. Therefore, applying the sliding-mode control algorithm in the motor control system is essential to enhance the control accuracy of the EPS system.

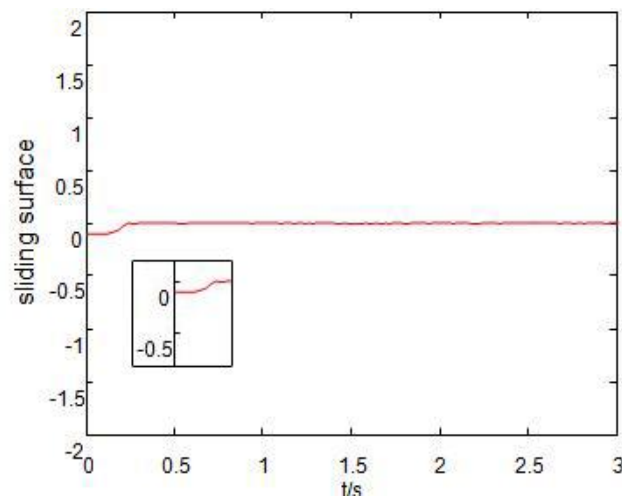


Fig. 3 - Sliding mode surface

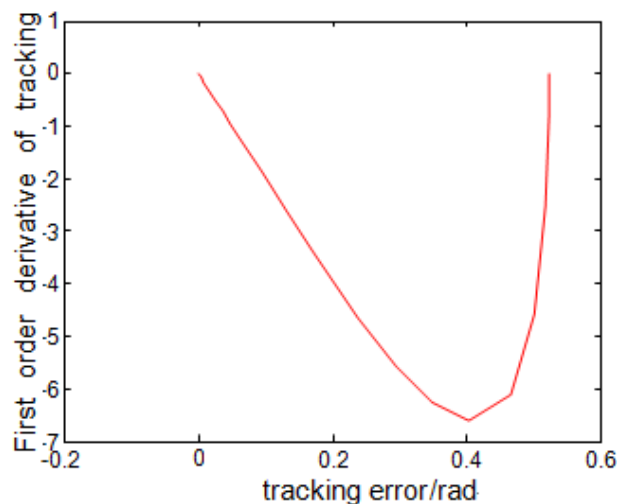


Fig. 4 - Phase trajectory

After adding the control algorithm of the global fast sliding mode into the EPS system, the tracking accuracy of the motor target current is increased by 5%. In Fig.6, the control algorithm of the global fast sliding mode increases the robustness of the system and weakens the jitter effect of the road surface impact on the motor current. In Fig.5, the traditional PID algorithm has obvious inadequate motor current tracking effect, whereas the motor current has a significant jitter. The effect of road surface impact is retained.

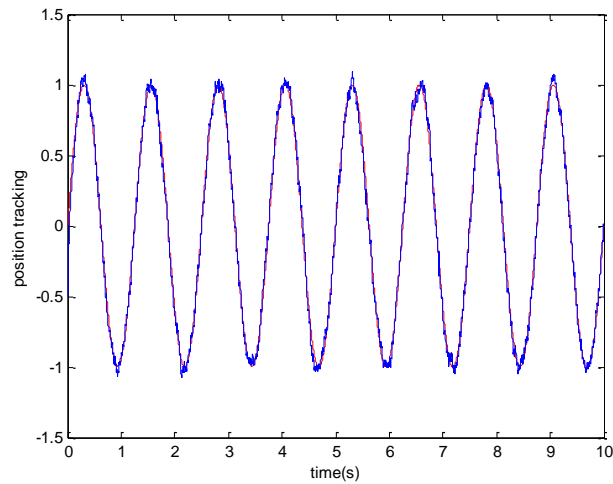


Fig. 5 - Traditional PID control

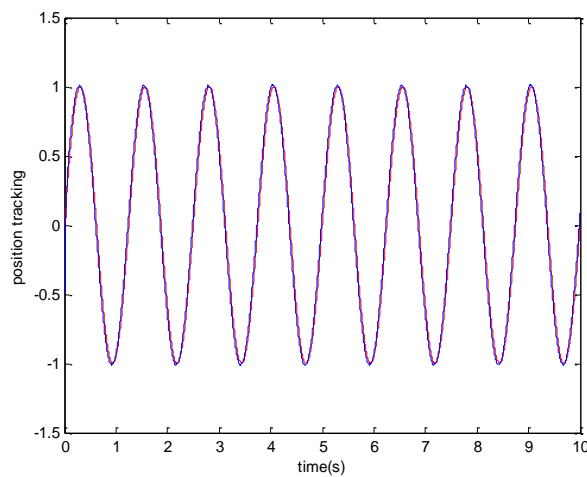


Fig. 6 - Global fast sliding mode control

Relationship between vehicle handling stability and road surface impact

Based on the simulation model of “road surface–EPS system vehicle,” this study compares the response curves of the yaw angular velocity with the lateral acceleration by using the sliding mode and the PID control and concludes that the yaw angular velocity response of the vehicle controlled by the global fast sliding mode control is zero under road surface impact, and the yaw angular velocity response residual of vehicle is 0.01 under control of traditional PID. The results indicate that the global sliding mode control can effectively overcome the impact of road direction input on the yaw angular velocity of the vehicles.

Fig.7 indicates the response of yaw angular velocity and Fig.8 indicates the response of lateral angular velocity.

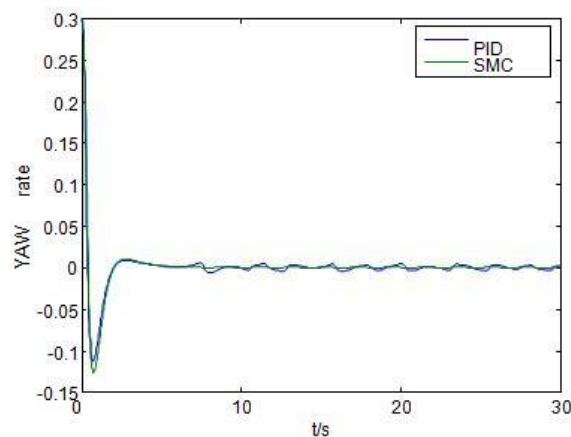


Fig. 7 - Response of yaw angular velocity

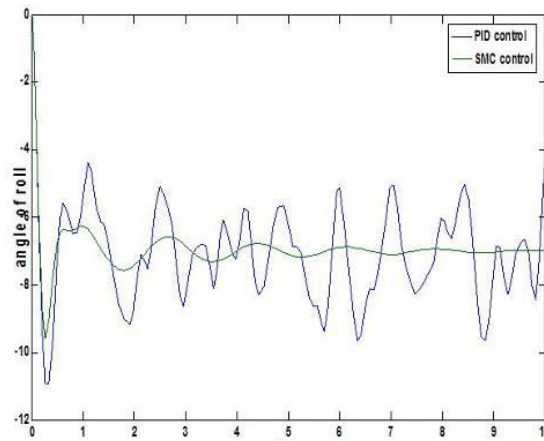


Fig. 8 - Response of lateral angular velocity

According to the judgment basis of the return-to-center conditions of the EPS system, Fig.9 analyzes the return-to-center residual angle of the steering wheel.

The results indicate that the steering-wheel residual angle of the EPS system that is added with the return-to-center control is 15° . This steering wheel angle does not cause a jitter phenomenon. Meanwhile, the steering-wheel residual angle of the EPS system that excludes the return-to-center control is 40° . This steering wheel angle generates significant jitter because of the effect of road surface impact.

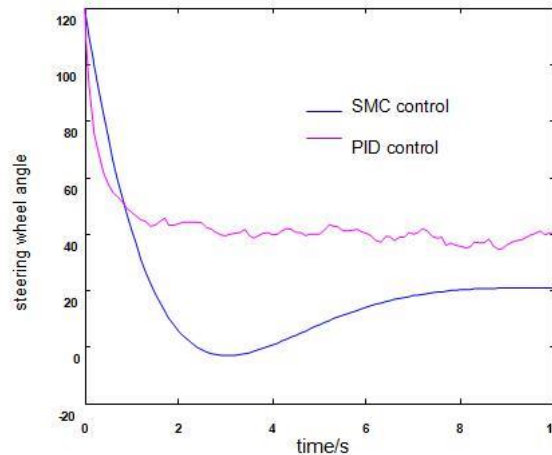


Fig. 9 - Diagram of steering wheel return-to-center results

CONCLUSIONS

In order to reduce the adverse effects of road surface impact on the handling stability and the smooth return-to-center of agricultural towing vehicles, the LH-UTV-400 low-energy-consumption agricultural towing vehicle was taken as research object, a road surface impact model was established, road surface impact model was combined with the whole vehicle model, the global fast terminal sliding mode control algorithm was added into the EPS control system, and a complete simulation model of “road surface - vehicle-EPS system” was established.

Finally, the main conclusions are presented below:

- when agricultural towing vehicles were steering, road surface impact increases the amplitude of the yaw motion and lateral motion of vehicles, and reduces the driving stability of vehicles.
- when steering wheel returns to center, the vibration caused by road surface impact was transmitted to steering wheel, resulting in the slight jitter of steering wheel, and reducing the stability of steering system. After global fast terminal sliding mode control algorithm was added into motor control algorithm, the tracking accuracy of motor current was improved significantly. After the steering wheel returns to the basic middle of angle, the return-to-center process of steering wheel was more smooth and stable.
- global fast terminal sliding mode control algorithm could make the power motor of the EPS system respond quickly to different steering conditions, improved the steering performance of vehicles in the condition of road excitation input, and it had great engineering practice significance in improving the steering stability of vehicles.

The steering stability response of the EPS system for agricultural towing vehicles under road surface impact is investigated, a motor current tracking control algorithm based on the global fast terminal sliding mode variable structure control algorithm is proposed, the accuracy of tracking and controlling motor current is improved, the return-to-center angle of steering wheel is calculated more accurately, and the jitter of steering wheel is weakened. Due to the limitations of models, the road surface impact investigated by this research is small-amplitude high-frequency impact. Based on this research, the influence of low-frequency large-amplitude road surface impact on the EPS system's return-to-center stability will be explored in future research, and the whole vehicle model will be further improved in the future.

ACKNOWLEDGEMENT

The work was supported by supported by the Fundamental Research Funds for the Central Universities (2572015AB19)

REFERENCES

- [1] Bing Zhou, Lu Fan, (2014), Integrated control of EPS and AFS to reduce steering vibration derived from road impact. *China Mechanical Engineering*, Vol.25, Issue 22, Editorial Department of China Mechanical Engineering, Wuhan, pp.3114-3118;
- [2] Champagne A., (2000), Correlation of Electric Power Steering Vibration to Subjective Ratings. *2000 SAE World Congress*, Vol.20, Issue 6, SAE International, Pittsburgh, pp.1-5;
- [3] Datong Qin, Jianjun Hu, Tong Li, (2008), Modeling and Simulation of Electric Power Steering System Based on Vehicle Whole Dynamics. *Journal of System Simulation*, Vol.20, Issue 6, Beihang University PRESS, Peking, pp.1577-1581;
- [4] Guobiao Shi, Rongwei Shen, Yi Lin, (2007), Model and simulation of electric power steering system, *Journal of Jilin University (Engineering and Technology Edition)*, Vol.37, Issue 1, Editorial Department of Journal of Jilin University, Changchun, pp.31-36;
- [5] Hamada H, Kurishige M, Sugiyama A et al., (2006), An EPS control strategy to reduce steering vibration associated with disturbance from road wheels, *2000 SAE World Congress*, Vol.20, Issue 6, SAE International, Pittsburgh, pp.1-5;
- [6] Hansong Xiao, Linfeng Zhao, Qidong Wang, (2014), Vehicle system dynamics and integrated control, vol.1, Science press Ltd., Peking, pp.102-113;
- [7] Heng Zhao, Shifu Lu, (1999), A vehicle's time domain model with road input on four wheels, *automotive engineering*, Vol.21, Issue 2, AutoFan magazine Ltd., Peking, pp.112-117;
- [8] Jinkun Liu, (2000), *MATLAB Simulation for Sliding Model Control*, vol.1, Tsinghua University Press, Peking, pp.360-370.
- [9] Kazemi R, Mohammadi H, (2003), Simulation of different types of electric power assisted steering (EPS) to investigate applied torque positions' effects, *2003 SAE World Congress*, Vol.20, Issue 6, SAE International, Pittsburgh, pp.1-5;
- [10] Konghui Guo, (1991), *Vehicle Handling Dynamics*, vol.1, Jilin Science and Technology Press, Changchun, pp.183-200;
- [11] Long Chen, Jingbo Zhao, Shaoyi Bei, (2011), Fuzzy-PID Control and Test of Automotive EPS System Under Return-to-center Condition. *Journal of Zhengzhou University (Engineering Science)*, Vol.32, Issue 5, Editorial Department of Journal of Zhengzhou University (Engineering Science), Zhangzhou, pp.112-116;
- [12] Lidong Miao, Ren He, (2009), Analysis of vibration modes for electric power steering system. *Journal of Jiangsu University*, Natural Science Edition, Vol.30, Issue 4, Editorial Department of Journal of Jiangsu University (NATURAL SCIENCE EDITION), Nanjing, pp.362-365,391;
- [13] Liangmo Wang, Songyan Li, Yongjun Min, (2009), Establishment and Simulation Analysis of Tire Dynamic Model, *Journal of Nanjing Institute of Technology (Engineering and Technology Edition)*, Vol.7, Issue 3, Editorial department of journal of Nanjing institute of technology, Nanjing, pp.34-38;
- [14] Můčka P., (2016), Road Roughness Limit Values Based on Measured Vehicle Vibration. *Journal of Infrastructure Systems*, Vol.10, Issue 6, ASCE, Reston, pp.1-23;
- [15] Sen A.K., Niewczas A, Litak G. etc., (2010), Vibrations of a vehicle excited by real road profiles, *Forschung im Ingenieurwesen*, Vol.74, Issue 2, Pamm, Darmstadt, pp.99-109.

THE EFFECT OF DRIPPER DISCHARGE ON THE WATER AND SALT MOVEMENT IN WETTED SOLUM UNDER INDIRECT SUBSURFACE DRIP IRRIGATION

滴头流量对间接地下滴灌下湿润体内土壤水盐运移的影响

Assoc.Prof. Qiaoxia An¹⁾, Assoc.Prof. Ph.D.Stud. Sanmin Sun^{1,2)}, M.S. Rong Xu¹⁾

¹⁾College of Water Conservancy and Architecture Engineering, Tarim University, Alar / China

²⁾College of Water Resources and Civil Engineering, China Agricultural University, Beijing/ China

Tel: +8609974680383; Email: ssmqx@126.com

Keywords: *dripper discharge, water and salt movement, indirect subsurface drip irrigation*

ABSTRACT

Jujube fruit, also called Chinese jujube (*Zizyphus jujuba* Mill.), is the main economic crop in Southern XinJiang province of China. However, due to the lack of suitable jujube irrigation technology, it not only wastes water resources, but also increases soil salinization. Indirect subsurface drip irrigation is a kind of high efficient water-saving irrigation technology, suitable for fruit tree irrigation. Dripper discharge is an important parameter in irrigation design. In this paper, an indoor experiment was adopted, and the effect of different dripper discharges on the distribution rules of water and salt were analysed in wetted body under indirect subsurface drip irrigation, and appropriate dripper discharges was selected to adjust the growth environment of crop root system. This study aims to provide theoretical guidance on using the indirect subsurface drip irrigation technology for jujubes in arid area.

摘要

特色林果—红枣是中国新疆南疆的主要经济作物，但由于缺乏适宜红枣的灌溉技术，不合理的灌溉技术不仅浪费水资源，而且加剧了土壤次生盐渍化。间接地下滴灌是一种高效节水的灌溉技术，适宜于果树灌溉。其滴头流量是灌溉设计中的重要参数，为研究滴头流量对间接地下滴灌下土壤水盐运移的规律，本文通过室内试验研究，分析不同滴头流量对湿润体特征及湿润体内水盐分布变化的影响规律，选择适宜的灌溉流量，以调节作物根系的生长环境。以期为间接地下滴灌技术在干旱区枣树中应用提供理论指导。

INTRODUCTION

Drought and soil salinization are the main factors that hinder the agricultural development of arid areas in southern XinJiang province of China (Yang Yu et al. 2016; Xiaodong Li et al., 2016; Xiaoming Li et al., 2011). In recent years, jujube fruit called Chinese jujube (*Zizyphus jujuba* Mill.) with a high economic value has been grown in large areas, enabled rapid development and promoted the local economy and ecological environment (Xiaocou Li et al., 2014; Ming Hong, et al., 2014). However, local irrigation technology not only wastes water resources but also causes serious soil salinization because of the lack of a suitable fruit irrigation technology. A suitable water-saving and salt-inhibiting irrigation technology for jujubes in arid areas should be identified.

Indirect subsurface drip irrigation is an efficient water-saving irrigation technology. This technology mainly consists of a surface drip irrigation system and a water-conducting device and it is characterized by the effect of using a surface-dripping method to achieve subsurface drip irrigation. In the process of irrigating fruit trees, a water-conducting device can be used to supply water to the root zone of fruit trees and to reduce surface evaporation and interception. This device is suitable for irrigating fruit trees. Experimental results show that compared to surface drip irrigation, indirect subsurface drip irrigation can better reduce evaporation among trees and improve water utilization efficiency (Meshkat et al., 1998).

Similar to surface drip irrigation, indirect subsurface drip irrigation is a type of partial root-zone irrigation that has a limited soil-wetting area. The size and distribution of the soil-wetting area can affect crop yield.

Dripper discharge is one of the most important elements in local irrigation design (Mingsi Li et al., 2006), with its size affecting not only the shape and moisture distribution of wetted body but also the salt leaching and salt distribution in wetted body (Shu Wang et al., 2005; Chunqin Liu et al., 2007). Accordingly, laboratory tests were adopted and the effect of different dripper discharges on the water and salt distribution

were evaluated in wetted body under the condition of using indirect subsurface drip irrigation in this study. This study aimed to provide theoretical guidance on using the indirect subsurface drip irrigation technology for jujubes in arid area.

MATERIAL AND METHODS

Water-conducting device components

The test system was composed of three parts (Sanmin Sun, *et al.*, 2015): a soil-box, a water supply device, and a water-conducting device. The soil-box was a 500 mm (L) × 500 mm (W) × 500 mm (H) cube made of 8 mm-thick plexiglass. The water supply device was composed of a water bottle and guide pipe with flow control valve. The water-conducting device was composed of water permeable boundary and impermeable boundary, impermeable boundary for PVC tube. In order to observe the water level in the PVC tube, the PVC tube was symmetrically divided along the tube diameter, placed into half of the inside wall of the soil box at a depth of 20 cm, and the testing soil was put into the box. Gravels screened in 2–5 mm were filled into the bottom of the PVC tube, which formed permeable boundary 5 cm high.

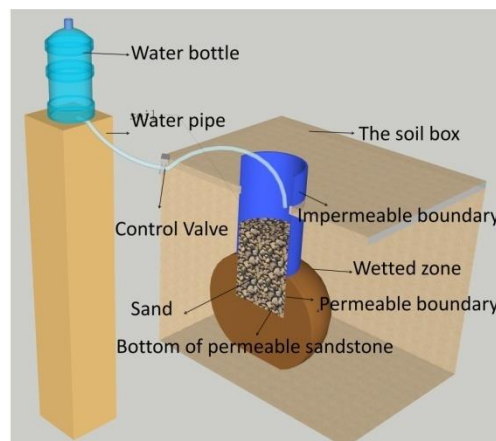


Fig. 1- Diagram of the components of indirect subsurface drip irrigation

Method and materials

The sample soils were selected from 0-50cm sandy loam soil of Tarim Irrigation Area in the southern Xinjiang province of China. The soil samples were air-dried and layered in the soil-box according to the predetermined soil bulk density of 1.40g/cm^3 , after the screening of the sieve with the pore size of 1 mm.

After 24 hours of irrigation, soil samples were collected from different profiles at 10, 20, and 30 cm (Profiles A, B, and C, respectively) away from the water-conducting device horizontally. The sampling depth of each profile was 40 cm, and every 5 cm depth was determined as one soil layer. Each treatment has 24 soil samples, and a total of 72 soil samples were collected. Soil moisture content was measured by the oven-drying method. After mixing 5 and 25 g of dried soil and water, respectively, and filtering the solution with filter paper, the electrical conductivity of the leach solution was measured with the DDSJ-308A electrical conductivity meter (INESA).

Testing program: The test-designed diameter for the water-conducting device and the height for the permeable stratum were fixed at 90 mm and 50 mm, respectively. Water flow was fixed at 1.5, 2, and 4 L/h, respectively. The irrigation amount was fixed at 4 L.

The purpose of the experiment was to study the distribution of water and salt under different water flow rates and the relationship between the distribution of water and salt in the wet body.

Data processing

The conversion between soil salinity content and soil conductivity was calculated according to the references (Yu Zhang *et al.*, 2011; Qiaoxia An *et al.*, 2016).

RESULTS

Effect of dripper discharge on soil moisture distribution

Under the subsurface drip irrigation condition, the capillary force of soil is the main force that affects water movement in soil. The force is equal in all directions. When the soil is dry, capillary force is greater than gravity. Thus, water flows evenly in all directions, including the upward direction. When the soil

becomes moist, soil pore reaches saturation, capillary force becomes weak, gravity exceeds capillary force and water flow downward (Zhenghua Wang et al., 2006). Along with the increasing irrigation time, a saturated area will be formed around the dripper. The saturated area has high water matric potential and gravitational potential. However, the soil outside the saturated area has low matric potential. Thus, water spreads in all directions from the dripper. When the distance between soil and dripper increases, soil water content decreases. Therefore, the area close to dripper has the highest water content in wetted solum. However, the water content decreases gradually in all directions. In this experiment, the water-conducting device was buried 20 cm deep into the ground. After irrigation, the soil layer at a depth of 20–30 cm had the highest water content. When the distance between soil and water outlet increased, the water content of each vertical soil layer gradually decreased in the upward and downward directions. In the horizontal direction, soil water content gradually decreased when the distance between soil and water outlet increased (Figure 2).

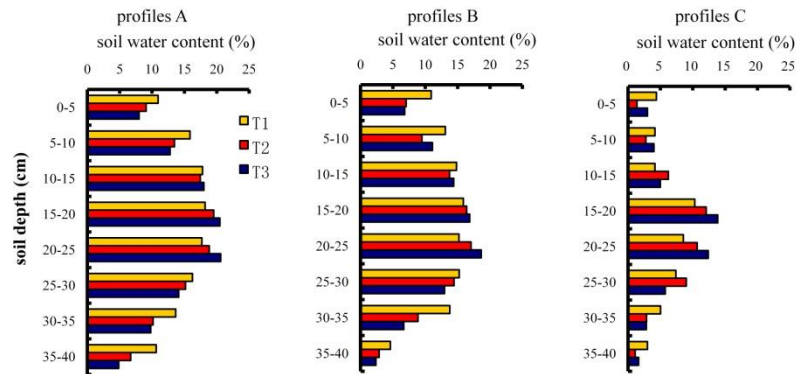


Fig. 2- Effect of dripper discharge on soil water distribution

Figure 2 shows that the dripper discharge had a significant effect on the distribution of water content in wetted solum. When the other conditions were the same, the soil water content of three soil profiles at a depth of 15–30 cm near the water outlet gradually increased with dripper discharge increase. By contrast, the soil water content of soil layers at depths of 0–15 cm and 30–40 cm gradually decreased. Accordingly, a large dripper discharge could facilitate water movement in the horizontal direction, whereas a small dripper discharge could facilitate water movement in the vertical direction.

Effect of dripper discharge on the soil salt distribution in the vertical profile

Under the indirect subsurface drip irrigation, water moves upward and downward in the vertical direction, and the water content of soil near the water outlet is large. Therefore, the water potential gradient of soil is large. Water moves rapidly, so that the soil salinity is effectively diminished. When the distance between soil and water outlet increases, soil water content decreases, soil matric potential decreases, soil suction capacity increases, salt content gradually decreases with water movement and salt content in soil accumulates at the upper and lower edges. In this experiment, a water-conducting device was buried 20 cm deep into the soil, so that the salt content of soil layer at 15–30 cm deep near the water outlet reached its minimum (Fig. 3).

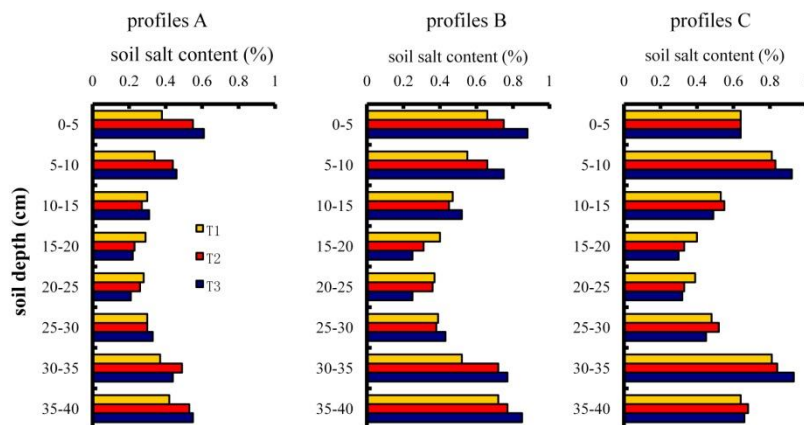


Fig. 3 - Effect of dripper discharge on the soil salt distribution in the vertical profiles

The salt contents of other soil layers in profiles A and B basically increased when the distance between soil layer and water outlet increased. The salt content of other soil layers in profiles C initially increased and then decreased when the distance between soil layer and water outlet increased. The salt content of soil layer at 5–10 cm and 30–35 cm was the highest, which might be caused by the decreased vertical wetting distance of profiles C. The 5–10 cm and 30–35 cm soil layers were at the edge of the wetting front. Salt accumulated in these soil layers, resulting in the highest salt content.

Effect of dripper discharge on the soil salt distribution in the horizontal section

The variation characteristics of salt content in each horizontal soil layer are shown in Figure 4. In the 5–35 cm soil layer, the salt content of all soil layers in profile A was the lowest. When the horizontal distance between soil layer and water outlet increased, salt spreads rapidly with water and gradually accumulated at each soil layer. Consequently, the salt content of each soil layer basically showed an increasing trend from profile A to profile B to profile C. By contrast, the 0–5 cm and 35–40 cm soil layers in profile B had the highest salt content. The soil salt content of each section initially increased and then decreased. This trend might be related to the relative position of different sections and wetting front edges. Profile B was only at the edge of the wetting front, where salt accumulated. Profile C was outside the wetting front and its salt content was substantially consistent with the base salt content of soil.

Dripper discharge had different salt-leaching effects on different sections. Figure 4 shows that, at the 10–30 cm soil layer, a large dripper discharge leads to a low soil salt content. The salt content of the 0–10 cm and 30–40 cm soil layers decreased when dripper discharge increased. This result indicated that a large dripper discharge could promote water and salt leaching, whereas a small dripper discharge could promote salt leaching in the vertical direction (Tao Li et al., 2010).

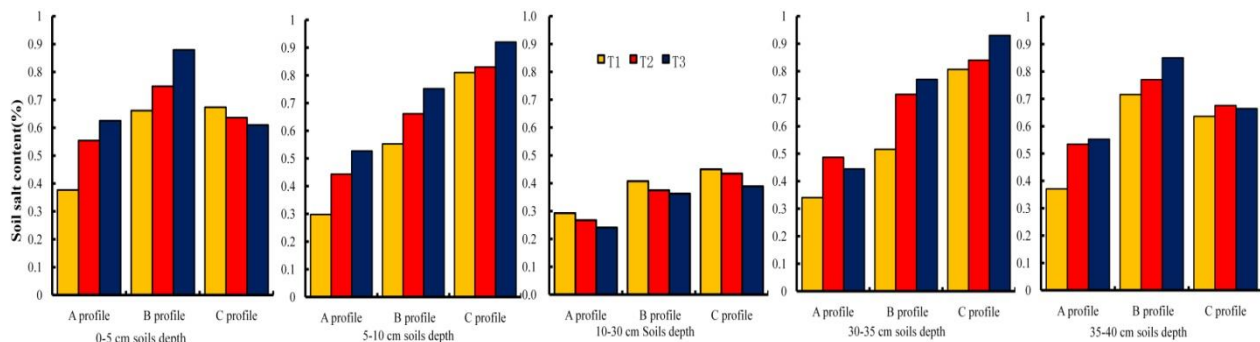
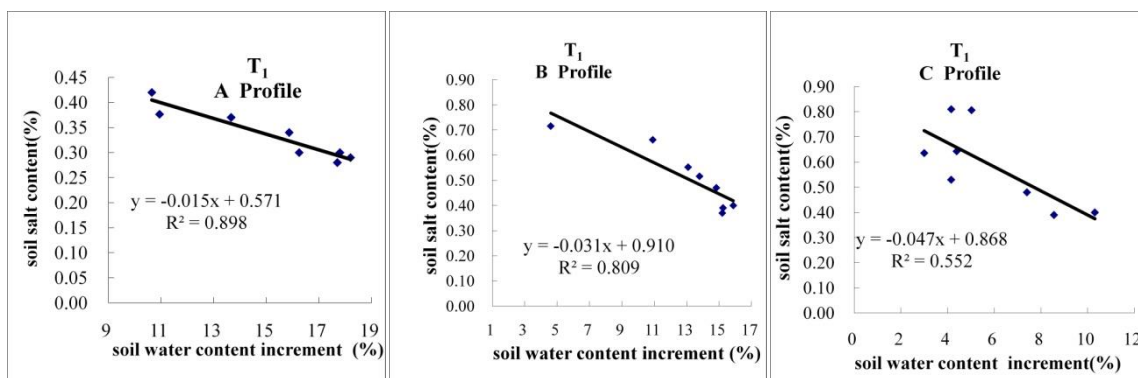


Fig. 4 - Effect of dripper discharge on the soil salt distribution in the horizontal section

Relationship between salt distribution and water content increment in wetted solum

The sampled soil was homogeneous air-dried loam soil and had a consistent salt content. Soil water content increases after irrigation, the soil water content increment is equal to the difference of the soil water content between after irrigation and before irrigation, the soil salt content at a certain area could represent the effect of water content on soil salt leaching, i.e., a low soil salt content could indicate a good desalination effect. In the experiment, the soil water content increment and the soil salt content of each section were fitted (Fig. 5).



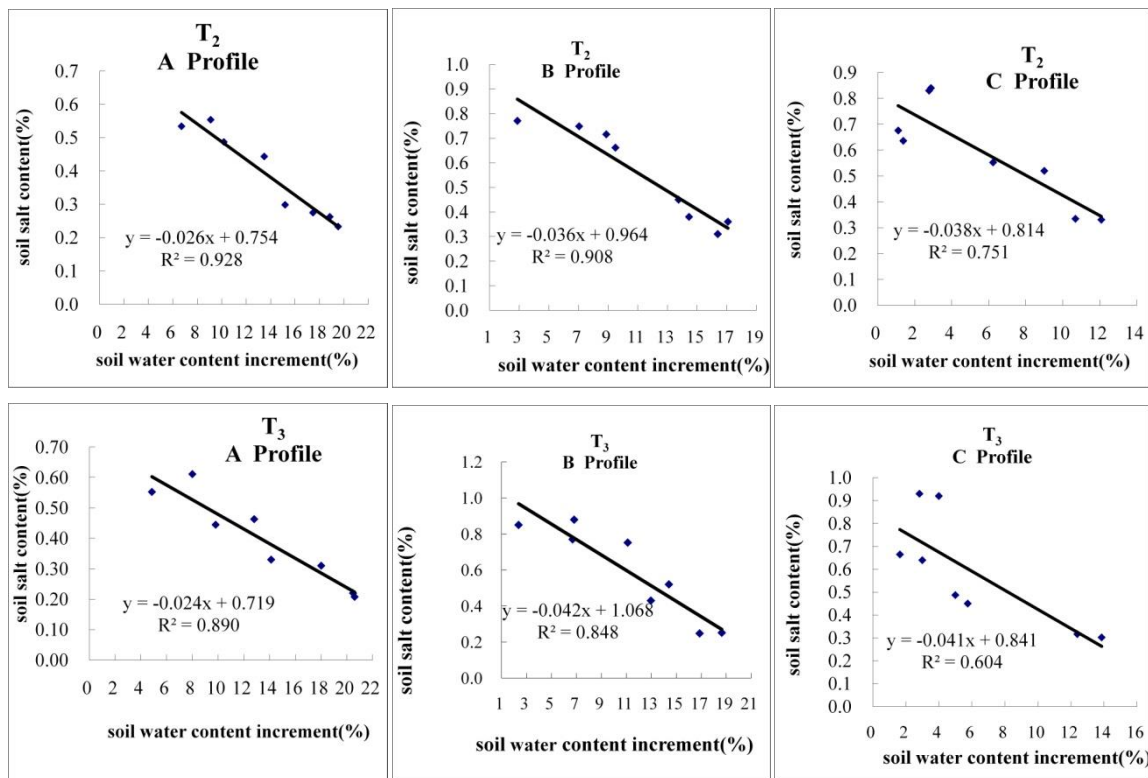


Fig. 5 - Relationship between salt distribution and water content increment in wetted solum

Figure 5 shows that, after three treatments, the soil moisture increment and the soil salt content in profile A and B had a good correlation. A high soil moisture increment had a good soil salt-leaching effect and could decrease soil salt content. The soil moisture increment and the soil salt content in profile C had a poor correlation. This result might be due to the fact that profile C was near the edge of wetted solum. Different sampling points and wetting fronts also had different relative positions (several points were not in the wetting front, several points were on the wetting front, and several points were in the wetting front). The fitting result indicated that, in wetted solum, a high soil moisture increment could have an evident salt-leaching effect.

CONCLUSIONS

(1) Under the experimental conditions, the 20–30 cm soil layer had the highest soil water content. As the distance between soil layer and water outlet increased, the soil water content of vertical soil layers gradually decreased in the upward and downward directions. In the horizontal direction, the soil water content gradually decreased when the distance between soil layer and water outlet increased. In wetted solum, the soil that was near the water outlet had a low soil salt content. When the distance between soil layer and water outlet increased, soil salt content increased.

(2) Dripper discharge had a significant effect on the distribution of water and salt movement in wetted solum. A large dripper discharge could promote water movement in the horizontal direction, whereas a small dripper discharge could facilitate water movement in the vertical direction. The corresponding large dripper discharge could promote salt leaching in the horizontal direction, whereas small dripper discharge could promote salt leaching in the vertical direction.

(3) In wetted solum, when the soil moisture increment in the same profile was high, then salt leaching would become evident.

ACKNOWLEDGEMENT

This work was financially supported by the National Natural Science Foundation of China (Nos. 51069013 and 51369028), the College Students' Innovative Projects of China (No. 201410757004), and the College Students' Innovative Projects of Tarim University (No. 2015027). The authors express their gratitude to Mr. Cai Huanjie, professor of Northwest Agriculture and Forestry University, for his help and encouragement in conducting this research.

REFERENCES

- [1] Chunqin Liu, Jinsong Yang, Xiaobing Chen, et al., (2007), Movement and redistribution of water and salt in relation emitter discharge (滴灌流量对土壤水盐运移及再分布的作用规律研究), *Acta Pedologica Sinica*, Vol.44, Issue 11, pp.1016-1020, Nanjing/China;
- [2] Meshkat M R C, Warner S R Workman, (1998), Comparison of water and temperature distribution profiles under sand tube irrigation, *Transactions of the ASAE*, Vol.41, Issue 6, pp.1657-1663, American Society for Agricultural /U.S.A.;
- [3] Mingsi Li, Shaozhong Kang, Haiyan Sun, (2006), Relationships between dripper discharge and soil wetting pattern for drip irrigation (点源滴灌滴头流量与湿润体关系研究), *Transactions of the CSAE*, Vol.22, Issue 4, pp.32-35, Beijing/China;
- [4] Ming Hong , Yingjie Ma, Haxi Mu, et al., (2014), Research and application of red jujube Micro-Irrigation Technology in Xinjiang (新疆红枣微灌技术研究及推广应用现状分析), *Water Saving Irrigation*, Issue5, pp.62-66, Wuhan/China;
- [5] Qiaoxia An, Sanmin Sun, Rong Xu, et al., (2016), Effect of permeable boundary of water-conducting device on water and salt transport under indirect underground drip irrigation, Vol.49, Issue 2, pp.31-36, *INMATEH-Agricultural Engineering Journal*, Bucharest/ Romania;
- [6] Sanmin Sun, Qiaoxia An, HuanJie Cai, et al., (2015), Research on salt movement law in jujube root zone under indirect subsurface drip irrigation (枣树间接地下滴灌根区土壤盐分运移规律研究), *Transactions of the Chinese Society for Agricultural Machinery*, Vol.45, Issue 1, pp.160-169, Beijing/China;
- [7] Shu Wang, Gangyong Li, Guoxia Meng, et al., (2005), Effects of dripper discharge and spacing on growth of cucumber in Chinese solar greenhouse under drip irrigation (日光温室滴灌条件下滴头流量和间距对黄瓜生长的影响), *Transactions of the CSAE*, Vol.21, Issue 10, pp.167-170, Beijing/China;
- [8] Tao Li, JianFeng Zhang, HuiJuan Cheng, et al., (2010),The wetting front distribution characteristic and the fitting model of single point free infiltration under deep pit irrigation in the field (深层坑渗灌田间单点入渗湿润锋分布特性及拟合模型研究), Vol.28, Issue 4, pp.36-39, *Agricultural Research in the Arid Areas*;
- [9] Xiaodong Li, Fenghua Zh, Yu Zhu, (2016), Agricultural irrigation water quality and soil salinization in typical areas of Southern Xinjiang (新疆南疆典型地区农业灌溉水质与土壤盐渍化关系的研究), *Xinjiang Agricultural Sciences*, Vol.53, Issue7, pp.1260-1267, Urumqi/China;
- [10] Xiaoming Li, Jingsong Yang, Meixian Liu, et al., (2011), Study on soil salt distribution with drip irrigation under mulch in cotton boll period in south Xinjiang (南疆膜下滴灌棉花花铃期土壤盐分分布研究), *Soils*, Vol.43, Issue2, pp.289-292, Nanjing/China;
- [11] Xiaoou Li, Guoxin Yu, (2014), Development status and construct countermeasure of Jujube brand in Xinjiang, (新疆红枣品牌发展现状及建设对策), *Northern Horticulture*, Issue8, pp.170-174, Harbin/China;
- [12] Yang Yu, Haibin Gu, Li Zhang, et al., (2016), Analysis of soil salt characteristics in oasis farmland (绿洲农田盐碱斑土壤盐分特征分析), *Journal of China Agricultural University*, Vol.21, Issue 3, pp.89-95, Beijing/China;
- [13] Yu Zhang, Lihong Wang, Sanmin Sun, et al. ,(2011), Indexes of salt tolerance of cotton in Akesu river irrigation district (阿克苏河灌区棉花耐盐指标的确定), *Scientia Agricultural Sinica*, Vol.44, Issue 10, pp.2051-2059, Beijing/China;
- [14] Zhenghua Wang, Desheng Lv, Xinming Wen,(2006), Experimental research on influence of discharge to soil water-salt transport under line source permeation of SDI (流量对地下滴灌土壤水盐运移影响的试验研究), *Journal of Irrigation and Drainage*, Vol.25, Issue 6, pp.61-65, XinXiang/China.

MATHEMATICAL MODEL VALIDATION AND ANALYSIS OF SOIL WATER AND NITROGEN TRANSPORT IN WATER STORAGE PITS

蓄水单坑土壤水氮运移的数学模型验证分析研究

Master Zhonghua Ni

College of Engineering and Technology, Shangqiu Polytechnic, No.566,

South Section of Shenhua Avenue, Shangqiu, Henan / China

E-mail: ni.zhonghua@yahoo.com

Keywords: water storage pit, water and nitrogen transfer, mathematical model, verification analysis

ABSTRACT

Water storage pit irrigation is a common irrigation method widely used in the northern part of China which can combine water-saving irrigation with soil and water conservation. Applying this method, this study analyzed different temperature and water content of the soil and established correlative models to study the water and nitrogen transport of soil in water storage pits. The results showed that the difference between the measured values of water and nitrogen obtained from the models and the actual values was small, either under different temperature or irrigation amount, suggesting that the models were correct.

摘要

蓄水坑灌法是北方地区普遍使用的浇灌方法，该方法浇灌的优点是将节水灌溉与保持水土有机结合起来，本文在此种浇灌方法上，对土壤的不同温度、不同水量进行分析研究，并建立相关模型，重点研究蓄水单坑下的土壤的水氮运移。结果发现，不同温度下，水分和氮素的模型测出来的值与实际测出来的值误差较低，不同灌水量的情况下也能准确检测出吻合度较高的数据，说明该模型是正确的。

INTRODUCTION

Since ancient times, China has long been a big agricultural country. Currently, despite its abundant total water resources, China is in a noticeable lack of fresh water resources (Holland et al., 2015).

The development of agriculture is inseparable from water and fertilizer and fertilizer is rich in nutrients and is an important nutriment for crop growth. Nitrogen is the mostly absorbed nutrient element by crops, so the use of fertilizer in China is also wide (Zhang, 2016). In recent years, with the continuous increase of population, the shortage of water resources is becoming more and more serious. At the same time, the combination of water resources and water fertilizer is an important way to realize agricultural high yield and high efficiency, thus how to achieve scientific irrigation of water and fertilizer on crops has become a key technology.

Water storage pit irrigation method was initially put forward for solving the water shortage and soil erosion problems in northern China (Fang, et al., 2014). For the fact that nitrogen cannot be adequately absorbed and used since agricultural irrigation and fertilization have long been carried out separately in China, the application of storage pit irrigation method can not only save water, but also reduce soil erosion (Ma, et al, 2010).

Many experts have studied this irrigation method. Fan Xiaobo et al (Fan et al., 2013) established a TRIME-PICO IPH system and revealed the water content in the soil under the condition of water storage pit irrigation, thereby improving the utilization of water. In an indoor soil column evaporation experiment, Wang Zengtao et al (Wang, et al., 2011) studied the law of soil evaporation, and analyzed the mechanism of soil water movement under the water storage pit irrigation condition during evaporation.

B Askri et al. (2014) used the HYDRUS-1D model on the basis of the water storage pit irrigation method in the study of the water of date palm and achieved good results.

Sepaskhah A R et al. (2012) studied the effects of different N rates and water-saving irrigation on rapeseed yield and nitrogen leaching.

In this paper, the soil water and nitrogen transport model in water storage pits was tested under different temperature and different irrigation amount. The results show that the model can well reflect the water and nitrogen transport situation in the soil, thus it is applicable.

MATERIAL AND METHODS

Water storage pit irrigation method

Water storage pit irrigation method is to dig around the trunk 5-7 water storage pits and place on the bottom of the water storage pits waterproof material to avoid deep percolation of the irrigation water. During irrigation, the water is led into the water storage pits through the circular canals and then penetrates into the root of the soil through the pit walls. In the farming areas, this method consists of water storage pits, solid wall facilities, annular ditches, covering facilities, and ditches (Li et al., 2016).

The specific design is shown in figure 1.

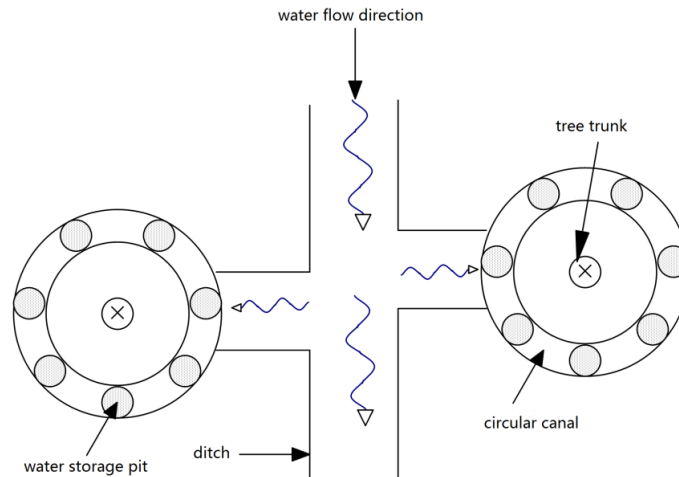


Fig. 1 – Field area engineering schematic diagram

The diameter of a single storage pit is determined according to the volume of irrigating water quota and is about 30 cm generally. The number of water storage pits needed by a single plant depends on the soil irrigation rate, which must ensure that the middle layer soil is completely wet in the neighbouring pit and realize the pit volume required by the irrigation rate. The circular canal locates at the lower part of the trunk and is a shallow canal which connects all the water storage pits. In addition to water delivery, it can also share the water volume under large rainfall conditions. The ditch is a fixed channel connecting the main irrigation system with the annular canal. It is generally divided according to the contour line and located in the upper trunk, which is beneficial to the artesian flow of the water during irrigation and can block the water produced by excessive rainfalls to reduce water and soil loss. The size of the section of the ditch is determined by the amount of water conveyed (Zhang et al., 2010).

MODEL CONSTRUCTION

Each layer of soil is assumed to be homogeneous and isotropic, ignoring the biological effects and chemical effects of soil on water production and the impact of solutes on soil moisture. The soil can be considered as porous media without skeleton deformation and soil water is a kind of incompressible continuous liquid. During the infiltration with different system temperature, the irrigation water achieves a uniform spread to the surrounding area, taking the centre axis of the water storage pit as the symmetric axis. Therefore, the water storage pit irrigation can be considered a two-dimensional plane situation.

Fig. 2 is the infiltration profile of the water storage pit, where:

OG is the water storage pit axis Oy;

OB - the ground plane r , (i.e., the soil surface);

AF - the puddle wall;

EF - the bottom of the pit;

EG, GH, BH are respectively the left border, lower border and right border of the model boundary.

H1 - initial depth of the puddle,

h2 - depth of the water storage pit,

h3 - total height of the soil,

r1 - radius of the water storage pit,

r2 - calculated radius of the soil.

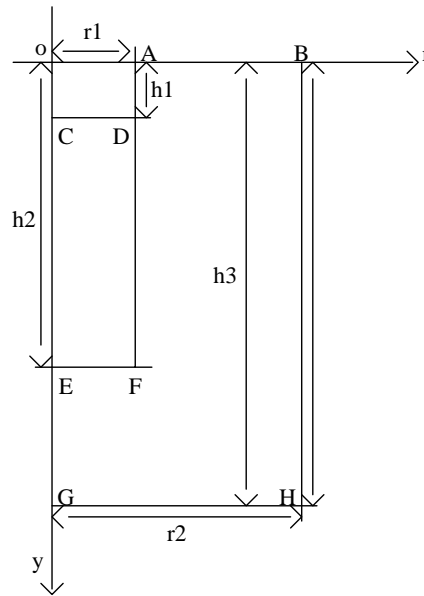


Fig. 2 – Profile diagram of a water storage pit

Water movement model

Because the water in the single reservoir is the positive pressure water and the pothole is the negative pressure, the governing equation of the model chooses the basic equation of the saturated-unsaturated soil water movement, and g is the dependent variable of the negative pressure head.

$$\frac{\partial \theta v}{\partial t} = \frac{\partial}{\partial r} \left(r K(g) \frac{\partial g}{\partial r} \right) + \frac{\partial}{\partial y} \left(K(g) \frac{\partial g}{\partial y} \right) - \frac{\partial K(g)}{\partial y} \quad (1)$$

where:

- θv is the water content in the soil;
- $K(g)$ - unsaturated soil hydraulic conductivity;
- t - infiltration time;
- r - horizontal coordinate of the puddle;
- y - depth of the soil below the surface.

In order to obtain the unsaturated hydraulic conductivity, the soil water characteristic curve and the soil saturated hydraulic conductivity were solved at first, as follows:

$$\theta(g) = \begin{cases} \theta r + (\theta m - \theta r) \left[1 + |\rho g|^{b_0} \right]^{-a_0} & (g < 0) \\ \theta m & (g \geq 0) \end{cases} \quad (2)$$

$$K(h) = Km \cdot S_w^{j_0} [1 - (1 - S_w^{1/a_0})^{a_0}]^2, \quad S_w = \frac{\theta - \theta r}{\theta m - \theta r} \quad (3)$$

where:

- θm is the volume water content of saturated soil;
- θr - soil residual volume water content;
- Km - saturated soil hydraulic conductivity;
- S_w - effective volume water content;
- ρ - inverse of the intake air pressure;
- b_0 - soil pore size distribution index;
- $a_0 = 1 - 1/b_0$;
- j_0 - porosity connectivity parameter.

The two-dimensional convection-diffusion equation describes the transformation process of urea in soil as follows:

$$\frac{\partial(\theta c_i + \mu m_i)}{\partial t} = \frac{\partial}{\partial r} \left(\theta D_{rr} \frac{\partial c_i}{\partial r} + \theta D_{ry} \frac{\partial c_i}{\partial y} \right) + r^{-1} (\theta D_{rr} \frac{\partial c_i}{\partial r} + \theta D_{ry} \frac{\partial c_i}{\partial y}) + \frac{\partial}{\partial y} (\theta D_{yy} \frac{\partial c_i}{\partial y} + \theta D_{ry} \frac{\partial c_i}{\partial r}) - \frac{\partial q_r c_i}{\partial r} - \frac{q_r c_i}{r} - \frac{\partial q_y c_i}{\partial y} + Q_i + H_i \quad (4)$$

where:

c is the soil volumetric quality;

j - nitrogen element,

q_r and q_y are soil moisture flux in the r -direction and soil moisture flux in the y -direction;

Q - source term of the transformation between nitrogen forms;

H - reminiscence of the transformation between nitrogen forms;

D_{rr} - the effect coefficients of the concentration gradient in the r -direction on the diffusion flux of the solute in the r -direction;

D_{ry} - the effect coefficients of the concentration-gradient in the y -direction on the diffusion flux in the r -direction solute.

EXPERIMENT DESIGN

Water and Nitrogen Experiments at Different Temperatures

The soil bulk density was 1.51 g/cm³, and the following experiments were carried out in the environments of 5°C, 10°C, 15°C, 20°C, 25°C, 30°C and 35°C, respectively:

(1) The orifice plate and the copper mesh are installed on one end of the plexiglass soil column, and the pressure in the semi-infinite soil column is pushed in line with the external pressure.

(2) The experiment was air-dried, blended with 2mm sieve, mixed and layered, and packed into plexiglass soil column according to the standard of 5cm per layer. Then, copper mesh and supportable porous plate are installed, covered with bottom plate to prevent the collapse of the soil edge.

(3) Preparation of 100mgN / L potassium nitrate solution, poured into the bottle. The temperature of the incubator was adjusted to 5°C, 10°C, 15°C, 20°C, 25°C, 30°C and 35°C, respectively, and the plexiglass soil column was placed in an incubator.

(4) The Markov bottle is made the constant water head for infiltration and the water level and the lower edge of the soil column is maintained in a balance.

(5) When the wet front is 2/3 that of the length of the soil column, the water supply is stopped. At the end of the experiment, the soil water content and the concentration of nitrate were determined by taking 5 g of soil in each layer. The soil water content was measured by oven-weighing method. The soil water content was measured by oven at 105°C, and the concentration of nitrate nitrogen was detected by flow analyzer.

Experiments on Different Irrigation Quantity

(1) On the first day after irrigation, soil samples were extracted with a 2 cm diameter, 1 m long soil drill. The soil samples were taken in plastic bags and aluminium boxes, and well marked for use in soil moisture and nitrogen measurements.

(2) Soil extraction was carried out along a same radial section every day. Sampling points are taken at the points where r is 20, 25, 30 and 35 cm in the radial direction. For the vertical direction, sampling points are chosen at the points where y is 10, 25 and 30 cm. The upper limit depends on the wet range.

(3) The soil moisture content was determined by dry weighing method. The oven temperature is adjusted to 105°C to bake the soil for 6-8 hours, and the soil is then removed and put into the desiccators for weighing after cooling. Finally, $(X - Y)/(Y - Q)$ is used for water content determination. In the equation, X is the container + wet soil weight and Y is the container + dry soil weight; Q is the container weight.

(4) According to the above steps, the water content and NO₃-N of the 3rd, 5th and 7th day of irrigation were measured.

RESULTS

Water and nitrogen transport at different temperatures

Water content

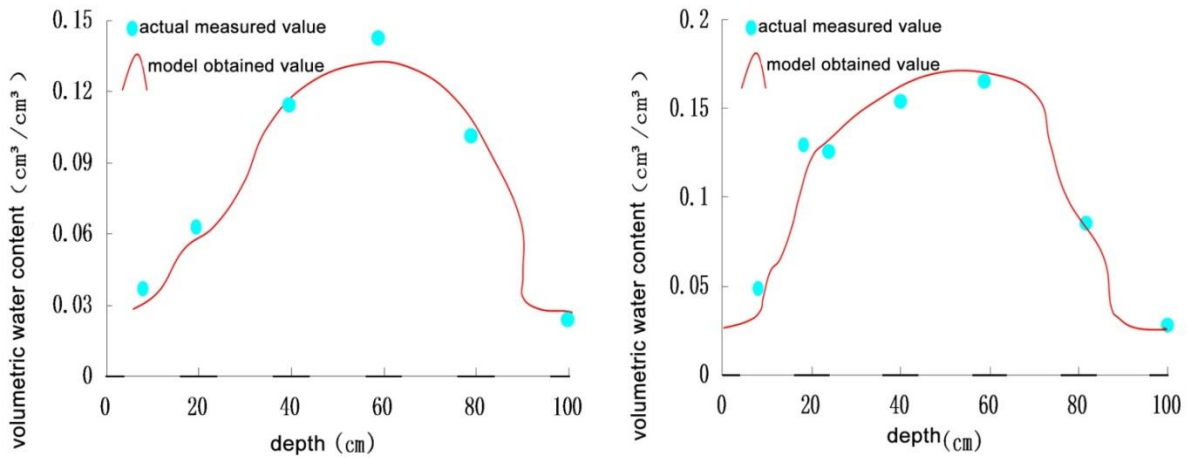


Fig. 3 –The measured and model values of soil water content at different temperatures

As shown in figure 2, the left figure is the comparison of the measured value and the model value of soil volumetric moisture content, changing with the vertical depth changes at 35°C system temperature, on the 15th day, when the radius is 45 cm.

The right figure is the comparison of the measured value and the model value of soil volumetric moisture content, changing with the vertical depth changes at 25°C system temperature, on the 5th day, when the radius is 25cm.

The left and right graphs show that the values obtained by the model agree well with the actual measured values. At the edge of the moist soil, the model value is slightly larger than the measured value, because the reduction rate of the volume of soil moisture around the wetting front of the moisture is faster than other regions. At the same time there is the possibility of human influence, that is, the operation of mixing with dry soil can lead to the result that the model value is greater than the measured value.

On the whole, the error range between the model value and the measured value is small and the error is within the allowable range. Therefore, the model can effectively verify that the water content determination model with constant volume head water infiltration is correct.

Nitric nitrogen

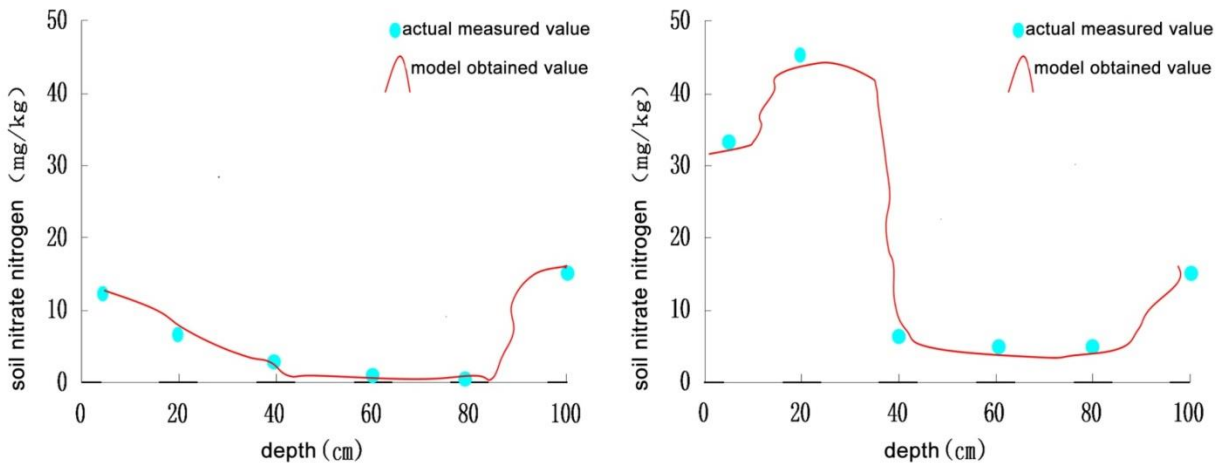


Fig. 4 – The measured and model values of soil nitric nitrogen at different temperatures

As shown in figure 3, the left graph shows the comparison chart of the simulated and measured values of vertical nitrate nitrogen distribution at 35°C, on the 5th day, when the radius is 25cm; the right graph shows the comparison chart at 25°C, on the 10th day, when the radius is 45cm.

From the figure, we can see that the content of NO₃-N in the more humid edge soil is higher, and in the middle part is smaller, with the model values close to the actual ones.

The average error is small, within the allowable range, so the model can effectively detect the situation of nitrogen in soil.

Water and nitrogen transport of different irrigation **Water content**

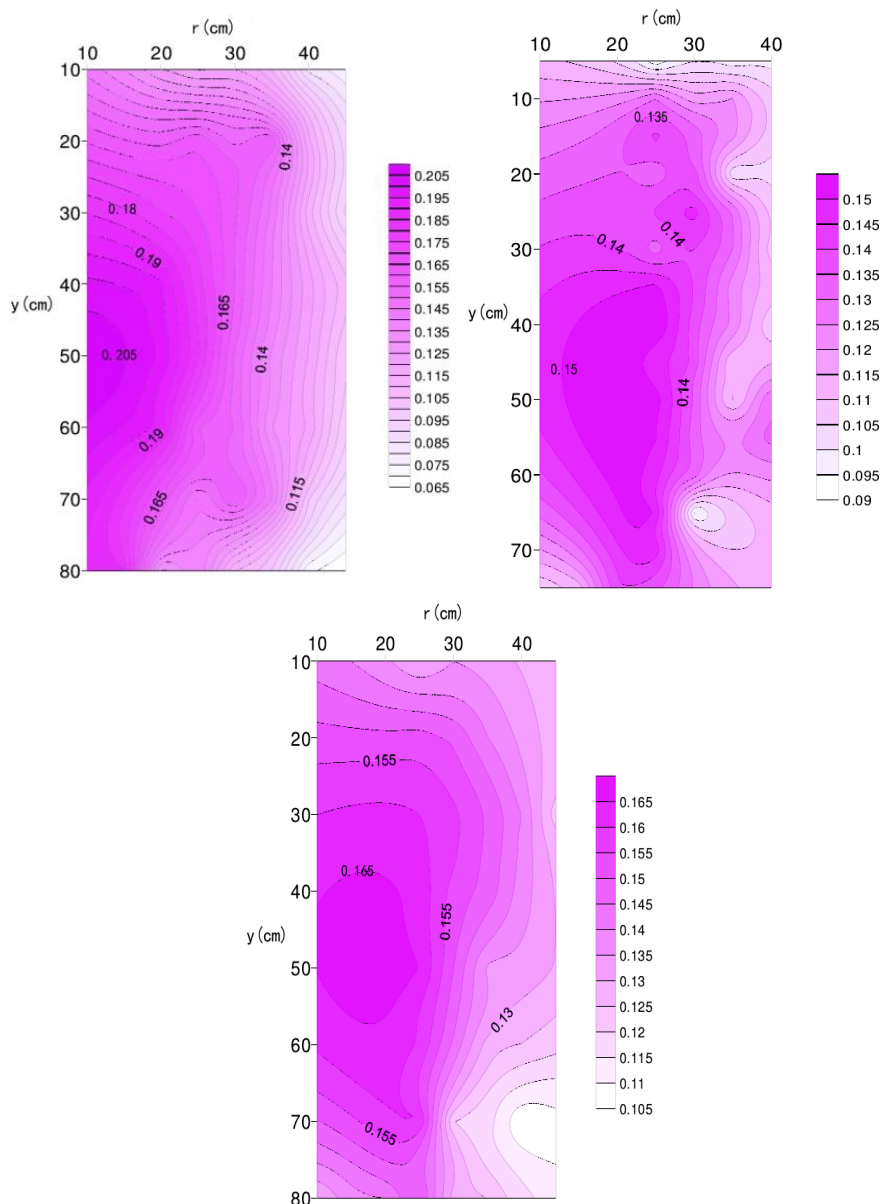


Fig. 5 – The contour map of soil water content under different irrigation water amount

As shown in Fig. 4, the distribution characteristics of the contours of the three water-cut maps are the same, representing the maps when the irrigation water amount is 6L, 8L and 10L. When the irrigation amount is 6L, the soil surface water content is low. With the increase of depth, water content begins to rise and is about 0.165 at 20 cm depth and 0.175 at 30 cm depth and reaches the maximum value at 50 cm depth. The depth area of the increase in water content is 40-60 cm, which is the same case when the irrigation water amount is 8L and 10L. It shows that in the water storage pit, the deep water content is larger and the water content in the middle and deep layers also increases with the increase in irrigation.

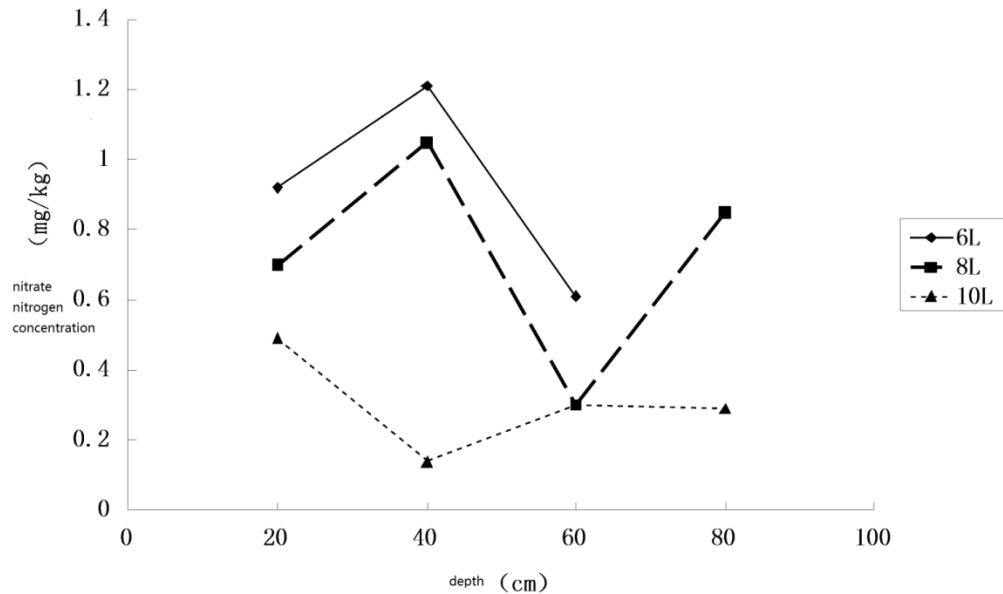
Nitrate nitrogen

Fig. 6 – The nitrate content at different irrigation water amount

As shown in Fig. 5, when the irrigation amount was 8 L, the concentration of nitrate nitrogen increased first and then decreased. The soil NO₃ - N concentration increased at the depth of 20-40 cm, and reached the maximum at 40 cm depth. The concentration of NO₃-N decreased in the depth of 40-60 cm and gradually increased after 60 cm. The middle and deep level irrigation of the puddle has good water retention feature and soil water can be considered as an important carrier of soil nutrient cycling and flow. From figure 5 and figure 6, we can see that the soil water content began to increase at 30-60 cm depth and peaked at about 50 cm. For NO₃-N, it dissolves in the soil solution and migrates soil colloid along the soil gap, so the adsorption capacity of soil on it is weak. The nitrate nitrogen in the soil below 40cm depth presents a decreasing trend. With the increase of soil depth, the nitrification was weakened, and the denitrification was gradually enhanced. Denitrification requires denitrifying bacteria, while most of denitrifying bacteria are isoxic bacteria and only a small part of denitrifying bacteria are good bacteria. At the depth of 70-80 cm, the nitrate content increased due to the accumulation of NO₃-N in the edge of the wetted soil. The other irrigation water had the similar characteristics. It should be pointed out that when the irrigation amount is 10L, the concentration of NO₃-N in the soil is obviously smaller than 1, indicating that the nitrate infiltration is more obvious in the lower soil layer.

CONCLUSION

The development of agriculture is inseparable from water, soil and fertilizer. To make the relationship among the three more clear, in this paper, water and nitrogen contents in soil under different temperature and different irrigation water conditions were studied.

The water and nitrogen values of the model were in good agreement with the measured values. With the increase in irrigation volume, the water content in the deep layer also increased. Besides, large irrigation volume led to the more obvious infiltration of nitrate nitrogen in the lower soil layer. The moisture movement model and the nitrogen transport model established in this experiment had certain accuracy and feasibility, and should be popularized and used.

REFERENCES

- [1] Askri B., Ahmed A.T., Abichou T., Bouhlila R., (2014), Effects of shallow water table, salinity and frequency of irrigation water on the date palm water use, *Journal of Hydrology*, Vol. 513, pp. 81-90;
- [2] Fan Xiao-bo, Sun Xi-huan, Guo Xiang-hong, MA Juan-juan, (2013), An Analysis of the Characteristics of Soil Moisture Distribution under Water Storage Pit Irrigations, *China Rural Water and Hydropower*, vol.3, pp. 69-72;

- [3] Fang D, Wang W Y., (2014), Comparative Analysis of Carrying Capacity of Water Resources in all Regions in Xinjiang, *Advanced Materials Research*, 962-965, pp. 2175-2179;
- [4] Holland R A, Scott K A, Flörke M., (2015), Global impacts of energy demand on the freshwater resources of nations, *Proceedings of the National Academy of Sciences*, vol.112(48), pp. 6707-16;
- [5] Li JJ, Guo X.H., Sun X.H., (2016), Analysis on Soil Moisture Distribution Characteristics under Different Irrigation Quantity of Water Storage Pit Irrigation, *People of the Yellow River*, vol.38(3), pp.140-143;
- [6] Ma Teng-fei, Wei Chang-zhou, Wang Juan, Hou Zhen-an, Wang Xiao-juan, Peng Zhen-bao, Zhang Bo., (2010), Soil Nitrate-N Distribution and Effect on Cotton Plant N Absorption under Different Irrigation method, *Xinjiang Agricultural Sciences*, volume 47(5), pp. 859-864;
- [7] Sepaskhah A R, Tafteh A., (2012), Yield and nitrogen leaching in rapeseed field under different nitrogen rates and water saving irrigation, *Agricultural Water Management*, 112(9), pp. 55-62;
- [8] Wang Zeng-tao, Sun Xi-huan, Ma Juan-juan, Guo Xiang-hong, (2011), Experimental Research of Soil Evaporation under Water Storage Pit Irrigation Condition, *Journal of Irrigation and Drainage*, 30(1), pp.84-86;
- [9] Zhang FR., (2016), The Position and Function of Soil and Fertilizer in the Sustainable Development of Agriculture, *Advisor for Farmers to Become Rich*, 28(10), pp. 32-32;
- [10] Zhang Yanxiong, Li Dan, Zhang Zuoyu, Liao Kejun, (2010), A Comparison Study of Two Methods for Mensuration of Soil Cation Exchange Capacity, *Guizhou Forestry Science and Technology*, 38(2), pp.45-49.

BIOREMEDIATION OF AGRICULTURAL SOIL CONTAMINATED WITH LEAD USING INTERACTION: COMMON BARLEY *HORDEUM VULGARE* AND EARTHWORM *LUMBRICUS SP*

/

BIOREMEDIATION D'UN SOL AGRICOLE CONTAMINÉ AU PLOMB A L'AIDE D'INTERACTION: ORGE COMMUNE *HORDEUM VULGARE* ET VER DE TERRE *LUMBRICUS SP*

As. Ph.D. Boukirat D.¹⁾, Prof. Ph.D. Maatoug M.¹⁾, As. Ph.D. Zerrouki D.¹⁾, As. Ph.D. Lahouel H.¹⁾,
Prof. Ph.D. Dr. Heilmeyer H.²⁾, Prof. Ph.D. Dr. Kharytonov M.³⁾

¹⁾Laboratory of Agro Biotechnology and Nutrition in Semi-arid Zones, Faculty of Natural Sciences and Life. Ibn-Khaldun University, Tiaret / Algeria; E-mail: boukirat_dyhia@live.fr

²⁾ Institute of Biosciences, TU Bergakademie Freiberg / Germany, E-mail: Hermann.Heilmeyer@ioez.tu-freiberg.de

³⁾ State Agrarian-Economic University, Dnipropetrovsk / Ukraine, E-mail: envteam@ukr.net
Tel: 0727651064; E-mail: boukirat_dyhia@live.fr

Keywords: earthworms, common barley, bioaccumulation, phytoremediation, lead pollution

ABSTRACT

The aim of this work is to study the possibility of remedying polluted agricultural soils by lead with the association: earthworms / barley. An experimentation of sixty pots was conducted in controlled conditions containing artificially contaminated soil by lead. It is divided into three systems: S1: soil-plant; S2: soil-earthworms; S3: soil-plant-earthworms, and five blocks representing lead concentrations: control; 500 $\mu\text{g g}^{-1}$; 1000 $\mu\text{g g}^{-1}$; 1500 $\mu\text{g g}^{-1}$ and 2000 $\mu\text{g g}^{-1}$ with 4 replicas each.

The results show that the S3 system (soil-plant-earthworm) has the highest remediation rate compared to the two other: S1 (soil-earthworm), S2 (soil-plant). The presence of earthworms *Lumbricus sp* decreases the bioaccumulation of lead by *Hordeum vulgare*, while concentrations recorded in earthworm tissues suggests that the presence of the plant considerably increase those concentrations.

The concentrations of lead in soil, earthworms and plants are influenced by the physical and chemical soil parameters; however, other factors related to the pollutant, the species of both earthworm and plant and their interactions can increase or decrease retention of lead by the soil and its bioaccumulation.

RÉSUMÉ

Le but de ce travail est d'étudier la possibilité de remédier les sols agricoles pollués au plomb à l'aide d'une association vers de terre / orge. Une expérimentation de soixante pots comportant des sols artificiellement contaminés au plomb a été menée dans des conditions contrôlées. Elle est répartie en trois systèmes : S1: sol-plante ; S2: sol-ver de terre; S3: sol-plante-ver de terre et cinq blocs représentant les concentrations de plomb : 500 $\mu\text{g g}^{-1}$; 1000 $\mu\text{g g}^{-1}$; 1500 $\mu\text{g g}^{-1}$; 2000 $\mu\text{g g}^{-1}$ et témoin avec 4 répliques chacun.

Les résultats montrent que le système S3 (sol-plante-ver de terre) présente le taux de remédiation le plus élevé comparé aux deux autres : S1 (sol-ver de terre), S2 (sol-plante). La présence des vers de terre *Lumbricus sp* diminue la bioaccumulation du plomb par *Hordeum vulgare*, alors que les concentrations enregistrées dans les tissus des vers de terre suggère que la présence de la plante accroît considérablement ces concentrations.

Les concentrations du plomb dans le sol, les vers de terre et la plante sont influencées par les paramètres physico-chimiques du sol cependant d'autres facteurs liés au polluant, à l'espèce du ver de terre et à celle de la plante et leurs interactions peuvent augmenter ou diminuer la rétention du plomb par le sol et sa bioaccumulation.

INTRODUCTION

Earthworms are one of the dominant groups of macro invertebrates of ground in several terrestrial ecosystems representing nearly 80% of the biomass of soil. They are identified as ecosystem engineers for their long-term effects on soil physical, chemical and biological properties (Edwards and Bohlen, 1996; Blouin et al, 2013; Bityutskii et al, 2016).

Due to their constant contact and their strong interaction with soil, earthworms can be profoundly affected by the soil pollution and accumulated contaminants in their bodies. Those characteristics among others allowed their use as indicator organisms of soil contamination (*Lanno et al, 2004; Xiao et al, 2006*).

Earthworms can concentrate some chemical products by involving selective absorption and excretion mechanisms, which vary according to species and families of chemicals. The toxic effects of a large number of chemical substances and the analysis of their absorption and metabolism have been identified to underline the importance of earthworms in biomonitoring of soil quality (*De Vauffleury et al, 2013*).

Human activity is the source of soil contamination by various organic and inorganic compounds. Heavy metals pollution caused by industrial enterprises activity and road traffic has reached high levels in the soil in some regions (*Ha et al, 2011; Jiang, Z.F., 2012; Adriano, D.C., 2001; Alkorta et al, 2004*).

It is established that such heavy metals as copper (Cu), zinc (Zn), lead (Pb) and cadmium (Cd) show a different effect of acute and chronic toxicity to animals and plants (*Cheng et al, 2002; Li M, et al, 2009; Li N et al, 2009*). Excessive levels of lead in soil inhibit the normal plant growth, disturb the ecosystem equilibrium and have an extremely negative impact on the environment and human health (*Mishra et al, 2006 Zeng et al, 2006*).

Studies on the ability of certain plant to accumulate heavy metals propose them as an alternative to the physical and chemical methods of decontamination.

Several studies were conducted using the plant / earthworms association for soil remediation. Earthworms increase the availability of heavy metals in some situations and aid in maintaining the structure and the quality of soil. The introduction of earthworms into metal contaminated soils has been suggested as an aid for the phytoremediation processes (*Lemtiri et al, 2015; Jusselme et al, 2012*).

The main objectives of this study are: i) to study the possibility of decontaminating a polluted by lead arable land using the association earthworm / plant; ii) to assess these two organisms impact on soil physics-chemical parameters.

MATERIAL AND METHODS

Samples and characterization of experimental soil

The soil samples were taken in uncontaminated arable land to the depth of 0 - 30 cm. All soil samples were air dried, crushed, sieved at 5 mm and mixed. This sieved soil was used for the pot experiment.

The soil samples were sieved at 2 mm additionally to provide physics-chemical analyses. The distribution of particles according to their size, or particle size analysis was determined by sedimentation using the Robinson pipette. Soil pH was measured using a soil suspension in a ratio (M/V) 1/5. The organic matter (OM) was determined by calcination in the oven at 500 °C according to NF ISO10694. The cation exchange capacity (CEC) was determined by percolation according to NF X 31-130. The electrical conductivity was measured in a soil suspension (M/V) 1/5 according to NF ISO 11265. The total lead concentration was determined by tri-acid attack following standard NF X 31-147, and measured by atomic absorption spectrometry (Agilent Technology. 55 AA). The characterization of experimental soil and the averages of lead concentrations in the soil, barley and earthworms ($\mu\text{g g}^{-1}$ dry weight) are represented in Table 1.

Lead contamination of soil

The soil was artificially contaminated with four levels of lead (500 $\mu\text{g/g}$, 1000 $\mu\text{g/g}$, 1500 $\mu\text{g/g}$ and 2000 $\mu\text{g/g}$) using lead nitrate powder [$\text{Pb}(\text{NO}_3)_2$] dissolved in distilled water, in addition to uncontaminated soil (control) with a lead concentration (<100 $\mu\text{g/g}$) in the international norms described by (*AFNOR X 31 in 1996*).

Experimental procedure

Three factors were involved in the experimental design: (i) lead concentration in soil; (ii) Presence / Absence of the earthworms and (iii) Presence / Absence of the plant. The experimentation is divided into three systems: S1: soil-plant; S2: soil-earthworms and S3: soil-plant-earthworms, five blocks representing lead concentrations: control, 500 $\mu\text{g g}^{-1}$, 1000 $\mu\text{g g}^{-1}$, 1500 $\mu\text{g g}^{-1}$ and 2000 $\mu\text{g g}^{-1}$ with 4 replicas each (see fig. 1). This disposition will allow to study and compare the effect of each organism alone on the soil and the effect of their association at different levels of pollution.

Table 1

Lead concentrations in the soil, plants and earthworms ($\mu\text{g g}^{-1}$ DW), and chemical parameters measured in the experimental soils

Parameters	Mean \pm SD	Minimum	Maximum
Soil (N=60)			
Clay (%) ^a	24,51 \pm 3,73	15,30	34,35
Silt (%) ^a	9,54 \pm 5,90	0,77	25,54
Sand (%) ^a	65,98 \pm 5,49	45,95	74,49
OM (%) ^b	2,30 \pm 0,37	1,50	3,12
pH _{water} ^c	7,42 \pm 0,57	6,39	8,34
CEC(meq100 ⁻¹ g) ^d	11,93 \pm 3,20	0,13	18,55
EC ($\mu\text{s/cm}$) ^e	831,27 \pm 273	335,00	1485,00
System 1(N=16)			
Pb soil ($\mu\text{g/g}$) ^f	331.86 \pm 66.95	200,00	430,00
Pb plant ($\mu\text{g/g}$) ^f	59.44 \pm 13.16	38,00	75,00
Remediation (%) ^g	17.93 \pm 1.87	14,85	21,50
Control 1 (N=4)			
Pb soil ($\mu\text{g/g}$) ^f	50.00 \pm 21.60	20,00	70,00
Pb plant ($\mu\text{g/g}$) ^f	11.75 \pm 3.10	9,00	16,00
Remediation (%) ^g	27.13 \pm 12.34	16.67	45.00
System 2 (N=16)			
Pb soil ($\mu\text{g/g}$) ^f	342.5 \pm 54.59	250,00	440,00
Pb EW ($\mu\text{g/g}$) ^f	24.01 \pm 10.97	12.55	54.54
Biomass (g)	2.11 \pm 0.45	1.40	2.90
Remediation (%) ^g	7.54 \pm 1.95	5,32	12.99
Control 2 (N=4)			
Pb soil ($\mu\text{g/g}$) ^f	70.00 \pm 16.33	50,00	90,00
Pb EW ($\mu\text{g/g}$) ^f	8.20 \pm 0.48	7.50	8.59
Biomass (g)	3.13 \pm 0.1	3.00	3.20
Remediation (%) ^g	12.29 \pm 1.49	10.38	14.00
System 3 (N=16)			
Pb soil ($\mu\text{g/g}$) ^f	316.25 \pm 87.25	150,00	430,00
Pb plant ($\mu\text{g/g}$) ^f	38.00 \pm 5.68	31,00	50,00
Pb EW ($\mu\text{g/g}$) ^f	26.01 \pm 6.66	16.53	39,00
Biomass (g)	1.18 \pm 0.47	0.90	2,50
Remediation (%) ^g	18.79 \pm 2.14	15.70	22.69
Control 3 (N=4)			
Pb soil ($\mu\text{g/g}$) ^f	67.5 \pm 9.57	60,00	80,00
Pb plant ($\mu\text{g/g}$) ^f	20.25 \pm 2.25	17,00	23,00
Pb EW ($\mu\text{g/g}$) ^f	12.84 \pm 1.09	11.36	13,93
Biomass (g)	2.78 \pm 0.13	2.60	2,90
Remediation (%) ^g	49.01 \pm 10.81	40.29	64.72

^a Size particles by sedimentation using the Robinson pipette method.
^b Organic matter was determined by calcination in the oven at 500°C according to NF ISO10694
^c pH_{water} with distilled water (w:v 1:5 ratio).
^d CEC determined by percolation according to NF X31-130.
^e Electrical conductivity water suspension with ratio 1:5.
^f Digestion with mixture of three acids inspired by the NF X 31-147.
^g calculated according to : $(R_1/R_0)*100$; [R₁: accumulated Pb in the system, R₀: accumulated Pb in soil].

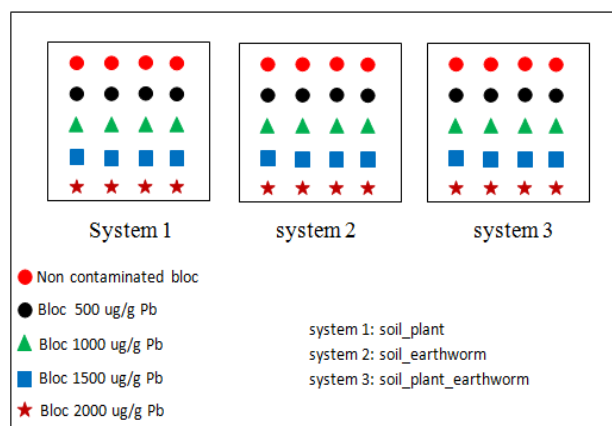


Fig. 1 - Experimental design

Sixty pots (18 cm diameter x 20 cm height) were prepared with 3 kg of dry soil, contaminated and mixed. The plant used in this experiment is a grass, common barley *Hordeum vulgare* L. Ten seeds were sown in the pots of the system S1 and S3. The experiment was conducted in greenhouses (temperature of $25 \pm 2^\circ\text{C}$ and $60 \pm 5\%$ relative humidity) and germination was determined visually. The pots of the three systems are watered daily to keep the soil moist. After 4 months, adult anecic earthworms *Lumbricus sp* were collected in an uncultivated and unpolluted soil of Tiaret. They were rinsed to remove the soil, kept in plastic box in the laboratory (24 h) for cleaning their gut. 2 - 3 earthworms (mass: 3 ± 0.5 g) were introduced into each pot of system S2 and S3; to provide a density of about 100 g m^{-2} (Blouin et al, 2006; Jusselme et al, 2013). The experiment was conducted under controlled conditions during 21 days.

Harvesting and treatment of samples

At the end of the experiment the samples were harvested, the aerial part of the plant was cut at ground level. The stems and leaves were separated and preserved in paper bags. Then the pots were overturned on plastic. Earthworms were gathered, their survival was determined by observing their activities in the hand; afterward they were rinsed, weighed and conserved for 48 hours in boxes containing moistened paper with distilled water to clean their gut (Lemtiri et al, 2015; Bityutskii et al, 2016).

The roots were collected, washed with distilled water to remove the soil and kept in paper bags, the soil dried in the open air for 48 h. The samples were the subject of a series of operations as follows:

- dehydration: the usual method is dehydration in an oven at $105^\circ \pm 2^\circ \text{C}$ for 72 hours, and the earthworms for 24 h.
- grinding: This step is highly critical as it can be source of contamination or loss. For this, the grinder used is an agate mortar; 0.5 to 1 g of the powder obtained is placed in quartz capsules and calcined in an oven, the temperature of which being gradually increased to 450°C for 3 h.
- mineralization and dissolution: after calcination, the sample are placed in an acid solution (10 ml of hydrofluoric acid HF 40% and 3 ml of perchloric acid ClHO_4 70%) and heated in a sand bath until total evaporation of the solution. Outside of the sand bath, we added 1 ml of nitric acid HNO_3 and 10 ml of distilled water and allowed 30 min, after that, it was placed in the sand bath for 30 min to 1 h.
- filtration and dilution: After filtration, the obtained extracts are diluted with 100 ml of distilled water (Durand, C., 2003). The lead concentration was determined by atomic absorption spectrometry.

Statistical analysis

The statistical treatment was performed using two software packages STATISTICA 8 and SPSS 20. The data obtained were subjected to several analyses: Descriptive statistics, ANOVA, ANOVAR and correlation analysis. Firstly, the effects of soil lead levels on the concentration of lead in earthworm's tissues and plant were evaluated through analysis of variance (ANOVA). Secondly, the effects of physicochemical parameters of soil on the concentration of lead in earthworm's tissues and plant were investigated. Finally, the effects of lead levels (block T, B1, B2, B3 and B4) and the systems (S1, S2 and S3) on Pb concentration in earthworms' tissues and plant were evaluated. Differences were considered significant at $P \leq 0.05^*$, highly significant at $P \leq 0.01^{**}$ and very highly significant at $P \leq 0.001^{***}$.

RESULTS

Levels of lead in soil

The concentrations of lead in soil within blocks of each system before and at the end of the experiment are represented in fig. 2.

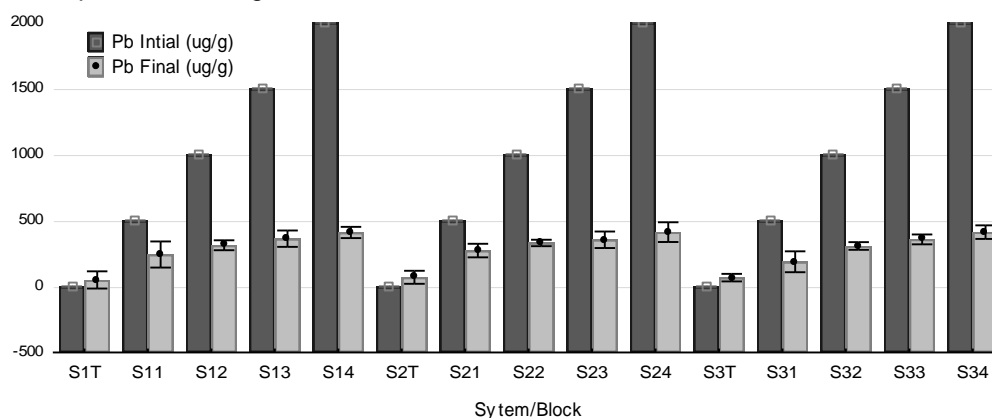


Fig.2 - Lead levels in the experimental soil

We see that the final concentrations of the soil have greatly reduced compared to the initial concentrations, a positive correlation was observed between the levels of contamination and soil concentrations with a correlation coefficient $r=0,94^{***}$ and a highly significant effect $p<0.001^{***}$.

The toxicity of metals does not depend only on the total concentration but also on their mobility and reactivity with other components of the ecosystem (Abollino et al, 2002). Many authors classify this reactivity in the order: $Ni>Zn>Cu>Pb$ (Harter, R. D., 1983; Kabala and Szerszen, 2002). Lead is generally found in surface horizons 0-20 cm than in deeper soil layers (Contat et al, 1991). Several factors affect its mobility and bioavailability: pH, soil texture especially clay content and organic matter content.

Concentrations of lead in the three systems

Remediation percentages of the three systems (including the five blocks) are shown in fig. 3. We observe that the association plant-earthworm (S3) shows the highest rate of remediation (accumulation) $24.83 \pm 13.26 \%$, a highly significant difference was observed between the three systems $p<0.001^{***}$. The concentrations of lead accumulated in the plant and earthworm increased significantly with the levels of lead in soil $p<0.001^{***}$.

The accumulation of lead by barley varies depending on the concentration of lead in the soil and the physic - chemical parameters of the soil (Maatoug et al, 2013). This concord with the results found in our study. Bioaccumulation of metals in earthworms depends a lot on the species and the characteristics of their environment, including soil composition and pH (Van Gestel and Ma 1988; Morgan J.E. and Morgan A.J. 1991; 1999). De Vauflery A. et al, 2013). The presence of the plant and earthworms can create a competition between them for the accumulation of lead. By producing exudates, plants can modify metal speciation and their behaviour in soil, particularly in the *rhizosphere* (Chaignon and Hinsinger, 2003; Uzu, G. et al, 2009). Therefore, plants can change the metal accumulation by earthworms (Lemtiri et al, 2015).

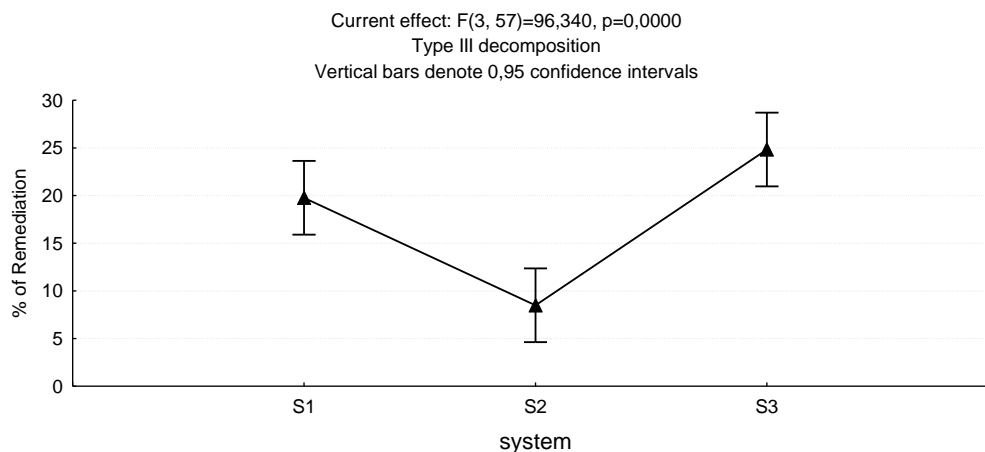


Fig. 3 - Percentage of remediation in the three systems S1: soil-plant; S2: soil-earthworm; S3: soil-plant-earthworm

Effects of the interaction plant / earthworms on the contaminated soil

Our study focused on the interaction between earthworm *Lumbricus sp* and the plant *Hordeum vulgare* for bioremediation of artificially contaminated soil with lead. In order to study the effects of the five lead concentrations used in this experiment which are divided into blocks, on the recorded soil concentrations, an ANOVA test was performed (fig. 4). A very highly significant difference is observed for the effect of lead dose added to the ground on the lead concentration in the soil, plants and earthworms $P<0.000^{***}$.

We notice an important fixative power of lead by the ground following the doses added at the beginning of the experiment.

The system S3 presents the highest concentration of lead extracted from the soil. We also observe that the plant accumulates more lead on its own $49.9 \pm 22.83 \mu\text{g g}^{-1}$ than in the presence of earthworms $34.45 \pm 8.92 \mu\text{g g}^{-1}$. The correlation matrix shows a positive correlation between Pb soil and Pb plant $r=0.688^{**}$.

The concentrations of lead in earthworm tissues after 21 days of exposure are positively correlated with soil concentrations with a correlation coefficient $r=0.919^{**}$ and a highly significant effect $p\leq 0.000^{**}$. We observed that concentrations of lead in earthworm tissues are higher in the presence of the plant $23.37 \pm 8.02 \mu\text{g g}^{-1}$ against $20.85 \pm 11.71 \mu\text{g g}^{-1}$ in its absence.

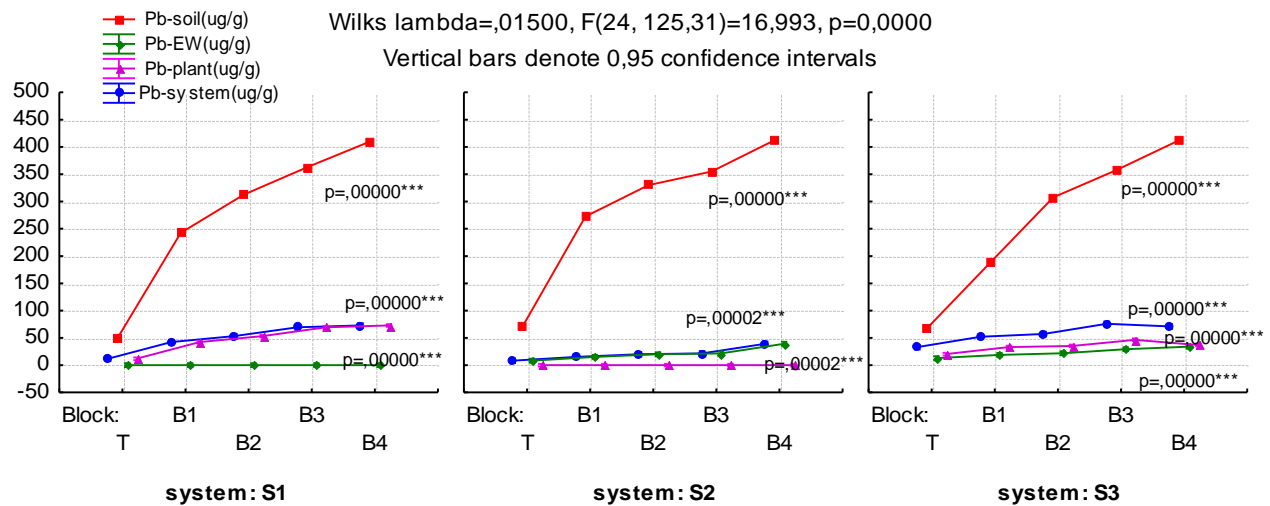


Fig. 4 - Effect of the interaction between bloc and Pb concentrations in plant, earthworm and soil for the three systems

Barley accumulates the trace elements to different degrees depending on the metal and its concentration in the soil. (Maatoug *et al.*, 2013) reported that in an agricultural soil close to a highway contaminated with lead $1714.39 \pm 512.62 \mu\text{g g}^{-1}$, barley accumulates until $36.28 \pm 14.90 \mu\text{g g}^{-1}$. In our study, we find that for lead concentrations in the soil of the order of $331.86 \pm 66.95 \mu\text{g g}^{-1}$ barley accumulates $59.44 \pm 13.16 \mu\text{g g}^{-1}$.

Lead contrary to the other elements (Zn, Cu) is not an essential element, although present in the plants, it does not participate to any known physiological or biochemical function (Marschner H., 1995). Pb is accumulated by the plant according to another uptake pathway than those of the essential elements Zn and Cu (Lemtiri *et al* 2015). In this study, lead being added in a highly soluble form may be more available and easily absorbed by the plant, which explains the high concentrations accumulated by barley.

Earthworms (of various species) that live in soils polluted by metals, mainly of anthropogenic source, have heavy metal contents much higher than those which develop in unpolluted areas (Ireland M.P., 1983; Morgan J.E. & Morgan A.J., 1988; Dai *et al*, 2004; De Vaufleury *et al*, 2013). Other studies report that concentrations in earthworms were weakly correlated with those of soils (Beyer and Cromartie, 1987; Abdul Rida and Bouché, 1995). The results found in this study indicate a very significant correlation between lead levels in soil and lead concentrations in earthworms *Lumbricus sp.*

An increase of metal concentration in plants was observed in the presence of earthworms (Wen and Hu, 2004). These results are opposite of what we observed in our study. Lead concentration in barley decreases greatly in the presence of *Lumbricus sp.* It can be explained by a different accumulation capacity and affinity according to the plant and the metal.

Earthworms can concentrate some chemicals involving selective absorption and excretion mechanisms, which vary according to earthworm species and chemical families (De Vaufleury A, 2013).

The ability of earthworms to accumulate heavy metals is widely studied (Morgan *et al*, 1986; Beyer W.N.*et al*, 1987; Morgan J.E. and Morgan A.J., 1992). Some differences in bioaccumulation were reported between ecophysiologicaly distinct earthworms (Morgan *et al*, 1993; Van Vliet *et al*, 2005; Kamitani and Kaneko, 2007). The presence of the plant increases the concentration of lead in earthworm tissues.

Effect of physicochemical soil parameters on Pb soil, Pb plant and Pb earthworms

In order to investigate the effect of physicochemical parameters of the soil on the accumulation of lead in the soil, plant and earthworms we performed a correlation analysis with a variance analysis (ANOVA).

Effect of pH

We observe a negative correlation between soil pH and lead soil, plants and earthworms with a correlation coefficient $r=-0.572^{**}$, $r=-0.396^{*}$, $r=-0.410^{**}$, respectively. ANOVA revealed a significant effect of soil pH on the Pb soil $p=0.037^{*}$ and Pb plant $p=0.002^{**}$, but no effect on the Pb earthworms $p=0.224$.

The pH is a factor whose role is crucial for the mobility of metal ions, because it influences the number of negative charges that can be brought into solution (McLaughlin, M.J., 2000). Generally, when

the pH increases, the cations are less soluble and less mobile (Blanchard C., 2000; Santillan-Medrano and Jurinak, 1975; Kabala and Szerszen, 2002). Different interpretations have been advanced to explain the influence of soil pH on the accumulation of lead (McBride, 1994). It was found that the Cd, Cu, Hg, Ni, Pb and Zn are strongly absorbed by the roots at $\text{pH} < 5.5$ (Blaylock and Huang, 2000).

The accumulation of metals in earthworms is influenced by their concentration in the soil, and in the case of Cd, by the pH (Spurgeon et al. 2006). The low bioavailability of metals (Cu, Pb and Zn) in a contaminated soil with an alkaline pH, and the absence of toxic effects were confirmed experimentally in *Lumbricus terrestris*, in urban soils little rich in nutriment of Montreal (Kennette D., 2002). Among the reasons that may explain the limited effects of pH change on the concentration of earthworm tissue (Oste et al. 2001) suggest firstly, an effect of pH on the absorption by the skin, and secondly, the influence of soil particles ingested.

Effect of CEC

The cation exchange capacity is positively correlated with lead soil $r=0.221$ and earthworms $r=0.215^{**}$ and is weakly correlated with the lead of the plant with a correlation coefficient $r=0.023^{**}$. ANOVA shows no significant effect of CEC on the Pb soil, Pb earthworms and Pb plant $p > 0.05$.

The pH influences the CEC, the nature of the organic matter and its decomposition via the fauna and flora of the soil. (Allan and Jarrell, 1989) have shown that CEC decreases gradually as decreases the external pH. The soil constituents thus modified will register increase or decrease the complexation capacity of the elements and therefore the mobility and bioavailability of trace elements (McBride et al 1997; Sauv   et al, 1997 Sauv   and McBride, 1998; Venditti D., 2000). Simultaneous measurements of the cation exchange capacity suggest that this soil parameter is a better indicator of the bioavailability of Cd and Zn because it takes into account the type of clay and organic matter (Lock K. & Janssen C.R., 2001).

Effect of clay rate

Concerning the clay content it has a positive correlation with Pb soil $r=0.234^{**}$ and Pb earthworms $r=0.102$ and negatively correlated with the Pb plant $r=-0,054^{**}$, the analysis of variance indicated a highly significant effect for Pb soil and Pb plant $p < 0.000^{***}$ and highly significant for Pb earthworms $p < 0.005^{**}$.

Clays and organic matter play a predominant role in the adsorption of lead by the plant. Trace elements show a high affinity for the humic substances with which they form stable humic-clay complex, eventually soluble. This explains the abundance of the trace elements on the surface mainly in the presence of organic matter (Baize D., 1997).

Lock and Janssen (2001) conducted experiments with *Enchytraeus albidus*, which show that the toxicity of Cd and Zn depends on the nature of the clay used and the organic matter.

Effect of organic matter

A weak correlation was observed between the organic matter and the three variables, however it is negative with Pb soil $r=-0,029^{**}$, Pb earthworms $r=-0,038$ and positive with Pb plant $r=0.052^{**}$. ANOVA shows no significant effect $p > 0.05$.

The assimilation of trace elements by plants is highly dependent on the bioavailability of these elements in the soil. The soil constituents, especially clays and organic matter can interact with the metal across different chemical interactions (electrostatic interactions etc.) All these interactions limit the bioavailability of the metals in the soil (Tanner and Headley, 2011).

The soil characteristics have a different impact from one earthworm species to another also depending on the studied metal (Peijnenburg W.J.G.M., 1999; Posthuma L., 1998). It was observed an increase of lead concentration in earthworms exposed in soil with high lead contamination (Grelle and Descamps, 1998; Scaps et al., 1997). Pb accumulation is proportional to the time of exposure. However the concentration in the earthworms remains much lower than that of soil. These results are similar with the results that we found in our experiments.

CONCLUSIONS

The present study shows that using the association *Hordeum vulgare* and *Lumbricus sp* significantly increases the concentrations of lead extracted from the soil. The concentrations of lead in *Lumbricus sp* tissues and *Hordeum vulgare* increase with increasing levels of lead in the soil.

The lead concentrations in the soil depend on the physico-chemical parameters. However, other factors (element content and mobility) may increase or decrease retention of lead by the soil. The system S3

(soil-plant-earthworm) has the highest rate of remediation 24.83 ± 13.26 % compared to the two others S1 (soil-earthworm) 8.49 ± 2.67 % and S2 (soil-plant) 19.77 ± 6.41 %.

The presence of earthworms *Lumbricus sp* decreases the bioaccumulation of lead by *Hordeum vulgare*, while content recorded in tissues of earthworms suggests that the presence of the plant significantly increases the element concentration. This can be explained by a competition between the two organisms in the absorption of trace elements.

Several studies report that the accumulation of trace elements differs from one species to another. However, the interaction between two organisms such as earthworms and plants can be complex and influenced by many factors: the species of the plant and the earthworm, the physico-chemical parameters of the soil, the levels of pollution and the nature of the pollutant.

The results of this study suggest that it is possible to use the association plant/earthworms for the bioremediation of agricultural soils polluted by lead.

REFERENCES

- [1] Abdul Rida A.M.M., Bouché M.B., (1995), The eradication of an earthworm genus by heavy metals in southern France, *Applied Soil Ecology*, vol.2, pp. 45-52;
- [2] Abollino O., Aceto M., Malandrino M., Mentasti E., Sarzanini C. & Barbaris R., (2002), Distribution and mobility of metals in contaminated sites, Chemometric investigation of pollutant profiles, *Environmental Pollution*, 119, pp. 177-193;
- [3] Alkorta I., Hernandez-Allica J., Becerril J.M., Amezcaga I., Albizu I. et Garbisu C., (2004), Recent findings on the phytoremediation of soils contaminated with environmentally toxic heavy metals and metalloids such as zinc, cadmium, lead and arsenic, *Environ. Sci. Biotechnol.*, vol.3, pp. 71-90;
- [4] Baize D., (1997), *Teneurs totales en éléments traces, métalliques dans les sols de France*, Edition INRA, p.408;
- [5] Beyer W.N., Cromartie E.J. (1987), A survey of Pb, Cu, Zn, Cd, Cr, As and Se in earthworms and soils from diverse sites, *Environ. Monit. & Assess.*, vol.8, pp. 27-36;
- [6] Beyer W.N., Hensler G. & Morre J., (1987), Relation of pH and other soil variables to concentrations of Pb, Cu, Zn, Cd and Se in earthworms, *Pedobiologia*, vol.30, pp. 167-172;
- [7] Bityutskii N., Kaidun P., Yakkonen K., (2016), Earthworms can increase mobility and bioavailability of silicon in soil. *Soil Biology & Biochemistry*, vol.99, pp. 47-53;
- [8] Blanchard C., (2000), *Caractérisation de la mobilisation potentielle des polluants inorganiques dans les sols pollués*, Thèse: Ecole Doctorale de Chimie de Lyon;
- [9] Blaylock M.J. and Huang J.W., (2000), Phytoextraction of metals. In: I. Raskin and B.D. Ensley eds. *Phytoremediation of toxic metals: using plants to clean-up the environment*, New York, John Wiley & Sons, Inc, pp. 53-70;
- [10] Blouin M, Barot S, Lavelle P. Earthworms (2006), *Millsonia anomala*, *Megascolecidae* do not increase rice growth through enhanced nitrogen mineralization, *Soil Biol Biochem*; 38, pp. 2063–8;
- [11] Blouin M., Hodson M.E., Delgado E.A., Baker G., Brussaard L., Butt K.R., Dai J., Dendooven L., Peres G., Tondoh J.E., Brun J.J., (2013), A review of earthworm impact on soil function and ecosystem services, *European Journal of Soil Science*, 64, pp.161–182;
- [12] Chaignon V., Hinsinger, P., (2003), A biotest for evaluating copper bioavailability to plants in a contaminated soil, *Journal of Environmental Quality*, 32, pp.824–833;
- [13] Cheng J., Wong M.H., (2002), Effects of earthworms on Zn fractionation in soils, *Biology and Fertility of Soils*, 36, pp. 72–78;
- [14] Contat F., Shariat Madari H et Stadelmann FX., (1991), Déposition et accumulation de Plomb le long de quatre secteurs autoroutiers de 1978 à 1988, Évolution en fonction des années, des saisons et de la météorologie. *Recherche Agronomique en Suisse*, 30(1/2), pp. 29–43;
- [15] Dai J., Becquer T., Rouiller J.H., Reversat G., Bernhard-Reversat F., Nahmani J. & Lavelle P., (2004), Heavy metal accumulation by two earthworm species and its relationship to total and DTPA-extractable metals in soils. *Soil Biology and Biochemistry.*, 36, pp. 91–98;
- [16] De Vaulfleury A., Gimbert F., Gomot L., (2013), *Bioaccumulation, Bioamplification des polluants dans la faune terrestre, Un outil pour la biosurveillance des écosystèmes*, ADEME, France, pp. 46–90;
- [17] Durand, C., (2003), *Caractérisation physico-chimique des produits de l'assainissement pluvial. Origine et devenir des métaux traces et des polluants organiques*, Thèse de doctorat, Université de Poitiers, 248 p;

- [18] Edwards, C.A., Bohlen, P.J., (1996), *Biology and Ecology of Earthworms*. Chapman and Hall, London.
- [19] Grelle C., Descamps M., (1998), Heavy metal accumulation by *Eisenia fetida* and its effects on glutathione-S-transferase activity, *Pedobiologia*, 42, pp. 289-297;
- [20] Ha, N.T.H., Sakakibara, M., Sano, S., Nhuan, M.T., (2011), Uptake of metals and metalloids by plants growing in a lead-zinc mine area, Northern Vietnam. *J. Hazard. Mater.* 186, pp. 1384-1391;
- [21] Harter, R. D., (1983), Effect of soil pH on adsorption of lead, copper, zinc, and Nickel, *Soil Science Society of America Journal*, 47, pp. 47-51;
- [22] Jiang, Z.F., Huang, S.Z., Han, Y.L., Zhao, J.Z., Fu, J.J., (2012), Physiological response of Cu and Cu mine tailing remediation of *Paulownia fortunei* (Seem) Hemsl, *Ecotoxicology* 21, pp. 579-767;
- [23] Jusselme MD., Poly F., Miambi E., Mora P., Blouin M., Pando A., (2012), Effect of earthworms on plant *Lantana camara* Pb-uptake and on bacterial communities in root-adhering, *Science of The Total Environment*, 416, pp. 200–7;
- [24] Jusselme MD., Miambi E., Mora P., Diouf M., Rouland-Lefèvre C., (2013), Increased lead availability and enzyme activities in root-adhering soil of *Lantana camara* during phytoextraction in the presence of earthworms, *Science of the Total Environment*, pp.445-446, pp.101–109;
- [25] Kabala, C., et Szerszen, L., (2002), Profile distributions of lead, zinc, and copper in Dystric Cambisols developed from granite and gneiss of the Sudetes Mountains, *Poland. Water, Air, & Soil Pollution*, 138, pp. 307-317;
- [26] Kamitani T., & Kaneko N., (2007), Species-specific heavy metal accumulation patterns of earthworms on a floodplain in Japan, *Ecotoxicology and Environmental Safety*, 66, pp. 82-91;
- [27] Kennette D., Hendershot W., Tomlin A. & Sauvé S., (2002), Uptake of trace metals by earthworm *Lumbricus terrestris* L. in urban contaminated soils, *Applied Soil Ecology*, 19, pp. 191-198;
- [28] Lanno, R., Wells, J., Conder, J., Bradham, K., Basta, N., (2004), The bioavailability of chemicals in soil for earthworm, *Ecotoxicology and Environmental Safety*, 57, pp. 39–47;
- [29] Lemtiri A., Liénarda A., Alabib T., Brostauxc Y., Cluzeaud D., Francisb F., Colineta G., (2015), Earthworms *Eisenia fetida* affect the uptake of heavy metals by plants *Vicia faba* and *Zea mays* in metal-contaminated soils, *Applied Soil Ecology*., <http://dx.doi.org/10.1016/j.apsoil.11.021>;
- [30] Li, M., Liu, Z.T., Xu, Y., Cui, Y.B., Li, D.S., Kong, Z.M., (2009), Comparative effects of Cd and Pb on biochemical response and DNA damage in the earthworm *Eisenia fetida* (Annelida, Oligochaeta), *Chemosphere* ,74, pp. 621–625;
- [31] Li, N.Y., Li, Z.A., Zhuang, P., Zou, B., McBride, M., (2009), Cadmium uptake from soil maize with intercrops. *Water Air Soil Pollution*, 199, pp. 45–56;
- [32] Lock K. & Janssen C.R., (2001), Effect of clay and organic matter type on the ecotoxicity of zinc and cadmium to the potworm *Enchytraeus albidus*, *Chemosphere*, 44, pp. 1669-1772;
- [33] Maatoug M., Amirat M., Zerrouki D., Ait Hammou M., (2013), Decontamination of Agricultural soil polluted with lead using the common barley (*Hordium vulgare*), *Arab Gulf Journal of Scientific Research*, 31 (1), pp. 23-35;
- [34] Marschner H., (1995), *Mineral Nutrition of Higher Plants*, Second edition, Academic press, London.
- [35] McBride M., Sauvé S. & Hendershot W.H., (1997), Solubility control of Cu, Zn, Cd and Pb in contaminated soils, *European Journal of Soil Science*, 48, pp. 337-346;
- [36] McBride M.B., (1994), "*Environmental chemistry of soils*". New York, Oxford University Press, 406 p., ISBN 0-19-507011-9;
- [37] McLaughlin M.J., Zarcinas B.A., Stevens D.P., Cook N., (2000), Soil testing for heavy metals. *Communications in Soil Science and Plant Analysis* 31, pp.11-14, pp. 1661-1700;
- [38] Mishra S., Srivastava S., Tripathi R.D., Kumar R., Seth C.S., Gupta D.K., (2006), Lead detoxification by coontail (*Ceratophyllum demersum* L) involves induction of phytochelatins and antioxidant system in response to its accumulation, *Chemosphere*, 65, pp. 1027-1039;
- [39] Morgan A.J., Morgan J.E., Turner M., Winters C. & Yarwood A., (1993), Metal relationships of earthworms, *Ecotoxicology of Metals In Invertebrates*, Dallinger R. & Rainbow P.S. (Eds), SETAC, Lewis Publ., USA, pp. 333-358;
- [40] Morgan A.J., Morris B., James N., Morgan J.E. & Leyshon K., (1986), Heavy metals in terrestrial macroinvertebrates: Species differences within and between trophic levels, *Chemistry and Ecology*, 2, pp. 319-334;
- [41] Morgan J.E., Morgan A.J., (1988), Earthworms as biological monitors of cadmium, copper, lead and zinc in metalliferous soils, *Environmental Pollution*., 54, pp. 123-138;

- [42] Morgan J.E., Morgan A.J., (1991), Differences in the accumulated metal concentrations in two epigeic earthworm species (*Lumbricus rubellus* and *Dendrodrilus rubidus*) living in contaminated soils. *Bulletin of Environmental Contamination and Toxicology.*, 47, pp. 296-301;
- [43] Morgan J.E., Morgan A.J., (1992), Heavy metal concentrations in the tissues, ingesta and faeces of ecophysiologicaly different earthworm species, *Soil Biology & Biochemistry.*, 24, pp. 1691-1697;
- [44] Morgan J.E., Morgan A.J., (1999), The accumulation of metals (Cd, Cu, Pb, Zn and Ca) by two ecologically contrasting earthworm species (*Lumbricus rubellus* and *Aporrectodea caliginosa*): Implications for ecotoxicological testing, *Applied Soil Ecology.*, 13, pp. 9-20;
- [45] Oste L.A., Dolfing J., Ma W.C., Lexmond T.M., (2001), The effect of beringite on Cd and Zn uptake by plants and earthworms: More than a liming effect?, *Environmental Toxicology and Chemistry.* 20, pp.1339-1345;
- [46] Peijnenburg W.J.G.M., Posthuma L., Zweers P.G.P.C., Baerselman R., de Groot A.C., Van Veen R.P.M., Jager T., (1999), Prediction of metal bioavailability in Dutch field soils for the oligochaete *Enchytraeus crypticus*, *Ecotoxicology and Environmental Safety.*, 43, pp. 170-186;
- [47] Posthuma L., Notenboom J., de Groot A.C., Peijnenburg W.J.G.M., (1998), Soil acidity as a major determinant of zinc partitioning and zinc uptake in two oligochaete worms (*Eisenia andrei* and *Enchytraeus crypticus*) exposed in contaminated field soils., *In: Advances in Earthworms Ecotoxicology.* Sheppard S., Bembridge J., Holmstrup M. & Posthuma L. (Eds), SETAC Publishers, Pensacola, FL, USA, pp. 111-127;
- [48] Raskin I., Kumar N.P.B.A., Dushenkov S., Salt D.E., (1994), Bioconcentration of heavy metal by plant. *Current Opinion in biotechnology* 5, pp. 285-290;
- [49] Salt D.E., Blaylock M., Kumar N.P.B.A., Dushenkov S., Ensley B.D., Chet I., Raskin I., (1995), Phytoremediation: a novel strategy for the removal of toxic metals from the environment using plants. *Biotechnology*, 5, pp. 285-290;
- [50] Santillan-Medrano J., Jurina, J.J., (1975), The chemistry of lead and cadmium in soil: solid phase formation. *Soil Science Society of America, Proceedings.*, 39, pp.851-856;
- [51] Sauvé S., McBride M., (1998), Lead phosphate solubility in water and soil suspensions. *Environmental Science and Technology*, 32, pp. 388-393;
- [52] Scaps P., Grelle C., Descamps M., (1997), Cadmium and lead accumulation in the earthworm *Eisenia fetida* (Savigny) and its impact on cholinesterase and metabolic pathway enzyme activity, *Comparative Biochemistry and Physiology.*, 116 C, pp. 233-238;
- [53] Spurgeon D.J., Lofts S., Hankard P.K., Toal M., McLellan D., Fishwick S., Svendsen C., (2006), Effect of pH on metal speciation and resulting metal uptake and toxicity for earthworms, *Environmental Toxicology and Chemistry.*, 25, pp. 788-796;
- [54] Tanner C. C., Headley T. R., (2011), Components of floating emergent macrophyte treatment wetlands influencing removal of stormwater pollutants, *Ecological Engineering.* 37(3), pp.474-486;
- [55] Uzu, G., Sobanska, S., Aliouane, Y., Pradere, P., Dumat, C., (2009), Study of lead phytoavailability for atmospheric industrial micronic and sub-micronic particles in relation with lead speciation, *Environmental Pollution*, 157, pp. 1178–1185;
- [56] Van Gestel C.A.M., Ma W.C., (1988), Toxicity and bioaccumulation of chlorophenols in earthworms, in relation to bioavailability in soil, *Ecotoxicology and Environmental Safety.*, 15, pp. 289-297;
- [57] Van Vliet P.C.J., Van der Zee S.E.A.T.M. & Ma W.C., (2005), Heavy metal concentrations in soil and earthworms in a floodplain grassland. *Environmental Pollution.*, 138, pp. 505-516;
- [58] Venditti, D., Durécu, S., Berthelin, J., (2000), A multidisciplinary approach to assess history, environmental risks, and remediation feasibility of soils contaminated by metallurgical activities, Part A: chemical and physical properties of metals and leaching ability, *Archives of Environmental Contamination & Toxicology.*, 38, pp. 411-420;
- [59] Wen, B., Hu, X., Liu, Y., Wang, W., Feng, M., Shan, X., (2004), The role of earthworms (*Eisenia fetida*) in influencing bioavailability of heavy metals in soils, *Biology and Fertility of Soils*, 40, pp. 181–187;
- [60] Xiao, N.-W., Song, Y., Ge, F., Liu, X.-H., Ou-Yang, Z.-Y., (2006), Biomarkers responses of the earthworm *Eisenia fetida* to acetochlor exposure in OECD soil, *Chemosphere*, 65, pp.907-912;
- [61] Zeng, L.S., Liao, M., Chen, C.L., Huang, C.Y., (2006), Effects of lead contamination on soil microbial activity and rice physiological indices in soil-Pb-rice (*Oryza sativa* L.) system, *Chemosphere*, 65, pp.567-574.

EXPERIMENTAL STUDY ON THE EFFECT OF WATER QUALITY ON RAINFALL EROSION

水质对土壤降雨侵蚀影响的实验研究

As.Ph.D.Stud. Ji Hengying^{1,2)}, Prof. Ph.D. Shao Ming-an^{*3,4)}, Ph.D. Jia Xiaoxu⁴⁾

¹⁾College of Resources and Environment, Northwest A & F University, Shaanxi/China; ²⁾ College of Chemistry and Chemical Engineering, Xinjiang Normal University, Urumqi/ China; ³⁾ State Key Laboratory of Soil Erosion and Dryland Farming on the Loess Plateau, Institute of Soil and Water Conservation, Northwest A & F University, Shaanxi /China; ⁴⁾Key Laboratory of Ecosystem Network Observation and Modeling, Institute of Geographic Sciences and Natural Resources Research, Chinese Academy of Sciences, Beijing /China
Tel: +86-010-648892788; E-mail: mashao@ms.iswc.ac.cn

Keywords: simulated erosion of rainfall, erosion, infiltration rate, sodium adsorption ratio

ABSTRACT

Considering the serious soil and water losses that impede the development of agricultural production in Loess Plateau in China, this study investigated the soil water infiltration, runoff yield, and sediment yield through simulated rainfall using rainfall water of different qualities; additionally, this study investigated the influence of water quality on rainfall-induced erosion. The effects of rainfall water quality on soil erosion under artificial simulation were studied in the State Key Laboratory of Soil Erosion and Dryland Farming on the Loess Plateau from 2015 to 2016. This experiment used four rainfall water types (water, natural precipitation, natural hydrops, and tap water) and three typical loess plateau soil samples (Loessal soil, Lou soil, and laminated Lou-Sand). The effect of water quality on soil erosion under the same rainfall intensity (60mm/H) and slope (5°) was determined. Results showed that the intensity of rainfall erosion was significantly affected by water quality, and soil erosion intensity gradually decreased with increased sodium adsorption ratio and conductivity (water<natural precipitation<natural hydrops<tap water) under natural hydrops; the runoff coefficient of soil erosion was the lowest (29.3%) under natural hydrops; stable infiltration rate and rainfall erosion were the lowest under rainfall hydrops; and soil erosion was the highest under water. Moreover, the influence of water quality on rainfall erosion was affected by soil type. Compared with the Loessal soil, which contains low amount of clay particles, the erosion of rainfall to the Lou soil with higher content of clay particle was more susceptible to the water quality. Water quality plays an important role in soil erosion and exerts more significant effects on soil with higher clay content. Therefore, water quality factors must be fully considered in studying and simulating rainfall erosion.

摘要

针对中国黄土高原水土流失严重, 阻碍农业生产发展的现状, 研究不同水质的水在模拟降雨条件下的土壤入渗和产流产沙特征, 揭示水质对降雨侵蚀过程的影响。于 2015-2016 年在黄土高原土壤侵蚀与旱地农业国家重点实验室, 开展了人工模拟条件下不同降雨水质对土壤侵蚀影响的研究。本实验设计了 4 种降雨水质(去离子水、天然降水、天然积水、自来水)和 3 种典型的黄土高原土壤(黄绵土、壤土和层状壤-砂), 在相同降雨强度(60mm/h)和坡度(5°)的条件下, 水质对土壤的侵蚀状况的影响。研究表明, 降雨侵蚀的强度受水质的显著影响, 随着水中钠吸附比和电导率的增加(去离子水<天然降水<天然积水<自来水), 土壤侵蚀强度逐渐降低(天然积水下的壤土径流系数最低, 为 29.3%); 降雨积水条件下, 土壤稳定入渗率最高, 降雨侵蚀程度最低, 而去离子水对土壤的侵蚀程度最大。水质对降雨侵蚀的影响特征还受土壤类型的影响, 粘粒含量较高的壤土降雨侵蚀受水质影响比粘粒含量较低的黄绵土更加明显。因此, 水质在土壤侵蚀过程中起着重要作用, 且对粘粒含量较高的土壤作用更加明显, 在模拟降雨侵蚀研究方面需要充分考虑水质因素。

INTRODUCTION

Agricultural development in arid and semiarid areas is achieved mainly by fully utilizing natural precipitation, by reducing surface runoff, and by increasing soil moisture. Given the fragility of the ecological environment, sustainable development of modern agriculture and the possibility of obtaining high yield of existing agricultural land have become very difficult. The quality of atmospheric precipitation will exert a direct impact on soil quality and crop yield.

The Loess Plateau in China has a fragmented terrain and scarce vegetation cover; moreover, rainfall commonly occurs as heavy rain, and variation in land is lacking. Erosion resistance of Loessal soil, especially its antiscourability, is quite weak and thus is not suitable for the implementation of agricultural cultivation measures, which in turn become the common leading factors of soil erosion (Jie *et al.*, 2004). For a long time, the erosion resistance of Loessal soil not only limited the sustainable development of agriculture in this area but also became the root cause of the low income of farmers. Loess Plateau mainly consists of loose Loessal soil, which is characterized by low fertility, low content of agglomerates, and high vulnerability to rainfall erosion. This region has a heterogeneous land structure, showing a layered distribution; with intensified rainfall erosion, the fertile topsoil thickness gradually decreases, and land production efficiency has become low and unstable.

Artificial rainfall simulation effectively regulates rainfall and rapidly realizes the erosion process; this approach is widely used in soil and water conservation research (Wenyan *et al.*, 2005; Guangyan *et al.*, 2011). The results have shown that the simulated rainfall water quality exerts a significant impact on soil erosion process, and the degree of influence is significantly affected by soil type (Lili *et al.*, 2015). Lorenzo found that rainfall water quality can change the process of soil erosion, and the influence of water quality on silty clay soil is larger than that on silty loam (Borselli *et al.*, 2001). Zhang showed that the soil erosion amount increases as the sodium adsorption ratio (SAR) of irrigation water increases, whereas it gradually decreases as conductivity increases (Lijun *et al.*, 2010). Therefore, studying the impact of water quality on rainfall erosion has important theoretical and practical significance in revealing the characteristics of rainfall erosion and the choice of water quality in simulated rainfall experiment. Moreover, the present research was conducted to provide some data useful in preventing soil and water losses in Loess Plateau region and improve the utilization rate of natural precipitation and promote agricultural development.

The physical and chemical properties of aqueous solution can significantly affect soil water potential and hydraulic conductivity (Yuli Zhao and Jianzhi Niu, 2012). Studies have shown that the type and content of solute in water affects the density, surface tension, and viscosity of water, affecting the movement of water in soil pores (Caijing Zhou, 2008). At present, the effects of solute on soil hydrodynamic parameters are mostly saline material. The hydraulic conductivity of soil has been suggested to be related to the composition and content of exchangeable cations in soil solution and soluble electrolyte concentration (Carter and Robbins, 1978; De and Wierenga, 1984), and the hydraulic conductivity decreases as SAR increases; when distilled water was used to simulate rainfall, hydraulic conductivity decreases (Oster and Frenkel, 1980). Xiao studied the impact of irrigation water quality on the hydraulic properties of unsaturated soil and found that highly mineralized irrigation water could increase soil hydraulic conductivity (Zhenhua Xiao and Hongfu Wan, 1998); Feign found that increased sodium ion content of irrigation water can cause soil particle contraction and colloidal particle dispersion and expansion, thereby affecting soil permeability (Feigin *et al.*, 1991). To a certain extent, increase in soil salt concentration can promote flocculation of soil particles, increase in aggregate ability, stabilization of soil structure, increase in soil macropores, and enhancement of permeability. Therefore, water quality is quite important in soil moisture movement and soil structure. However, studies on rainfall erosion have devoted little attention on the impact of water quality. Investigations on soil erosion will not only help to improve the existing theory on soil erosion but will also provide an important basis for accurate prediction of soil erosion under different rainfall conditions.

Loess Plateau is characterized by loose soil, sparse vegetation, serious erosion, and fragile ecology. Soil erosion has long been a core problem that constrains ecological civilization construction and regional sustainable development in Loess Plateau. Discussing the influence of water quality on rainfall erosion process is of great significance in understanding the process, intensity, and model prediction of soil erosion in this area, and it is a kind of sustainable circular agriculture with very important ecological protection significance. In Loess Plateau, a large number of artificial simulated rainfall experiments were conducted, and the water used for the simulated rainfall was mostly tap water or well water. Given that water quality in different places obviously varies, the effects of water qualities on rainfall erosion will also vary in artificial simulated rainfall experiments. In this study, where Loessal soil and Lou soil were used as research objects, artificial simulated rainfall experiments were conducted using deionized water, tap water, natural precipitation, and natural hydrops, and the influence of water quality on slope runoff and sediment yield and soil water infiltration was analysed to reveal the influence of water quality on rainfall erosion, providing a scientific basis for accurate prediction of soil erosion process.

MATERIAL AND METHODS

Rainfall simulator

A simulated rainfall experiment was conducted in the Hall of Artificial Simulated Rainfall in the State Key Laboratory of Soil Erosion and Dryland Farming of Loess Plateau, Northwest A & F University, China from 2015 to 2016. Disturbed soils were studied, and homogenous Lou soil, Loessal soil, and Lou-sand laminated soil were used as samples. Loessal soil was collected from Ansai County of Shaanxi Province (109°19'46"N, 36°51'44"E); Lou soil was collected from Yangling Demonstration Zone of Shaanxi Province (108°5'40"N, 34°16'20"E); and river sand was collected from the riverbed of Weihe, Yangling (108°4'39"N, 34°14'9"E). Table 1 shows the physical and chemical properties of the soil samples. The soil samples were air-dried, pressed, crushed, screened through 5 mm sifter, and mixed for subsequent use. Bulk density was controlled based on the bulk density of the undisturbed soils (Sandy soil, Lou soil, and Loessal soil). For the air-dried soils, the required soil quality for each processing was calculated according to the volumetric moisture content (approximately 2%) and soil bulk density for layered filling. Special plate was used to blur the layer to prevent vertical layering of soil.

Table 1

Physical and chemical properties of soil samples

Particle sizes [mm]	Particle composition /%			Texture	Dry bulk density [g/cm ³]	Ks [mm/min]
	Non-mulching					
	0-0.002	0.002-0.05	0.05-1.00			
Homogenous Lou soil	22.8	68.5	8.7	silty loam	1.4	0.020
Sand soil	4.49	20.87	75.64	medium sand soil	1.8	2.791
Loessal soil	9.10	61.80	29.10	silt loam soil	1.2	0.577

Materials and experimental design

Experiments were performed using a fully saturated design. Three types of soil exist: Lou soil (L), Loessal soil (Lo), Lou soil (L)-Sandy soil (S); four types of rainfall water exist: water (C), natural precipitation (R), natural hydrops (J), and tap water (Z). After different combinations of soil types and rainfall water quality were made, 12 treatments were designed, and each treatment was performed three times. The experiment involved the use of water supply device, rainfall simulator, and soil bin (Figs.1 and Figs.2). The rainfall simulator was a movable needle-type sealed box with a height of $H_2=40\text{cm}$, a length of $L_1=145\text{cm}$, a width of $W_1=145\text{cm}$, and a needle spacing of $D=2\text{ cm}$. The average diameter of the raindrops is $d = 2.97 \pm 0.05\text{ mm}$, the rainfall height is $H_1=220\text{ cm}$ and the rainfall uniformity was greater than 94%. Rain intensity was controlled by a peristaltic vacuum pump. An erosion soil bin (100 cm × 40 cm × 30 cm) was self-manufactured. Evenly distributed holes were created at the bottom of the soil bin to exclude gravity water. The rainfall intensity was 60 mm/h, and the soil bin slope was set as 5°, which was quite common in Loess Plateau, and the duration of rainfall was 60 min.

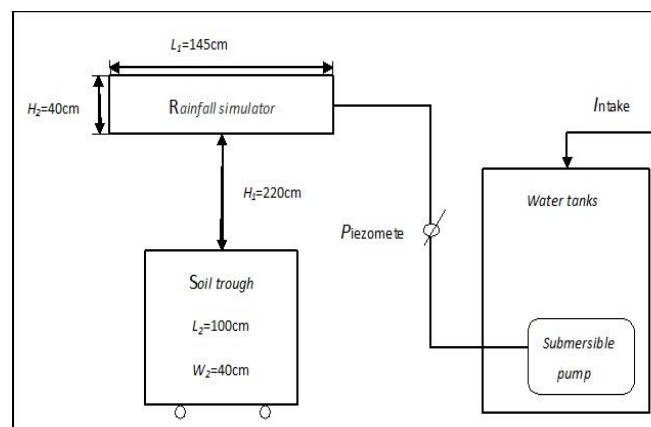


Fig. 1 - Schematic of artificial simulated rainfall device



Fig. 2 - Artificial simulated rainfall device

During rainfall, runoff and sediment samples were collected every 3 min from the time when the flow yield was observed on the slope. After the rainfall was finished, the runoff collected was measured, the sediment was separated, and the amount of sediment was measured by using the drying method. The infiltration rate was calculated as follows equation (1) (Yuanjun Zhu and Ming-an Shao, 2006):

$$i = R \cos \theta - \frac{F - A}{K \cdot A \cdot T} \quad [\text{cm/min}] \quad (1)$$

where:

i is the infiltration rate, [cm/min]; R is the rainfall [cm]; T is the duration of rainfall [min]; θ is the slope of soil bin [°]; F is the flow yield within the interval [g/min]; S is the sediment yield within the interval [g/min]; K is the conversion ratio [1g/cm³]; A is the cross sectional area of soil bin [cm²].

Prior to the rainfall test, three rain gauges were placed in the areas where the soil bins were located. Calibration was performed after the rainfall intensity stabilized. The mean was determined and taken as the rainfall intensity. The formula was as in the following equation (2) (Qianhua et al., 2015):

$$P = \frac{P_1 + P_2 + P_3}{3 \times T} \quad [\text{mm/min}] \quad (2)$$

where:

P is the average rainfall intensity [mm/min]; T is the rainfall duration [min].

The water types used in the artificial simulated rainfall include water, tap water, natural precipitation, and rainfall hydrops. The water was produced by the Institute of Soil and Water Conservation, CAS&MWR; compounds and ions were not detected. The tap water was collected from the residents of Yangling District, Shaanxi; natural precipitation was collected from natural rainfall in Yangling, Shaanxi. Rainfall hydrops was a natural precipitation that has been stored for more than one year. Table 2 shows the SAR, pH value, and conductivity of the four water types.

Table 2

Physical and chemical properties of different types of rainfall water

Type of water quality	sodium adsorption ratio [m•Mol/L]	pH	conductivity [μS/cm]
Water[D]	0.00	7.04	3
Natural precipitation[P]	0.03	7.76	36
Natural hydrops[H]	1.47	7.97	452
Tap water[T]	2.24	7.78	634

Data analysis

SPSS software was used for correlation analysis, and Excel and Origin were used for correlation calculation and chart drawing.

RESULTS

Changes in soil flow yield and runoff coefficient

Flow yield time and runoff coefficient are important indexes that characterize soil water infiltration; these indexes are affected by factors such as soil type, rainfall intensity, and slope (*Zhixin Xu and Mengli Zhao, 2001*). Initially, rainfall completely infiltrates into the soil, and no runoff yield is observed in the slope. When the rainfall intensity is greater than the infiltration capability of the soil, the excess rainfall will cause slope runoff. The initial flow yield time is the main factor affecting the runoff process and the degree of rainfall (*Tianxu et al., 2011*).

Table 3 shows the flow yield time and runoff coefficient in different soils as a function of water quality. We could see that:

Table 3

Flow yield time of soils under different water qualities

Water quality	Flow yield time, s			Runoff coefficient, α		
	Lou soil	Loessal soil	Lou soil-sandy soil	Lou soil	Loessal soil	Lou soil-sandy soil
Water [D]	240.0	1800.0	180.0	0.618	0.264	0.683
Natural precipitation [P]	480.0	1560.0	360.0	0.458	0.297	0.502
Natural hydrops [H]	978.0	1320.0	840.0	0.293	0.299	0.378
Tap water [T]	540.0	1620.0	360.0	0.440	0.287	0.498

For the homogenous Lou soil and Lou soil-sandy soil (Top Lou soil layer and bottom Sand layer), as SAR and conductivity of rainfall water increased, the flow yield time was postponed and the duration of natural hydrops was extended. Moreover, as soil and water erosions and conductivity of rainfall increased, the flow yield time started to decrease, indicating that SAR and conductivity of rainfall water showed the highest threshold values. This result suggested that water quality could reduce the intensity of rainfall-induced soil and water erosions. The flow yield time of Loessal soil was longer than that of Lou soil because the infiltration capability of the Loessal soil was stronger than that of Lou soil, and it was characterized by loose particles and strong water absorption capacity. For the Loessal soil, as the SAR of rainfall, the flow yield time decreased and the natural hydrops showed the shortest duration. Moreover, as the SAR of rainfall increases, the flow yield time decreased once again; this pattern was opposite that of the variations in Lou soil and Lou soil-sandy soil. The infiltration rate was related to the physical properties of soil, as follows: (1) Soil texture. The structure and texture of soil were not uniform, facilitating blockade of water. Therefore, the infiltration capability of Lou soil-sandy soil was weaker than that of Lou soil. (2) Bulk density of soil. Previous results showed that the higher the bulk density, the lower the infiltration rate (*Jiangsu Wen, 2012*) and the shorter the flow yield time. The increasing flow yield times were as follows: Lou soil-sandy soil < homogenous Lou soil < Loessal soil. The slope runoff was calculated using the water balance method, that is, runoff was the difference between rainfall amount and infiltration amount. Therefore, the slope runoff was closely related to soil water infiltration rate. If the infiltration rate was large, the runoff amount was small. If the soil pores of Loessal soil were large, the flow yield time was long, and the runoff generation time would be postponed. Therefore, the runoff coefficient would be low. The soil water infiltration rates of Lou soil and Lou soil-sandy soil were low, the bulk densities were large, the flow yield times were short, and the runoff coefficients were large. Additionally, due to the laminated structure of Lou soil-sand soil, the sandy soil of lower layer blocks the water (*Wenyan et al., 1995; Wenyan et al., 2005*). As a result, the permeability of the soil to water was considerably small, the runoff increased, and the runoff coefficient was the greatest. From the perspective of rainfall water quality, the runoff coefficient of natural hydrops was the lowest, whereas that of the deionized water was the highest. The type of rainfall water displaying the appropriate SAR and conductivity can relatively relieve the erosion effect of soil with high viscosity.

Influence of water quality on soil water infiltration

Infiltration rate is the amount of water that infiltrated the soil within a given time, reflecting the infiltration capability of soil. Generally, for the three soil types under any rainfall water quality, soil water

infiltration rates decreased as time was shortened (Fig.3). The results of the independent sample T examination showed that for Lou soil and Lou soil-sandy soil, the soil water infiltration rate of the deionized water was significantly lower than that of the three other rainfall water types ($p < 0.05$), and the rainfall hydrops showed the highest soil water infiltration rate. The soil water infiltration rate of tap water and natural precipitation did not significantly differ ($p > 0.05$). Different from Lou soil, under four water qualities, the Loessial soil didn't display significant difference in terms of soil water infiltration rate ($p > 0.05$). The soil water infiltration rates of the four water types were quite close for the first 30 min after infiltration. Therefore, the influence of water quality on soil water infiltration rate depends on soil type.

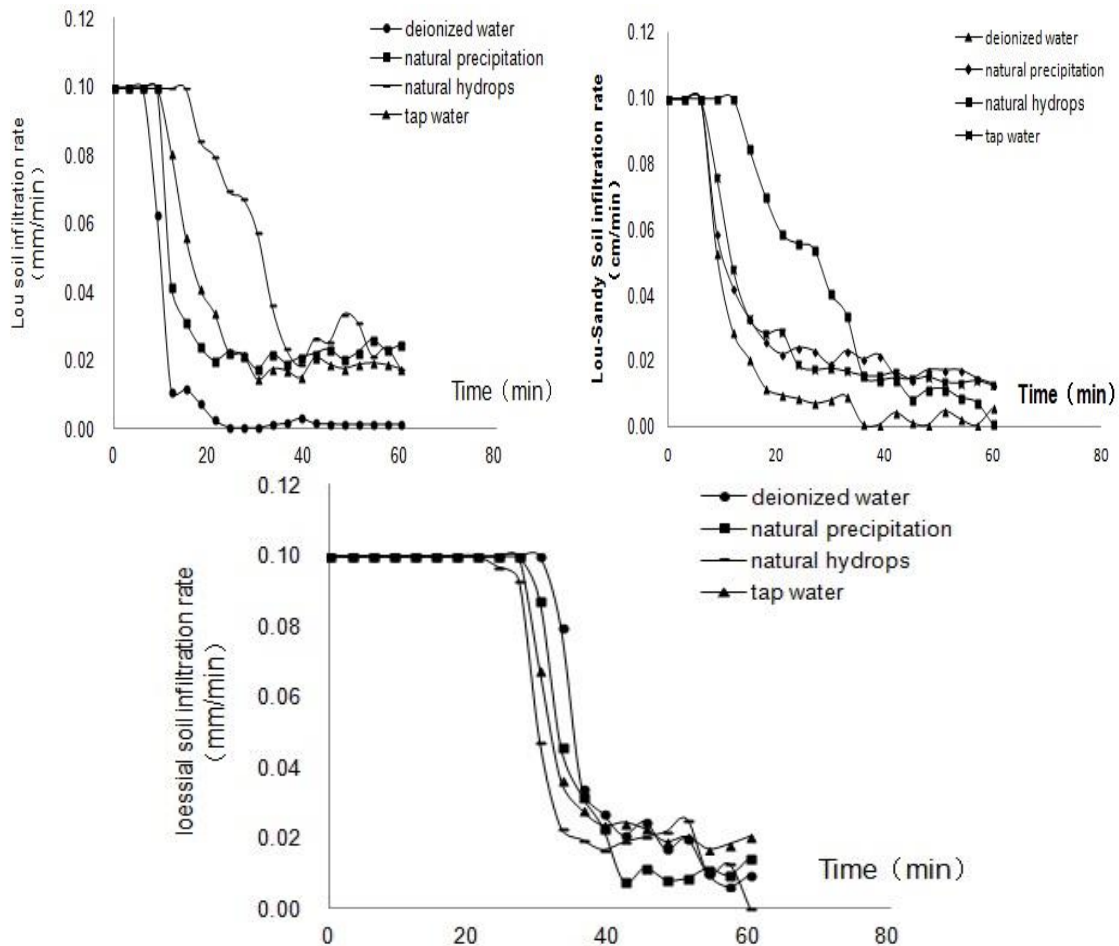


Fig. 3 - Changes in soil water infiltration rate of artificial simulated rainfall

Water quality matters only for heavy clay soil; thus, for Lou soil and Lou soil-sandy soil, the soil water infiltration rate was higher under the natural hydrops than that under the four other rainfall water types. The decreasing infiltration rate of the different water types was as follows: natural precipitation > tap water > natural precipitation > deionized water. With the SAR and conductivity of rainfall, the infiltration rate of soil increased while the soil erosion decreased. However, the rate of soil erosion was the lowest under natural hydrops. As the SAR increased, the soil water infiltration rate decreased, whereas the erosion worsened, indicating that the SAR and conductivity had a range of threshold values. The SAR of deionized water was 0; thus, when deionized water infiltrated into the soil, no spectrometer exchange occurred. By contrast, the sodium ions would be dissolved, which changed the flocculation of clay particle and promoted the dispersion. As a result, soil pores were blocked, and soil water infiltration rate decreased. Figure showed that in terms of SAR, an inflection point was observed under the effect of natural hydrops. The tap water showed the highest SAR, and the infiltration rate of tap water was lower than that of natural hydrops. Therefore, the SAR of rainfall water that promotes soil water infiltration was confined within a certain range.

Flocculation of soil clay particle and the stability of soil aggregates are determined by the composition of ion concentration of soil solution, which further determine the conductive capability and infiltration rate in soil and the difficulty of runoff generation on earth's surface (Fahu Li and Guojing Rong, 2004). The different water qualities of artificial simulated rainfall will lead to the different electrolyte

concentrations and conductivities. The increase in electrolyte concentration in soil solution will promote the formation and development of soil crust, and the increase in conductivity of soil solution will inhibit the formation of soil crust, which will further affect the runoff and sediment yield during rainfall erosion. Hydration will occur if rainfall water of different qualities acts on the soil. The base cations will cause the soil to swell and explode. The aggregates are damaged, and the particles are dispersed, blocking the pores. As a result, the hydraulic conductivity or infiltration rate of soil decreases. In this study, the clay particle content of Lou soil (22.8%) was higher than that of Loessal soil (9.1%). The influence of water quality on the infiltration rate of Lou soil is higher than that on the infiltration rate of Loessal soil, consistent with the results of Ben-Hur et al. (Ben-Hur et al., 1985).

Influence of water quality on flow and sediment yields

Fig.4 showed the runoff and sediment yield caused by erosion of Lou soil, Loessal soil, and laminated soil under the four types of rainfall water. During erosion, natural hydrops showed the lowest runoff and sediment yield, whereas the water showed the highest runoff and sediment yield (Fig.4). In the two-layered structure of Lou soil and laminated Lou soil-sandy soil, the decreasing erosion capabilities of rainfall water types were as follows: water > natural precipitation > tap water and natural hydrops. Therefore, in the artificial simulated rainfall experiment, the water quality greatly influenced the test results and thus was a factor that cannot be ignored. Moreover, a proper increase in SAR of rainfall water with different qualities (contents of sodium, magnesium, and calcium ions in aqueous solution) can prevent slope erosion. These ions will prevent slope erosion to some extent.

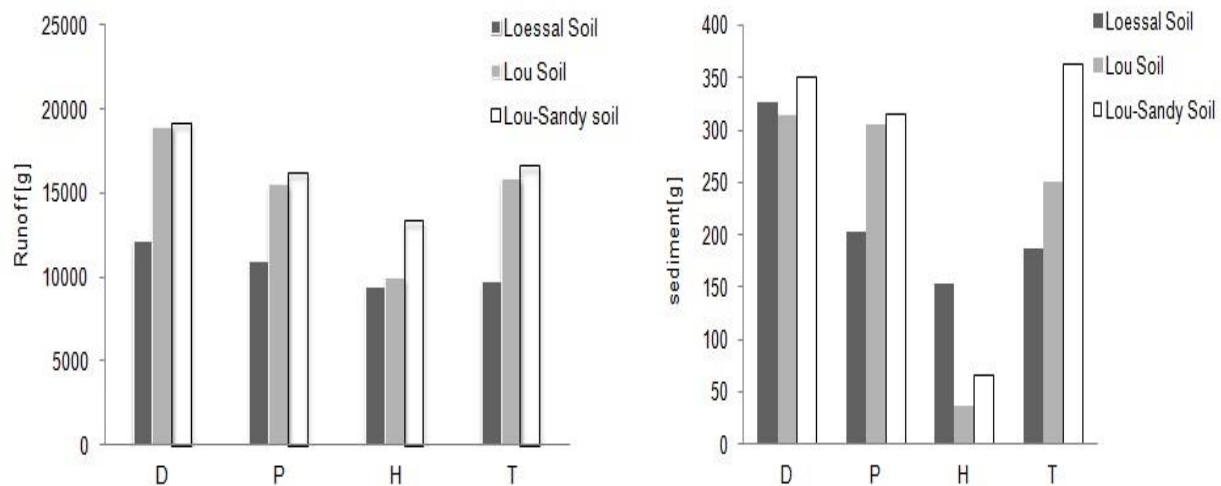


Fig. 4- Changes in rainfall runoff and sediment yield under different types of rainfall water.

Application of Philip infiltration model in rainfall infiltration process by using different SARs

The influence of SAR on the characteristics of soil water infiltration is simulated using a Philip infiltration model, and the infiltration of rainfall water types with different SAR changes with time. The Philip model assumes that at any moment of infiltration, the infiltration rate displays the relationship of power series with time, and the specific infiltration model was as follows equation (3) (Zhongdong Wu and Quanjiu Wang, 2008):

$$I(t) = S t^{0.5} + A \quad [\text{cm}] \quad (3)$$

Where:

I is the accumulated infiltration amount [cm]; S is the infiltration rate [$\text{cm}/\text{min}^{0.5}$]; A is the stable infiltration rate [cm/min]; and t is the infiltration time of rainfall [min].

In equation (3), the relationship between accumulated infiltration amount and was expressed as a quadratic equation (the intercept is 0). After being fitted, the coefficients of the quadratic term were the stable infiltration rate A . The coefficient of one degree term was the infiltration rate S . Moreover, because $A = i(\infty)$, during rapid infiltration, it could be considered as $A = 0$ ($A = i(\infty)$). The fitted equation was the straight line passing through the origin, and its slope was the soil infiltration rate S .

Table 4

Physical and chemical properties of different types of rainfall water

Type of water quality	Type of water quality	Water	Natural precipitation	Natural hydrops	Tap water
Homogenous Lou soil	S	0.277	0.302	0.338	0.329
	R^2	0.988	0.955	0.971	0.978
	Fitting equation (I)	$0.277t^{0.5}$	$0.302 t^{0.5}$	$0.338 t^{0.5}$	$0.329 t^{0.5}$
Lou soil-sandy soil	S	0.257	0.301	0.391	0.292
	R^2	0.995	0.980	0.954	0.990
	Fitting equation (I)	$0.257 t^{0.5}$	$0.301 t^{0.5}$	$0.391 t^{0.5}$	$0.292 t^{0.5}$

Note: R^2 -Pearson product-moment correlation coefficient

The water quality did not significantly influence the Loessal soil. Therefore, the Philip infiltration model was used to simulate the Lou soil and Lou soil-sandy soil. Table 4 showed that the sequence of infiltration rate (as determined using the Philip model) for the homogenous soil and the Lou soil-sandy soil with similar initial moisture content under the one-dimensional rainfall infiltration was as follows: natural hydrops → tap water → natural precipitation → water. Comparison of the result of the Philip model with the observation results suggested that when SAR was relatively low, (its SAR was smaller than that of natural hydrops), the results of the Philip infiltration model is similar to the experimental results; when the SAR was relatively high (its SAR was smaller than that of natural hydrops), and the experimental demonstrated that as SAR increases, the infiltration rate of soil reached the highest when the SAR was the one of natural hydrops. As the SAR increased, the infiltration rate decreased. Therefore, when SAR was relatively low (its SAR was smaller than that of natural precipitation), the results of the Philip infiltration model was opposite to the experimental results. This finding indicated that when the Philip infiltration model was applied to study the infiltration rates of rainfall waters of different qualities, the calculation results would be more accurate for the rainfall water type with low SAR. For the water quality with a relatively high SAR, the calculation results showed certain deviations, consistent with the results of Zhongdong Wu, although the specific mechanism remains to be studied.

CONCLUSIONS

Artificial simulated rainfall experiment was conducted to study the influence of the quality of four types of rainfall water (water, tap water, natural precipitation, and natural hydrops) on soil water infiltration and soil erosion under the same rainfall intensity and slope, as well as determine the influence of the water quality of rainfall and farmland irrigation on soil quality. In this study, Loessal soil and Lou soil were used as soil samples. The following conclusions were drawn.

(1) Water quality significantly influenced the infiltration rate in Lou soil and Lou soil-sandy soil. Water showed the lowest soil water infiltration rate, which was significantly different from that of tap water, natural precipitation, and rainfall hydrops, whose soil water infiltration rates did not significantly vary. Water quality did not significantly influence the rainfall infiltration rate. Therefore, the influence of water quality on soil water infiltration rate depended on soil type. The low infiltration rate worsened the soil condition, promoted water erosion, and reduced soil quality, affecting soil productivity.

(2) Water quality significantly influenced the characteristics of erosion runoff and sediment yield. As the salt concentration of rainfall water increased, the erosion intensity of the soil gradually decreased. The influence of water quality was considerably more significant in Lou soil with relatively high clay particle contents; in Loessal soil, as salt concentration of rainfall water increased, the degree of soil erosion gradually decreased, indicating that the influence of transportation process of eroded sediment was made more complicated by water quality relative to the influence of the runoff process. For this reason, the influence of water quality on the erosion intensity varied depending on the soil type.

(3) When the Philip model was adopted in simulating the infiltration of rainfall water of different qualities, relatively accurate calculation results for the rainfall water with relatively low SAR were obtained. For the aqueous solution with relatively high SAR, the results obtained using the Philip model displayed a

certain degree of deviation. That is, the SAR of rainfall water had certain range of threshold value. In this experiment, rainfall erosion was lowest when the SAR equals the SAR of natural hydrops.

Studies on water quality are conducted in irrigated farmland. In this work, the problem on water quality was incorporated in the rainfall experiment to study the influence of water quality on soil erosion process. Meanwhile, it is combined with the laminated soil structure, providing a new theoretical basis for soil infiltration mechanism. Given that the water containing different solutes enters into the soil, the solute content of soil solution will change, and the soil solute will undergo chemical and physical processes during movement of solution on the earth's surface and underground. A complex material migration system is formed due to multiple factors and the interactions of these factors. A more comprehensive analysis of the quantitative relationship between soil erosion and migration of soil is necessary, and a mathematical model of soil erosion must be established to provide scientific basis for agricultural production and disaster prevention and control.

ACKNOWLEDGEMENT

This research project was funded by the Nation Science Foundation Project (41530854) of China.

REFERENCES

- [1] Ben-Hur M., Shainberg I., Bakker D., et al., (1985), Effect of soil texture and CaCO_3 content on water infiltration in crusted soil as related to water salinity, *Irrigation Science*, Springer-Verlag/Germany, Vol. 6, Issue 4, pp. 281-294;
- [2] Borselli L, Torri D, Poesen J, et al., (2001), Impact of rainwater quality on infiltration, runoff and interrill erosion processes *Earth Surface Processes & Landforms*, Hoboken/USA, Vol.26, Issue3, pp.329-342;
- [3] Caijing Zhou, (2008), Effect of irrigation water quality on soil hydraulic and physical properties. MSc dissertation, *Northwest Agriculture & Forestry University*, Shaanxi/China;
- [4] Carter D L, Robbins C W, (1978), Salt outflows from new and old irrigated lands1. *Soil Science Society of America Journal*, Madison/USA, Vol. 42, Issue 4, pp.623-627;
- [5] De S F, Wierenga P J, (1984), Solute transfer through columns of glass beads, *Water Resources Research*, Hoboken/USA, Vol.20, Issue 2, pp. 225-232;
- [6] Feigin A, Ravina I, Shalhevet J, (1991), Effect of Irrigation with Treated Sewage Effluent on Soil, Plant and Environment, *Irrigation with Treated Sewage Effluent*, Berlin Heidelberg/Germany Springer Publishing House, Issue 17, pp.34-116;
- [7] Fahu Li, Jingrong Guo, (2004), Research status and future development of effects of chemical factors on soil water erosion, *Transactions of the Chinese Society of Agricultural Engineering*, Beijing/China, Vol. 20, Issue 5, pp.32-37;
- [8] Guangyan Wu, Zhenhua Zhu, Qian Cheng, et al., (2011), Runoff and sediment characteristics of slope under simulated rainfall, *Water Saving Irrigation*, Beijing /China, Issue 6, pp.44-47;
- [9] Jiangsu Wen, (2012), Experimental Study on Different Soil Bulk Density Affecting Soil Erosion under Simulated Rainfall Conditions, MSc dissertation, *Jiangxi Agricultural University*, Jiangxi/China;
- [10] Jie Gong, Liding Chen, Bojie Fu, et al., (2004), Effects of land use and vegetation restoration on soil quality in a small catchment of the loess plateau, *Chinese Journal of Applied Ecology*, Beijing/China, Vol.15, Issue 12, pp.2292-2296;
- [11] Jie Wang, Shaowei Hu, Yue Zhou, (2005), Analysis of properties and problems about artificial rainfall simulation tests, *Research of Soil and Water Conservation*, Shaanxi/China, Vol.12, Issue 4, pp.188-190,194;
- [12] Lijun Zhang, Fahu Li, Liguang Wan, (2010), Effect of brackish water quality and slopes on soil erosion in furrow irrigation, *Water Saving Irrigation*, Beijing /China, Issue 4, pp.26-28,34;
- [13] Lili Luan, Guanghui Zhang, Ruxin Liu, et al., (2015), Effects of water quality on soil infiltration in rainfall simulation, *Journal of soil and water conservation*, Shaanxi/China, Vol.26 Issue 2, pp.122-127;
- [14] Qianhua Shi, Wenlong Wang, Mingming Guo, et al., (2015), Runoff and sediment yielding processes on red soil engineering accumulation containing gravels by a simulated rainfall experiment, *Chinese Journal of Applied Ecology*, Beijing /China, Vol.26, Issue 9, pp.2673-2680;
- [15] Oster J D, Frenkel H., (1980), The chemistry of the reclamation of sodic soils with gypsum and lime, *Journal of the Soil Science Society of America*, Madison / USA, Vol.44, Issue 1, pp. 41-45;

- [16] Tianxu Mao, Yuanjun Zhu, Ming-an Shao, (2011), Characteristics of runoff and infiltration in stony soils under simulated rainfall conditions, *Chinese Journal of Soil Science*, Shenyang/China, Issue 5, pp.1214-1218;
- [17] Wenyan Wang, Jianfeng Zhang, Zhirong Wang, et al., (1995), Experiment and study on water-tightness and infiltration reduction of sand layer in loess soils, *Transactions of the Chinese Society of Agricultural Engineering*, Beijing /China, Vol.11, Issue 1, pp.104-110;
- [18] Wenyan Wang, Jianfeng Zhang, Zhirong Wang, et al., (2005), Infiltration reduction effect of sand layer in loess, *Journal of Hydraulic Engineering*, Beijing /China, Vol.36, Issue 6, pp. 0650-0655;
- [19] Yuanjun Zhu, Ming-an Shao, (2006), Processes of rainfall infiltration and sediment yield in soils containing different rock fragment contents, *Transactions of the Chinese Society of Agricultural Engineering*, Beijing/China ,Vol.22, Issue 2, pp. 64-67;
- [20] Yuli Zhao, Jianzhi Niu, (2012), Analysis of properties and problems about artificial rainfall simulation tests, *Research of Soil & Water Conservation*, Shaanxi/China, Vol.19, Issue 4, pp.278-284;
- [21] Zhenhua Xiao, Hongfu Wan, (1998), Effect of irrigation water quality on soil hydraulic and physical properties, *Acta Pedologica Sinica*, Beijing/China, Vol.35, Issue 3, pp.359-366;
- [22] Zhixin Xu, Mengli Zhao, (2001), Influence of overgrazing on soil erosion of grassland, *Grassland of China*, Beijing/China, Vol.23, Issue6, pp.59-63;
- [23] Zhongdong Wu, Quanjiu Wang, (2008), Study on impact of sodium adsorption ratio of saline water on soil physical and chemical properties and infiltration characteristics, *Agricultural Research in the Arid Areas*, Shaanxi/China, Vol.26, Issue 1, pp.231-236.

WRITING NORMS

Article Types

Three types of manuscripts may be submitted:

1. **Regular articles:** These should describe new and carefully confirmed findings, and experimental procedures should be given in sufficient detail for others to verify the work. The length of a full paper should be the minimum required to describe and interpret the work clearly (max.10 pages, **even number**);
2. **Short Communications:** A Short Communication is suitable for recording the results of complete small investigations or giving details of new models or hypotheses, innovative methods, techniques or apparatus. The style of main sections has not necessarily to be in accordance with that of full-length papers (max. 6 pages, **even number**);
3. **Reviews:** Submissions of reviews and perspectives covering topics of current interest are welcome and encouraged (max.10 pages, **even number**).

Manuscripts should be written in English (American or British usage is accepted, but not a mixture of these) and submitted **electronically** at the following e-mail addresses: inmatehjournal@gmail.com

Please be sure to include your full affiliation and e-mail address (see Sample manuscript)

The authors are responsible for the accuracy of the whole paper and references.

There are allowed 2 papers by each first author.

The text layout should be in single-column format. To avoid unnecessary errors it is strongly advised to use the “spell-check” and “grammar check” functions of your word processor.

Review Process

All manuscripts are reviewed by 2 members of the Scientifically Review Office. Decisions will be made as rapidly as possible and the journal strives to return reviewers' comments to authors in approx.3 weeks.

The editorial board will re-review manuscripts that are accepted pending revision.

NOTE:

Submission of a manuscript implies: that the work described has not been published before (excepting as an abstract or as part of a published lecture or thesis) that it is not under consideration for publication elsewhere.

1. REGULAR ARTICLES

- Manuscripts should be concise, in **1.15 line spacing**, and should have 2 cm all over margins. The font should be **Arial 10 pt**. Ensure that each new paragraph is clearly indicated, using **TAB at 1 cm**.
- Title will be **Arial 12 pt** and explicit figures will be **Arial 9 pt**.
- Text will be written in English.
- Chapters' titles are written by **Arial 10 pt, Bold, Uppercase** (e.g. **INTRODUCTION, MATERIAL AND METHODS**), between chapters is left a space for 10 pt. At the beginning of each paragraph, TAB of 1 cm.
- The paper body will be written in **Arial 10 pt., Justify alignment**.

TITLE **Arial 12 pt., Uppercase, Bold, Center (in English language)** and **Bold Italic (in native language)**.

Should be a brief phrase describing the contents of the paper. Avoid long titles; a running title of no more than 100 characters is encouraged (without spaces).

AUTHORS **ARIAL 9, Bold, Centre alignment**

Under the paper's title, after a space (enter) 9 pt., write **authors' names** and **affiliations (Arial 8 pt.-Regular)**

When the paper has more than one author, their name will be followed by a mark (Arabic numeral) as superscript if their affiliation is different.

Corresponding author's name (next row), (**Arial 8 pt.**). Should be added also: phone, fax and e-mail information, for the paper corresponding author (**font: 8 pt., Italic**).

KEYWORDS (**In English**) about 4 to 10 words that will provide indexing references should be listed (**title: Arial 10pt, bold italic, text Arial 10 pt., italic**).

A list of non-standard Abbreviations should be added. In general, non-standard abbreviations should be used only when the full term is very long and used often. Each abbreviation should be spelled out and introduced in parentheses the first time it is used in the text. Standard abbreviations (such as ATP and DNA) need not to be defined.

ABSTRACT (in English and Native language, Arial 10 pt.), the title *bold*; the text of abstract: *italic*) should be informative and completely self-explanatory, briefly present the topic, state the scope of the experiments, indicate significant data, and point out major findings and conclusions. The Abstract should be max.250 words. Complete sentences, active verbs, and the third person should be used, and the abstract should be written in the past tense. Standard nomenclature should be used and abbreviations should be avoided. No literature should be cited.

INTRODUCTION (Arial 10 pt.) should provide a clear statement of the problem, the relevant literature on the subject, and the proposed approach or solution. It should be understandable to colleagues from a broad range of scientific subjects. We should refer to the current stage of researches performed in the field of the paper to be published, by quoting up-to-date specialty studies, preferably published after 2006, excepting certain referential specialty books/studies, especially papers issued in magazines/journals/conferences/ISI quoted symposia or in other international data bases, which are well known and available.

MATERIALS AND METHODS (Arial 10 pt.) should be complete enough to allow experiments to be reproduced. However, only truly new procedures should be described in detail; previously published procedures should be cited, and important modifications of published procedures should be mentioned briefly. Methods in general use need not be described in detail.

RESULTS (Arial 10 pt.) should be clearly presented. The results should be written in the past tense when describing findings in the authors' experiments. Results should be explained, but largely, without referring to the literature. Discussion, speculation and detailed interpretation of data should not be included in the Results, but should be put into the Conclusions section.

CONCLUSIONS (Arial 10 pt.) The main conclusions drawn from results should be presented in a short Conclusions section. Do not include citations in this section.

Formulae, symbols and abbreviations: Formulae will be typeset in Italics (preferable with the Equation Editor of Microsoft Office 2003) and should be written or marked as such in the manuscript, unless they require a different styling. They should be referred to in the text as Equation (4) or e.g. (4). The formulae should be numbered on the right side, between brackets (Arial 10 pt.):

$$P = F \cdot v \quad (1)$$

Terms of the equation and the unit measure should be explained, e.g.

P is the power, [W];

F – force, [N];

v – speed, [m/s]

SI units must be used throughout.

Tables should be self-explanatory without reference to the text. The details of the methods used in the experiments should preferably be described in the legend instead of in the text. [The same data should not be presented both in table and graph form or repeated in the text.](#)

Table's title will be typed **Arial 9 pt, Bold, Centered**

In the table, each row will be written Arial 9 pt, single-spaced throughout, including headings and footnotes.

The table should be numbered on the right side, between brackets (Arial 10 pt):

Figure (Arial 9 pt., Bold, Center) should be typed in numerical order (Arabic numerals). Graphics should be high resolution (e.g.JPEG). Figure number is followed by what represent the figure or graph e.g.:

Fig.1 – Test stand

Legend: Arial 8 pt, Italic, Center, e.g.

1 - plansifter compartments; 2- break rolls; 3 – semolina machines; 4 – reduction rolls; 5 – flour

ACKNOWLEDGMENTS (Arial 10 pt.) of people, grants, funds etc should be brief (if necessarily).

REFERENCES (Arial 10 pt.)

(in alphabetical order, in English and in the original publication language).

Minimum 10 references, last 10 years, minimum 3 references from the last 2 years

It can be used “References” tool from the *Word Editor*.

References should be cited in the text in brackets as in the following examples:

(Babicu P., Scripnic V., 2000)

All references must be provided in English with a specification of original language in round brackets.

Authors are fully responsible for the accuracy of the references.

References should be alphabetically, with complete details, as follows:

Examples:

Books: Names and initials of authors, year (between brackets), title of the book (Italic), volume number, publisher, place, pages number or chapter, ISSN/ISBN:

[1] Vlăduț V., (2009), *Study of threshing process in axial flow apparatus (Studiul procesului de treier la aparatele cu flux axial)*, vol.1, "Terra Nostra" Publishing House, Iași/Romania;

Journal Article: Names and initials of authors, year (between brackets), full title of the paper, full name of the journal (Italic), volume number, publisher, place, page numbers:

[1] Lizhi Wu, Yan Di., (2005), *Demonstrational study on the land consolidation and rehabilitation (LCR) project of saline-alkali soil in arid areas: a case study of Lubotan LCR project in Pucheng County, Shaanxi Province (干旱区盐碱化土地整理工程实证研究-以陕西蒲城县卤泊滩土地整理项目为例)*, *Transactions of the Chinese Society of Agricultural Engineering*, vol.21, no.1, Madison/Wisconsin, pp.179-182;

[2] Leonov I.P., (1973), *Basic machine theory for tobacco stringing. Post-harvest care of tobacco and rustic tobacco (Основы теории машин для закрепления табака на шнуры. Послеуборочная обработка табака и махорки)*, *Collection of scientific articles (сборник научно-исследовательских работ)*, pp.37-45;

Conference or Symposium: Names and initials of authors, year (between brackets), full title of the paper (Regular), full name of the conference/symposium (Italic), volume number, publisher, place, page numbers

[1] Bungescu S., Stahl W., Biriș S., Vlăduț V., Imbrea F., Petroman C., (2009), *Cosmos program used for the strength calculus of the nozzles from the sprayers (Program Cosmos folosit pentru calculul de rezistență la zgomot al aparatelor de distribuție)*, *Proceedings of the 35 International Symposium on Agricultural Engineering "Actual Tasks on Agricultural Engineering"*, Opatija / Croatia, pp.177-184;

Dissertation / Thesis: Names and initials of authors, year (between brackets), full name of the thesis (Italic), specification (PhD Thesis, MSc Thesis), institution, place;

[1] Popa L., (2004), *Research on the influence of structural and functional parameters of the braking system on the braking performance of agricultural trailers (Cercetări privind influența caracteristicilor constructive și funcționale ale sistemelor de frânare asupra performanțelor de frânare ale remorcilor agricole)*, PhD dissertation, Transylvania University of Brașov, Brașov / Romania.

Patents: Names and initials of authors, year (between brackets), patent title (Italic), patent number, country:

[1] Grant P., (1989), *Device for Elementary Analyses*. Patent, No.123456, USA.

Legal regulations and laws, organizations: Abbreviated name, year (between brackets), full name of the referred text, document title/type (Italic), author, place:

[1] *** EC Directive, (2000), *Directive 2000/76/EC of the European Parliament and of the Council of 4 December 2000, on the incineration of waste, Annex V, Official Journal of the European Communities, L332/91, 28.12.2000, Brussels.*

Web references: The full URL should be given in text as a citation, if no other data are known. If the authors, year, and title of the documents are known and the reference is taken from a website, the URL address has to be mentioned after these data:

The title of the book, journal and conference must be written in Italic, the title of the article, chapter of the book, must be written Regular.

Citation in text

Please ensure that every reference cited in the text is also present in the reference list (and vice versa). Do not cite references in the abstract and conclusions. Unpublished results, personal communications as well as URL addresses are not recommended in the references list.

Making personal quotations (one, at most) should not be allowed, unless the paper proposed to be published is a sequel of the cited paper. Articles in preparation or articles submitted for publication, unpublished, personal communications etc. should not be included in the references list.

Citations style

Text: All citations in the text may be made directly (or parenthetically) and should refer to:

- **single author:** the author's name (without initials, unless there is ambiguity) and the year of publication: "as previously demonstrated (Brown, 2010)".

- **two authors:** both authors' names and the year of publication: (Adam and Brown, 2008; Smith and Hansel, 2006; Stern and Lars, 2009)

- **three or more authors:** first author's name followed by "et al." and the year of publication: "As has recently been shown (Werner et al., 2005; Kramer et al., 2000) have recently shown"

Citations of groups of references should be listed first alphabetically, then chronologically.

Units, Abbreviations, Acronyms

- Units should be metric, generally SI, and expressed in standard abbreviated form.
- Acronyms may be acceptable, but must be defined at first usage.



Edited by: INMA Bucharest

6 Ion Ionescu de la Brad Blvd., sect. 1, Bucharest, ROMANIA

Tel: +4021.269.32.60; Fax: +4021.269.32.73

<http://www.inmateh.eu>

E-mail: inmatehjournal@gmail.com